Evaluation of In Situ and Ex Situ Remediation Technologies for Iodine-129: Final Bench Scale Results

September 2019

Jim E Szecsody   Nik P Qafoku
Guohui Wang   Hilary P Emerson
Carolyn I Pearce   Elizabeth C Gillispie
Amanda R Lawter   Brandy N Gartman
Kirk J Cantrell   Sara R Kimming
Elsa A Cordova   Vanessa Garayburu-Caruso
Vicky L Freedman   Chris F Brown

U.S. DEPARTMENT OF ENERGY

DISCLAIMER

This report was prepared as an account of work sponsored by an agency of the United States Government. Neither the United States Government nor any agency thereof, nor Battelle Memorial Institute, nor any of their employees, makes **any warranty, express or implied, or assumes any legal liability or responsibility for the accuracy, completeness, or usefulness of any information, apparatus, product, or process disclosed, or represents that its use would not infringe privately owned rights**. Reference herein to any specific commercial product, process, or service by trade name, trademark, manufacturer, or otherwise does not necessarily constitute or imply its endorsement, recommendation, or favoring by the United States Government or any agency thereof, or Battelle Memorial Institute. The views and opinions of authors expressed herein do not necessarily state or reflect those of the United States Government or any agency thereof.

Evaluation of In Situ and Ex Situ Remediation Technologies for Iodine-129: Final Bench Scale Results

September 2019

Jim E Szecsody
Guohui Wang
Carolyn I Pearce
Amanda R Lawter
Kirk J Cantrell
Elsa A Cordova
Vicky L Freedman

Nik P Qafoku
Hilary P Emerson
Elizabeth C Gillispie
Brandy N Gartman
Sara R Kimming
Vanessa Garayburu-Caruso
Chris F Brown

Pacific Northwest National Laboratory
Richland, Washington 99354

Summary

At the U.S. Department of Energy's (DOE's) Hanford Site, located in southeastern Washington State, iodine-129 (I-129) was produced as a byproduct of nuclear fission in the site's nine Pu production reactors. Currently, there are large dilute I-129 groundwater plumes at Hanford, including a groundwater plume in the 200-UP-1 operable unit (OU), located within the Central Plateau. The interim Record of Decision (ROD) for the 200-UP-1 OU requires that DOE evaluate potential treatment options for I-129 before a final ROD is issued. A remedy evaluation plan was subsequently published and identified the approach for this effort.

The laboratory evaluation reported herein is part of the remedy evaluation. This report builds from information gathered in previous literature reviews of potential remedy technologies and provides laboratory testing results for promising candidates in support of determining which candidates warrant additional evaluation through treatability testing.

Based on samples of 200 West Area groundwater, iodine is present in the plume as a mix of iodide (I-), iodate (IO_3^-), and organo-I species, with iodate as the dominant species in most groundwater samples analyzed to date. Thus, evaluation of technologies focused on the two most common iodine species, iodide and iodate. Candidate in situ technologies and materials for use in aboveground treatment processes [e.g., as part of a pump-and-treat (P&T) system] were tested in the laboratory to evaluate their effectiveness under conditions relevant to the 200-UP-1 OU. Within this report, the technologies are organized into three broad categories: in situ sequestration or removal of iodine from groundwater, in situ mobilization of iodine to enhance extraction efficiency, and ex situ removal of iodine from groundwater to support P&T operations.

For in situ sequestration, co-precipitation of iodate with calcium carbonate was investigated using three methods. The first method evaluated iodate uptake as a function of calcite precipitation rate. The second method explored the impact of solution chemistry on iodate uptake by calcite, and the final approach examined the impact of surface area on iodate uptake. While all three approaches demonstrated the ability to remove iodate from Hanford-representative solutions at relevant total iodine solution concentrations, none of them were effective at removing more than 70% iodate from solution. This presents a serious shortcoming for in situ application; therefore, further testing of in situ formation of calcite for remediation of I-129 is not recommended.

Precipitation of initially amorphous calcium-phosphate (which slowly crystallizes to apatite), another potential in situ treatment approach, inconsistently removed a small amount of iodate from solution at pH 11 and above, and none at pH 9.0 and 7.5. In the 40 experiments performed as part of this study, many showed greater uptake during initial amorphous calcium phosphate precipitation, and less iodate uptake as the precipitate crystallized to hydroxyapatite. Iodate removal from solution via either sorption onto or incorporation into apatite was insufficient to meet the maximum contaminant level of 1 pCi/L in groundwater; therefore, further testing of this technology for remediation of I-129 is not recommended.

A series of batch adsorption/desorption experiments were also conducted to determine the effectiveness of several organic materials for sequestering iodate and iodide from Hanford groundwater. The organic materials that were evaluated in this study were chitin, lignin, and humic acid sorbed to a representative Hanford sediment. Of the three organic carbon materials tested, only chitin showed potential as an in situ remediation technology for iodide (average K_d value of 74.9 ± 4.3 mL/g). However, iodine within the groundwater at 200-UP-1 is primarily in the form of iodate, which limits the effectiveness of chitin as a removal technology. As such, further testing of this technology is not recommended.

Laboratory results indicated that iodate and iodide are effectively removed from Hanford groundwater by in situ iron oxide precipitation, especially ferrihydrite (HFO), either through sorption or co-precipitation processes. This HFO precipitation technology evaluated in 1- and 3-meter columns for source area treatment showed 23% to 47% iodate capture, likely in HFO. For permeable reactive barrier application, 1-D columns showed 100% removal of 100 μg/L iodate for 170 PVs, after which 50% to 60% of the iodate remobilized. This is a reasonable capacity, but long-term performance and potential unintended consequences still need to be identified.

The use of dithionite was identified as a potential remedial approach for enhancing pump-and-treat extraction. Results demonstrated that dithionite-treated sediments enabled much greater (4 times or more) and rapid (one to three orders of magnitude) leaching of I-127 from the sediment compared to leaching of untreated sediment. In addition, it appears that I-129 is more easily removed from sediments than I-127, suggesting low concentration of Na-dithionite would be effective. This technology is a promising candidate to accelerate removal of iodine from the surface by P&T in areas where sorption and I-129 mass in Fe-oxide precipitates limit extraction efficiency. However, further testing of this technology is recommended for this type of application.

A wide range of materials for ex situ treatment were also tested for their capacity to remove iodate from groundwater. Synthetic groundwater was used in the experiments to evaluate iodate removal in the presence of the competing anions. Ferrihydrite, bismuth oxy(hydroxide), and bismuth-cobalt-aluminum are the most promising materials, and the observed batch-test removal efficiency is sufficient to reduce concentrations of I-129 from 30 pCi/L to 1 pCi/L, even in the presence of a total iodine concentration (i.e., including I-127) 1000 times higher than I-129. When available in sufficient quantities, these promising materials were engineered into viable form for deployment in the P&T system. In some cases, a viable form of the material was available commercially as hybrid ion exchange resins from ResinTech, Inc. The ResinTech CHM-20 resin, a cerium oxide/hydroxide hybrid with a Type 2 (dimethylethanolamine) parent anion exchange, performed the best with respect to iodate removal in a column system using 200 West Area groundwater with an influent iodine concentration of 100 μg/L (added as sodium iodate) and a flow rate of 25 mL/h. The performance of the CHM-20 hybrid resin can be characterized as marginal, with an iodine capacity under the conditions tested of 33 μg/g at 100% breakthrough. There is a potential for improving resin performance by optimizing the parameters for the column experiments and tuning the resin composition. However, the CHM-20 resin capacity is substantially lower in relation to the influent contaminant loading based on expected I-127 concentration in groundwater than the capacity/loading ratio of the current resins in use at the 200 West P&T facility for uranium and Tc-99. Therefore, significant improvements through resin development would be needed to enable its use as an effective iodate treatment application.

Acknowledgments

Acronyms and Abbreviations

AGW	artificial groundwater
BSN	bismuth-based material
BTC	1,3,5-benzenetricaboxylate
CAC	Carbon Activated Corporation
CPN	cationic polymeric network
CPS	calcium polysulfide (CaSx)
DDI	double deionized
DDW	degassed and deionized water
DMSO	dimethyl sulfoxide
DOE	U.S. Department of Energy
EDS	energy dispersive X-ray spectroscopy
GAC	granulated activated carbon
HA	humic acid
HF	Hanford fine sand
HFO	2-line-ferrihydrite
I/P	iodine/phosphorous
IC	inorganic carbon
ICP-OES	inductively coupled plasma – optical emission spectroscopy
ICP-MS	inductively coupled plasma – mass spectrometry
MOF	metal organic framework
NAPL	non-aqueous phase liquids
OU	operable unit
P&T	pump-and-treat
PAN	polyacrylonitrile
PDA	polydopamine
PNNL	Pacific Northwest National Laboratory
PRB	permeable reactive barrier
PV	pore volume
ROD	record of decision
SAGW	sediment with artificial groundwater
SEM	scanning electron microscopy
SSA	specific surface area
TIPE	1,1,2,2-tetrakis(4-(imidazolyl-4-yl) phenyl)ethane
TMAH	tetramethylammonium hydroxide
TOC	total organic carbon
VZPW	artificial vadose zone porewater

XANES	X-ray absorption near edge structure
XAS	X-ray absorption spectroscopy
XPS	X-ray photoelectron spectroscopy
XRD	X-ray diffraction

Contents

Figures

Tables

1.0 Introduction

Due to its long half-life (15.7 Ma) and relatively unencumbered migration in subsurface environments (Sheppard et al. 1995; Bird and Schwartz 1997; Cantrell et al. 2003; Um and Serne 2005), 129I has been recognized as a contaminant of concern at numerous federal and international nuclear facilities (DOE 1996; Hou et al. 2003; Kekli et al. 2003; Hartman et al. 2004). At the U.S. Department of Energy's (DOE's) Hanford Site, located in southeastern Washington State, ^{129}I was produced as a byproduct of nuclear fission in the site's nine Pu production reactors. Release of waste solutions (both purposeful and inadvertent) to the environment has resulted in ^{129}I being the second-most widespread radionuclide in the Hanford groundwater system (DOE 2016). Currently, there are large, dilute ^{129}I groundwater plumes, including a groundwater plume in the 200-UP-1 operable unit (OU) located within the Central Plateau (Figure 1.1). The interim Record of Decision (ROD) for the 200-UP-1 OU requires that DOE evaluate potential treatment options for I-129 before a final ROD is issued (DOE 2012). A remedy evaluation plan was subsequently published and (DOE 2017) identified the approach for this effort. The laboratory evaluation reported herein is part of the remedy evaluation. This report builds from information gathered in a literature review of potential remedy technologies (Strickland et al. 2017a,b) and provides laboratory testing results for promising candidates in support of determining which candidates warrant additional evaluation through treatability testing.

Based on samples of 200 West Area groundwater, iodine is present in the plume as a mix of iodide (I-), iodate (IO$_3$-), and organo-I species, with iodate as the dominant species in most groundwater samples analyzed to date. Thus, evaluation of technologies focused on the two most common iodine species, iodide and iodate. Candidate in situ technologies and materials for use in aboveground treatment processes [e.g., as part of a pump-and-treat (P&T) system] were tested in the laboratory to evaluate their effectiveness under conditions relevant to the 200-UP-1 OU. Detailed descriptions of the ^{129}I plume and factors important for remediation technologies are provided in a series of reports describing the conceptual model for iodine behavior in the Hanford Site subsurface (Truex et al. 2015, 2016, 2017; Qafoku et al. 2017), and were considered in designing the laboratory tests used to evaluate technologies.

Strickland et al. (2017a) identified several potential technologies. The set of technologies evaluated was expanded based on a literature review by Strickland et al. (2017b). Within this report, the technologies are organized into three broad categories: in situ sequestration or removal of iodine from groundwater, in situ mobilization of iodine to enhance extraction efficiency, and ex situ removal of iodine from groundwater to support P&T operations. Evaluated technologies are summarized in the following sections.
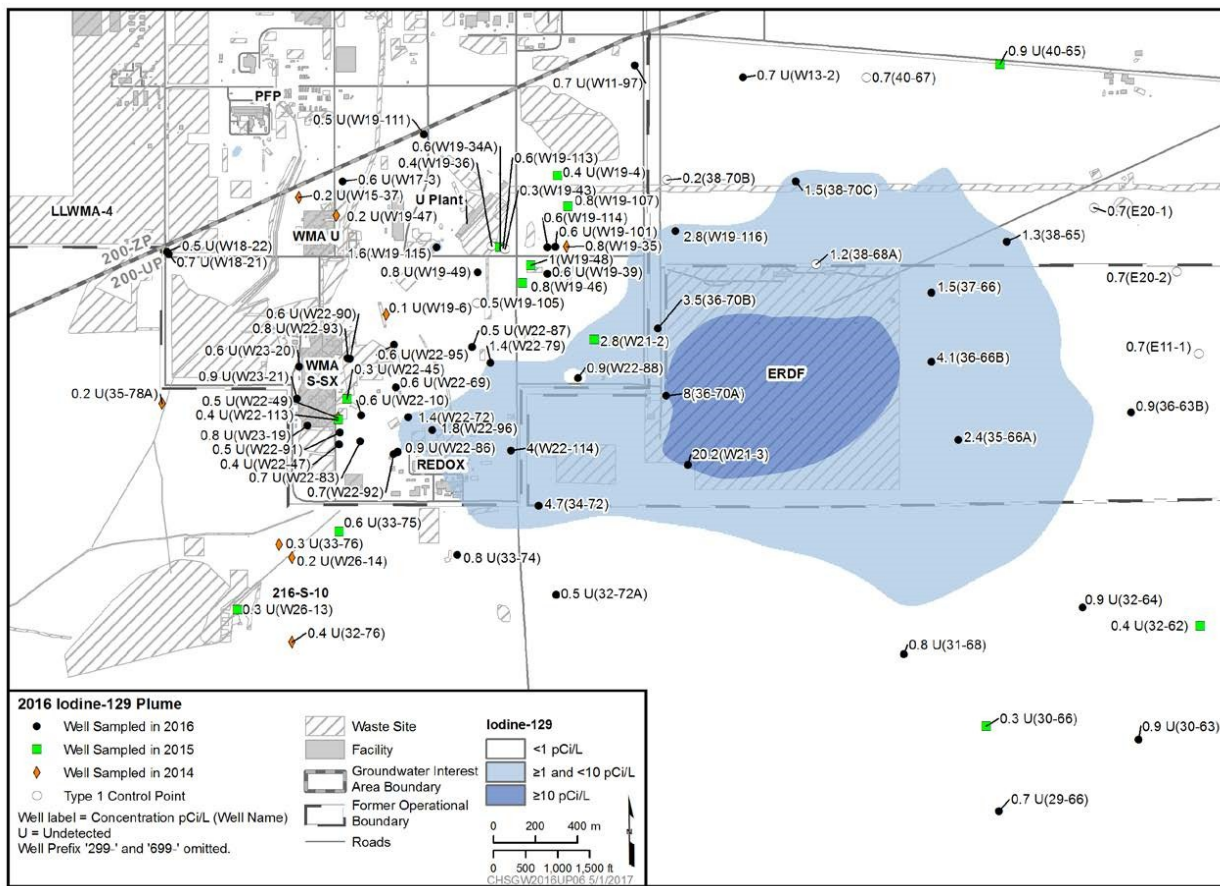
Figure 1.1. 2016 I-129 plume map (from DOE 2016).

1.1 Category 1: In Situ Sequestration or Removal of Iodine from Groundwater

1.1.1 Co-precipitation and Enhanced Sorption by Calcite

The laboratory study focused on evaluating methods to induce calcite precipitation in situ over a large radial distance from an injection well. Key to this effort was ensuring a suitable precipitate mass to create slow-release conditions for iodate while not clogging aquifer pores. Previous calcite precipitation experiments showed removal of iodine by incorporation into calcite during calcite precipitation (50% aqueous iodate removed) (Truex et al. 2016). However, there was a need to further increase iodate uptake by calcite to make this a viable in situ remediation strategy. The calcite precipitation method used during previous years was modified to determine if iodate uptake could be increased. Modifications included calcite formation in synthetic vadose zone porewater (VZPW) instead of double deionized (DDI) water, precipitation of nano-calcite to increase surface area, and use of alternative precipitation methods to enhance iodate sorption/uptake.

1.1.2 Co-precipitation and Enhanced Sorption by Iron Oxides

Interaction of iodide and iodate with iron oxides was evaluated, building on the work by Couture and Seitz (1983) and Fuhrman et al. (1998). Laboratory-scale efforts focused on two tasks: (1) understanding the interactions of iodate/iodide with iron oxides (sorption/desorption, and co-precipitation), and

(2) evaluating methods to induce iron oxide precipitation in situ over a large radial distance from an injection well and at a suitable mass to create enhanced sorption and slow-release conditions for iodine species without clogging aquifer pores. For task 1, batch experiments were conducted to investigate the immobilization of iodine through association with iron oxides (in terms of distribution coefficient K_d). Building on the previous test results that focused on iodate/iodide sorption onto pure iron oxides in artificial groundwater (AGW) (Strickland et al. 2017a), testing was expanded to include reversibility testing (i.e., desorption) of iodate/iodide on iron oxides in AGW, as well as iodate/iodide behavior during iron oxide transformation between different phases, such as ferrihydrite to goethite or to magnetite. Experiments also involved 1-D flow through soil columns using amendments identified to induce iron oxide precipitation in situ.

1.1.3   Enhanced Sorption by Organic Carbon

These laboratory tests focused on evaluating types of organic carbon that could be injected as a permeable reactive (sorption) barrier. Candidates included chitin, lignin, and humic/fulvic acids sorbed to a Hanford sediment. Batch partitioning and desorption studies were conducted for the candidate materials. In the case of humic/fulvic acids sorbed to Hanford sediment, both as is and sterilized sediments were evaluated to determine potential impacts of microbial activity. Selected samples were analyzed for iodine speciation to determine if any changes in iodine speciation occurred during the course of the experiments.

1.1.4   Co-precipitation and Enhanced Sorption by Apatite

Previous work (Campayo et al. 2011) identified up to 7% iodate incorporation into solid apatite with a pH 10 to 12 solution. Apatite technology evaluation focused on adapting and testing this technology under Hanford groundwater conditions. Tests were conducted by adding apatite-forming chemicals to solutions containing iodate and iodide. The loss of iodine from solution was monitored as a function of time. Additionally, adsorbed iodine species and measurement of incorporated iodine species were quantified through analysis of the solid-phase materials (by acid dissolution of the precipitated apatite). The test matrix included multiple tests to evaluate the effect of pH, iodine concentration, iodine/phosphate ratio, and the addition of carbonate on iodine species uptake.

1.2 Category 2: In Situ Mobilization of Iodine to Enhance Extraction Efficiency

1.2.1   Dithionite-Enhanced Mobility

The enhanced mobility screening tests focused on using a low-concentration solution of sodium dithionite to reduce iodide to iodate, thereby reducing its sorption potential by up to a factor of four (Xu et al. 2015; Truex et al. 2016). This technology is targeted at accelerating removal of iodine from the surface by P&T in areas where sorption limits extraction efficiency. This laboratory study focused on identifying appropriate concentration ranges of dithionite to release and maintain iodine mobility by converting iodate to iodide and by dissolving iron oxides on sediment surfaces, releasing iodine species to aqueous solution. Batch experiments were conducted to bound the appropriate concentration ranges and evaluate potential analytical interferences with iodine quantification. Samples were also analyzed to determine the magnitude of other constituents released by the dithionite treatment. Soil column experiments were used to quantify water quality after treatment and to determine if released ferrous iron that is oxidized downgradient of the treatment would sequester the iodine and nullify the enhanced mobilization.

1.3 Category 3: Ex Situ Removal of Iodine from Groundwater to Support Pump-and-Treat Operations

1.3.1 Materials for Iodine Immobilization

The objective of this task was to conduct a set of batch sorption experiments with selected materials for ex situ iodate immobilization in a representative synthetic Hanford groundwater. The materials that were evaluated in this study included iron oxides (ferrihydrite, micro-magnetite, nano-magnetite, goethite, ferrous hydroxide), sulfides (potassium metal sulfide, iron sulfide), organoclays (PM-199 and MRM, Cetco), bismuth-based materials (bismuth nitrate), metal organic frameworks (SCU-101, SCU-102, SCU-CPN, FeBTC-PDA) and aerogels (sulfur functionalized aerogels, copper-functionalized aerogels). These materials were tested alongside the baseline materials currently used in the 200 West pump-and-treat (P&T) facility (Purolite A530E Ion Exchange Resin and Carbon Activated Corporation 011-55 Granulated Activated Carbon) because previous work has demonstrated that strong base anion exchange resins can remove iodine from Hanford groundwater (Parker et al. 2014; Levitskaia et al. 2017). Silver-based materials were not included for testing because silver is a *Resource Conservation and Recovery Act* metal and its use for remediation activities may be restricted. It is notable that an in situ treatment zone created through injection of submicron silver chloride particle is being evaluated at the Savannah River Site (Denham and Eddy-Dilek 2016).

2.0 Co-precipitation with Calcite

Previous experiments have shown removal of iodine by incorporation into calcite during precipitation (~50% aqueous iodate removed); however, there is a further need to increase iodate uptake for this approach to be a viable remediation strategy. Various modifications to the calcite co-precipitation approach were made to determine if iodate uptake could be improved. Modifications included calcite formation in the presence of silica gel, which slows down the rate of calcite precipitation, and is expected to result in greater iodate incorporation into calcite. The effects of other background solutions on iodate incorporation into calcite (including synthetic VZPW and/or AGW instead of DDI) were evaluated. In addition, methods to precipitate nano-calcite to increase surface area with the aim of greater iodate incorporation were assessed.

2.1 Experimental Methods

2.1.1 Iodate Co-precipitation with Calcite in the Presence of Si Gel

Iodate-doped calcium carbonate in a sodium metasilicate gel was synthesized using a modified procedure described by Podder et al. (2017). The starting materials included analytical grade sodium metasilicate (Na_2SiO_3; 18-mesh granular and purity ≥95.0% Alfa Aesar), calcium chloride ($CaCl_2$; ≥97% Sigma-Aldrich), ammonium carbonate (($NH_4)_2CO_3$; Purity Grade Fisher Scientific), sodium iodate ($NaIO_3$; ≥99% Acros Organics), acetic acid ($C_2H_4O_2$; ACS Grade ≥99.7% Fisher Scientific), and Milli-Q water (18.2 MΩ cm at 21°C). Five batches of Na_2SiO_3 + 1 M acetic acid were made, which corresponded to five concentrations of iodate spiked in calcite. First, 2.5 g Na_2SiO_3 was added in 50 mL of distilled deionized water, stirred for 30 min, and then left undistributed for another 30 min. Subsequently, a 1 M acetic acid solution was prepared and stirred for 15 min. In order to prepare the Na_2SiO_3 gel (specific gravity of approximately 1.05 g/cm³), the 50 mL Na_2SiO_3 solution was added drop-wise to 50 mL of 1 M acetic acid in 150-mL high-density polyethylene bottles (Fisher Scientific, USA) using a transfer pipette, while constantly stirring the solution at 100 rpm. One hundred milliliters of 0.1 M ammonium carbonate was impregnated into the gel solutions for each batch. Additionally, $NaIO_3$ at concentrations of 100 (0.51 μM), 250 (1.3 μM), 500 (2.5 μM), and 395784 (2.0 mM) μg/L was added to the gel solution separately. Concentrations between 100 and 500 μg/L were chosen in order to closely mimic elevated environmental levels and the 2.0-mM concentration was the lowest concentration used in Podder et al. (2017) and was chosen for a comparison of technique. Approximately 25 mL of each combined solution was slowly placed into five 50-mL polypropylene centrifuge tubes (Corning Incorporated) and left to settle (ca. 5 min). Each tube was then covered with 20 mL of 0.1 M $CaCl_2$, gently agitated, and capped. Solutions gelled after roughly 2 weeks and small amounts of calcite precipitation occurred after 4 weeks.

To quantify the amount of iodine from calcite precipitation, the solution was centrifuged (Thermo Electron Corporation; HN-SII Bench-Top) from gel + calcite material at approximately 2500 rpm, decanted, filtered (0.2 micron), and measured for total iodine using inductively coupled plasma mass spectrometry (ICP-MS). Currently, there are no effective methods for complete separation of calcite from Si gel matrix. Therefore, several techniques were tested for complete separation and evaluated below.

2.1.1.1 Separation Considerations

Several techniques (i.e., centrifuging, sonication, rinsing and filtration, dissolution) were considered to separate solution and calcite from Si gel. Centrifuging the samples twice, once to extract the bulk solution and a second time to extract any remaining solution within the gel, was an effective technique to remove all solution from the remaining gel. Most solutions were fully separated from the gel + calcite material

after only one time centrifuging (20 min, ca. 2500 rpm). During this process, calcite appeared uniformly trapped in the gel and no visible calcite was present or decanted with the solution. Due to the novelty of this technique, it was assumed that iodate captured in the gel + calcite material would be immobilized in field conditions whether bound to calcite or the Si gel. Additionally, it is likely that calcite would have a greater affinity for iodate than silicate, and therefore iodine is expected to be mostly bound to calcite. However, it will be important to better understand the mechanism of immobilization prior to deploying Si gel as a remediation tool.

Sonication was considered as a possible technique to further separate calcite from Si gel. A 50-mL centrifuge tube with solution, Si gel, and calcite were placed into a rack and put into a bench-top sonicator (Fisher Scientific; FS30H) filled with DDI water and left to sonicate for 15 min. After 15 min, some Si gel migrated toward the bottom of the centrifuge, leaving roughly 5 mL of solution as a layer at the top. Due to the amount of time it would take to separate the solution from gel using this technique, and the fact that calcite still remains in the gel, centrifuging is a better technique for solution separation. Further tests could be conducted to evaluate just gel and calcite separation using either a bench sonicator or a sonic dismembrator.

Calcite and Si gel material were placed onto a 0.45-micron filter (Millipore Express®; Stericup vacuum driven disposable filtration system), rinsed with DDI water during vacuum, and set aside to air dry in a fume hood. After a week, solids appeared to be crystalized calcite minerals, where the crystallization could have incorporated small amounts of silica. This technique has the potential to separate out calcite from Si gel; however, further tests need to be conducted to determine if the mass balance of iodate uptake matches that from solution and if the chemical composition of the solid is pure calcite or contains silica impurities. Qualitative analyses of the initial tests suggest that not all of the Si gel is removed with the process of rinsing and drying.

2.1.1.2 Differences from Podder et al. Synthesis and Separation Methods

According to Podder et al. (2017), solid products were washed with deionized water and air dried. Once dry, samples were examined under a microscope and were hand-picked to separate calcium carbonate minerals. Based on testing, washing of solid products did not effectively separate gel material from calcite and the calcite was too well mixed and small in size to be hand-picked. This approach would likely result in loss of the majority of calcite and thus be an inadequate representation of the amount of iodine that was co-precipitated with calcite.

Additionally, iodine in calcite and vaterite was dissolved using HF-HNO_3, which could result in the volatilization of iodine due to the extreme acidic conditions and loss of total iodine actually found in these minerals. Therefore, samples were digested using alkaline fusion and analyzed via ICP-MS.

2.1.2 Iodate Co-precipitation with Calcite from VZPW and AGW

Calcite was precipitated in Hanford VZPW and AGW to test the extent of iodate uptake in calcite. Calcite-forming solutions were prepared in VZPW and AGW and contained 0.1 M $CaCl_2$ and 0.1 M $(NH_4)_2CO_3$ (Truex et al. 2017). The VZPW solution was composed of 12 mM $CaSO_4*2H_2O$ (Acros Organics), 1.7 mM NaCl (ACS Grade Spectrum Chemical, 0.4 mM $NaHCO_3$ (ACS Grade Fisher Scientific), 3.4 mM $NaNO_3$ (≥99% Sigma-Aldrich), 2.6 mM $MgSO_4$ (J.T. Baker), 2.4 mM $MgCl_2*6H_2O$ (ACS Grade Fisher Scientific), and 0.7 mM KCl (ACS Grade Fisher Scientific) adjusted to a pH of 7.14 (Serne et al. 2015) (Table 2.1). The AGW solution was composed of 0.20 mM $H_2SiO_3*nH_2O$, 0.11 mM, KCl, 0.15 mM $MgCO_3$, 0.26 mM NaCl, 0.49 mM $CaSO_4$, and 1.5 mM $CaCO_3$ and measured a pH value range of 7.5–7.6 (Table 2.2). In addition to VZPW and AGW, calcite was precipitated in DDI water spiked with and without iodate as controls. Iodate uptake during calcite precipitation was tested by spiking

VZPW, AGW, and DDI water solutions with 100 (0.51 µM), 250 (1.3 µM), 500 (2.5 µM), and 395784 (2.0 mM) µg/L $NaIO_3$, concentrations consistent with those discussed in Section 2.1. Batch experiments were conducted in duplicate in 250 mL high-density polyethylene bottles (Fisher Scientific, USA).

The VZPW was made by addition of the reagents in Table 2.1 to DDI water in the order identified in Table 2.1. Once the reagents had all been added, the solution pH was adjusted with the addition of sodium hydroxide or sulfuric acid to a final pH of between 7.0 and 7.2.

Table 2.1.   Vadose zone porewater simulant recipe (from Serne et al. 2015).

Order to Dissolve	M	Reagent	MW	g/L
1	0.012	$CaSO_4*2H_2O$	172.1723	2.0661
2	0.0017	NaCl	58.4430	0.0994
3	0.0004	$NaHCO_3$	84.0068	0.0336
4	0.0034	$NaNO_3$	84.9948	0.2890
5	0.0026	$MgSO_4$	120.3660	0.3130
6	0.0024	$MgCl_2*6H_2O$	203.3034	0.4879
7	0.0007	KCl	74.5515	0.0522
Adjust pH to 7.0 to 7.2 with sodium hydroxide or sulfuric acid.				

The AGW was made by addition of the reagents in Table 2.2 to DDI water in the order identified in the table. Once the chemicals were dissolved, an excess of calcium carbonate ($CaCO_3$) was added and the solution was stirred. After approximately 1 week, the solution was filtered to remove excess $CaCO_3$ using a 0.45-µm filter.

Table 2.2.   Artificial Hanford groundwater.

Constituent	Conc. (mg/L)	Mass for 1 L (g)
$H_2SiO_3*nH_2O$, silicic acid	15.3	0.0153
KCl, potassium chloride	8.20	0.0082
$MgCO_3$, magnesium carbonate	13.0	0.0130
NaCl, sodium chloride	15.0	0.0150
$CaSO_4$, calcium sulfate	67.0	0.0670
$CaCO_3$, calcium carbonate	150	0.1500

After the VZPW and/or AGW were prepared, the calcite-forming solutions were made. To remain consistent with previous calcite formation studies (Truex et al. 2017), 1M or 0.1M $CaCl_2$ and $(NH_4)_2CO_3$ were used as the calcite-forming solutions. These calcite-forming solutions were prepared in VZPW, AGW, and/or DDI water. Table 2.3 provides the appropriate amount of each chemical added for the two molarities.

Table 2.3. Calcite-forming solutions.

Constituent	Molarity	Mass for 1 L (g)
CaCl$_2$, calcium chloride	0.1M	11.098
	1M	110.98
(NH$_4$)$_2$CO$_3$, ammonium carbonate	0.1M	19.218
	1M	192.18

To precipitate calcite, equal volumes of the CaCl$_2$ and (NH$_4$)$_2$CO$_3$ solutions of equal molarity were slowly added together in a PTFE poly bottle (e.g., 50 to 250 mL of each solution). Iodate spikes (from a stock NaIO$_3$ solution to achieve concentrations in the range 100 to 500 µg/L) were added to the CaCl$_2$ solution prior to the (NH$_4$)$_2$CO$_3$ addition. Once the calcite-forming solutions were combined, calcite precipitation was visible immediately. Calcite was precipitated from solutions made in DDI water, as well as DDI water without calcite-forming solutions (but spiked with NaIO$_3$) to serve as controls for these experiments.

After the calcium carbonate precipitation started, pH was measured and 2 mL of supernatant was sampled at approximately 0, 4, 24, and 72 h, and then weekly for a minimum period of 28 days. The 2-mL samples were filtered with a 0.2-µm syringe filter. The contents of the bottles were gently swirled daily during regularly scheduled workdays, and were otherwise undisturbed between samplings. Following the completion of sampling events, the contents of the poly bottles were filtered with a 0.45-µm vacuum filter to collect the produced solids. After drying in a fume hood, the solids were collected for solid phase characterization by alkaline fusion and scanning electron microscopy (SEM) energy dispersive X-ray spectroscopy (EDS).

2.1.3 Iodate Co-precipitation with Nano-Calcite

Nano-sized calcite was synthesized using a modified procedure from Montes-Hernandez et al. (2007). A 1M calcium hydroxide (Ca(OH)$_2$) solution was made by adding 1.85 g of Ca(OH)$_2$ (> 96% purity; Sigma-Aldrich) to a volumetric flask and filling up to 25 mL with DDI. A 25-mL Parr pressure reactor (Parr Instrument Company) was used to react the Ca(OH)$_2$ solution with CO$_2$ (800 psi) at 30°C. A rigid mantle heater with a heat controller receiving feedback directly from a J-type thermocouple (OMEGA Engineering Inc.; Precision Fine Wire) was used to maintain the reactor at 30°C. Solutions were spiked with either 100 or 500 µg/L sodium iodate and reacted for 4 and 24 h.

Samples were centrifuged and the solution decanted. Solids were dried at 80°C for 48 h. The weight of the decanted solution was recorded and a 4-mL aliquot was filtered using a 0.2-µm syringe filter (Merck Millipore; Millex – GV) and analyzed for total iodine using ICP-MS.

2.1.4 Analyses

2.1.4.1 Elemental Analyses

Total iodine was analyzed on two different ICP-MS instruments based on equipment availability. The first instrument was an X-Series II ICP Mass Spectrometer from Thermo Fisher Scientific and the second instrument was an ELAN DRC II ICP Mass Spectrometer from PerkinElmer. The detection limit for total iodine is 0.0126 µg/L for both instruments.

A suite of elements were analyzed based on the VZPW: aluminum, calcium, magnesium, potassium, silicon, sodium, sulfur, and tin. Detection limits for each element were 16, 33, 2.7, 161, 54, 44, 47, and 13 µg/L, respectively.

2.1.4.2   Scanning Electron Microscope

The SEM instrument used for calcite size and morphology was an FEI Helio 600 dual beam. Samples were prepped by attaching double sticky carbon (C) tape to aluminum holders (Ted Pella) and sprinkling a small amount of sample powder to the C tape. Samples were then coated with a 10-nm C layer using a sputter coater to avoid charging.

2.1.4.3   Alkaline Fusion

Alkaline fusion was used to solubilize iodine from calcite using a Pacific Northwest National Laboratory (PNNL) technical procedure (PNNL-ESL-Fusion, Rev. 2). In short, the calcite sample was mixed with a potassium hydroxide-potassium nitrate (KOH-KNO$_3$) solution in a nickel (Ni) crucible (Metal Technology; 20-0075HC) and dried. The crucible was then heated at approximately 550°C in a furnace (OMEGALUX; LMF – 3550) for about 60 min. KNO$_3$ is used as an oxidant to improve the dissolution potential of the flux. To recover samples from the crucibles after heating, samples were cooled and then rinsed with DDI and 5 mL of sulfuric acid into funnels over 50-mL polypropylene centrifuge tubes (Corning Incorporated) and brought to a volume of 30 to 35 mL. All Ni crucibles were new and were cleaned by washing the crucibles and lids with 2% nitric acid (HNO$_3$), rinsed with DDI water, pre-heated in an oven (Thermo Scientific) to 150–200°C, cleaned again, and air dried. All chemicals were ACS grade or equivalent. Each fusion process had 1 to 3 samples, a blank, a blank spike, at least one duplicate of a sample, and a sample matrix spike. An aliquot was then filtered using a 0.2-μm syringe filter and analyzed for total iodine using ICP-MS.

2.2 Results

2.2.1   Iodate Co-precipitation with Calcite in the Presence of Si Gel

Iodate co-precipitation with calcite in the presence of Si gel was chosen as a potential method of iodate removal in the subsurface due to Si gel's ability to slow down the rate of formation of calcium carbonate minerals. In general, calcite formation is almost instantaneous and preliminary data has shown that the majority of iodate uptake occurs during this time. By slowing the precipitation of calcite, it is possible that more iodate could be removed over time. Results demonstrated that in the presence of Si gel, greater than 50% of total iodine in solution is removed within the calcite and gel mixture for all concentrations of iodate. Figure 2.1 shows that, compared to initial spiked concentrations, calcite in Si gel removed the most iodine when the initial spike was 500 μg/L. Overall, 84% of iodine was removed when initial concentrations were 500 μg/L and 56% at 100- and 250-μg/L concentrations.
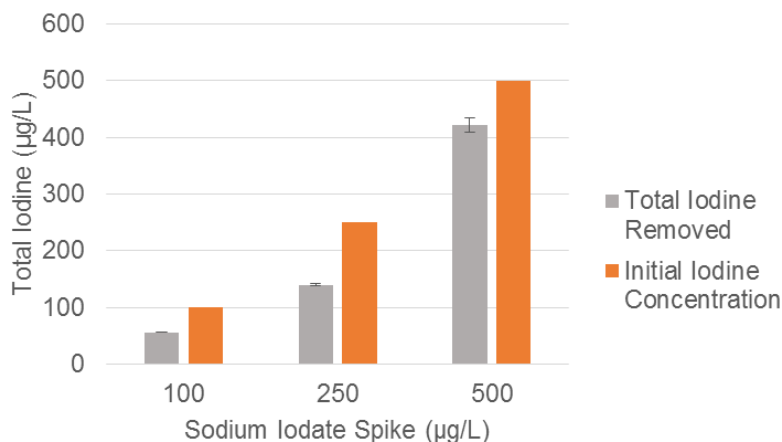
Figure 2.1. Removal of iodate after calcite precipitation in metasilicate gel. Treatments of Si gel and calcite were spiked with 100, 250, and 500 µg/L sodium iodate in a stock solution relative to the spike. Five replicates of each treatment were performed and left to sit for approximately 5 weeks until calcite formation. Orange bars represent initial iodine concentrations spiked into solutions. Gray bars represent the difference between the average measured iodine concentration and the original spike amount, assuming that the spike and solution were distributed evenly throughout the five centrifuge tubes. Error bars represent the standard deviation of the replicates for total iodine in solution.

As the concentration of iodate in solution increased (i.e., increase in spike), calcite removed the same percentage of iodate in both 100- and 250-µg/L treatments, yet the amount of iodine co-precipitated with calcite increased (Figure 2.1; Table 2.4). This suggests that calcite can indeed remove and bind more iodine but that other chemical mechanisms are having an effect, such as equilibrium between how much iodine is in the system and how much gets sorbed. Furthermore, an elevated concentration of iodine was tested (396 ppm) to compare to the lowest concentration of Podder et al. (2017). Results were similar to spikes with 100 and 250 µg/L iodine, where approximately 58% of iodine was removed from solution and resulted in 1129 µg of iodine loaded onto 1 g of calcite (Table 2.4).

Table 2.4. Iodine concentrations in calcite precipitated in Si gel.

Sodium Iodate Spike (µG/L)	Total Iodine in Solution (µG/L)	Amount of Iodine Removed (µG IO_3^-/G of calcite)
100	44 ± 0.5	0.278
250	110 ± 1.2	0.689
500	79 ± 13	1.59
395784	167800 ± 2588	1129

2.2.2   Iodate Co-precipitation with Calcite from VZPW and AGW

Various concentrations of sodium iodate were introduced into Hanford VZPW and AGW to better understand the effect of the chemical composition of solution on iodine removal in the presence of calcite. Our results indicate that the greatest amount of iodine was removed over time in VZPW at any given concentration and that removal of iodine was almost instantaneous for all solutions (Figure 2.2). After 28 days, calcite VZPW had removed 71, 168, 324, and 51,284 µg/L of iodine for each respective spike (100, 250, 500, and 395,784 µg/L), whereas calcite in AGW removed only 46, 121, 224, and 32,784 µg/L. Overall, the calcite in VZPW treatment removed 15–20% more iodate than in AGW or DDI. For

treatments with 100 and 250 µg/L iodate, calcite in VZPW was able to remove up to 80% of the iodate in solution, whereas AGW removed 46% and 48%, respectively, and DDI 32% and 36%, respectively. When concentrations were extremely elevated with iodine (i.e., 396-ppm spike), only 8–12% of the iodine was removed across all solutions. Despite the differences in iodine removal, all solutions removed most of the iodine within the first 4 h but slightly increased in removal by day 28 (Figure 2.2). Varying iodate concentrations without calcite were also mixed with VZPW, AGW, and DDI, and no significant difference was noticed among samples on any iodine removal and concentrations remained at the initial levels (Figure 2.3).
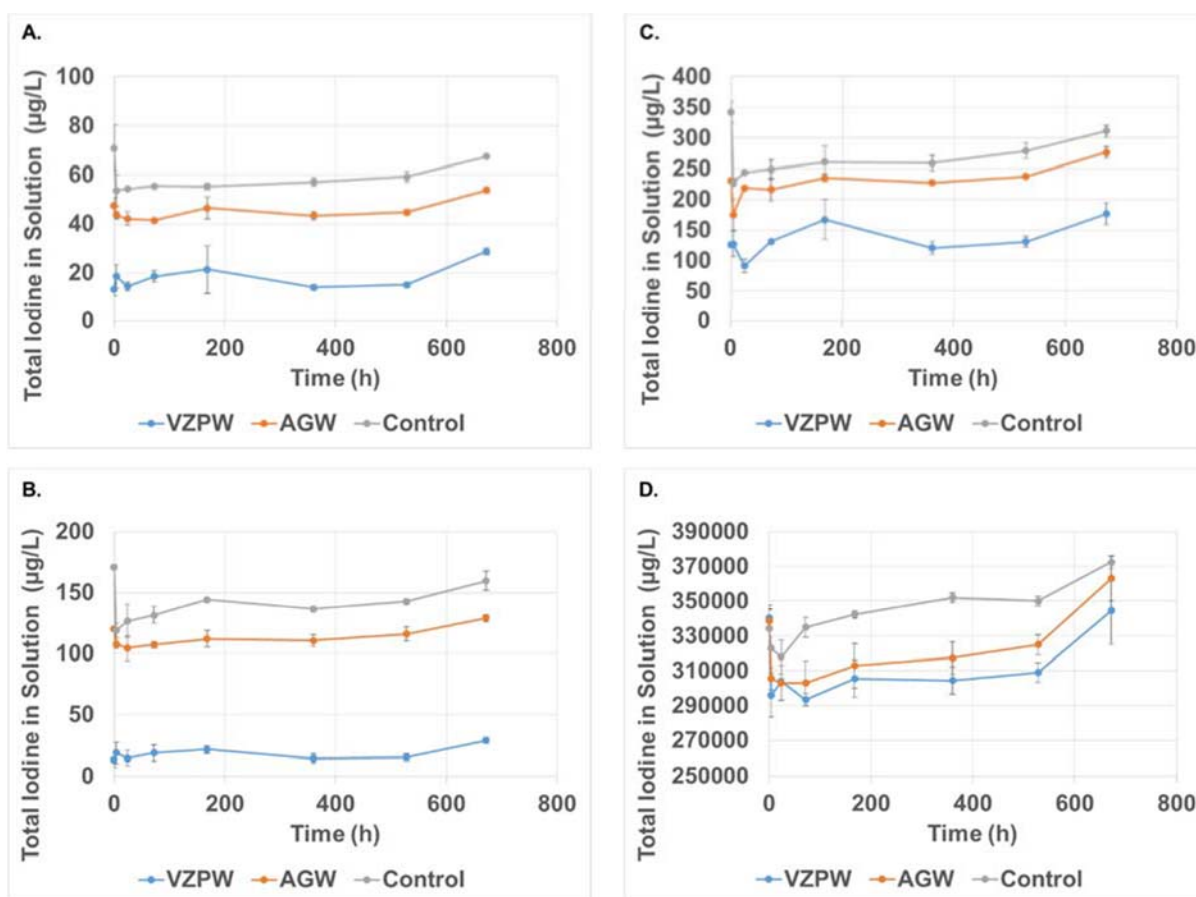
Figure 2.2.   Iodine in solution after calcite precipitation in VZPW and AGW over time. Four concentrations of iodine—100 µg/L (A), 250 µg/L (B), 500 µg/L (C), and 395,784 µg/L (D)—were added to VZPW (blue line) and AGW (orange line) in the presence of calcium carbonate. Total iodine in solution was measured over a period of 28 days and sampled at 0 h, 4 h, 24 h, 3 d, 7 d, 15 d, 22 d, and 28 d. Gray lines represent iodine concentrations over time in DDI in the presence of calcite. Samples were performed in duplicate. Error bars represent the standard deviation of replicates for each time point.

Results from SEM images reveal that AGW and DDI produced purely calcite minerals, whereas VZPW produced a mixture of calcite and aragonite (Figure 2.4). This can be seen by the needle-like structures of aragonite and cubic structure of calcite. These results could suggest that the solution chemical composition and mineralogy of calcium carbonate influences the effectiveness of iodate uptake. Within the chemical composition of VZPW, concentrations of the constituents, especially magnesium (Mg), were at much high molarities than in AGW (Table 2.5). Because of this, it is possible that a more complex structure composed of aragonite and calcite might be better at removing iodate than if just calcite was present.

Lastly, alkaline fusion digestions were performed on VZPW, AGW, and DDI solutions with calcite spiked at 500 µg/L and resulted in 66.5, 48.5, and 40.9 µg/g of iodine present in calcite from the VZPW, AGW, and DDI solutions, respectively.
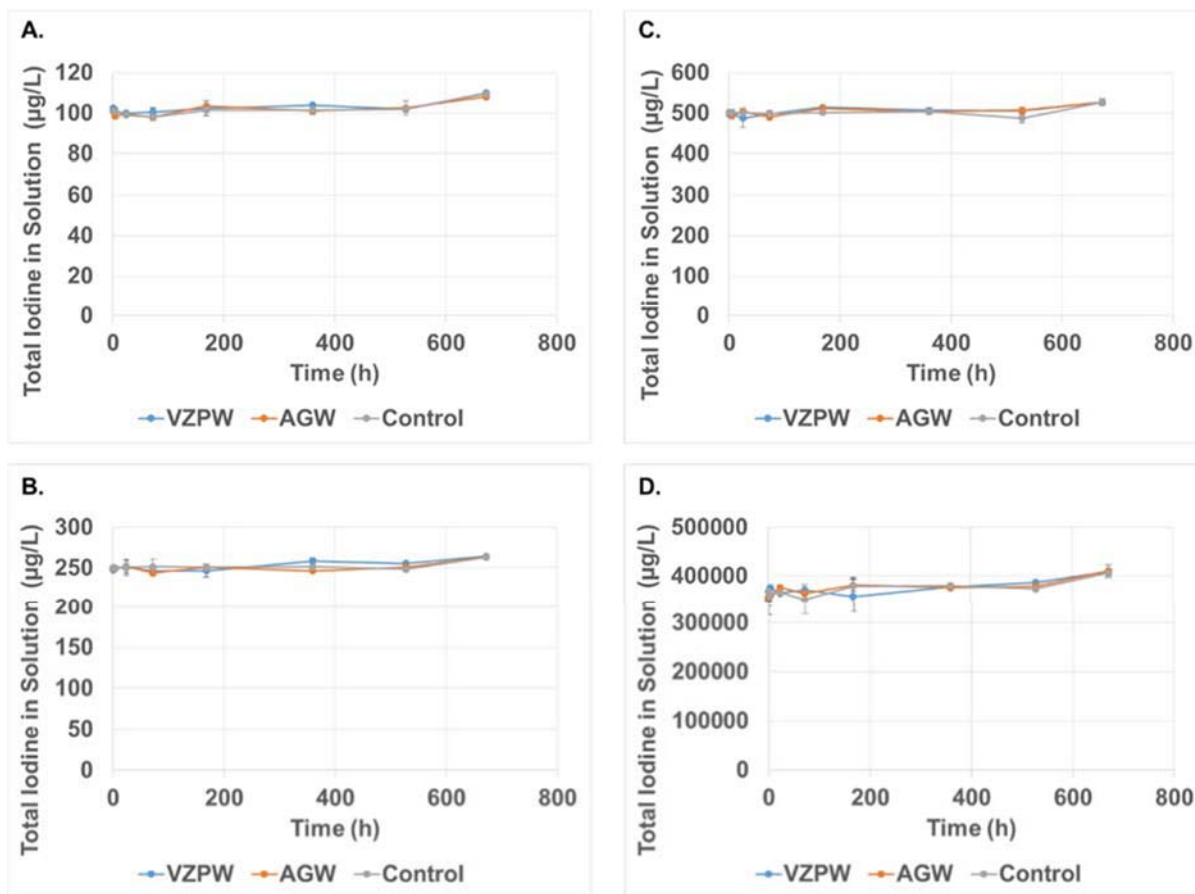
Figure 2.3. Iodine in VZPW and AGW over time. Four concentrations of iodine—100 µg/L (A), 250 µg/L (B), 500 µg/L (C), and 395,784 µg/L (D)—were added to VZPW (blue line) and AGW (orange line) and contained no calcite. Total iodine in solution was measured over a period of 28 days and sampled at 0 h, 4 h, 24 h, 3 d, 7 d, 15 d, 22 d, and 28 d. Gray lines represent iodine concentrations over time in DDI. Samples were performed in duplicate. Error bars represent the standard deviation of replicates for each time point.
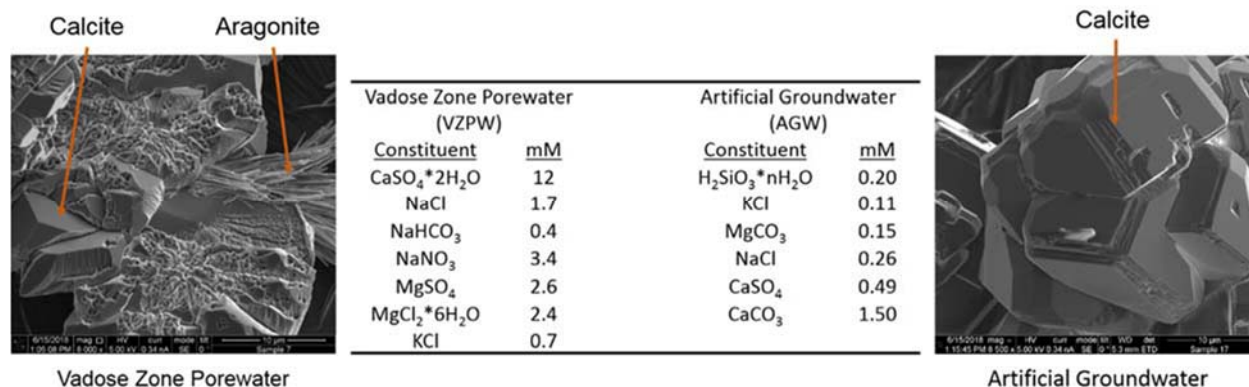
Figure 2.4.   SEM image of calcium carbonate minerals after 28 days for 500 µg/L iodine in VZPW and AGW. Two types of calcium carbonate minerals were formed—aragonite (needle-like crystals) and calcite (cubic crystals)—in VZPW, a solution containing higher concentrations of groundwater constituents compared to AGW. Only calcite crystals formed in AGW.

Table 2.5.   Chemical composition of AGW, VZPW, and DDI solutions with calcite after 28 days.

Analyte (mg/L)	AGW			VZPW			DDI		
	100 ppb Spike	500 ppb Spike	396 ppm Spike	100 ppb Spike	500 ppb Spike	396 ppm Spike	100 ppb Spike	500 ppb Spike	396 ppm Spike
Aluminum	BDL	BDL	BDL	6 ± 1	5 ± 1	4 ± 1	BDL	BDL	BDL
Calcium	180 ± 25	205 ± 3	270 ± 25	680 ± 26	681 ± 23	682 ± 48	214 ± 6	206 ± 1	276 ± 4
Magnesium	3 ± 0.1	3 ± 0.1	3 ± 0.1	102 ± 5	99 ± 1	98 ± 3	BDL	BDL	BDL
Potassium	BDL	BDL	BDL	31 ± 2	30 ± 1	30 ± 0.1	BDL	BDL	BDL
Silicon	8 ± 0.2	8 ± 0.3	8 ± 0.2	BDL	BDL	BDL	BDL	BDL	BDL
Sodium	6 ± 0.4	5 ± 0.1	75 ± 0.1	126 ± 6	121 ± 0	191 ± 6	BDL	BDL	71 ± 2
Sulfur	12 ± 0.2	12 ± 0.8	15 ± 0.2	449 ± 19	441 ± 4	455 ± 9	BDL	BDL	BDL
Tin	BDL	BDL	BDL	3 ± 0.2	2 ± 0.3	3 ± 0.1	BDL	BDL	BDL

2.2.3   Iodate Co-precipitation with Nano-Calcite

Nano calcite was synthesized for 4 and 24 h with 100- and 500-µg/L iodate spikes. According to SEM results, calcite formed two types of particles: Type 1 was a single, well-formed calcite crystal and Type 2, which tended to be the rest of the particles, were small nanoparticles around 40 nm in size (Figure 2.5). Results from the Parr reactor experiments showed that after 4 h, ~79% and 76% iodate was removed from the 100- and 500-µg/L treatments, respectively. However, results also indicated that an increase in synthesis time (i.e., 24 h) increased the amount of iodate removed, where 83% and 78% of iodate was removed from the 100- and 500-µg/L treatments, respectively (Figure 2.6).
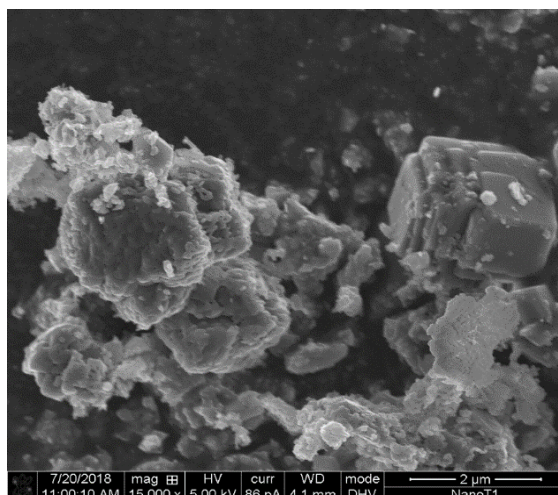
Figure 2.5. Nano calcite with 500-µg/L spike of iodate after 4 h. Two different types of calcite minerals formed after being synthesized for 4 h with 500 µg/L sodium iodate. Type 1 consists of large, well-formed calcite cubes that look like single crystals (i.e., flat particles and not composed of aggregates). Type II consists of small nanosize calcite particles (rest of particles) that are likely aggregates of small nanocrystals (~40 nm).
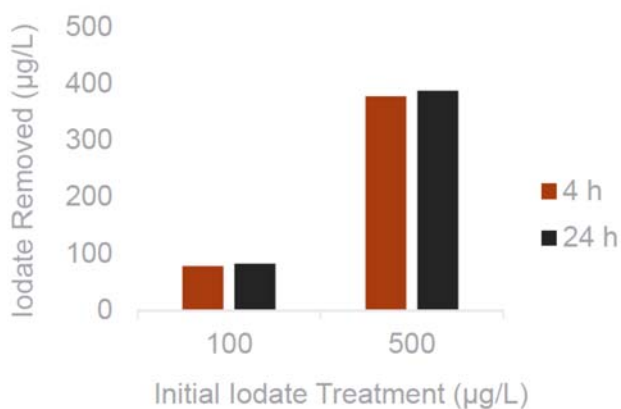
Figure 2.6. Iodate removal in nanocalcite after 4 and 24 h. Red and black bars represent iodate removed in nanocalcite after 4 and 24 h, respectively, for both 100- and 500-µg/L treatments. Experiments were not duplicated and therefore values do not have error bars.

3.0   Incorporation into Apatite/Carbonated Apatite

This laboratory study focused on evaluating (1) the effect of different geochemical conditions on iodate uptake by apatite with an attempt to replicate conditions in a previous study (Campayo et al. 2011) that showed 7% iodate incorporation into solid apatite from a pH 10 to 12 solution, and then with conditions that progressively approached Hanford groundwater conditions, and (2) use of a carbonate-substituted apatite material under conditions informed by results of item 1. Assessment of potential field application will also need to consider the I-127 present in the groundwater in addition to I-129. Experiments were initially conducted in batch tests where apatite-forming chemicals were added in the presence of iodate and iodide. Measurements quantified the loss of iodate or iodide from solution over time (i.e., before and after precipitation), the amount of adsorbed iodine species, and iodine species incorporated (by acid dissolution of the precipitated apatite). The baseline apatite treatment was 4 mM phosphate, 6.67 mM Ca, 1.33 mM iodate [i.e., iodine/phosphorous (I/P) aqueous ratio of 0.33], and pH 11 in oxic AGW. Apatite treatments included variation in (1) pH 11, 9.0, 7.5; (2) iodate concentration from 13 mM (2330 mg/L) to 0.00133 mM (233 µg/L); (3) I/P ratio from 33 to 0.0033; and (4) addition of carbonate (CO_3/PO_4 ratio = 0.4). A limited number of treatments also included iodide and carbonated apatite.

The phosphate sources used in these experiments were orthophosphate and a polyphosphate mixture. Orthophosphate (i.e., Na-phosphate) and $CaCl_2$ at pH 7.5 results in immediate precipitation of amorphous Ca-phosphate, with the slow crystallization over weeks to months (Sumner 2000). A Ca-citrate-phosphate solution, which relies on citrate complexing with Ca to prevent immediate precipitation, was not used because the reducing conditions created reduce iodate. Note that phosphate precipitation does use H^+, so the pH can decrease. At field scale with high sediment/water ratios where minerals buffer pH change, the pH decrease is small (i.e., 7.5 to 7.3), but in a batch system with no sediment and no other aqueous species to buffer the pH, the pH change can be large (i.e., pH 11 initially and pH 6 after precipitation). A polyphosphate solution (i.e., 33% Na-orthophosphate, 33% Na-pyrophosphate, 33% Na- tripolyphosphate) also does not immediately precipitate in the presence of $CaCl_2$. The slow hydrolysis of the polyphosphates into orthophosphate delays Ca-phosphate precipitation for tens of hours (Wellman et al. 2006). A similar decrease in pH from 7.5 to 7.1 was observed at field scale and was simulated (Metha et al. 2017).

It is hypothesized that rapid precipitation of amorphous Ca-phosphate may incorporate a greater amount of iodate, then, during the subsequent crystallization into hydroxyapatite, less iodate may be incorporated. Experiments with rapid Ca-phosphate precipitation used $CaCl_2$ and Na-phosphate at pH 7.5 to 13. Experiments with slow precipitation of apatite used the polyphosphate mixture described above may incorporate less iodate into the more crystalline apatite precipitate. The advantage of this solution over Ca-citrate-PO_4 is that the polyphosphate solution does not change the redox conditions during precipitation, so iodate is not reduced to iodide and can incorporate into the apatite. Experiments were not conducted with a Ca-citrate-phosphate solution as the citrate biodegradation results in a reducing environment sufficient for iodate to be reduced to iodide (based on previous year's preliminary experiments).

3.1   Experimental Methods

3.1.1   Batch Iodate Uptake Experiments with Variable Iodate Concentrations

A series of batch experiments was conducted where iodate concentrations were varied while keeping the pH and iodine/phosphorous ratios constant with Na phosphate, as indicated in Table 3.1. Additional selected experiments were conducted with iodide (not iodate). The batch experiments consisted of 35 mL of the listed solution (made with AGW, Table 2.2) in a 40-mL Teflon centrifuge tube, with 3.0-mL samples taken at multiple time periods ranging from 0.1 to 1000 h. Samples were filtered with a

0.1-micron filter before iodine species analysis. Analysis was conducted by ion chromatography or ICP-MS.

Table 3.1.   Iodate and phosphate concentrations, iodine/phosphorus ratios, and pH used for variable iodate batch experiments.

Iodate (mg/L) (mM)	PO$_4$ (mM)	I/P (M/M)	pH
3400 13.3	40.0	0.333	11.0
340 1.33	4.0	0.333	11.0
34 0.133	0.40	0.333	11.0
0.34 0.0133	0.04	0.333	11.0
x n	3n	0.333	11.0

n = selected experiments may be conducted at additional concentrations.

3.1.2   Variable Initial pH

A series of batch experiments was conducted in which the pH was varied and the iodate concentration and I/P ratios were kept constant with Na phosphate. The parameters used in these experiments are listed in Table 3.2.

Table 3.2.   Iodate and phosphate concentrations, iodine/phosphorus ratios, and pH used for variable pH batch experiments.

Iodate (mg/L) (mM)	PO$_4$ (mM)	I/P (M/M)	pH
340 1.33	4.0	0.333	11.0
340 1.33	4.0	0.333	9.0
340 1.33	4.0	0.333	7.5
340 1.33	4.0	0.333	m

m = selected experiments may be conducted at additional pH values.

3.1.3   Variable Iodine/Phosphate Molar Ratio

A series of batch experiments was conducted in which the I/P ratio was varied and the iodate concentration and pH were held constant with Na phosphate. The parameters used in these experiments are listed in Table 3.3.

Table 3.3.   Iodate and phosphate concentrations, iodine/phosphorus ratios and pH used for variable I/P ratio batch experiments.

Iodate (mg/L) (mM)	PO$_4$ (mM)	I/P (M/M)	pH
340 1.33	0.04	33.3	11.0
340 1.33	0.4	3.33	11.0
340 1.33	4.0	0.333	11.0
34 0.133	4.0	0.033	11.0
3.4 0.0133	4.0	0.0033	11.0
p	4.0	p	11.0

p = selected experiments may be conducted at additional I/P ratios.

3.1.4   Carbonated Apatite and Iodate Uptake

A series of batch experiments was conducted with variable carbonate addition (to precipitate a carbonated apatite, while keeping the iodate concentration, I/P ratio, and pH constant with Na phosphate). The parameters used in these experiments are listed in Table 3.4.

Table 3.4.   Iodate and phosphate concentrations, iodine/phosphorus ratios, and pH used for variable carbonate addition batch experiments.

Iodate (mg/L) (mM)	PO$_4$ (mM)	I/P (M/M)	CO$_3$ (mM)	pH
340 1.33	4.0	0.33	0.0	11.0
340 1.33	4.0	0.33	2.2	11.0
0.34 0.0013	0.004	0.33	0.0	11.0
0.34 0.0013	0.004	0.33	0.0022	11.0
340 1.33	4.0	0.33	q	11.0

q = selected experiments may be conducted at additional CO$_3$ concentrations.

3.1.5   Use of Polyphosphate

A series of batch experiments was conducted using a mixture of polyphosphates. The polyphosphate reagents are an equimolar mixture of orthophosphate (Na$_2$HPO$_4$), pyrophosphate (Na$_4$P$_2$O$_7$), and tripolyphosphate (Na$_4$P$_3$O$_{10}$), which hydrolyzes slowly over time into orthophosphate. Selected batch experiments with the polyphosphate mixture were conducted while varying the iodate and phosphate concentrations, following methods similar to those in Section 3.1.1. Selected batch experiments with the polyphosphate mixture were also conducted while varying the pH following procedures similar to those described in the previous section. Selected batch experiments with the polyphosphate mixture were conducted while varying the I/P ratio, following the methods previously described. Selected batch experiments with the polyphosphate mixture were conducted while varying the addition of carbonate.

3.1.6   Solid Phase-Associated Iodine by Liquid Extraction and Solid Phase Analysis

After liquid sampling from the various batch experiments was completed, additional analyses were conducted on the apatite precipitates to evaluate (1) adsorbed iodate, (2) incorporated iodate, and (3) precipitate phase (to determine if different from non-iodate apatite). After the last liquid samples in the

batch experiments were taken, liquid extractions were conducted on the solids to measure adsorbed and incorporated iodine. If sufficient iodate was incorporated into precipitates selected samples would undergo solid phase analysis by X-ray diffraction (XRD) or other methods. No precipitates contained sufficient iodate mass to be able to evaluate iodate-substituted apatite. The adsorbed iodide and iodate was determined by extraction with a 0.5-mol/L Mg-nitrate solution. The iodide or iodate that was incorporated into apatite was determined by extraction with a weak acid (0.5M HCl). When the weak acid extraction is conducted after the adsorbed extraction, then the remaining iodine mass measured in this extraction is all incorporated.

Long-term stability of iodate-substituted apatite was initially planned in batch experiments at different pH levels and through long-term leaching. None of the 40 iodate/apatite experiments produced sufficient iodate in precipitates, so long-term stability experiments were not conducted.

3.2   Results

A total of 40 batch experiments were conducted in a wide variety of geochemical conditions to evaluate iodate and iodide substitution into apatite (or $Ca-PO_4$) precipitates (Table 3.5).

3.2.1   Initial pH and Iodate Uptake

In phosphate experiments with different initial pH levels, there was some iodate uptake with an initial pH of 11, 12, and 13, and no iodate or iodide uptake with an initial pH of 7.5 or 9.0 (Figure 3.1). In most experiments, there was no iodate uptake (Figure 3.1b). In some experiments, as much as 70% of the iodate was removed from solution at short times, likely into the initial amorphous precipitate, and less iodate uptake at later times when the precipitate crystallized into apatite. The calculated moles of iodate per mole of phosphate precipitated was calculated (Table 3.1) and the fraction of adsorbed and incorporated iodate was measured in some precipitates. There was a fair degree of variability between experiments with the $CaCl_2$ and $Na-PO_4$ solutions, likely caused by slight differences between the amorphous and semi-crystalline precipitates formed. There was no uptake from the polyphosphate solutions (Figure 3.1b). At a much higher phosphate to iodate ratio (Figure 3.1c), there was more fraction iodate uptake. The pH of solutions decreased significantly, typically to pH 6 after precipitation. Adjusting the pH to the initial higher pH after every sample decreased iodate uptake (Figure 3.1d), perhaps because iodate is outcompeted by OH^- in the hydroxyapatite ($Ca_{10}(PO_4)_6(OH)_2$) at higher OH^- concentrations.

3.2.2   Iodate/Phosphate Ratio and Iodate Uptake

In phosphate precipitation experiments varying the molar ratio of iodate to phosphate, results generally show high excess phosphate results in greater iodate uptake (Figure 3.2). Experiments with the greatest iodate uptake from field-relevant iodate concentrations (i.e., < 200 µg/L) (Table 3.1, 67–73% uptake of aqueous iodate, E64, E65, E67, E71) had P/I molar ratios of 4100 to 16,900. This is equivalent to an iodate loading in the apatite of 11 to 30 µg/g (Table 3.1). Experiments with much higher iodate concentration had significantly greater iodate loadings (as high as 10,000 µg/g). However, in none of the 40 experiments conducted was all of the iodate removed from solution (to detection limits of ~1 µg/g), even with a starting concentration of 21 µg/L (E66, Table 3.1). Therefore, it is highly unlikely that the use of apatite at field scale would be effective at decreasing iodate concentrations to < 1 µg/L. Experiments in which the pH was readjusted to the initial alkaline pH resulted in a decrease in iodate uptake (Figure 3.2d) compared to experiments in which the final pH was not adjusted (Figure 3.2c).

3.2.3 Iodate Concentration and Uptake

Experiments conducted with a range of iodate concentrations, maintaining an I/P ratio of 0.33 (Campayo et al. 2011) showed little uptake (Figure 3.3). In most experiments, there was greater uptake at short times (<100 h), but iodate uptake decreased at later times. This may have been caused by initial iodate uptake in the amorphous Ca-phosphate precipitate, but upon subsequent crystallization to apatite, there was less (or none) iodate incorporation. In addition, none of the experiments exhibited significant iodate sorption.

Table 3.5.   Phosphate experiments to evaluate iodate and iodide uptake.

#	Iodate (μg/L)	Iodide (μg/L)	PO$_4$ (mM)	CO$_3$ (mM)	I/P (mol/mol)	Initial pH	% Aq. Uptake	% Incorp.	Time (h)*	Uptake Ratio (mol P/mol I)	IO$_3$ Loading (mg/g)	Uptake Rate (μmol IO$_3$ h^{-1} mol^{-1}apatite)
D32	3.40E5	0	4.0	0	0.33	11.0	20	1.8	350	1.52E+01	8.35	3.88E+01
D33	3.00E4	0	0.4	0	0.33	11.0	4	0.9	350	7.58E+01	1.67	8.21E+00
D34	3400	0	4.0E-02	0	0.33	11.0			350			
D35	340	0	4.0E-03	0	0.33	11.0	25		350	1.21E+01	10.4	2.78E+02
D36	3.40E5	0	4.0	0	0.33	9.0	5.0	1.4	350	6.06E+01	2.09	1.19E+01
D37	3.40E5	0	4.0	0	0.33	7.5	0.0	0.57	350			
D47	3.40E5	0	4.0	0	0.33	7.5	4.0		350	7.58E+01	1.67	8.23E+00
D39	3.40E54	0	4.0	0	3.3E-02	11.0	12.0	6.4	350	2.53E+02	0.50	2.16E+00
D40	3400	0	4.0	0	3.3E-03	11.0		2.1	350			
D41	3400	0	4.0	0	3.3E-04	7.5	5.0	0	350	6.06E+04	2.1E-3	9.72E-01
D44	3.40E5	0	4.0	2.2	0.33	11.0	13	1.4	350	2.33E+01	5.43	3.78E+01
D45	300	0	4.0E-03	2.2E-03	0.33	11.0	0		30			
D46	300	0	4.0E-03	2.2E-03	0.33	7.5	24		100	1.26E+01	10.0	2.50E+02
D42	0	3.82E5	4.0	0	0.33	7.5	0	0	350			
D43	0	980	4.0E-03	0	0.33	7.5	0		350			
D50	1.8E+06	0	40**	0	0.33	11.0	0		1500			
D51	3.02E5	0	4.0**	0	0.33	11.0	0		1500			
D52	3.02E5	0	4.0**	0	0.33	11.0	0		1500			
D53	2.96E5	0	4.0**	0	0.33	9.0	0		1500			
D54	2.78E5	0	4.0**	0	0.33	7.5	0		1500			
D55	2.3E+06	0	40**	0	3.3E-02	11.0	29		1500	1.04E+02	1.21	1.09E-01
D56	3.60E5	0	0.4**	0	3.3	11.0	0		1500			
D57	3.60E5	0	0.04**	0	33.2	11.0	0		1500			
D58	0	2.95E5	4.0**	0	0.33	11.0	35		1500	8.66E+00	14.6	1.69E-02
D59	0	3.41E4	4.0**	0	3.3E-02	11.0	0		1500			

#	Iodate (µg/L)	Iodide (µg/L)	PO_4 (mM)	CO_3 (mM)	I/P (mol/mol)	Initial pH	% Aq. Uptake	% Incorp.	Time (h)*	Uptake Ratio (mol P/mol I)	IO_3 Loading (mg/g)	Uptake Rate ($\mu mol\ IO_3\ h^{-1}\ mol^{-1}$apatite)
E64	180	0	4.0	0	3.6E-04	11.0	67		336	4.15E+03	3.05E-2	1.26E-01
E65	78	0	4.0	0	1.5E-04	11.0	69		336	9.66E+03	1.31E-2	5.43E-02
E66	21	0	4.0	0	3.0E-05	11.0	33		336	1.01E+05	1.25E-3	5.58E-03
E67	204	0	4.0	0	3.6E-04	12.0	67		336	4.15E+03	3.05E-2	1.26E-01
E68	227	0	4.0	0	3.6E-04	13.0	46		336	6.04E+03	2.09E-2	8.63E-02
E69	190	0	40.0	0	9.1E-05	11.0	65		336	1.69E+04	7.48E-3	1.22E-02
E70	38	0	40.0	0	7.5E-06	11.0	15		336	8.89E+05	1.42E-4	4.84E-04
E71	180	0	4.0	0	3.6E-04	11.0	73		336	3.81E+03	3.32E-2	1.36E-01
E72	341	0	4.0	0	3.6E-04	11.0	0		294			
E73	254	0	4.0	0	3.6E-04	11.0	19		294	1.46E+04	8.65E-3	4.17E-02
E74	254	0	4.0	0	3.6E-04	11.0	17		294	1.63E+04	7.74E-3	3.66E-02
E75	508	0	4.0	0	3.6E-04	12.0	9		294	3.09E+04	4.10E-3	3.57E-02
E76	508	0	4.0	0	3.6E-04	13.0	8		294	3.47E+04	3.64E-3	3.23E-02
E77	254	0	16.0	0	9.1E-05	11.0	0		294			
E78	254	0	16.0	0	9.1E-05	11.0	27		294	4.07E+04	3.11E-3	1.49E-02
E79	341	0	4.0	0	3.6E-04	11.0	26		294	1.07E+04	1.18E-2	7.57E-02

* Final exp. time of measured uptake
** Equal molar mixture of ortho-, pyro-, and tripolyphosphate
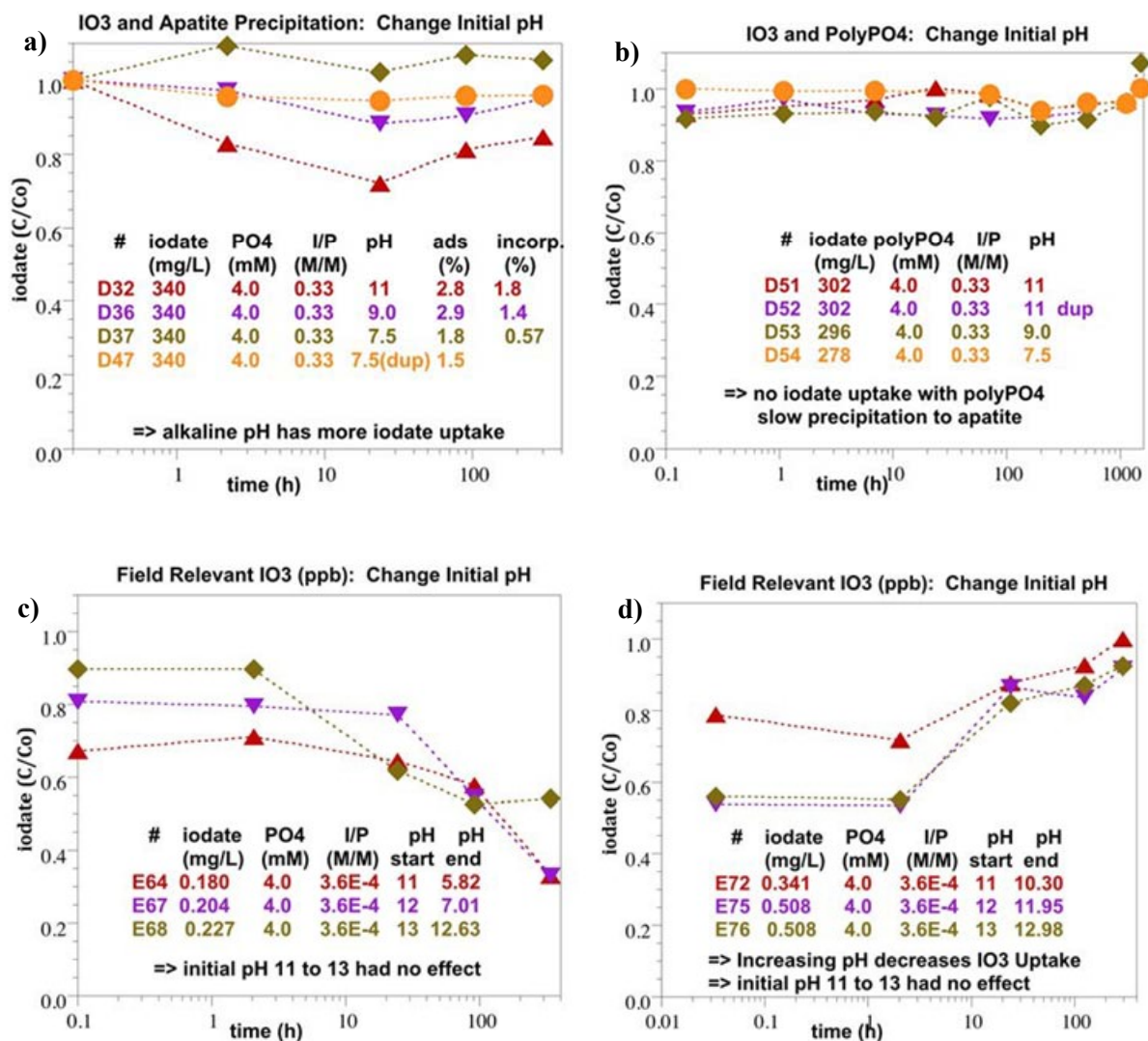
Figure 3.1. Apatite precipitation experiments conducted at different pH with a) CaCl$_2$ and Na-PO$_4$ solution, b) polyphosphate solution, c) CaCl$_2$ and NaPO$_4$ at low iodate concentration, and d) CaCl$_2$ and NaPO$_4$ at low iodate concentration readjusting pH to initial pH.
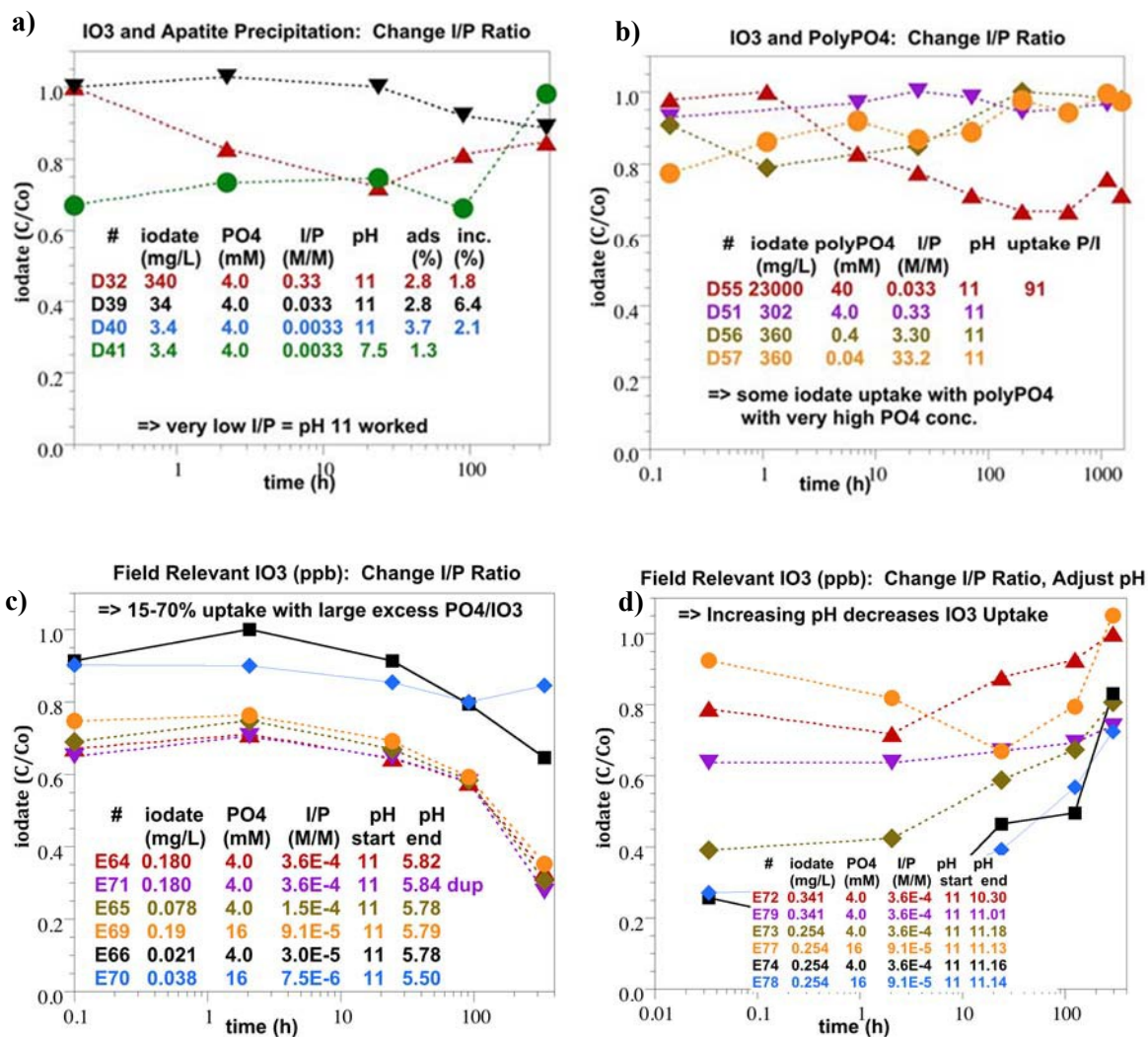
Figure 3.2.   Apatite precipitation experiments conducted at different I/P ratio with a) CaCl$_2$ and NaPO$_4$ solution, b) polyphosphate solution, c) CaCl$_2$ and NaPO$_4$ at low iodate concentration, and d) CaCl$_2$ and NaPO$_4$ at low iodate concentration readjusting pH to initial pH.
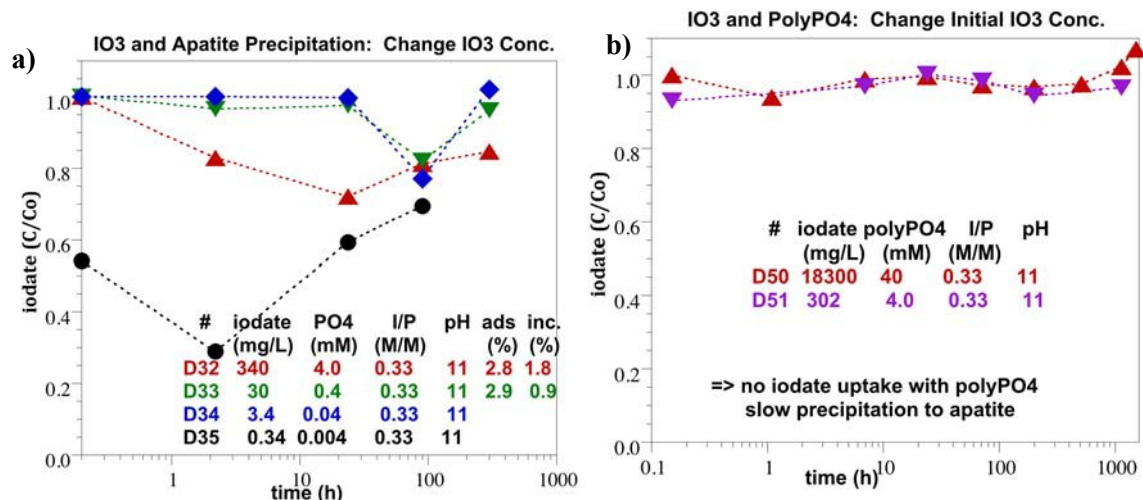
Figure 3.3. Apatite precipitation experiments conducted at different iodate concentration and constant I/P ratio of 0.33 with a) CaCl₂ and Na-PO₄ solution, and b) polyphosphate solution.

3.2.4 Carbonated Apatite and Iodate Uptake

Phosphate precipitation experiments conducted with a high carbonate content in the apatite (i.e., the solution contained 33% carbonate and 67% phosphate) resulted in the same or less iodate uptake (Figure 3.4) at pH 11 and 7.5.
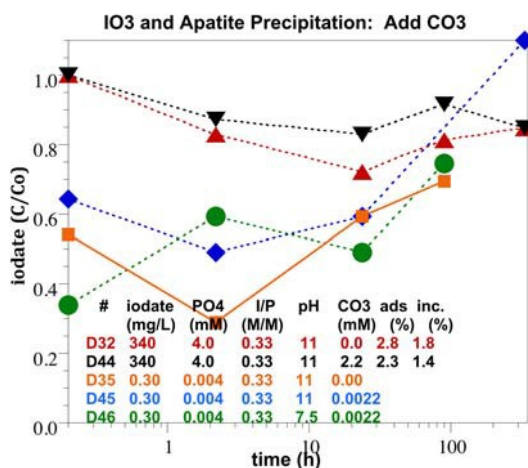
Figure 3.4. Iodate uptake in a solution precipitating carbonate-substituted apatite.

3.2.5   Iodine Uptake

There was no iodide uptake in precipitation experiments conducted with Na-phosphate or polyphosphate solutions (Figure 3.5).
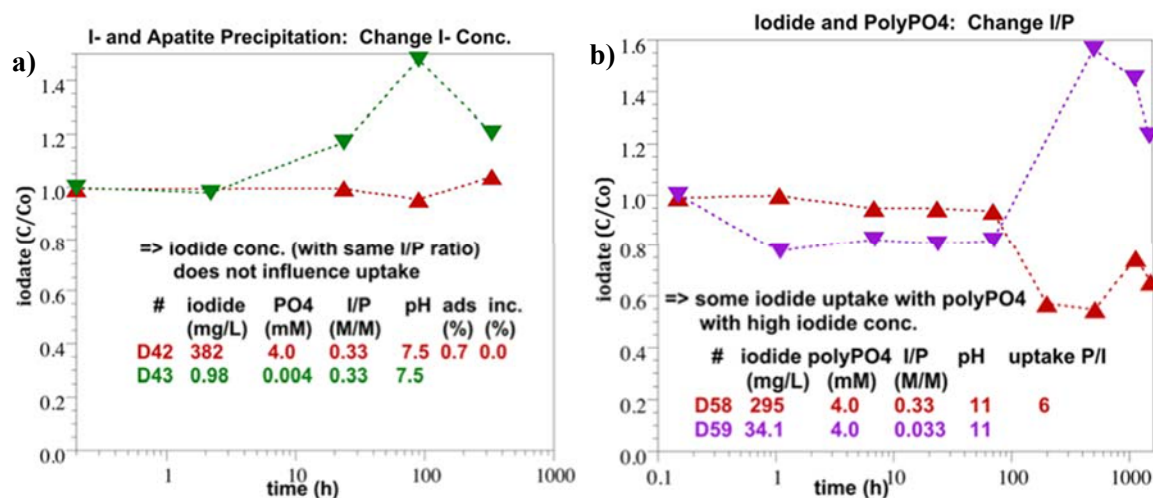
Figure 3.5.   Iodide uptake during Ca-phosphate precipitation from a) orthophosphate solutions, and b) polyphosphate solutions.

3.2.6   Apatite in 1-D Columns and Iodate Uptake

In an earlier study, Ca-citrate-phosphate solution was injected into an iodide/iodate-contaminated sediment column to evaluate the change in iodine concentration that would result if iodate were uptaken in the precipitating apatite. In contrast to batch experiments, these 1-D sediment columns additionally have a high pH buffering capacity, and the Ca-citrate-PO_4 solution will create a reducing environment. A sediment sample sequential extraction showed a total of 0.9 µg/g iodine, with 5.5% aqueous and adsorbed. About 85% of the iodine was present as iodide and 15% as iodate. Addition of just AGW into the sediment column as a control showed removal of 0.035 µg/g iodine or 3.9% of the mass (Figure 3.6, black diamonds). Injection of 40 mM phosphate in a Ca-citrate-phosphate solution did not decrease iodate, and in fact increased the total aqueous iodine to 0.067 µg/g (Figure 3.6a) or 7.4% of the total iodine in the sediment. This was because (1) most of the iodine present in the sediment was iodide, and (2) reducing conditions created by citrate biodegradation reduced any iodate to iodide, which adsorbs to sediment less than iodate. In a second column, the same iodine-contaminated sediment was added, but additionally with 150 µg/L iodide and 150 µg/L iodate (for a total of 0.96 µg/g iodine). Iodine mass was again increased by the addition of the Ca-citrate-phosphate solution (0.075 µg/g or 7.8%, Figure 3.6b). Clearly, Ca-citrate-phosphate addition to iodine-contaminated sediment was not effective for iodate immobilization. For comparison, a pH 9.3 carbonate solution added to the same sediment extracted about the same iodine as water, suggesting iodine mass is not incorporated into carbonates.
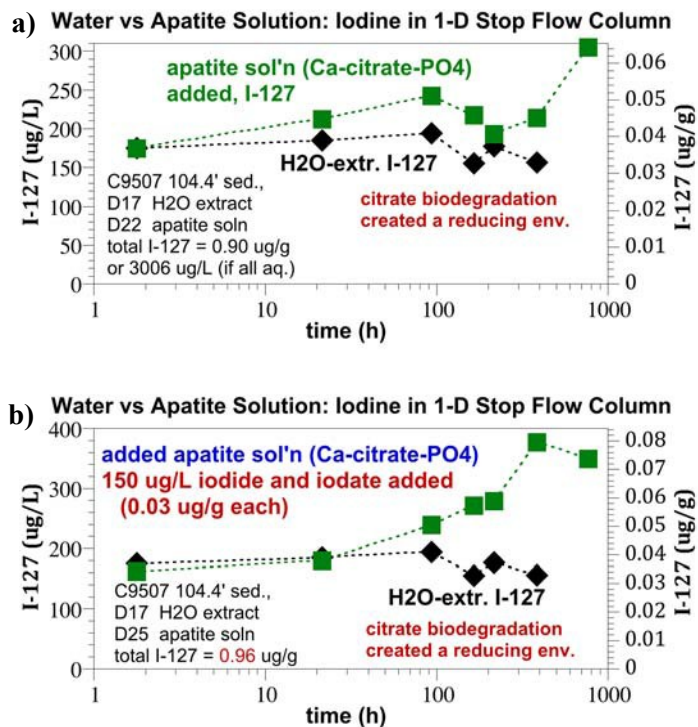
Figure 3.6. Measured total aqueous iodine as a result of phosphate addition to iodine-contaminated sediment with Ca-citrate.

4.0   Enhanced Sorption by Organic Carbon

A series of batch adsorption/desorption experiments was conducted to determine the effectiveness of several organic materials for sequestering iodate and iodide from groundwater. Organic materials that were evaluated in this study were chitin, lignin, and humic acid (HA) sorbed to a representative Hanford sediment. In the case of humic/fulvic acids sorbed to Hanford sediment, both as is and sterilized sediments were evaluated to determine potential impacts of microbial activity. Selected samples were analyzed for iodine speciate to determine if any changes in iodine speciation occurred during the experiments.

4.1   Experimental Methods

The organic materials used were chitin (from shrimp shells, practical grade, powder, Sigma-Aldrich), lignin, alkali (Sigma-Aldrich), and Hanford sediment amended with humic acid sodium salt (technical grade, Sigma-Aldrich). Each batch adsorption/desorption experiment was conducted in a 50-mL polypropylene centrifuge tube at room temperature (~22°C) in duplicate. Equilibration times of 1, 3, 7, and 28 days were used for the adsorption experiments, and 28 days for the desorption experiments. The experiments were performed at an organic material-to-solution ratio of 0.2 g organic material to 40 mL synthetic groundwater. A duplicate set of the humic acid experiments was conducted in which the groundwater was amended with 2% glutaraldehyde to evaluate the potential impact of microbial growth. Separate experiments for each sorbent were conducted at initial iodide and iodate concentrations of approximately 75 mg/L. All experiments were conducted in duplicate and a set of control samples containing the solution but no sorbents was also conducted in duplicate for each equilibration time.

The recipe used to make the AGW was shown previously in Table 2.2. In the case of the HA experiments, approximately 10 g of Hanford sediment from borehole C9567 (depth interval 283.0 to 283.5 feet) was treated with a solution of 0.2 g humic acid sodium salt dissolved in 40 mL of the synthetic groundwater. The solution was allowed to contact the sediment for 24 h on an orbital shaking table. After this initial contact with the humic acid sodium salt solution, the solution was decanted and 40 mL fresh groundwater was equilibrated for 24 h and then decanted (then repeated). After this, 40 mL of groundwater containing approximately 75 mg/L of iodide or iodate was added to start the adsorption phase of the experiment. A separate set of humic acid adsorption/desorption experiments was conducted in which the groundwater was amended with 2% glutaraldahyde to sterilize the sediments. Total organic carbon (TOC) was measured on the humic acid treated sediments after the 1, 3, and 7-day equilibration periods. TOC for the 28-day equilibration period was not measured to allow these experiments to be used to determine desorption K_d values. Both TOC and total inorganic carbon measured on the untreated Hanford sediments was below the detection limit.

4.2   Results

4.2.1   Adsorption K_d Values

The measured adsorption K_d values for iodate and iodide on chitin and lignin are shown in Table 4.1 as a function of contact time. Very little if any sorption of iodate onto either chitin or lignin occurred, with average values and standard deviations of 3.2 ± 4.0 and 4.8 ± 4.8 mL/g, respectively. It appears that slightly greater adsorption (higher K_d values) may have occurred at longer contact times, but this is difficult to discern due to the high relative uncertainty. Similar results were observed for iodide sorption onto lignin, with an average and standard deviation of 3.6 ± 3.5 mL/g. In contrast to these results, significant sorption of iodide onto chitin occurred, with an average and standard deviation of 74.9 ± 4.3 mL/g. Shigeno et al. (1980) reported that adsorption of iodine onto chitosan is caused by charge-

transfer complexes between amino groups of chitosan and iodine molecules. A similar mechanism may apply to chitin. Overall, these results suggest that adsorption of iodate and iodide onto chitin and lignin reaches equilibrium relatively quickly (possibly in less than 1 day). Although, the moderately high sorption of iodide onto chitin is a favorable result, the fact that iodate is the dominant species in Hanford groundwater means that chitin is not likely (under typical Hanford groundwater conditions) to be a useful material for iodine remediation at Hanford. However, it could potentially be an effective sorbent when used in combination with reducing conditions.

Table 4.1. Iodate and iodide K_d (mL/gm) values measured on the chitin and lignin.

Contact Time (days)	Iodate		Iodide	
	Chitin	Lignin	Chitin	Lignin
1	2.8	6.3	80.6	6.4
1	0.3	4.1	76.8	1.2
3	-2.0	-2.1	73.3	4.6
3	1.5	-2.1	81.1	2.5
7	5.8	6.8	70.2	3.6
7	0.3	7.4	70.7	6.6
28	9.4	11.8	74.5	-3.3
28	7.5	6.4	71.9	7.3
Average and Std. Dev.	3.2 ± 4.0	4.8 ± 4.8	74.9 ± 4.3	3.6 ± 3.5

The measured adsorption K_d values for iodate onto a represent Hanford sediment, humic acid treated sediments, and sterilized HA treated sediments as a function of contact time are shown in Table 4.2. In addition, K_d values calculated on a TOC weight basis rather than the weight of the sediments are also provided. Sorption of iodate was quite low for both treated and untreated sediments. The K_d value for humic acid treated sediments ($K_d = 0.58 ± 0.27$ mL/g) was actually less than for the untreated sediments ($K_d = 1.13 ± 0.06$ mL/g). This could be the result of competitive effects of the humic acid anions for sorption sites on the sediment that would have been available for iodate; however, the overall effect is fairly small. The sterilized humic acid treated sediments actually had higher adsorption ($K_d = 1.84 ± 0.50$ mL/gm) than that of both the sediment alone and the humic acid treated sediment. It is hypothesized that sorption of glutaraldehyde to the sediment (a neutrally charged molecule) may be responsible for this slight enhancement of iodate adsorption to the sterilized sediment. A small increase in iodate adsorption with time may have occurred with the H-treated sediments (both sterilized and non-sterilized). This was most noticeable for the sterilized HA-treated sediments.

Table 4.2. Iodate K_d values (mL/g) measured on sediment and humic acid (HA) treated sediments.

Contact Time (days)	Sediment Only	HA Treated Sediment	Sterilized HA Treated Sediment	TOC Weight Basis	Sterilized TOC Weight Basis
1	1.13	0.40	1.12	591	481
1	1.10	0.39	1.37	250	619
3	1.06	0.53	1.74	421	347
3	1.17	0.76	1.72	1030	439
7	1.08	0.16	1.74	201	379
7	1.17	0.60	1.99	303	972
28	1.06	0.96	2.48	-	-
28	1.24	0.83	2.55	-	-
Average and Std. Dev.	1.13 ± 0.06	0.58 ± 0.27	1.84 ± 0.50	466 ± 284	539 ± 212

Iodate K_d values determined on a TOC weight basis were considerably higher than on a sediment weight basis, ranging from 250 to 1030 mL/g. In addition, the K_d values determined on a TOC weight basis were highly variable. The amount of TOC measured in the sediments (Table 4.3) was also highly variable, but does not appear to be correlated with the K_d values determined on a TOC weight basis as one might expect. The TOC values measured on the sediment were small relative to what was added (200 mg), indicating that 11% or less of the HA added actually adsorbed to the sediment.

Table 4.3. TOC content of sediment after HA treatment (mg) measured on sediment and humic acid treated sediments.

Contact Time (days)	Iodate		Iodide	
	HA Treated Sediment	Sterilized HA Treated Sediment	HA Treated Sediment	Sterilized HA Treated Sediment
1	6.73	23.2	7.97	18.6
1	15.6	22.1	9.77	23.1
3	12.7	50.2	22.4	23.8
3	7.39	39.2	18.2	22.1
7	7.85	46.0	18.0	29.7
7	19.8	20.5	4.89	26.7
Average and Std. Dev.	11.7 ± 4.8	33.5 ± 12.1	13.5 ± 6.3	24.0 ± 3.5

The measured adsorption K_d values for iodide on a representative Hanford sediment, humic acid treated sediments, and sterilized humic acid treated sediments as a function of contact time are shown in Table 4.4. In addition to K_d values calculated based on the weight of sediment, K_d values calculated on a TOC weight basis rather than the weight of the sediments are provided in Table 4.4. Sorption of iodine was quite low for both treated and untreated sediments and was significantly less than those for iodate for the sediment only and the sterilized humic acid treated sediments. The K_d values for humic acid treated sediments (K_d = 0.46 ± 0.05 mL/g) were slightly higher than for the untreated sediments (K_d = 0.34 ± 0.05 mL/g). The sterilized humic acid treated sediments had higher adsorption (K_d = 0.54 ± 0.12 mL/g) than that of both the sediment alone and the humic acid treated sediment, but the differences were very small. In addition, sorption of iodide may have increased slightly with time for the sterilized humic acid treated sediments.

Table 4.4. Iodide K_d values (mL/g) measured on sediment and humic acid treated sediments.

Contact Time (days)	Sediment Only	HA Treated Sediment	Sterilized HA Treated Sediment	TOC Weight Basis	Sterilized TOC Weight Basis
1	0.35	0.51	0.38	648	206
1	0.30	0.53	0.47	548	205
3	0.30	0.41	0.47	181	198
3	0.32	0.38	0.39	209	177
7	0.34	0.47	0.60	259	200
7	0.37	0.43	0.65	872	246
28	0.33	0.46	0.66	-	-
28	0.44	0.50	0.68	-	-
Average and Std. Dev.	0.34 ± 0.05	0.46 ± 0.05	0.54 ± 0.12	453 ± 256	205 ± 20.5

As with iodate, iodide K_d values determined on a TOC weight basis were considerably higher than those determined on a sediment weight basis, ranging from 181 to 872 mL/g. In addition, the K_d values determined on a TOC weight basis were highly variable. The amount of TOC measured in the sediments (Table 4.3) was also highly variable, but does not appear to be correlated with the K_d values determined on a TOC weight basis as one might expect.

4.2.2   Desorption K_d Values

For the case of iodide desorption from chitin (28 days), approximately 52% of the adsorbed iodide desorbed. This resulted in an average desorption K_d value of 190 ± 3 mL/g. Iodate desorption from chitin, as well as both iodide and iodate desorption values, is not reported because their relative high variability renders it useless. The high variability is due to the fact that very little iodine was sorbed and the K_d values are calculated from the difference between small numbers (amount of iodine sorbed and the amount desorbed) with relatively high uncertainty. The duplicate 28-day desorption K_d values measured on the untreated sediment, HA treated sediments, and sterilized HA treated sediments are shown in Table 4.5. The desorption K_d values on the untreated sediments for both iodate and iodide were similar to those determined for the adsorption K_d values determined at 28 days (Table 4.2 and Table 4.3), indicating that sorption of iodate and iodide is reversible for untreated sediments. The desorption K_d values for the HA treated sediments for both iodate and iodide were significantly higher than those determined for adsorption (Table 4.2 and Table 4.3), indicating that sorption of iodate and iodide onto HA treated sediments is not completely reversible at 28 days. For the sterilized HA treated sediments, the desorption K_d values for iodate are only slightly higher than those determined for adsorption (Table 4.2), indicating that sorption of iodate onto sterilized HA treated sediments is close to reversible at 28 days. The desorption K_d values for iodide sterilized HA treated sediments are only significantly higher than those determined for adsorption (Table 4.3), indicating that sorption of iodide onto sterilized HA treated sediments is not completely reversible at 28 days.

Table 4.5. Desorption K_d values (mL/g) measured on sediment and humic acid (HA) treated sediments (28-day desorption period).

Sediment Only	HA Treated Sediment	Sterilized HA Treated Sediment	Sediment Only	HA Treated Sediment	Sterilized HA Treated Sediment
	Iodate			Iodide	
1.08	3.68	2.80	0.39	2.66	2.77
1.48	2.63	3.52	1.30	2.56	3.32

4.2.3   Iodine Speciation after the Adsorption Experiments

Total iodine and iodine speciation results for the various adsorption experiments at the 28-day contact time are shown in Table 4.6. In general, the final speciation of iodine is consistent with the iodine species that was added at the start of the experiments. A notable exception is for the lignin adsorption experiments in which iodine was added as iodate. For these experiments, it appears that the added iodate was completely reduced to iodide by the lignin during the course of the experiment. The reason for this has not been determined.

Table 4.6. Total measured iodine and speciation results in adsorption experiments after 28 days contact.

| Experiment | Total Measured Iodine (μg/L) | | Iodate (μg/L, as I) | Iodide (μg/L) |
	Added as Iodate	Added as Iodide		
Chitin-1	70.3	-	73.2	ND
Chitin-2	70.9	-	72.4	ND
Lignin-1	69.4	-	ND	68.7
Lignin-2	71.3	-	ND	74.6
Blank	73.5	-	77.5	ND
Blank	73.9	-	80.4	ND
Chitin-1	-	54.1	ND	46.8
Chitin-2	-	55.0	ND	52.9
Lignin-1	-	75.6	ND	70.9
Lignin-2	-	71.7	ND	57.8
Blank	-	74.3	ND	61.1
Blank	-	74.5	ND	85.4
HA-1	59.2	-	51.9	ND
HA-2	60.8	-	58.5	ND
HA-S-1	55.1	-	47.3	ND
HA-S-2	54.6	-	48.3	ND
Sediment-1	58.0	-	53.3	ND
Sediment-2	56.0	-	44.2	ND
HA-1	-	66.6	ND	59.9
HA-2	-	66.0	ND	57.1
HA-S-1	-	65.5	ND	56.3
HA-S-2	-	65.2	ND	53.5
Sediment-1	-	68.6	ND	59.6
Sediment-2	-	66.8	ND	53.9

ND = not detected

5.0 Co-precipitation with Iron Oxides

Laboratory studies of batch adsorption/desorption of iodate, column reactive barrier adsorption/desorption of iodate and co-precipitation of iodate and iodide with 2-line-ferrihydrite (HFO), and in situ formation of HFO in column experiments were conducted to evaluate the potential of these approaches for in situ remediation of iodine.

5.1 Experimental Methods

5.1.1 Iron Oxide Preparation

Batch sorption/desorption of iodate (IO_3^-) was conducted on iron oxides at neutral pH prepared in DDI, artificial Hanford groundwater (AGW), and Hanford sediment with AGW (SAGW). HFO in DDI was synthesized by adding ferric nitrate [8.0089 g of $Fe(NO_3)_3 \cdot 9H_2O$] to 100 mL DDI in a polyethylene bottle at room temperature, followed by addition of approximately 59 mL of 1 M NaOH dropwise while stirring until a pH of approximately 7 to 7.5 was achieved. The precipitated HFO was washed five times using approximately 100 mL DDI followed by centrifugation. The final HFO slurry was filtered using a 0.45-µm vacuum filter and air-dried at room temperature. The air-dried bulk solid HFO was ground to powder using a mortar and pestle.

Goethite in DDI was synthesized by adding ferric nitrate [8.0089 g of $Fe(NO_3)_3 \cdot 9H_2O$] to 100 mL DDI water in a polyethylene bottle at room temperature, followed by addition of approximately 1 M NaOH dropwise while stirring until a pH of approximately 12 was achieved. The slurry was stirred for 30 min, followed by heating at 70°C for 60 h, which allowed the initial HFO precipitate to age to goethite. The same washing, filtering, and drying procedures used for HFO were applied to the goethite precipitates.

Methods to prepare HFO and goethite in AGW were the same as those used to prepare the materials in DDI. The recipe used to make the AGW was the same as that listed in Table 2.2. Preparation of HFO with AGW involving sediment was done using two methods. In the first method, ferric nitrate [16 g of $Fe(NO_3)_3 \cdot 9H_2O$] was dissolved into 200 mL AGW in a polyethylene bottle, followed by addition of 7 g of sediments [Hanford fine sand (HF)]. Then, approximately 118 mL of 1 M NaOH was added dropwise while stirring the slurry until a pH of 7 to 7.5 was achieved. Approximately 4 g of HFO was produced, which was precipitated in the sediment matrix.

In the second method, instead of 1M NaOH, calcite-dominated rock collected from the Hanford Cold Creek Unit was pulverized and added to neutralize the solution pH. In this case, ferric nitrate [4 g of $Fe(NO_3)_3 \cdot 9H_2O$] was dissolved into 50 mL AGW in a polyethylene bottle, followed by addition of 2 g of the rock powder. The solution was gently mixed on an orbital shaker for 20 days while the slurry pH was monitored until the pH reached approximately 7 to 8.

Preparation of goethite in AGW with sediment was performed as follows. Ferric nitrate [16 g of $Fe(NO_3)_3 \cdot 9H_2O$] was dissolved into 200 mL AGW in a polyethylene bottle, followed by addition of 7 g of sediment (HF). The pH of the slurry was increased to ~pH 12 by adding 1 M NaOH dropwise. The slurry was then stirred for 30 min, followed by heating at 70°C for 60 h.

In this work, the above laboratory-synthesized HFO and goethite were named as DDI-HFO, DDI-goethite, AGW-HFO, AGW-goethite, SAGW-HFO, and SAGW-goethite, corresponding to the solution matrix of DDI, AGW, and AGW with sediments, respectively. Figure 5.1 shows the iron oxides prepared in polyethylene vessels. The HFO precipitated through pH buffering by calcite dissolution was named as

calcite-HFO. In addition, in the AGW and SAGW systems, the 1M NaOH solution used was prepared by dissolving 10M NaOH (initially prepared in DDI) into AGW solutions to minimize any ionic strength effects in AGW due to large volumes of NaOH addition.

Each of the iron oxide minerals was characterized using XRD, SEM, and N_2-BET, for mineralogy, particle morphology, and size, as well as specific surface area (SSA).

Figure 5.1. Iron oxides [HFO (*left*) and goethite (*middle*)] preparation in polyethylene vessels; the conversion of AGW-HFO to AGW-goethite (*right*) was visible by color changing, where no obvious color changed in the SAGW systems, indicating the conversion of HFO to goethite was strongly retarded when sediment was included.

5.1.2   Iodate Sorption/Desorption on Iron Oxides

Batch sorption/desorption experiments were conducted using iodate concentrations of 10, 50, and 200 ppb with solid to solution ratios of 2 g/L (for HFO) or 10 g/L (for goethite) in 50-mL centrifuge tubes. These experiments were run in triplicate. In addition to the sorption test samples, duplicate controls consisting of 25 mL of the iodate-spiked solutions with no sorbent were also run. After assembly, the samples were gently mixed on a shaker table for 7 and 30 days. After the 7- or 30-day contact period, the pH of the samples was measured and then the tubes were centrifuged at 3500 rpm for 30 min. Supernatant was then collected and filtered (0.20 μm) for total iodine analysis by ICP-MS. Selected samples were also analyzed for iodine speciation.

After the adsorption phase of the experiments was complete, the quantity of residual solution in the centrifuge tube was determined and fresh iodate-free AGW solution was added and recorded. After the respective 7- or 30-day contact periods, the pH of the samples were measured and then the tubes were centrifuged at 3500 rpm for 30 min. Supernatant was then collected and filtered (0.20 μm) for total iodine analysis by ICP-MS. Selected samples were analyzed for iodine speciation (ICP-MS) and for iron concentrations [inductively coupled plasma – optical emission spectroscopy (ICP-OES)]. The sorption K_d was calculated based on the iodine mass balance in the batch reactor.

In order to investigate the sorption of iodine on iron oxides using microscopy techniques, two extra sets of sorption experiments with higher iodate concentrations [1.0×10^{-2} and 5.76×10^{-4} M (=100 ppm)] in the AGW/DDI solution matrix were conducted. The sorption contact time was 7 days, and sorption was confirmed by the decrease in solution iodine concentrations (data not shown). At the end of the experiments, the solids were air-dried and analyzed by X-ray photoelectron spectroscopy (XPS).

5.1.3   Iodate Column (Reactive Barrier) Sorption/Desorption Experiments

Column iodate adsorption/desorption experiments were conducted with HFO and goethite synthesized with AGW (AGW-HFO and AGW-goethite). The columns were packed with silica sand (0.21 to 0.30 mm) mixed with ~1% to 6% iron oxides in the center of the column with pure silica sand (~1 cm

thickness) at both ends of the columns. Filters were also emplaced at each end of the columns (5 µm pore sized PEEK frit and 15 to 45 µm pore-sized poly-filter at the inlet and outlet of the column, respectively). A control column with only silica sand was run in parallel. The columns were composed of PEEK with inside diameters of 0.76 cm and lengths of 10 cm. Prior to running the sorption/desorption experiments, the columns were conditioned by pumping AGW through the columns at a constant flow rate with a residence time of approximately 1 to 2 h to remove any fine particles for column stabilization. Figure 5.2 is a schematic of the column packing structure.
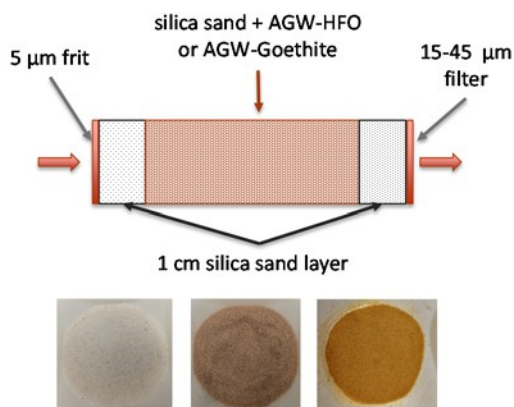
Figure 5.2. Sorption/desorption reactive barrier column packing with an 8-cm-long layer of silica sand mixture either containing 1.0% AGW-HFO or ~ 5.5% AGW-Goethite. The three images (*left* to *right*) are of the materials of the control silica sand, silica sand + AGW-HFO, and silica sand + AGW-Goethite, respectively.

The adsorption phase of the experiments was conducted by injecting iodate-spiked AGW solution (50 ppb) into the bottom of the column (positioned vertically) at a constant flow rate with an approximate residence time of 1.6 h. Samples were collected at the outlet of the column in sufficient number and frequency to measure the changes in iodate concentrations until breakthrough. After breakthrough, desorption was initiated by injecting iodate-free AGW at the same constant flow rate as applied during the sorption phase of the experiment.

The effluent samples were collected automatically using a programmable fraction collector. The sampling intervals (10 min to 2 h) were pre-determined based on the K_d results in the batch adsorption experiments. Two stop-flow events were performed during both the sorption and desorption phase of the experiments. The duration of the stop-flow events was 48 h. Bromide tracer tests were conducted after the sorption/desorption column tests. Selected effluent samples were analyzed for iodate and iodine speciation.

5.1.4   Iodate and Iodide Co-precipitation with HFO

Co-precipitation of iodate/iodide with HFO in DDI, AGW, and with sediment (SAGW) systems was performed using methods similar to those described in Section 5.1.1 for HFO synthesis. However, in this case, the DDI and AGW solutions were first spiked with iodate or iodide at three concentrations (5, 50, and 200 ppb). The co-precipitation experiments were conducted in duplicate in 125-mL polyethylene bottles. Within an hour of precipitation of the iron oxides, the reaction vials were centrifuged at 3500 rpm for 25 min. The solution supernatant was filtered through a 0.20-µm filter for iodate or iodide analysis using ICP-MS. The final pH of the solution slurry was measured, and then the solid precipitates were washed three to five times with approximately 100 mL DDI water, air-dried, and ground for weight measurements and for solid characterization analysis.

5.1.5   Long-Term Sorption of Iodate/iodide on Iron Oxides

This work is an extension of sorption experiments initiated in FY17 (Strickland et al. 2017a), where batch sorption experiments for iodate and iodide on HFO, goethite, magnetite, and hematite were conducted in duplicate in 50-mL centrifuge tubes at room temperature under neutral pH ($\sim$ pH 7.4) conditions. The batch experiments were carried out with a solid to solution ratio of 2.0 g/L for HFO and 10.0 g/L for magnetite, hematite, and goethite. A 48-h contact time between the iron oxide samples with a Hanford synthetic ground water (similar to AGW) was applied to reach sorption equilibrium based on the kinetic study results. At the end of the reaction time (48 h), the batch reactors were centrifuged at 3500 rpm for 20 min to separate the sorbent particles from the supernatant. About 3 mL of supernatant solution was sampled from each reactor using a pipette, followed by filtration through a 0.2-µm filter. The remaining supernatant ($\sim$ 22 mL) and the iron oxides in the tubes were re-mixed with a vortex mixer and the reaction was allowed to continue for up to 200 days. The weight of the reactor tube was recorded for determining the remaining solution volume and the remaining iodate mass in the reactor after the 48-h sampling event. The reactors were shaken by hand once per month during the entire test period. On day 200, the batch reactors were centrifuged at 3500 rpm for 20 min and about 3 mL of supernatant solution was collected and filtered (0.2 µm) for iodate concentration measurement by ICP-MS and the final solution slurry pH was measured. The solids from certain selected reactor tubes were collected and air-dried for XRD analysis to characterize any potential iron oxide mineral transformation during the long-term reaction period.

5.1.6 In situ Precipitation of HFO for Iodate Remediation

Whereas traditional P&T approaches can be costly and produce high-concentration wastes ex situ, in situ remediation approaches can be advantageous because they can limit site disruption, lower costs and secondary waste generation, reduce worker exposure, and treat at depth or under obstructed sites (DOE 1994). In situ technologies have the potential to provide treatment with minimal long-term operational requirements, and to stabilize contaminants that may slowly diffuse out of low-permeability zones after active P&T applications.

This section identifies a practical approach for in situ HFO precipitation for iodine immobilization under field-scale conditions at the Hanford Site. Since carbonate and clay minerals are widely present in sediments, self-pH buffering of an injected acidic ferric solution will occur due to mineral dissolution, leading to HFO precipitation under neutral pH conditions. This hypothesis is supported by the observed pH neutralization and zonation that occurred at Hanford resulting from historical acidic and alkaline subsurface waste discharges (Wan et al. 2004; Szecsody et al. 2013; Wang et al. 2017). HFO precipitation was tested here under different flow rates, and 1-D, 1- to 3-meter-long column experiments were carried out using Hanford sediments and AGW that mimicked the geochemical signature of Hanford groundwater. Iodate was injected into the HFO-laden sediment column (to serve as a reactive barrier) or was injected together with the HFO-forming solution into the iodine-contaminated sediment column to test the iodine-HFO co-precipitation/adsorption effects.

5.1.6.1 Materials and Methods

Hanford Fine Sand (HF). Hanford Fine Sand (HF), collected at near-surface burial ground excavation at 218-E-12B location and composed of the silty sand facies from the Hanford formation in the Hanford 200 Area, was used to represent the sediments at the Hanford sites. The HF, which contains 0.23 wt% gravel, 72.61wt% sand, and 27.16 wt% silt and clay (Serne et al. 2008), was sieved to remove the size fraction greater than 2 mm prior to experiments. The HF is typical of Hanford formation sediments and contains quartz, K/Na-feldspar and smectite, along with illite and chlorite, as the dominant mineral phases with a low calcium carbonate content (1.75 wt%), as identified by mineralogical analysis in Serne et al. (2008).

Preparation of acidic ferric solution and iodate solution. Ferric nitrate [Fe(NO$_3$)$_3$ · 9 H$_2$O] (≥98%; Sigma-Aldrich) was used as the Fe(III) source for ferric solution preparation. Briefly, 80.089 g of Fe(NO$_3$)$_3$ · 9 H$_2$O was dissolved into 1 L of AGW (~pH 7.9) at room temperature, resulting in a brown-colored acidic 0.1 M Fe(III) solution with a pH value of ~1.5. Sodium iodate (>99%; ACROS Organics Corp.) was dissolved into AGW to make an IO$_3^-$ solution for the adsorption/co-precipitation experiments. The concentration of the prepared IO$_3^-$ solution was of 100 ppb based on certain iodine plume conditions in the field (Truex et al. 2015). In addition, one IO$_3^-$ solution (100 ppb) was prepared in the 0.1 M Fe(III) solution matrix to test the IO$_3^-$ co-precipitation with the produced Fe oxides.

5.1.6.2   In Situ HFO Precipitation by Ferric Iron Injection into 1- and 3-Meter Columns

HFO in situ precipitation experiments were conducted in four 1-D columns packed with HF sediments, including two glass columns of 1 cm ID by 100 cm length and two PVC columns of 1.5 cm ID by 300 cm length. The glass columns enable visible observation of the in situ HFO precipitation as well as its distribution within the columns. The two glass columns were also used for IO$_3^-$ immobilization experiments in a reasonable laboratory experimental time scale. Replicating injecting amendment at a field-scale length was accomplished by evaluating the spatial distribution of HFO precipitation in the two longer PVC columns. Briefly, 823-861 g and 118-119 g of HF were dry-packed into the 3-meter PVC (named as 3mP) and 1-meter glass (named as 1mG) columns, leading to porosities of 0.41–0.42 and 0.30–0.32, respectively. A narrow range of solid to solution ratio of 3.8–5.1 was achieved in all the tested columns. The four packed columns were saturated through pumping AGW into the columns, where the column porosity was determined based on the pumped AGW mass balance. After column saturation, to investigate in situ HFO precipitation, the prepared 0.1 M acidic ferric solution was pumped into the columns at a controlled flow rate using a syringe pump for the in situ HFO precipitation. For the two 3mP columns, a constant average linear flow velocity of 2.0 or 21.4 m/day, corresponding to solution residence times of 35.5 and 3.4 h, respectively, was applied to mimic a single well injection time scale to a 10 to 15 m radius. For the two 1mG columns, a single constant average linear flow velocity of 3.1–3.3 m/day, leading to a solution residence time of 7.3–7.6 h, was used for the ferric solution delivery. The effluent pH was monitored during the entire reaction process by an Accumet pH meter. The injection ceased when the effluent solution color turned into brown, where the effluent solution pH of ~ 4.0 was normally observed. After the 0.1 M ferric solution injection, each column (except 1mG-2 column) was flushed with AGW under the same flow velocity as used for ferric solution injection, in order to test the stability of the in situ precipitated HFO in the column sediments through a Fe mass balance calculation. Effluent samples were collected and analyzed using ICP-OES for Fe, Ca, Si, Sr, and Al concentrations. All the column experimental setup and flow conditions are listed in Table 5.1.

5.1.6.3   Injection of Iodate into HFO-Modified Sediment Columns to Evaluate Immobilization

The IO$_3^-$ transport and immobilization experiments were conducted with the two glass columns described above. The performance of the in situ precipitated HFO for iodate immobilization in this study was evaluated under two scenarios: (1) injecting IO$_3^-$ solution into the HFO-laden sediments (column 1mG-1 in Table 5.1) where the newly-precipitated HFO served as a permeable reactive barrier (PRB); and (2) injecting IO$_3^-$-spiked acidic ferric solution into IO$_3^-$-contaminated sediments (column 1mG-2 in Table 5.1) to mimic a remediation scenario within iodine plumes (source term) in the subsurface. To test the PRB scenario, 100 ppb IO$_3^-$ solution in AGW was injected at a constant average linear velocity of 8.3 m/day into the 1mG-1 column after the acidic ferric solution injection (for HFO precipitation) and the followed 45.5-pv AGW flushing. This extended AGW flushing before the IO$_3^-$ injection enabled the elimination of any potential HFO particle-facilitated IO$_3^-$ transport, if there were any. For the source term scenario, the packed HF sediments in 1mG-2 column were first contaminated through 100 ppb IO$_3^-$ solution injection, followed by the injection of a 100-ppb IO$_3^-$-spiked 0.1 M Fe(III) solution for the HFO-

IO_3^- co-precipitation. After the IO_3^- uptake procedures, leaching was immediately performed using neutral AGW to evaluate the long-term retention capacity of the adsorbed and co-precipitated iodine in the HFO-amended sediments. The leaching used the same flow velocity as that for the IO_3^- uptake process, and extended to more than 100 PVs. The iodine concentrations in the effluent samples were analyzed using ICP-MS. All the iodine column experimental conditions applied in this study are also listed in Table 5.1.

Solid characterization. After the entire column experimental procedures, the total Fe contents (mg/g) in the HFO-amended sediments collected at five column locations for each column was determined using 8 M HNO_3 acid extraction (Demirkanli et al. 2018). The column locations are presented in Table 5.2. Before acid extraction, the samples were air-dried. The in situ precipitated Fe content was calculated by subtracting the extracted Fe content in the untreated HF sediments from that of each HFO-amended sample. Briefly, triplicate extraction vials containing 2 g of air-dried solid sample plus 6 mL 8 M HNO_3 solution was heated for 3 h at 95°C in a heating box. After cooling to room temperature, the supernatant was passed through a 0.45-µm filter and analyzed for Fe concentrations using ICP-OES. The solution volume was determined by the reactor mass balance combined with the solution density measurements to calculate the final extracted Fe mass. In addition to extraction using 8 M HNO_3, extractions with 0.5 M HCl or 1 M $CaCl_2$ in an anaerobic chamber were also conducted for the (exchangeable) Fe(II) contents (Demirkanli et al. 2018). The Fe(II) concentration in the extracted solution was determined using Hach 8147 method by reaction with ferrozine. XRD was used to identify the precipitated Fe oxide mineral phases as well as any potential mineral changes in the sediments before and after the treatment with the acidic ferric solution. Select sediment samples were also characterized using SEM-EDS to identify crystal geomorphology and to look for relatively high-Fe content domains in the treated sediments, which may reflect the HFO precipitation. In addition to Fe, iodine concentration in the treated sediments was extracted by the KOH-KNO_3 fusion method (Geiszler 2016) for mass balance calculation, to identify the final immobilized iodine percentage after the experiments. The immobilized IO_3^- percentage was calculated as: (IO_3^- extracted from the reacted sediments – IO_3^- extracted from the untreated sediments) / the total injected IO_3^- * 100. The detailed calculation terms are listed in Table 5.3.

5.2 Results

5.2.1 Solid Characterization on Synthesized Iron Oxides

The detailed XRD analysis results and SEM images of the synthesized iron oxides under different conditions are shown in Figure 5.3 and Figure 5.4. For ferrihydrite, its powder XRD pattern contains only two or six scattering bands in its most disordered state. The observed two broad XRD patterns of the both synthesized HFO in DDI water (DDI-HFO) and in the AGW system (AGW-HFO) in the present study were typical for 2-line ferrihydrite, which agrees with its bulk material morphology in the SEM image (Figure 5.4). The synthesized DDI-goethite and AGW-goethite showed well-crystalized, needle-shaped micrometer-sized minerals that matched well with their JADE XRD reference peak. For the SAGW-HFO, synthesized using the first method with NaOH addition, where 7 g of HF was added in the solution system, the dominant minerals observed in the collected bulk solids were HF minerals quartz, feldspar, and mica, among others. However, the XRD analysis on the dark brown particles, which were handpicked out of the collected bulk solids, clearly showed the presence of HFO. This implies that the HFO generated in the SAGW system was likely physically mixed with the sediment minerals. A similar mineral mixing pattern was observed in the SAGW-goethite synthesis system, but without goethite present. Instead of the expected SAGW-goethite, materials similar to SAGW-HFO were observed (Figure 5.3), even after heat-treatment (70°C) for 60 h. This is because silicate retards the conversion of ferrihydrite to goethite (Schwertmann and Cornell 2000). In the SAGW-goethite synthesis system, Si dissolution from the Hanford sediment minerals, such as quartz and feldspar, can be expected in the strongly alkaline media (pH ~12).

Table 5.1.   Column experimental setup for HFO in-situ precipitation, IO_3^- sorption, and desorption.

Column	ID * Length (cm)	Porosity (-)	Solid: Solution Ratio (g: mL)	Fe(III) Solution Resident Time (h)	Fe(III) Injection Velocity (m/day)	Fe(III) Injection Volume (PV)	AGW Flushing Volume After Fe(III) Injection (PV)	IO_3 Injection Velocity (m/day)	Fe+IO_3- Injection Velocity (m/day)	IO_3 Desorption Velocity (m/day)	Natural/ Anthropogenic Iodine AGW- Leaching Velocity (m/day)
1mG-1	1*100	0.30	5.1	7.3	3.3	8.77	45.5	8.3	NA	8.3	NA
1mG-2	1*100	0.32	4.7	7.6	NA	7.74	NA	7.7	3.1	3.1	3.1
3mP-1	1.5*300	0.42	3.8	35.5	2.0	6.54	4.1	NA	NA	NA	NA
3mP-2	1.5*300	0.41	4.0	3.4	21.4	6.49	3.65	NA	NA	NA	NA

Table 5.2.   Sample collection locations in columns (cm from the column inlet) for Fe and IO_3^- extraction after experiments.

Position	Sample 1	Sample 2	Sample 3	Sample 4	Sample 5
3mP columns	0–10	72.5–82.5	145–155	222.5–232.5	290–300
1mG columns	0–16	28–44	44–56	56–72	86–100

Table 5.3.   Iodine mass recovery calculation.

Column	KOH-KNO3- Extracted IO_3^- Mass from the Reacted Sediments (μg)	KOH-KNO3- Extracted IO_3^- Mass from the Untreated Sediments (μg)	Total Injected IO_3^- (μg)	Effluent IO_3^- Mass During the Initial AGW Leaching (μg)	Effluent IO_3^- Mass During IO_3^- Injection (μg)	Effluent IO_3^- Mass During Desorption Leaching (μg)	IO_3^- Mass Recovery[a] (%)	Immobilized IO_3^- After Experiment[b] (%)
1mG-1	325.8	51.1	561.4	NA	307.8	226.4	140.4	48.9
1mG-2	72.7	51.1	52.2	22.8	35.5	13.9	140.2	41.3

(a) Mass recovery = (KOH-KNO3-extracted IO_3^- from the reacted column sediments + effluent IO_3^- during the initial AGW leaching + effluent IO_3^- during IO_3^- solution injection + effluent IO_3^- during desorption leaching) / (KOH-KNO3-extracted IO_3^- from the untreated HF sediments + total injected IO_3^-) *100

(b) Immobilized IO_3^- after experiment = (KOH-KNO3-extracted IO_3^- from the reacted column sediments - KOH-KNO3-extracted IO_3^- from the untreated HF sediments) / total injected IO_3 *100

Figure 5.5 shows the XRD spectra and an SEM image of the calcite-HFO prepared using the second method) (without NaOH addition). The XRD pattern clearly shows that the solids were dominated by 2-line ferrihydrite, with quartz and calcite also present. The SEM image shows the bulk fine particle morphology is similar to the images of the DDI- or AGW-HFO (Figure 5.4). The pH evolution of the synthesis solution through the self-buffering process by calcite-dissolution is shown in Figure 5.6. It illustrates that he solution pH approached pH 7 after a reaction period of 20 days.

The SSAs measured by N_2-BET for each synthesized iron oxide are listed in Table 5.4. As expected, high specific surface areas were observed in DDI- and AGW-HFO products (~336 to 337 m^2/g). These values agree well with literature values (Schwertmann and Cornell 2000). Calcite-HFO shows a somewhat lower SSA (~216 m^2/g), which could be due to the presence of quartz in the final product. Interestingly, SAGW-HFO shows an SSA of ~75 m^2/g. Assuming that no significant interactions between the synthesis solutions and sediments occurred, 2 g of HFO could be expected in the SAGW-HFO experiment (Schwertmann and Cornell 2000). Ignoring the much lower SSA contributions from the added 7 g HF sediments, the HFO contributed a surface area of ~339 m^2/g [75.4 m^2/g x (2 g HFO + 7 g HF)/2 g HFO], almost the same SSA as the DDI- and AGW-HFO. This agrees with the XRD findings, where the produced HFO was physically mixed with the sediments. Geochemical modeling should be conducted in the future to confirm these assumptions. Compared to HFO, lower SSA values were observed in the DDI- and AGW-goethite samples (~62 to 63 m^2/g), which is still much higher than that of normal Hanford sediments. Similar SSA values for SAGW-goethite (~78 m^2/g) and SAGW-HFO (~75 m^2/g) were found in these experiments, which confirms that no significant goethite conversion occurred from HFO due to the dissolved silica retardation effects.

Table 5.4.   Specific surface area of the synthesized iron oxides determined by N_2-BET method.

Sample	DDI-HFO	AGE-HFO	SAGW-HFO	DDI-Geothite	AGW-Geothite	SAGW-Geothite	Calcite-HFO
SSA (m^2/g)	337.56	336.49	75.43	61.75	62.81	78.12	216.20
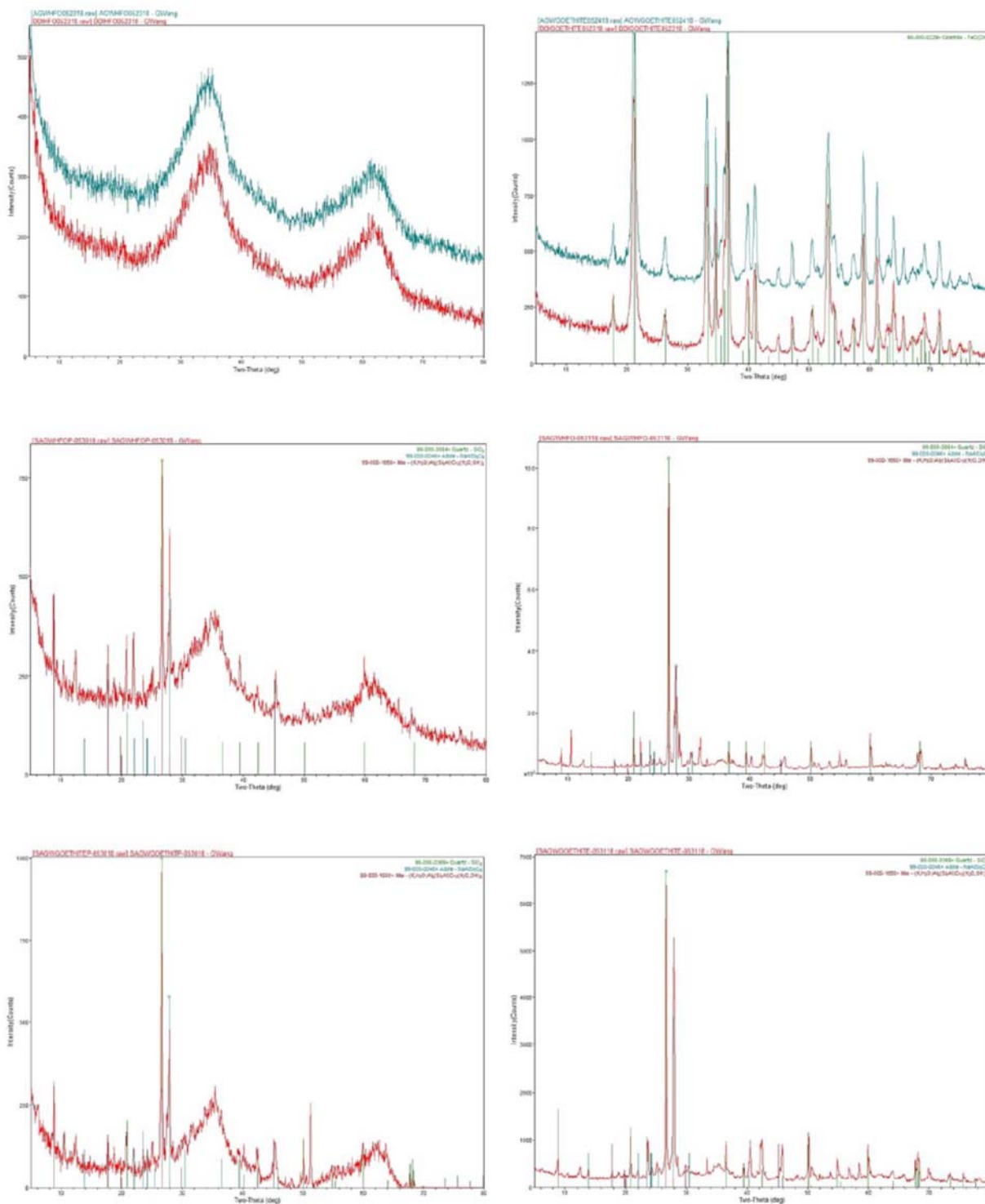
Figure 5.3.   XRD analysis showing the typical 2-line-ferrihydrite or goethite patterns for each iron oxides synthesized in the present study.
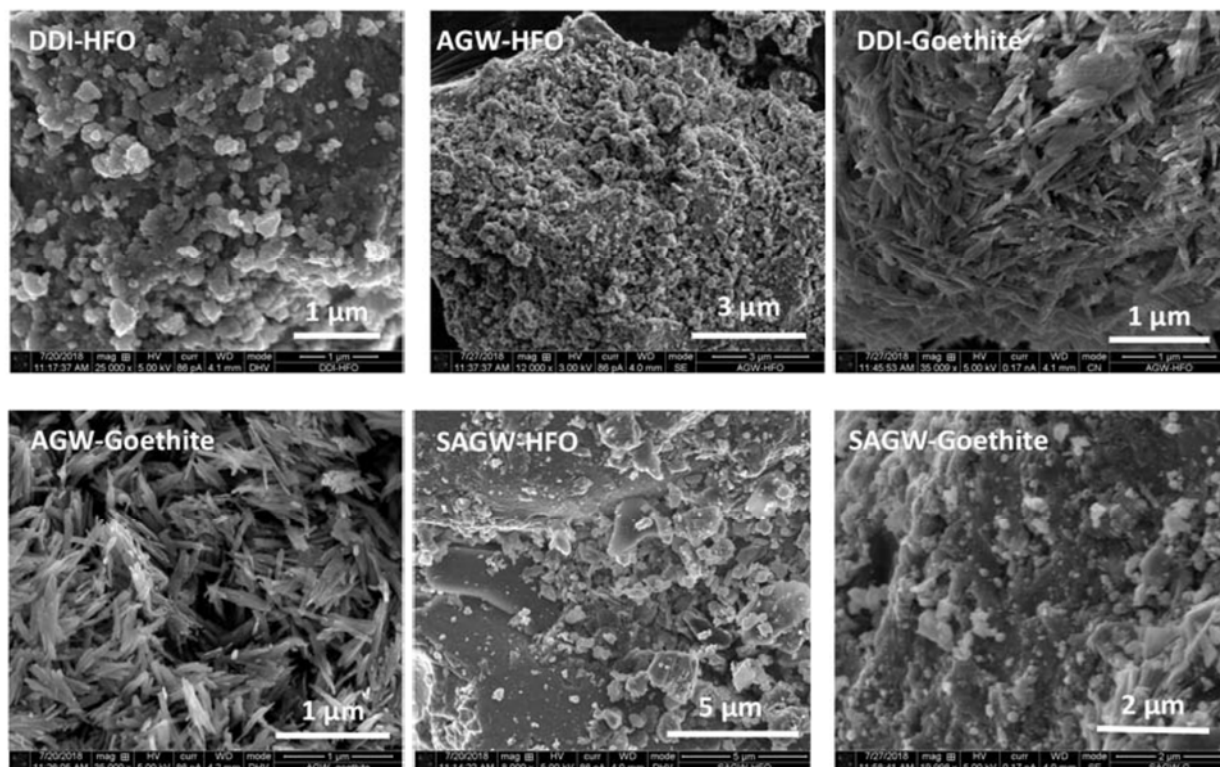
Figure 5.4. SEM analysis showing the typical 2-line-ferrihydrite or goethite crystal morphology for each iron oxides synthesized in the present study.
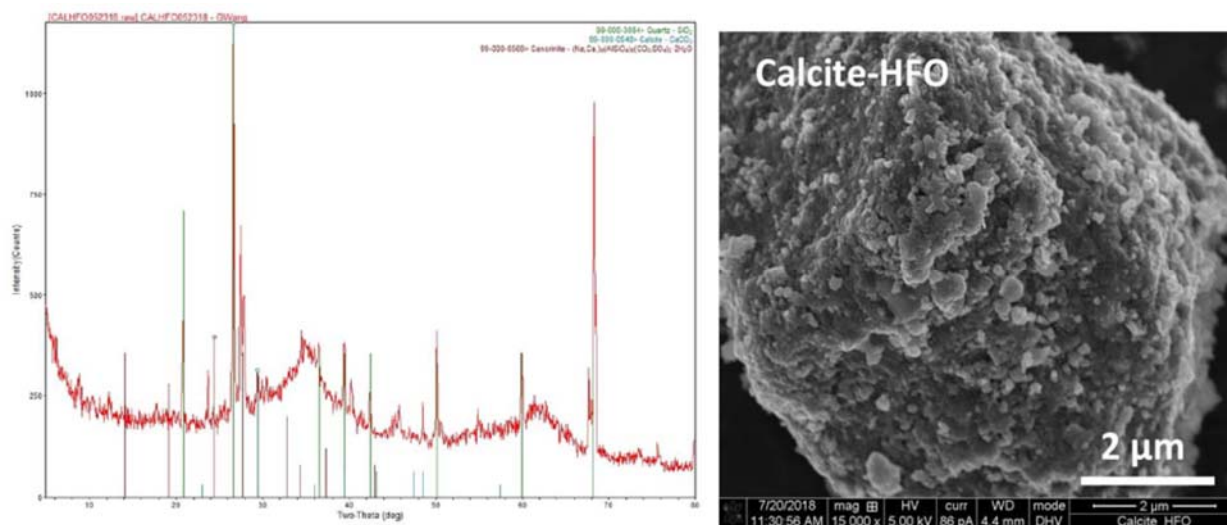
Figure 5.5. XRD analysis showing the 2-line ferrihydrite containing a certain amount of quartz and tiny calcite in the calcite-HFO. The SEM images show a similar mineral morphology as in DDI- or AGW-HFO products (Figure 5.4).
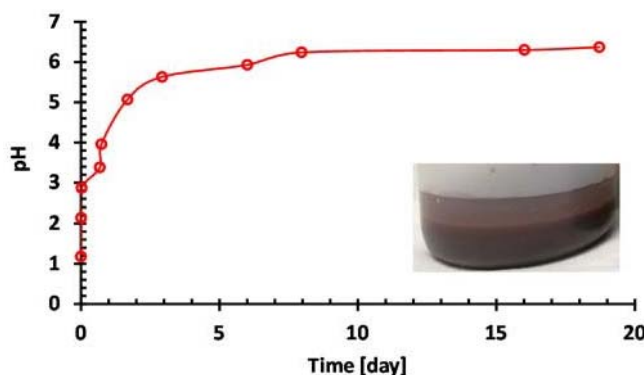
Figure 5.6. Evolution of solution pH with time in the calcite-HFO precipitation system [4 g
Fe(NO$_3$)$_3$·9H$_2$O + 50 mL DDI + 2 g calcite rock powder], resulting in calcite-HFO
precipitations through solution pH self-buffering.

5.2.2   Sorption/Desorption of Iodate on Iron Oxides

The sorption of iodate (IO$_3^-$) on the synthesized DDI-, AGW-, and SAGW-HFO or goethite at room
temperature for 7 and 30 days at three different concentrations at neutral pH (pH ~7.3) is plotted in
Figure 5.7. A linear regression of the data indicated R2 values of 0.94 to 1.00, demonstrating near linear
sorption onto these synthesized iron oxide materials. Among the tested samples, the sorption coefficients
(K$_d$) were found to be in the order of DDI-HFO (goethite) > AGW-HFO (goethite) > SAGW-HFO
(goethite) (Figure 5.7 and Table 5.2). Between the DDI- and AGW-samples (either HFO or goethite),
considering their similar SSA values (~336 and ~62 m^2/g for -HFO and -goethite, respectively) and the
same experimental conditions, the significantly lower sorption for AGW-samples may be the result of
differences in the sorbent properties. For AGW-samples, which were synthesized in the artificial ground
water, cation (Ca, Mg, etc.), substitution or other anion-incorporation into HFO or goethite may have
occurred, which could affect the material's affinity for iodine. Previous sorption experiments conducted
in FY17 (Strickland et al. 2017a) showed that higher solution ionic strength resulted in lower sorption
capacity of iodine on iron oxide minerals. The SAGW-HFO and SAGW-goethite showed much lower
sorption compared to that of the iron oxides synthesized without sediments. The lower sorption on
SAGW-HFO or -goethite can be explained by the sorbent's much lower SSA (~75 to 78 m^2/g). The
dissolution of sediment minerals in the SAGW system may also have resulted in sorption decreases
through higher solution ionic strength effects or because of the more complex aqueous composition.
Consistent with their differences in SSA, HFO showed a far higher sorption affinity for IO$_3^-$ than did
goethite, indicating the strong control of surface area on iodate adsorption.

The calculated sorption K$_d$ values for each synthesized sample with 7-days reaction time are listed in
Table 5.2. In general, high K$_d$ values were observed on the HFO samples synthesized in the DDI and
AGW systems (3253.4 to 5712.2 L/kg after 7-days reaction), followed by the goethite (164.8 to
436.9 L/kg), and then the HFO and goethite samples synthesized in the systems involving sediments
(149.5 to 312.4 L/kg). Higher sorption K$_d$ values for SAGW samples could be expected if the observed K$_d$
values were normalized by the iron oxide mass in the iron oxide-sediment mixtures. Similar to the SSA
normalization method described in Section 5.2.1, iron oxide mass normalized K$_d$ values of 672.8 to
1405.8 L/kg [(149.5 or 312.4) × (2 g HFO + 7 g HF)/2 g HFO] can be estimated. The iron oxide mass-
normalized K$_d$ values are listed in parentheses in Table 5.2. Sorption experiments with the dark brown
HFO particles separated from the precipitate-sediment mixtures should be conducted in the future to
determine iodate affinity on SAGW-HFO precipitates. A lower K$_d$ compared to the normalized K$_d$ value
might be possible because more element-substituted HFO precipitates may have formed due to the
presence of the sediment, resulting in lower sorption.
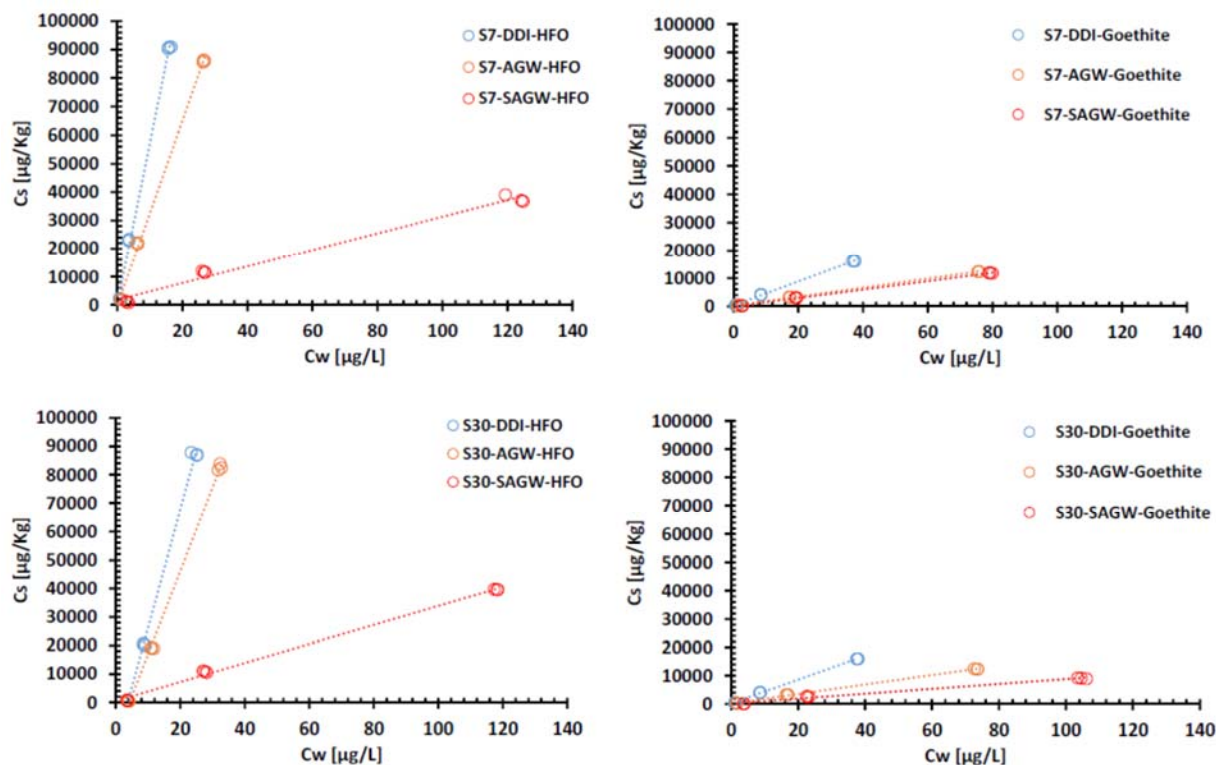
Figure 5.7. Linear iodate sorption on the synthesized iron oxides at room temperature for 7 and 30 days.

Table 5.5. Calculated sorption and desorption K_ds on the synthesized -HFO and -goethite samples at neutral pH in Hanford artificial ground water for 7-day and 30-day reaction times.

Samples	Linear Regression Parameters*	Sorption after 7-day Reaction (L/kg)	Desorption after 7-day Reaction (L/kg)	Sorption after 30-day Reaction (L/kg)	Desorption after 30-day Reaction (L/kg)
DDI-HFO	K_d	5712.2	3633.5	3329.2	2618.3
	R^2	1.00	0.99	0.94	0.97
AGW-HFO	K_d	3253.4	2958.3	2430.4	2403.7
	R^2	1.00	1.00	0.95	0.97
SAGW-HFO	K_d	312.4	411.9	339.7	383.2
		(1405.8)	(1853.6)	(1528.7)	(1724.4)
	R^2	0.98	0.99	1.00	1.00
DDI-goethite	K_d	436.9	401.7	427.7	374.2
	R^2	1.00	1.00	1.00	1.00
AGW-goethite	K_d	164.8	199.3	172.2	192.1
	R^2	1.00	1.00	1.00	1.00
SAGW-goethite	K_d	149.5	174.7	89.0	115.0
		(672.8)	(786.2)	(400.5)	(517.5)
	R^2	1.00	1.00	0.99	0.99

The comparison of iodate sorption between the contact times of 7 days and 30 days is plotted in Figure 5.8. For both DDI-goethite and AGW-goethite, the data for both periods nearly overlap, indicating

that sorption equilibrium was reached within 7 days. Of particular interest for both DDI- and AGW-HFO was the significantly lower sorption (~25% to 42%) observed for the 30-day reaction period compared to the 7-day reaction period. This decrease in K_d with increasing reaction time was not observed on the SAGW-HFO sample. The reasons for these observations are not currently apparent. Re-dissolution of the precipitated HFO solids into the batch sorption system was eliminated as a possible cause by the solution analysis, which showed no detectable Fe by the ICP-OES (data not shown).
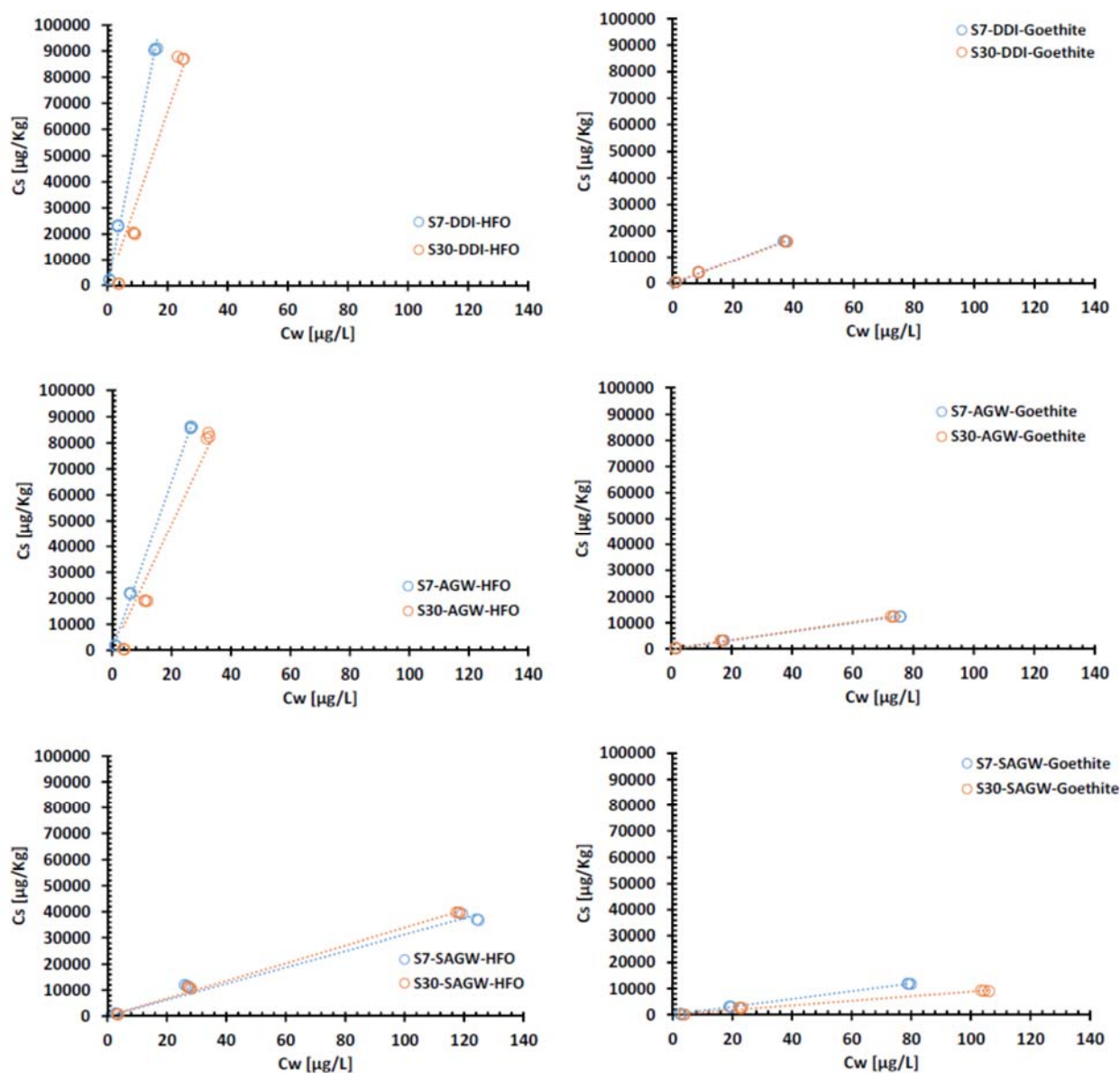
Figure 5.8. Comparison of iodate sorption on the synthesized iron oxides between the reaction time of 7 and 30 days.

The results for iodine desorption (for both 7 days and 30 days) are illustrated in Figure 5.9 and Figure 5.10, with the calculated desorption K_d values listed in Table 5.2. In general, the measured sorption and desorption K_d values were quite comparable, with a variation of ± 1% to 30%, indicating reversible sorption/desorption of iodine for the iron oxides tested in this study. However, different sorption/desorption behavior occurred among the different samples. For example, compared to sorption,

samples of DDI-HFO showed lower desorption K_d values of ~ -36% and ~ -21% for 7-day and 30-day reaction times, respectively, whereas the samples in SAGW-HFO and SAGW-goethite showed an increased desorption K_d (~ +13% to 32%) for both reaction times. Considering the observed nearly identical sorption K_d values on the sample SAGW-HFO between 7- and 30-day reaction times (discussed above), it appears that sorption of iodine on SAGW-HFO was readily reversible in the synthesized AGW conditions.
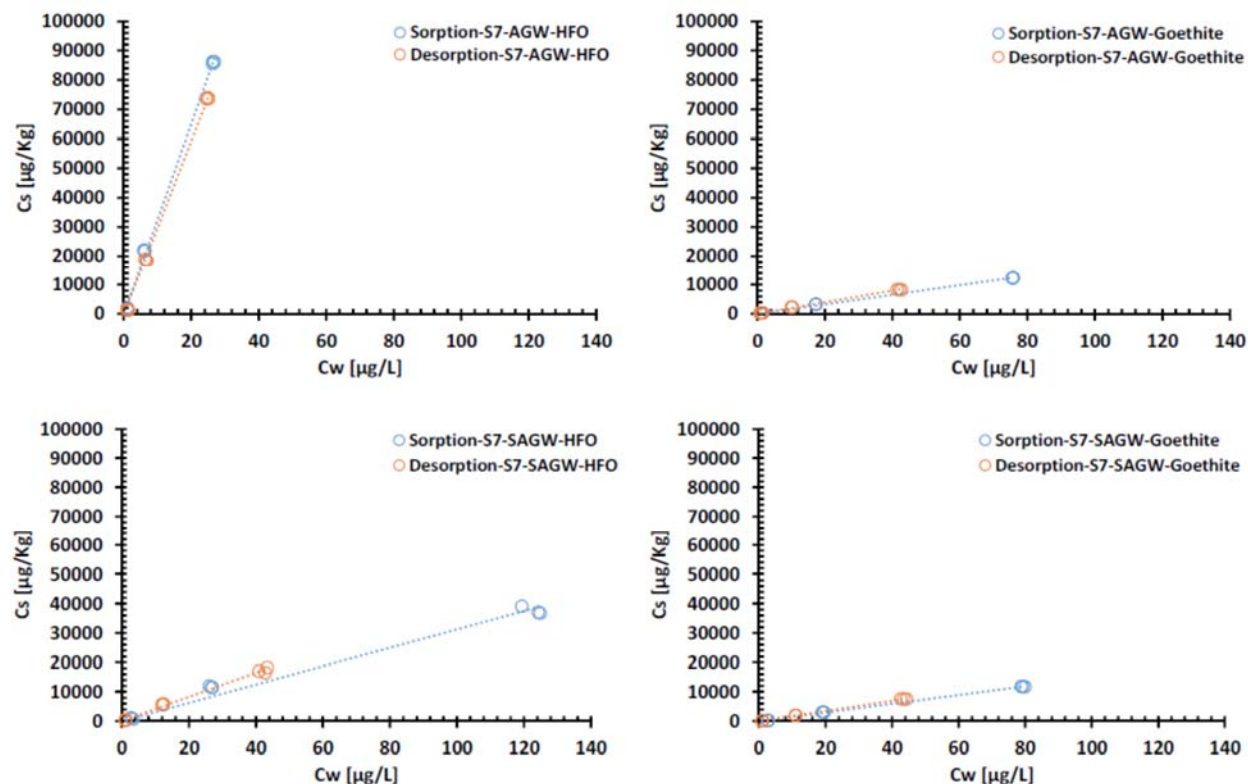
Figure 5.9.   Sorption and desorption of iodate on the synthesized iron oxides at room temperature for 7 days.
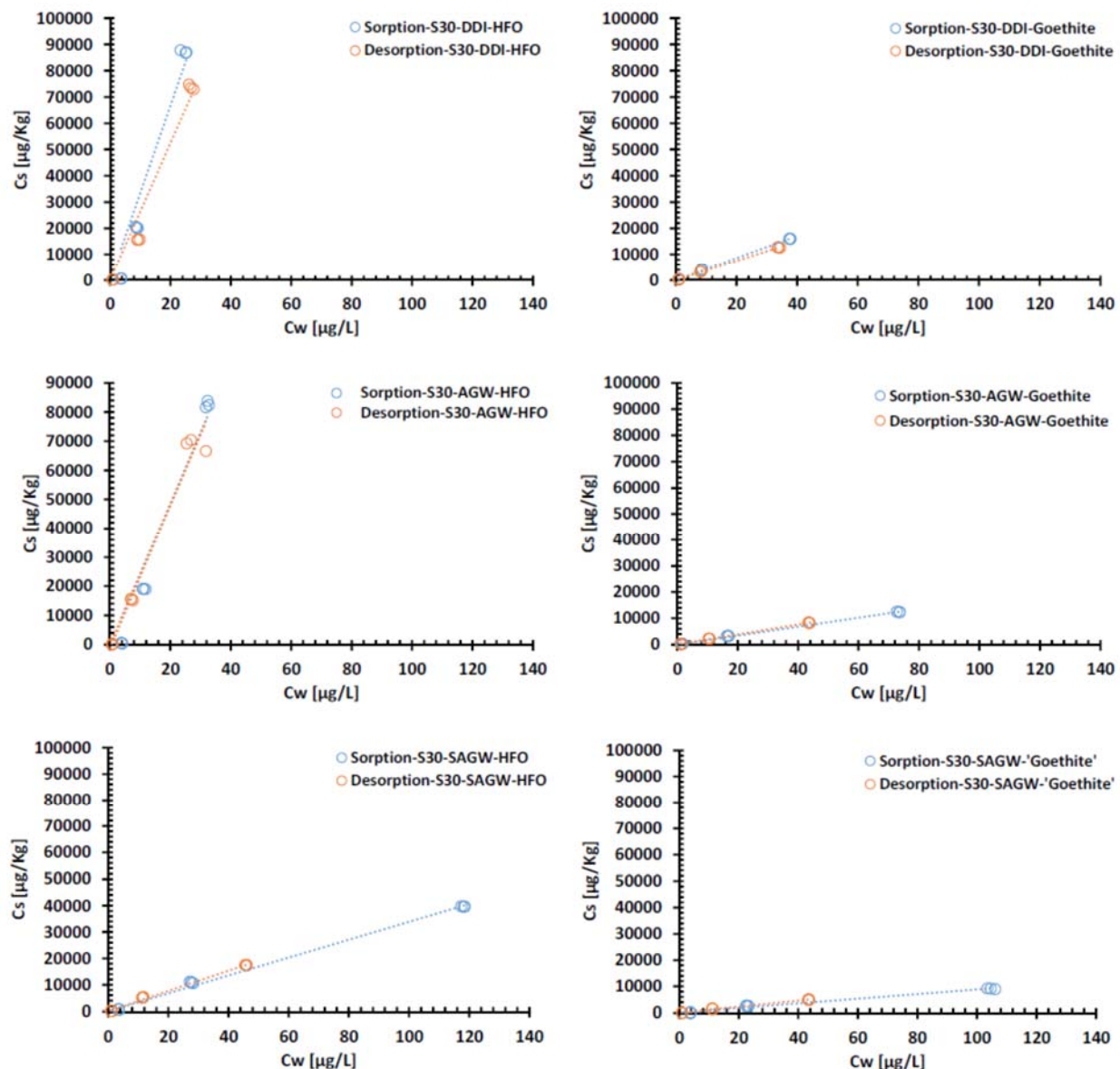
Figure 5.10. Sorption and desorption of iodate on the synthesized iron oxides at room temperature for 30 days.

5.2.3   Sorption/Desorption Reactive Barrier Column

The measured concentrations of total iodine in the effluents of columns packed with AGW-HFO, AGW-goethite, and silica sand are shown in Figure 5.11. As expected, the iodine breakthrough from the control silica sand column occurred after ~1 pore volume (PV), indicating conservative iodine flow without detectable iodine-silica sand interactions. In contrast, the iodate transport was significantly retarded in the AGW-goethite and is due to sorption processes. The iodine breakthrough time at $C/C^0 = 0.5$ occurred after ~27 and ~59 PV in AGW-goethite and AGW-HFO columns, respectively, resulting in retardation factors of about 27 and 59 under the current column packing and flow conditions.

If the iron oxide content of the AGW-HFO column (~1.0%) were more similar to that of the AGW-goethite column (~5.5%), then much later iodine breakthrough would be expected. The large iodine

retardation differences between the two packed iron oxides is consistent with the batch sorption experimental results, in which a much higher sorption K_d value was observed for AGW-HFO (4936 L/kg) compared to AGW-goethite (260 L/kg) at an initial iodine concentration of 50 ppb.
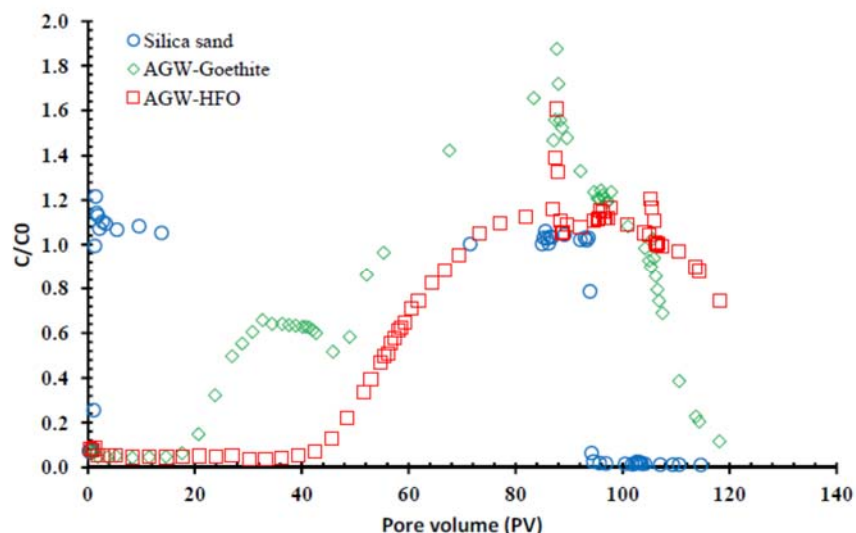
Figure 5.11. Breakthrough curves of the total iodine in the reactive barrier flow-through column experiments [AGW-HFO, AGW-goethite, and the (control) silica sand].

The measured iodine concentrations, selected sample pH, as well as the sorption/desorption stop-flow events are illustrated in Figure 5.12. The effluent samples from the AGW-HFO or AGW-goethite columns were also filtered with a 0.2-µm filter for iodine concentration measurements to check for potential release of iron oxide particles that could result in particle-facilitated iodine transport in the experimental setup. For the AGW-HFO and AGW-goethite columns, the nearly identical iodine concentration values between the 0.2-µm-filtered and non-filtered effluent samples indicated that no > 0.2-µm-sized colloid-facilitated iodine transport occurred. For both columns, the 48-h stop-flow event during the sorption phase resulted in a significant increase in iodine concentrations in the effluent. Similar to the iodine behavior in the 48-h desorption stop-flow events, iodine concentration increases during the stop-flow event of the sorption phase indicate release of iodine from the initial sorbed phase back into solution.

This phenomenon is consistent with the iodine breakthrough curves before the sorption stop-flow and before the desorption phase of the experiment, where for both AGW-HFO and AGW-goethite columns, the relative effluent iodine concentrations (C/C^0) > 1.0 were observed, up to 1.16 and 1.88 for AGW-HFO and AGW-goethite, respectively. The reason for this is not yet clear. Any pH effect can be ruled out by the pH monitoring results, which indicated nearly constant pH values (pH 7.16 to pH 7.45) during the entire sorption/desorption test. One possible explanation for the unexpectedly high C/C^0 values in the effluent could be that the initial sorbed iodine released back in the solutions at a later time, overlapping with the freshly injected iodine solution. This phenomenon could potentially be the result of a change in iodine speciation during the experiment. After the initial iodate sorption to the AGW-HFO or AGW-goethite surfaces, part of the iodate may have been reduced to iodide, which then was released due to its much low sorption K_d.
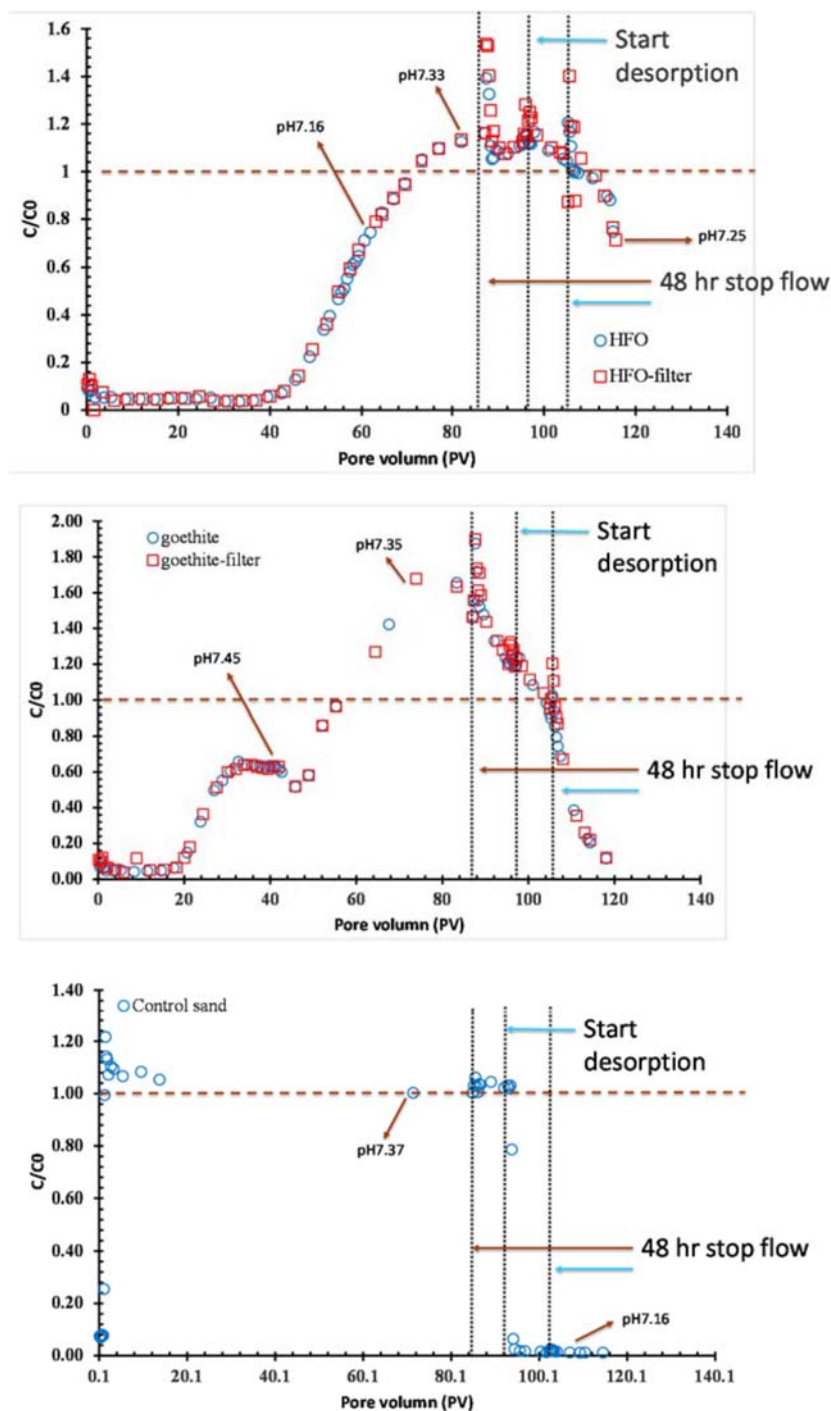
Figure 5.12. The breakthrough curves of iodine in the reactive barrier column packed with the synthesized iron oxides (AGW-HFO, AGW-goethite, and silica sand). The brown dashed lines indicate where the effluent iodine concentrations (C) is equal to the injected iodine concentration (C^0). The empty blue circle and red square represent unfiltered effluent samples and filtered (0.2-μm) effluent samples. The vertical black dashed lines and related arrows illustrate the locations stop-flow events. Selected effluent pH values are shown.

This hypothesis is supported by the XPS characterization results (discussed in Section 5.2.6), in which iodide was observed on the iron oxide surfaces after reaction with iodate solutions. This finding appears to be consistent with some of the batch results presented in Section 5.2.2, where decreased sorption K_d on DDI-HFO and AGW-HFO samples was found for the sorption duration (7 days to 30 days). Iodine speciation measurements on some selected column effluent samples are currently ongoing to validate this hypothesis. The redox mechanisms responsible for this phenomenon is not fully understood; however, microbial reduction is a possibility.

The redox assumption above is based on the premise that the packed silica sand, AGW-HFO or AGW-goethite, is initially free of iodine. Table 5.6 lists the flow-through solution volumes during the sorption/desorption processes and the calculated total iodine mass. Within ICP-MS analytical errors, good mass recoveries from the control silica sand column (104.3%) and AGW-goethite column (98.7%) were observed. The mass recovery of ~ 67.9% from the AGW-HFO column indicates that some iodine (~ 32%) was still sorbed to the solid after flushing with ~ 20 PV AGW. Nevertheless, the mass recovery, especially for AGW-goethite, which showed much higher C/C_o values, confirmed that the packed column samples were iodine-free.

Table 5.6. Flow-through solution volumes during the sorption/desorption processes and the calculated total iodine mass.

Samples	Iodate AGW Solution Injected during Sorption (PV)	Total Iodate Mass Injected during Sorption (µg)	Calculated Effluent Iodine Mass during Sorption (µg)	AGW Desorption Volume (PV)	Calculated Effluent Iodine Mass during Desorption (µg)	Mass Recovery (%)
AGW-HFO	95.35	6.71	3.12	20.32	1.44	67.91
AGW-goethite	95.33	6.71	5.48	22.77	1.11	98.2
Silica sand	92.72	7.03	7.17	21.90	0.17	104.3

5.2.4   Long-Term Iodate Sorption on Iron Oxides

The 200-day and 2-day sorption results for iodate (IO_3^-) on HFO, goethite, magnetite, and hematite at initial concentrations ranging from 5 to 200 ppb and neutral pH (~pH 7.3) are shown in Figure 5.13. Linear regressions of the data produced R^2 values of 0.96 to 1.00, indicating near linear sorption on these iron oxide materials. The zero-intercept linear regression fitted K_d values are listed in Table 5.7. Similar to the 2-day reaction results (Strickland et al. 2017a), Table 5.7 shows that the HFO showed the highest sorption capacity (1210 L/kg), followed by goethite (125 L/kg), magnetite (30.3/kg), and hematite (12.5 L/kg). In general, compared to the 2-day reaction, an increase of sorption K_d (~ +27% to 48%) was observed when the reaction time approached 200 days. The limited K_d increase may have resulted from sorption kinetics or from changes in the solid/solution ratio [in the 2-day reaction, the solid/solution ratio increased from 2.0 to 2.2 for HFO and 10.0 to 10.9 for the other iron oxide samples, because 3 mL of supernatant was removed for sampling in 2-day experiments (see Section 5.1.5)].

No significant mineral transformation of the synthesized HFO was observed after the 200-day reaction period. The XRD patterns of the HFO (synthesized in FY17; containing ~20% hematite) before and after 200-day reaction periods (Figure 5.13) showed a small goethite peak (~ 21 deg) generated after the reaction. The 200-day reaction HFO sample was further heat-treated at 70°C for a week. The XRD results still showed a very limited transformation to goethite (Figure 5.14). These findings imply that the synthesized HFO is relatively stable within the experimental conditions and duration of the study.
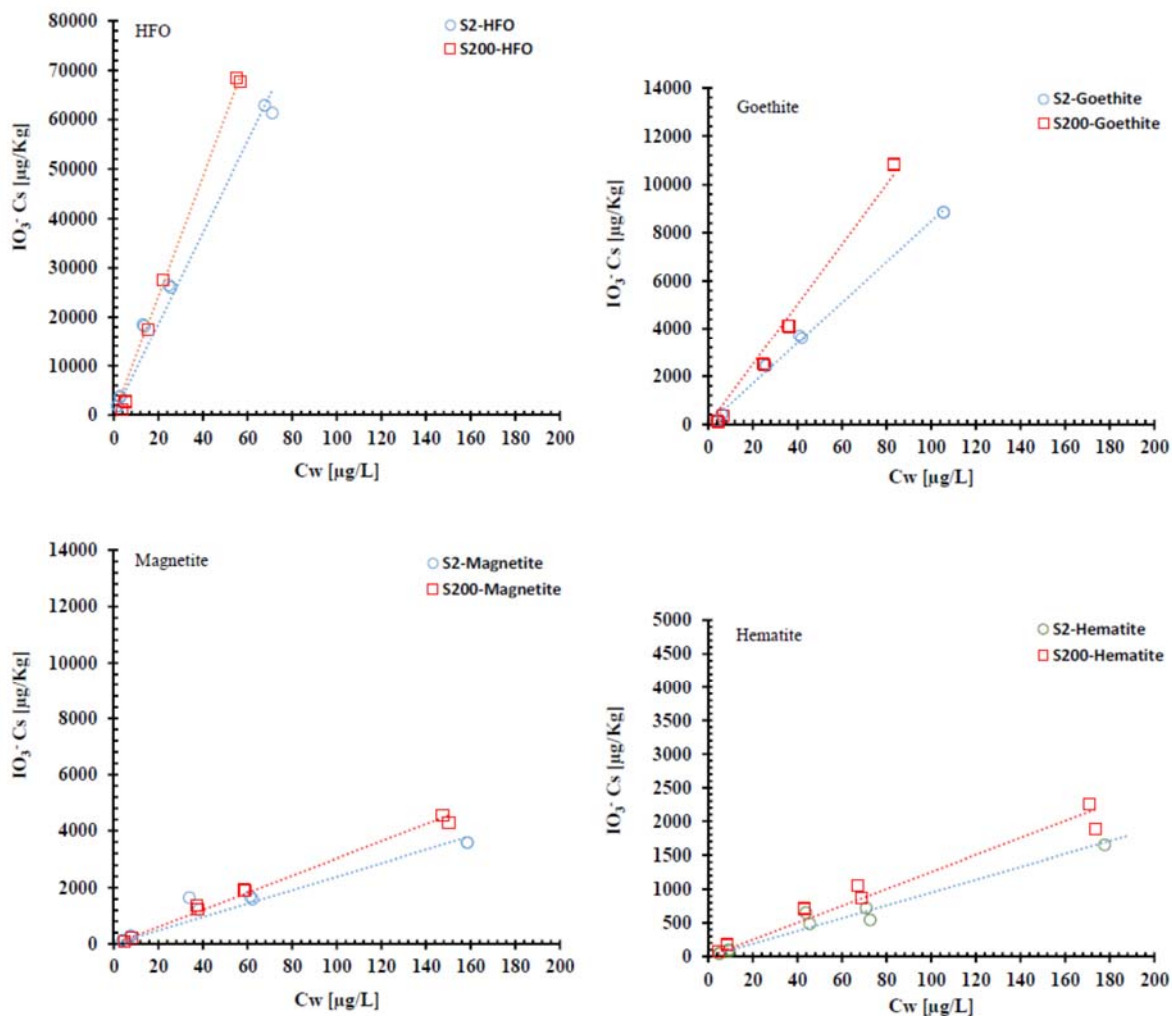
Figure 5.13. Long-term (200 days) extended iodate sorption experiments with HFO, goethite, magnetite, and hematite. The 2-day reaction results are also shown for comparison purpose.

Table 5.7. Calculated sorption K_d in the extended long-term (200 days) sorption experiments, and comparison with the 2-day sorption results.

Samples	Linear Regression Parameters* (ppb)	K_d after 2-day Reaction (L/kg)	K_d after 200-day Reaction (L/kg)	K_d Differences between 2- and 200-day Reaction Time (%)
HFO	K_d	927.5	1212.5	30.7
	R^2	0.98	0.99	
Goethite	K_d	84.9	125.2	47.5
	R^2	1.00	0.98	
Magnetite	K_d	23.8	30.3	27.3
	R^2	0.94	0.99	
Hematite	K_d	9.5	12.5	31.6
	R^2	0.96	0.96	

*Zero intercept linear regression model.
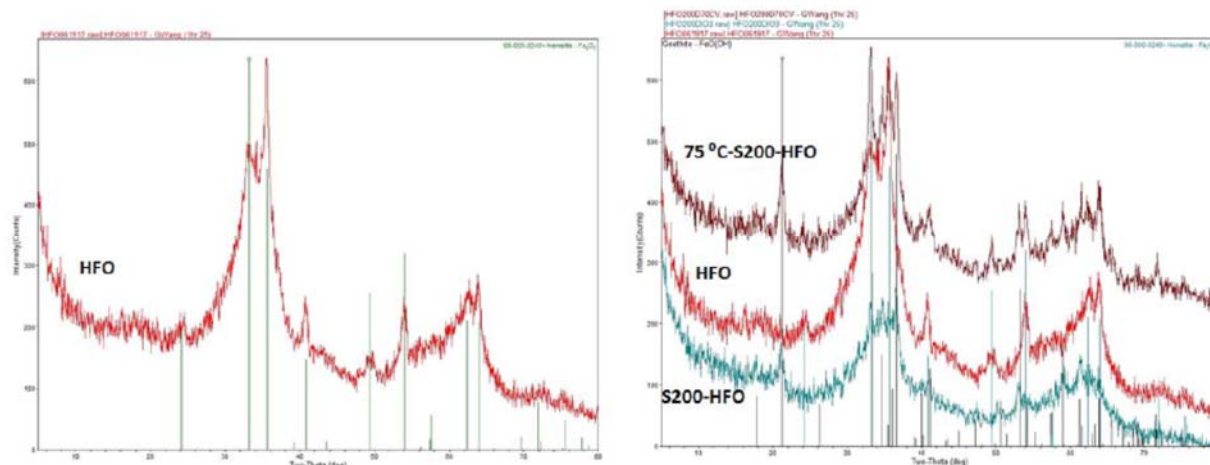
Figure 5.14. XRD analysis on the synthesized HFO (FY17; containing ~20% hematite) before (HFO) and after the 200-day reaction (S200-HFO), as well as a sample further heat-treatment at 70°C for a week (75°C-S200-HFO).

5.2.5   Iodine Uptake during HFO Precipitation (Co-precipitation)

Results of iodate and iodide removal efficiency through co-precipitation with HFO in the three different solution systems of DDI, AGW, and SAGW are shown in Figure 5.15. Greater than 90% of the iodate was removed from solution through co-precipitation with DDI-HFO, AGW-HFO, and SAGW-HFO for initial concentrations ranging from 5 to 200 ppb (except SAGW-HFO at 5 ppb, which showed an average value of 68.3%). For iodide, lower removal efficiencies (20% to 70%) were observed among all the tested systems. The iodate and iodide co-precipitation efficiencies were also presented in terms of iodine loading (mg/kg), in which the solid mass used in the iodine loading calculation referred to the collected, air-dried solid precipitate weights. Figure 5.16 and Table 5.8 show the co-precipitated loadings for iodate and iodide with different initial iodine concentrations in the three tested systems. In general, much higher co-precipitation of iodate (~0.21 to 7.97 mg/kg) was found than for iodide (0.04 to 4.35 L/kg). Although lower than that of iodate, the iodide loadings are still much higher than for sorption on natural sediments, which implies a potential iodide sequestration approach. For either iodate or iodide, similar iodine loading values were observed at each concentration level (except "iodide-SAGW-200 ppb" batch) for each of the three testing conditions (DDI, AGW, and SAGW). These findings are different from the batch sorption experiment results (where a sorption K_d of DDI- > AGW- > SAGW- was observed), which might reflect a different iodine-iron oxide association mechanism.
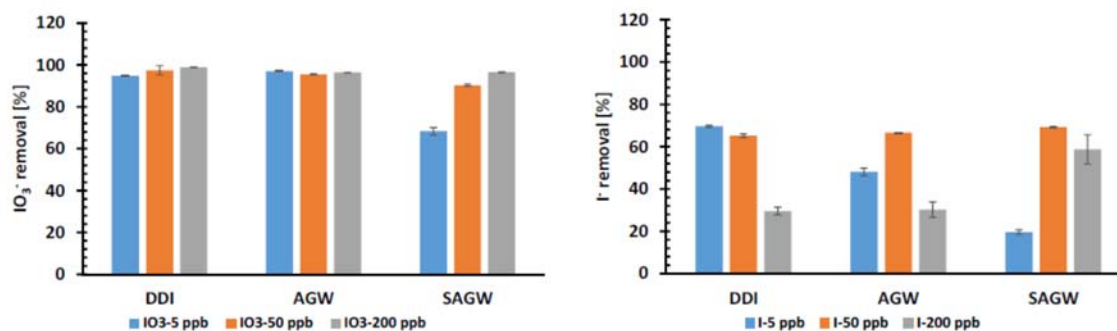
Figure 5.15. Removal efficiency of iodate and iodide through HFO co-precipitation in three different solution systems (DDI, AGW, an SAGW) under a concentration range of 5 to 200 ppb.

Figure 5.16. Calculated loadings of iodate and iodide (mg/kg) through HFO co-precipitation in three different solution systems (DDI, AGW, an SAGW) under a concentration range of 5 to 200 ppb.

Table 5.8. Calculated loadings of iodate and iodide through HFO co-precipitation in three different solution systems (DDI, AGW, and SAGW) under three initial concentrations of 5, 50, and 200 ppb.

Initial Iodine Concentrations	DDI-IO$_3^-$ Loading (mg/kg)	AGW-IO$_3^-$ Loading (mg/kg)	SAGW-IO$_3^-$ Loading (mg/kg)	DDI-I Loading (mg/kg)	AGW-I Loading (mg/kg)	SAGW-I Loading (mg/kg)
5 ppb	0.21 ± 0.00	0.39 ± 0.00	0.27 ± 0.01	0.22 ± 0.00	0.10 ± 0.00	0.04 ± 0.00
50 ppb	1.96 ± 0.04	1.97 ± 0.00	1.86 ± 0.01	1.10 ± 0.01	1.18 ± 0.00	1.23 ± 0.00
200 ppb	7.97 ± 0.01	7.91 ± 0.00	7.92 ± 0.02	1.99 ± 0.12	2.24 ± 0.27	4.35 ± 0.51

5.2.6   XPS Analysis on Iodine Sorption

XPS is a versatile surface analysis technique that can be used for compositional and chemical state analysis. To enhance understanding of iodate sorption on iron oxide surfaces, XPS spectra were collected on four selected samples: DDI-HFO, DDI-goethite, magnetite, and hematite. The iron oxide samples were reacted with iodate-spiked AGW solutions with initial concentrations of 1.0×10^{-2} and 5.76×10^{-4} M (100 ppm).

A full-range XPS spectra was conducted for each sample. An example spectra (AGW-goethite after reaction with 1.0×10^{-2} M iodate solution in AGW system) is shown in Figure 5.17. It clearly revealed the presence of iodine on the goethite, and I 3d peaks were clearly identified in the survey scan spectrum after iodate adsorption.
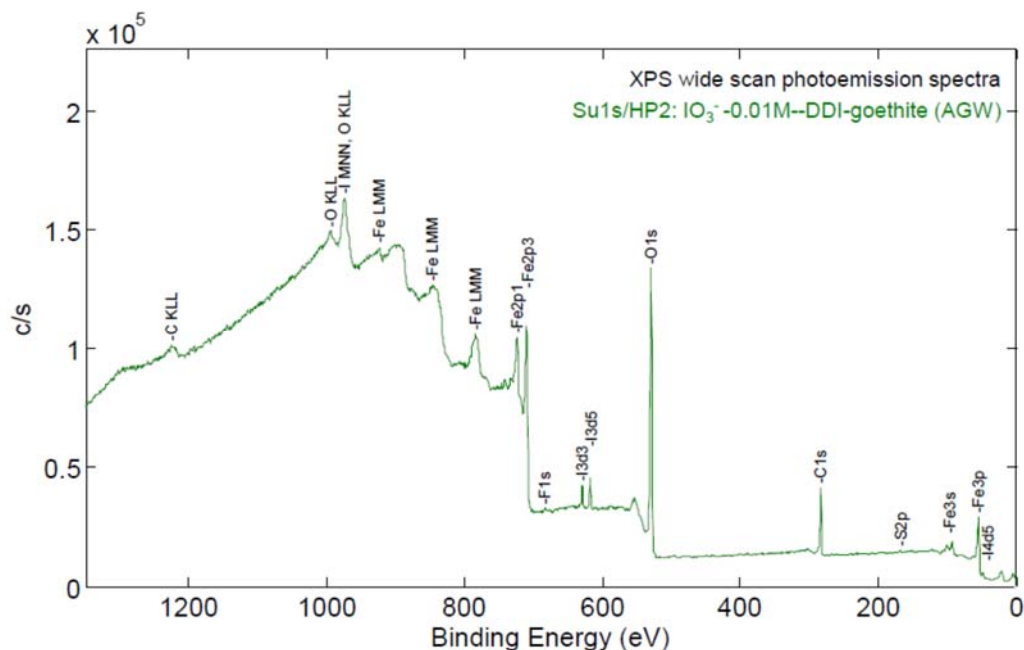
Figure 5.17. Full-range XPS spectra of AGW-goethite after iodate sorption in 0.01 M iodate AGW solution.

To determine the chemical environment of iodine, high-resolution XPS spectra of the I 3d peaks of the samples before and after 7-days reaction with 1.0×10^{-2} or 5.76×10^{-4} M iodate (IO_3^-) AGW solutions were collected and are shown in Figure 5.18. Two major peaks located at 624.1 eV and 635.2 eV appear to result from the I 3d spin-orbital doublet (I $3d_{5/2}$ and I $3d_{3/2}$, respectively) with a splitting of 11.1 eV. These two peaks were expected and are assigned to iodate based on literature values (Li et al. 2016). According to previous work (Du et al. 2004; Li et al. 2016), the peak of I $3d_{5/2}$ at the binding energy of 624.1 eV might be associated with the formation of iron iodate because of the strong interaction between iodate and surface iron atoms. Unexpectedly, Figure 5.18 also has two major peaks at the binding energy of 619.2 eV and 630.5 eV, which are consistent with iodide (I-) signals (Li et al. 2016). It is not clear what the chemical bonding was between iodide and the iron oxide surfaces. In addition, no significantly detectable sorption of iodide on iron oxides can be reported in our FY17 scoping batch experiments (Strickland et al. 2017a). High-resolution XPS spectra of the I 3d peaks on the control samples (the samples reacted with AGW without iodine) were also collected, and indicated no iodate or iodide contamination in the samples (Figure 5.18).
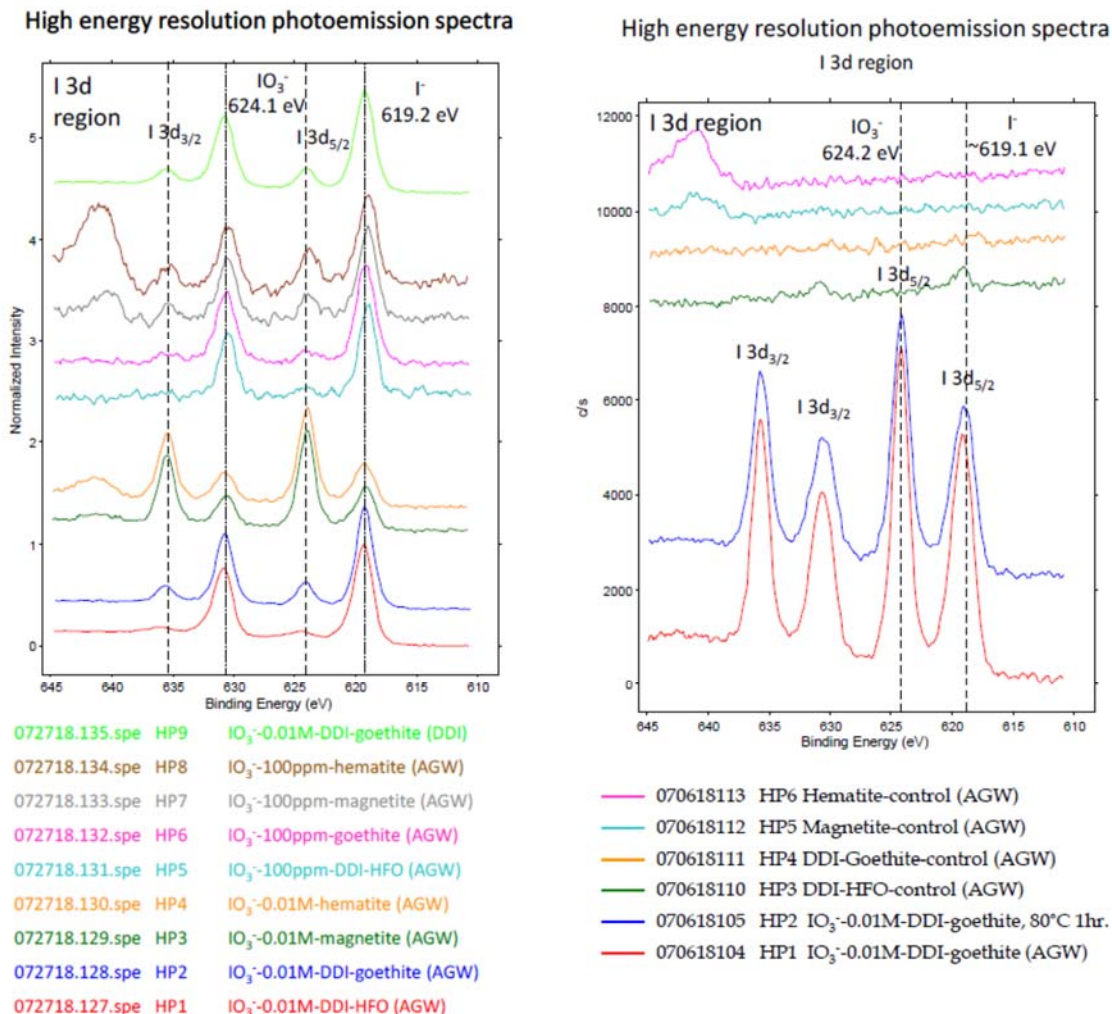
Figure 5.18. High-resolution XPS spectra of the I 3d peaks on the samples reacted with AGW solutions of 100 ppm or 0.01 M iodate (*left*), as well as the XPS spectra on the control samples (*right*). The sample label "IO_3^--0.01M-DDI-goethite, 80°C 1hr" represented the 1.0E-02 M IO_3^- reacted DDI-goethite sample was further heat-treated at 80°C for 1 h.

To understand the presence of iodide, one can consider the possibility that the added iodate was reduced to iodide on the iron oxides in the AGW system (reduction potential of the IO_3^-/I^- : 1.085 V for acid solution and 0.26 V for alkaline solution). This scenario does not appear to be likely because the iron oxides were synthesized with ferric iron (except magnetite) and is supported by the Fe XPS spectra (Figure 5.19) where no clear indication of Fe^{2+} was found. To evaluate any redox artifacts resulting from the XPS beam, multiple sequential XPS beam scans were conducted to monitor any potential changes in the IO_3^- : I^- peak ratio (Figure 5.20). No clear indication of peak ratio changes were found in sample DDI-HFO and hematite, whereas a limited IO_3^-/I^- decrease was observed in magnetite and DDI-goethite. The results indicate that the XPS X-ray beam might result in limited reduction of iodate, depending on the sample; however, it is not possible to quantify the magnitude of iodate reduction that occurred during the first beam exposure.
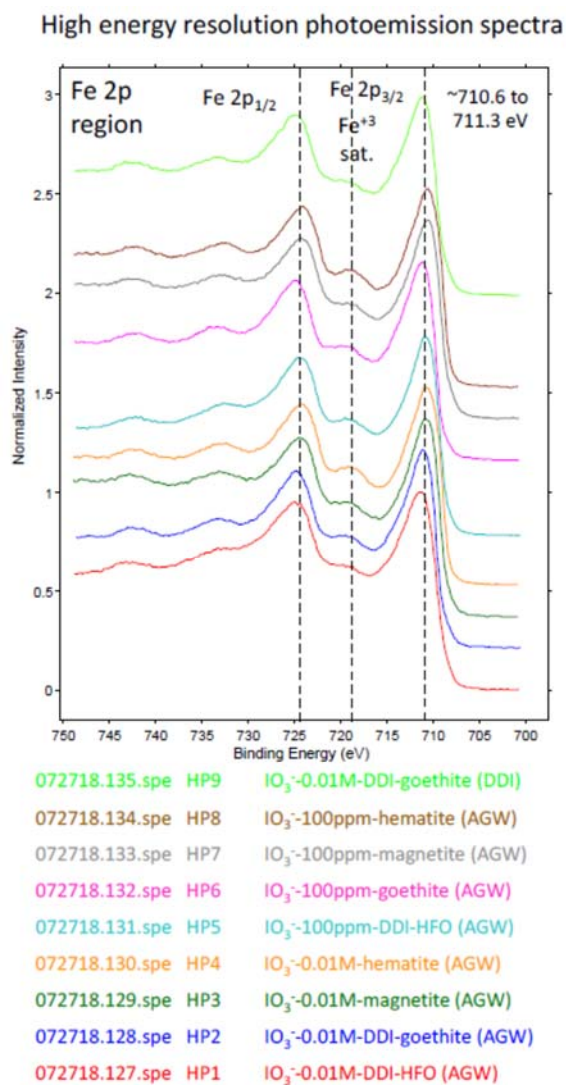
Figure 5.19. High-resolution XPS spectra of the Fe 2p peaks on the samples reacted with AGW solutions of 100 ppm or 0.01 M iodate. Two major peaks at 710.6–711.3 eV and ~724.6 eV were assigned to Fe^{3+}, while the Fe 2p$_{3/2}$ peak has associated satellite peaks at ~718.5 eV (Yamashita and Hayes 2008).
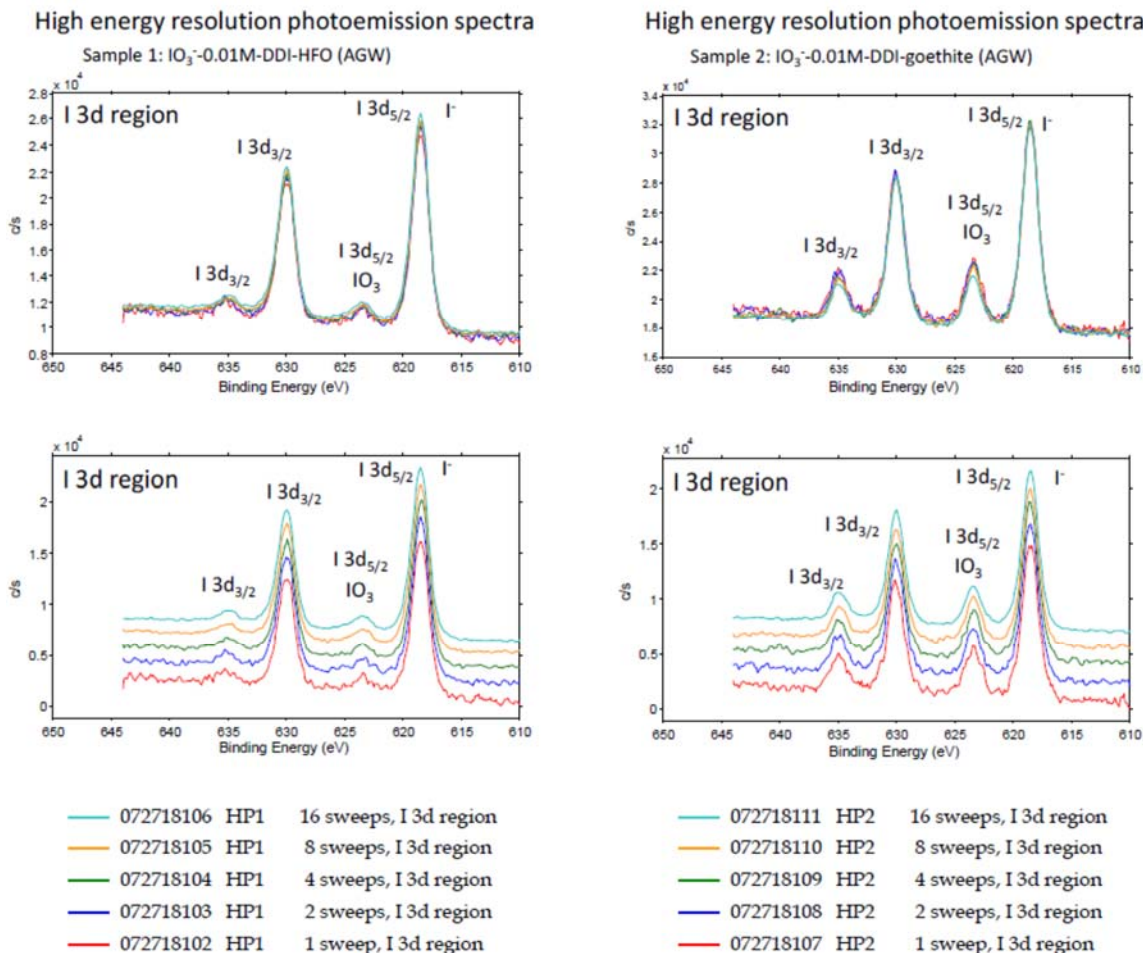
Figure 5.20. Multiple sequential scans for high-resolution XPS spectra of the I 3d peaks on selected samples (DDI-HFO, DDI-goethite, reacted with AGW solutions of 0.01 M iodate) for potential iodate reduction monitoring caused by XPS beam energy.

5.2.7 Injection of Ferric Iron into 1- and 3-Meter Columns and In Situ HFO Precipitation

5.2.7.1 Aqueous Measurements during Ferric Iron Injection and HFO Precipitation

In situ HFO precipitation was apparent in the two transparent glass columns due to a visibly significant color change of the packed sediment, where the grayish HF sediment matrix turned brown, indicating the precipitation of HFO (Figure 5.21). As expected, the self-pH buffering of the injected acidic ferric solution occurred, leading to nearly 100% injected Fe precipitating out of the solution in the column. Figure 5.22 clearly illustrates that the injected acidic solution (pH 1.5) was immediately buffered to above ~ pH 6 (pH 5.5 in 3mP-2 column) after the first pore volume effluent (~ pH 7.9). The relative higher pH from the first pore volume resulted from the AGW column saturation injection before the acidic ferric solution. Fe signals in all the column effluents were almost near or under the ICP-OES detection limit (41.1 μg/L), indicating that Fe precipitated in the columns under neutral pH conditions (Figure 5.22). Among all the columns, the effluent solution became brown in color after about 6.5–8.5 PVs, accompanied by a dramatic decrease in effluent pH (to ~4.0) and a concomitant increase in Fe

concentration. This indicated that the injected acidic ferric solution overwhelmed the HF acid's neutralization capacity and the injection was stopped.

Figure 5.21. Color comparison between treated (brown) and untreated (gray) HF sediments. The seven brownish samples located in the middle are the reacted sediments from column 1mG-1 after in-situ HFO precipitation, which, from left to right, represented the samples collected following the column flow direction (0 to 100 cm); the two grayish samples at far left and right are the untreated HF sediments.
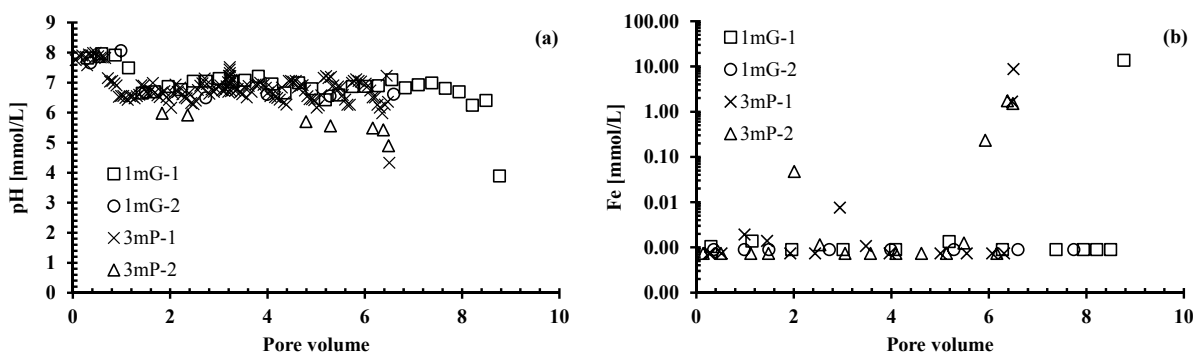
Figure 5.22. (a) Neutralized solution pH through self-buffering due to mineral dissolution in the tested columns; (b) ignorable Fe presented in column effluent during acidic ferric solution injection in the tested columns.

The pH self-buffering of the injected ferric solution in the columns mainly resulted from calcite carbonate dissolution. Figure 5.23 shows the measured concentrations of Ca, Al, Si, and Sr in the effluents during the acidic ferric solution injection. As expected, carbonate dissolution in HF sediments was rapid, where the Ca concentration in all tested columns was dramatically increased to ~120 mmol/L after the first pore volume, and a concentration plateau was maintained during the entire ferric solution injection process. The elevated Ca concentration and the constant concentration plateau indicated a dominant carbonate dissolution process, because the cation exchangeable Ca is much smaller for Hanford sediments (Szecsody et al. 2013). The carbonate dissolution was also indicated by the continuous gas bubbles observed in the effluents. This is because the carbonate concentrations were well above aqueous carbonate solubility, which resulted in most carbonate outgassing as CO_2 gas.
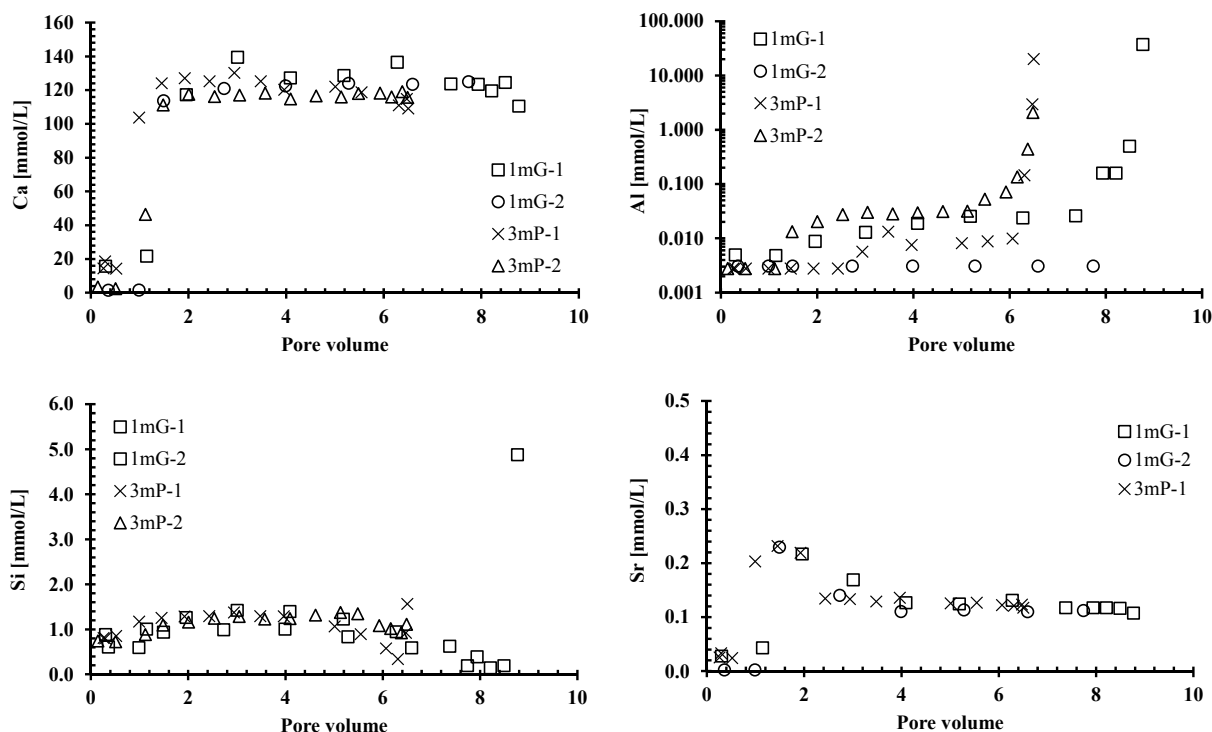
Figure 5.23. Effluent Ca, Al, Si, and Sr concentrations during the injection of the 0.1 M acidic ferric solution.

5.2.7.2   Measurement of Ferric Iron Precipitates in Sediments by Fe Extractions

The in situ precipitated HFO mass in the columns was quantified by the total ferric iron extracted with 8 M HNO_3 minus the background ferric iron determined in the untreated sediments. Figure 5.24 shows that the Fe contents extracted from the treated samples were relatively constant (~10–12 mg/g among all the tested columns despite differences in the column length (1 or 3 meters) and the ferric solution injection rates (2.0–21.4 m/day). In the 1-meter glass columns, the precipitated HFO was evenly distributed throughout the columns, with a HFO content range of ~ 5.3–10.6 mg/g. For the two 3-meter PVC columns, higher HFO precipitation occurred in the middle of the columns (6.94–12.02 mg/g at 72.5–232.5 cm), with less mass (3.98–4.63 mg/g) and limited precipitation (0.40–0.85 mg/g) at the column inlet (0–10 cm) and outlet areas (290–300 cm). For column 3mP-2 (3-m), HFO precipitation increased in the direction of flow. This might be due to the high injection velocity (21.4 m/day) applied on this column. The resulted residence time (3.4 h) may not be supportive of local pH buffering. Under high flow conditions, the low pH solution was quickly refreshed. Further from the inlet, HFO precipitation occurred because the pH increased to near neutral conditions.
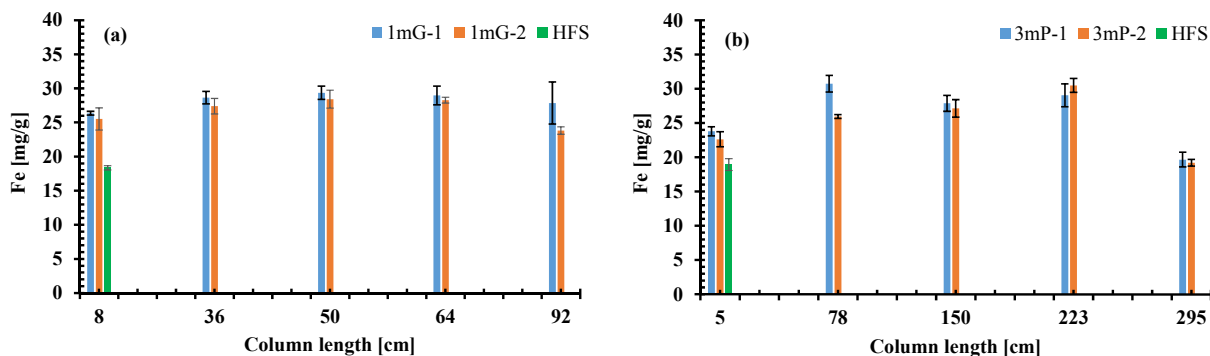
Figure 5.24. Fe contents determined by 8 M HNO_3 extraction in the tested 1D columns along the column length from the column inlet. (a) 1-meter glass columns; (b) 3-meter PVC columns.

In addition to the total Fe extraction, Fe(II) extraction using 0.5 M HCl was also conducted on the reacted sediments collected from column 3mP-1, 3mP-2, and 1mG-1 at the same sample locations described above. Figure 5.25 shows the extraction results with an extracted Fe(II) value range of ~0.49–0.77 mg/g. As expected, no significant Fe(II) difference between the untreated and column-treated sediments was observed, and the extracted Fe(II) contents were constant among the samples collected at different column locations. These results indicate that no significant Fe(II)-containing minerals in the HF sediments were dissolved. These results were further confirmed by the 1 M $CaCl_2$ extraction, where no significant ion-exchangeable Fe(II) was observed (data not shown).
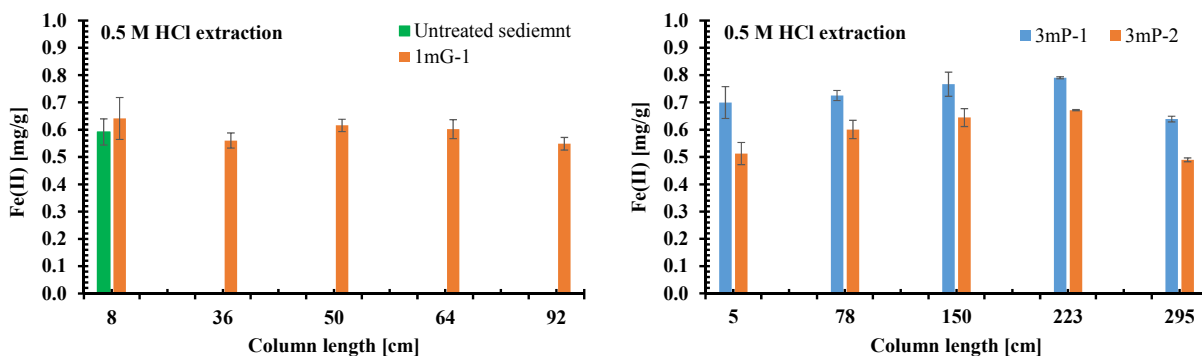
Figure 5.25. Fe(II) contents by 0.5 M HCl extraction on the column-treated and untreated HF sediments.

5.2.7.3   Measurement of Other Phase Changes by XRD and SEM/EDS

HFO precipitates were identified in the XRD analysis at low precipitate concentrations (10 mg/g). However, the XRD pattern did not show any other Fe oxides or hydroxides such as goethite, magnetite, hematite, lepidocrocite, or akageneite. Although not identified in the XRD analysis, the chemical composition analysis through SEM-EDS provided strong evidence for HFO precipitation (Figure 5.24, right). Figure 5.26 shows that 49–59 at% and ~4.5 at%, Fe was detected on the more bright and grey areas, respectively. Results indicated that the nanometer-sized HFO presumably precipitated on a feldspar grain in the reacted sediments.

The dissolution of calcium carbonate was supported by the XRD analysis. Figure 5.24 (left) compares the collected XRD patterns between the untreated and the treated sediments collected from column 1mG-1. The comparison illustrated the disappearance of calcite (indicated by the strongest calcite peak at 29.4° 2Θ) after the column reaction process. No significant changes of other minerals were observed in the XRD analysis. This is consistent with the Si and Al signals presented in Figure 5.23, where very limited Si with initial-dissolution (up to 1.5 mmol/L) and likely later-precipitation, as well as almost no detectable Al, were observed in the effluent solutions.
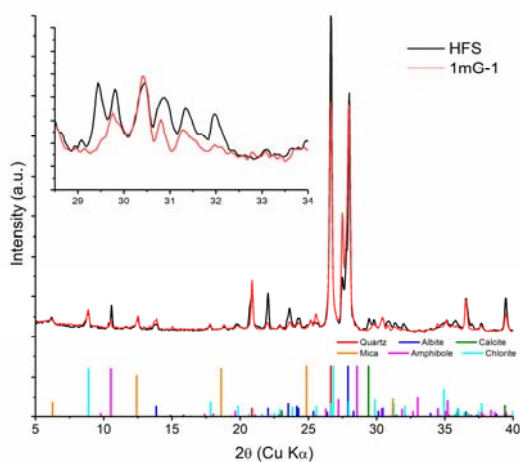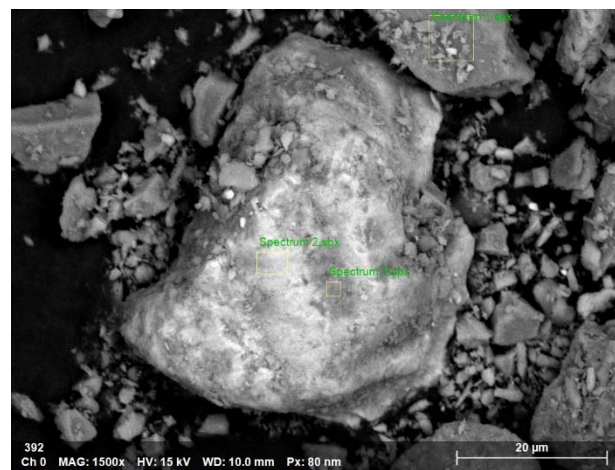
| (a) | (b) |

Spectrum	Carbon	Oxygen	Sodium	Magnesiu	Aluminiur	Silicon	Potassium	Calcium	Titanium	Iron
Spectrum 1.spx	0	0	1.399078	1.471652	20.41968	55.34444	15.66991	0.914562	0.289179	4.491507
Spectrum 2.spx	0	0	0.814016	2.856408	7.340665	28.39187	0.658454	1.001627	0.213511	58.72345
Spectrum 3.spx	0	0	0.594277	2.663641	10.71076	33.20933	1.104807	2.213982	0.264815	49.23839

Figure 5.26. (a) XRD showing the disappearance of calcite after treatment by the injected acidic ferric solution. The inset shows the absence of the strongest calcite peak at 29.4° 2Θ; other peaks vary in intensity due to preferred orientation effects; Electron backscatter image (b) shows bright Fe coatings, presumably precipitated HFO on a feldspar grain from the reacted sediment, where the EDS analysis shows that 49–59 at% and ~4.5 at% Fe was detected on the Fe-coated and non-coated areas, respectively.

5.2.8   Long-Term Stability of Precipitated Ferric Oxide

After HFO in situ precipitation, the stability of the precipitated HFO was tested with an extended AGW leaching process up to 135 PVs. The flow velocity for the AGW leaching was the same as the velocity used for ferric solution injection on each column (2.0–21.4 m/day). Figure 5.27 shows that very limited Fe was detected in the flushing effluent, except the first two pore volumes, which mainly resulted from the remaining ferric solution in the pores after the Fe injection stopped. The Fe mass balance calculation from the two 1-meter glass column indicated that only < ~ 3.16 wt.% of the injected Fe was leached out of the column after more than 100 PVs.
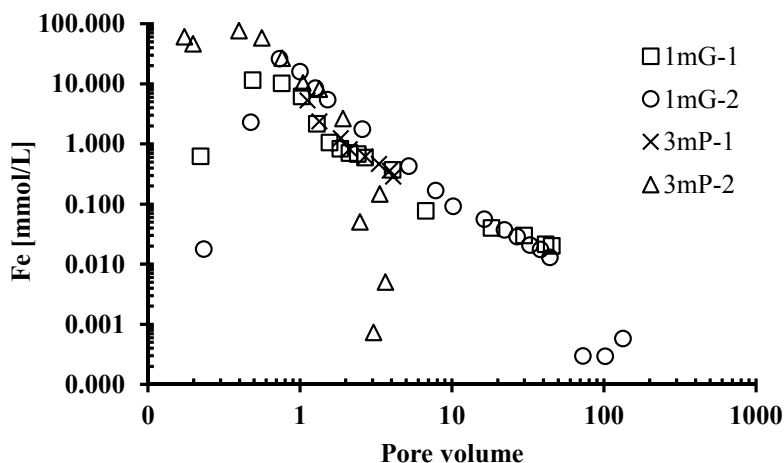
Figure 5.27. Effluent Fe signals during AGW leaching over 100 PVs. The low concentrations indicated ignorable amount of Fe leached out of the columns.

5.2.9 Iodate Immobilization using In-situ Precipitated HFO

One-dimensional column studies of iodate injection in the 1-meter glass columns were used to evaluate IO_3^- immobilization by the in-situ precipitated HFO, which served either as a PRB or through the adsorption/co-precipitation process in iodine plumes for a source term remediation. Because natural and anthropogenic I-127 (as iodate and iodide) in the HF sediments is present as aqueous, adsorbed (5% to 15%) and one or more precipitate phases (i.e., incorporated in Fe oxides and calcite), the performance of the HFO-precipitated sediments was tested against untreated sediments.

5.2.9.1 Iodate Source Area Remediation Evaluation

To evaluate source area remediation of iodate in aqueous solution and in precipitates, three 1-D column injection experiments were conducted: (1) pre-equilibration of the sediment, (2) injection of aqueous iodate into untreated sediment, and (3) simultaneous injection of aqueous iodate and the pH 1.5 ferric iron solution into sediment. For the pre-equilibration step, 12 PVs of AGW was injected (at 3.1 m/day, Table 5.1) into the untreated sediment. Effluent iodate concentrations were initially very high (> 2000 µg/L) and decreased to 5 µg/L by 11.5 PVs (Figure 5.28a), indicating high anthropogenic I-127 in the sediments. The fast iodine release may have resulted from an injection water with a different pH relative to the sediment. However, the iodine concentration rebounded after the 72-h stop-flow event, and the later tailing phase also indicated slow desorption or dissolution kinetics.

To evaluate iodate behavior in this pre-equilibrated, untreated sediment, an iodate solution of 100 µg/L was injected into the 1mG-2 column for ~13.5 PVs at an average linear velocity of 7.7 m/day (Figure 5.28b) Iodate breakthrough averaging 4.5 PVs (K_d ~0.8) indicates minimal sorption of the injected iodate in the untreated sediment.

Finally, iodate source area treatment was approximated by the simultaneous injection of the 0.1 M acidic ferric solution with 100 µg/L IO_3^- into the untreated sediment column (Figure 5.28c). As HFO precipitates, some iodate is incorporated. In addition, iodate (an anion) sorbs to HFO and other minerals strongly in the highly acidic water (i.e., anions sorb at low pH). Sorption of an ion is less in the presence of competing ions (i.e., the high ionic strength 0.1M acidic ferric iron solution). Results show that the IO_3^- concentration ratio of the effluent vs. injected (C/C_0) ranged from 0.53–0.77 under the injection average linear velocity of 3.1 m/day (Figure 5.28c, Table 5.1). The injection was stopped after ~8 PVs when the

effluent solution color turned brown in color. The elevated solution ionic strength in this system resulted from mineral dissolution during the acidic ferric solution injection (see Section 5.2.7). The adsorption contribution in the total IO_3^- immobilization here could be limited because low IO_3^- adsorption on HFO was expected under high ionic strength conditions (Wang et al. 2019). Therefore, co-precipitation could be the dominant process here for the IO_3^- immobilization. However, further investigation is needed to identify the respective contributions from the adsorption and co-precipitation processes.
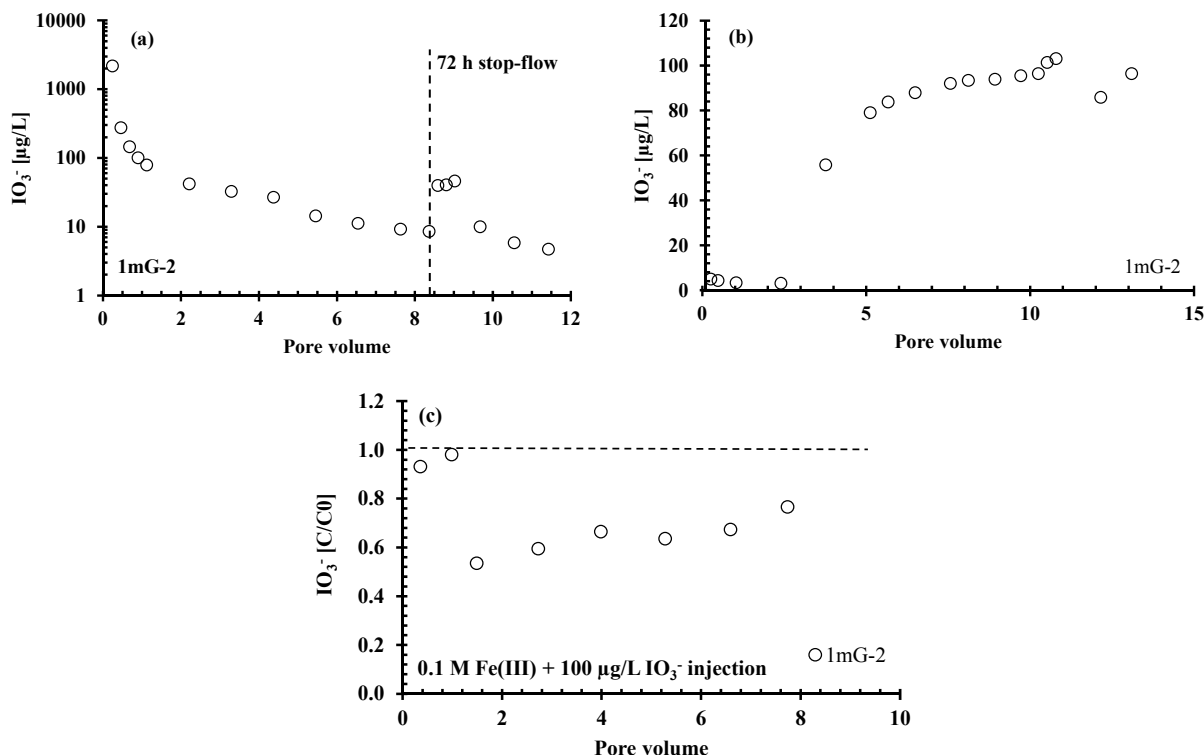
Figure 5.28. Source area evaluation of iodate with (a) pre-equilibration of the iodate-contaminated sediment with pH 8 AGW, (b) injection of 100 µg/L IO_3^- in the untreated sediment, and (c) simultaneous injection of 100 µg/L IO_3^- and 0.1 M ferric solution (pH 1.5) into the untreated sediment (i.e., source area treatment).

5.2.9.2   HFO Permeable Reactive Barrier Capture of Iodate

For the PRB test, HFO was first precipitated in the 1mG-1 column through the acidic ferric solution injection (8.77 PVs), followed by AGW (pH 7.9) flushing to return the column pH from the acidic solution injection condition to neutral. However, the effluent pH was still ~4.5, even after 45.5 PVs AGW flushing. Under this weak acidic condition, an IO_3^- solution of 100 µg/L was injected at an average linear velocity of 8.3 m/day. No IO_3^- breakthrough was observed until ~174 PVs, during which the effluent solution pH was kept nearly constant with an average value of pH 4.7 (Figure 5.29). This result indicated that the IO_3^- transport was strongly retarded through adsorption onto the HFO-amended sediments in the column. Unfortunately, it is not possible to directly compare this IO_3^- transport behavior with the one conducted on the untreated sediments because of the different pH conditions. Solution pH will strongly impact IO_3^- adsorption on to HFO where higher IO_3^- adsorption is expected at lower pH conditions (Wang et al. 2019). The effluent solution pH dramatically increased to ~pH 7.9 within several pore volumes after 174 PVs. Correspondingly, the effluent IO_3^- concentrations jumped, up to a maximum value of ~571.5 µg/L. This phenomenon may indicate that certain amount of the earlier-adsorbed IO_3^- desorbed and released back into the solution at the elevated pH conditions. The IO_3^- back-release process continued to

the end of the IO_3^- injection (238 PVs), where the effluent IO_3^- concentration was of 131.1 µg/L, close to, but still higher than the injected IO_3^- concentration of 100 µg/L. The 328-h stop-flow event conducted at ~221 PVs resulted in IO_3^- concentration rebound up to 258.9 µg/L, indicating a slow release of the adsorbed IO_3^- from the HFO-amended sediments.
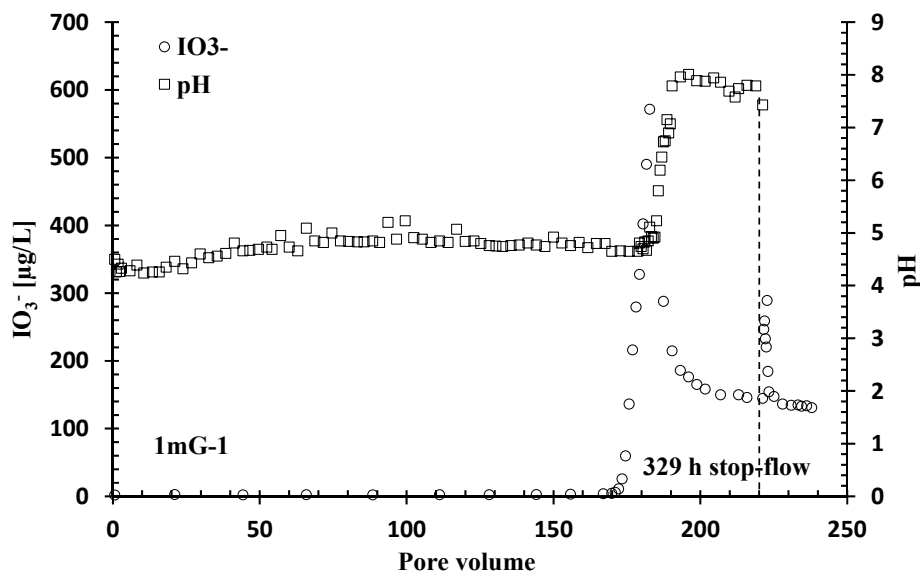
Figure 5.29. Strongly retarded IO_3^- transport through HFO-amended sediments in column 1mG-1 as a PRB at a pH <5 condition; earlier-adsorbed IO_3^- desorbed and released back into solution after pH increases to 8.0; the secondary Y-axis shows the corresponding pH changes during the adsorption process.

Desorption of IO_3^- from HFO-amended sediments. Leaching studies were conducted using AGW for more than 100 PVs after the IO_3^- injection in both the PRB- (1mG-1) and source term (1mG-2) columns. The leaching flow velocity used was the same as that used for IO_3^- injections, i.e., 8.3 or 3.1 m/day for 1mG-1 and 1mG-2 columns, respectively (Table 5.1). The effluent IO_3^- concentrations along the leaching are illustrated in Figure 5.30. For the source term-column (1mG-2; Figure 5.30(a)), after the initial 3-PV leaching, the effluent IO_3^- concentration was rapidly decreased to a tailing level of ~ 1.8 µg/L. This might indicate a strong retention of IO_3^- through the in situ HFO-IO_3^- adsorption/co-precipitation processes. In the case of the PRB-column (1mG-1), Figure 5.30(b) shows a slow rate of desorptive release of IO_3^- over the entire leaching process, including a concentration rebound signal after the 160-h stop-flow event conducted at 130 PVs. However, a direct comparison between the two column leaching is not possible, since the effluent solution pH from the source term column was still lower than 5.0 after more than 120-PV leaching; whereas, the leaching on the PRB column was conducted under neutral condition during the entire leaching process.

(a)   (b)
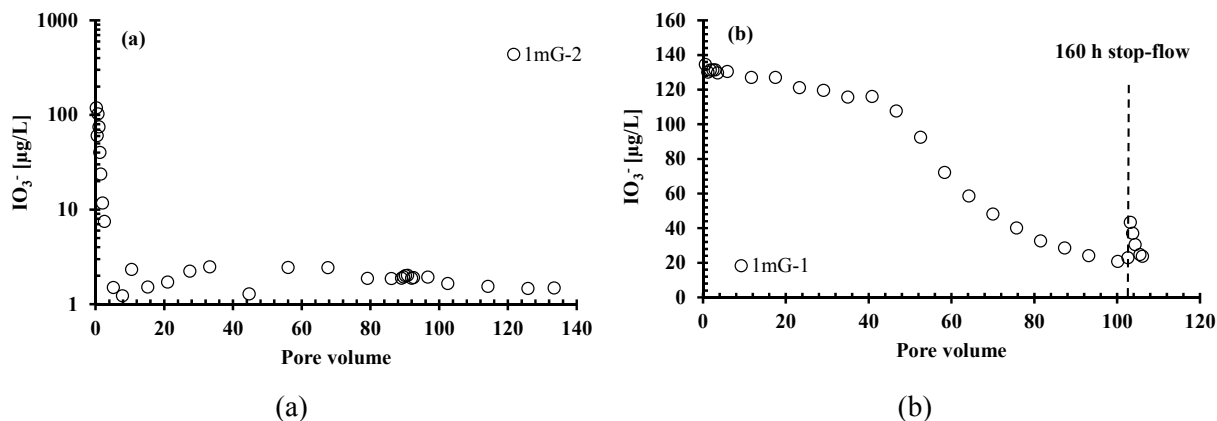
Figure 5.30. Long-term leaching of IO_3^- from (a) source term-column (1mG-2) and (b) PRB-column
            (1mG-1) using AGW under different pH conditions: the effluent pH values were < 5.0 and
            ~7.9 for 1mG-2 and 1mG-1 column, respectively.

Iodate mass balance. The iodine mass balance in the two reacted glass columns (1mG-1 and 1mG-2)
was calculated after experiments and the results are listed in Table 5.3. For each column, two sediment
samples were collected from different column locations (0–10 and 56–72 cm from column inlet), and the
extracted averaged IO_3- concentration was used for the total IO_3- mass calculation. Although the mass
recovery was relatively poor (~140%), the percentage of the immobilized IO_3^- was calculated based on
the alkaline-fusion-extracted IO_3^- on the treated sediments minus the extracted IO_3^- amount from the
untreated sediments; thus, the results are likely reliable. The results indicated that, after over 100 PVs of
leaching, about 48.9% and 41.3% injected IO_3- was still sequestrated in the HFO-amended PRB and
source term columns, respectively. However, more IO_3^- will be released back into solution along the
extended leaching process.

5.3 Summary of In Situ Ferric Iron Emplacement in Sediments and Use for Iodine Sequestration

A ferric iron solution at pH 1.5 was injected into 1- and 3-meter columns, resulting in precipitation of
HFO. The low pH front migrated slowly, with a retardation factor of about 170. Significant calcite
dissolution occurred during the acidic injection, as evidenced by increased aqueous carbonate, gas phase
CO_2, and increased aqueous calcium. Calcite precipitated downgradient as the pH was buffered. This
calcite dissolution/precipitation could be problematic at the field scale, lowering the permeability at some
distance downgradient of the point of injection. AGW injected into the treated columns at two velocities
for 135 PVs showed very low iron leaching (< 3.2%), indicating the precipitated HFO was stable in the
pH buffered sediment.

The use of HFO precipitation was tested for immobilization of iodate in Hanford formation sediments
was tested as (a) source area treatment of iodine-contaminated sediment, and (b) PRB to capture
upgradient aqueous iodate. For source area treatment, the simultaneous injection of 100 µg/L iodate with
the pH 1.5 ferric iron solution resulted in precipitation of 23% to 47% of the iodate, likely within
ferrihydrite (HFO). There may be additional decrease in iodine leaching release from precipitates in the
sediments due to the HFO coating on surfaces, because iodine-contaminated sediments contain 5% to
15% aqueous iodine with the remainder of mass incorporated in one or more precipitate phases including
Fe oxides and calcite.

As a PRB, injection of 100 µg/L iodate into HFO-modified sediment showed complete removal for 170)PVs due to the low pH (i.e., high iodate sorption in the pH 1.5 to 5.0 sediment), after which 50% to 60% of the iodate was rapidly released into aqueous solution at a high concentration (up to 600 µg/L). The breakthrough curve is characteristic of ion exchange, and may indicate that initially H^+ saturated sites (with iodate sorption under acidic conditions) were exchanged by Ca^{2+} and Mg^{2+} (and to a lesser extent Na^+ and K^+) in the AGW by 170 PV, after which the pH 8 solution exhibits minimal iodate sorption. In a study of cation exchange in Hanford formation sediments from the 100N Area, the retardation factor for Ca^{2+} was determined to be 125 based on the sediment with a cation exchange capacity of 2.0 meq/g (Szecsody et al. 2008). The Hanford sediment used in this study may have a slightly higher cation exchange capacity.

The fraction of iodate that remained immobile (40% to 50%) after 170 to 300 PVs is significant for experiments that lasted several weeks, but it still underperforms relative to the need to reduce radioiodine concentrations from 30 to 1 pCi/L in the field. Moreover, stable iodine concentrations can be up to 1000 times higher in groundwater than radioiodine, which will behave geochemically the same. The simultaneous I-127 (high concentration) and I-129 (low concentration) injection into an HFO-modified sediment column and evaluation of I-129 uptake has not been investigated. Iodate incorporation into HFO is likely responsible for this long-term behavior. However, potential negative impacts from HFO precipitation include: (a) localized metals mobilization in the treatment zone from the pH 1.5 solution, (b) permeability change resulting from the calcite dissolution and downgradient precipitation, (c) potential permeability change resulting from the HFO precipitation, and (d) density effects of the pH 1.5 solution injection. While some aspects of the side effects were evaluated in 1- to 3-meter columns, additional experiments are needed in field-realistic radial flow systems to determine the potential for deleterious impacts.

6.0 Dithionite-Enhanced Iodine Mobility

6.1 Introduction

The purpose of investigating an aqueous reductant, Na-dithionite, for remediation of iodine in Hanford sediments is to remove aqueous iodide and iodate as well as some iodate incorporated into iron oxides. Sequential liquid extractions conducted on vadose zone sediments beneath the Hanford Site B, T, and S complexes showed that 2% to 15% of the total I-127 mass was aqueous and adsorbed, with the remainder in unidentified precipitates (Truex et al. 2017; Szecsody et al. 2017). It is hypothesized that iodine-contaminated Hanford sediments have a higher proportion of iodine in Fe oxides than in calcite. Dithionite treatment of sediments dissolves some ferric oxides (20% to 40%), and reduces ferric species to ferrous, which precipitate as multiple ferrous phases. The dithionite also reduces aqueous and adsorbed iodate removed from the dissolved ferric oxides. Because iodine is actually made more mobile, this reduction technology is designed to be used to enhance the P&T system by removing more iodine from the sediments more quickly compared with just pumping groundwater. As a laboratory study of the potential use of a technology for iodine remediation, the specific objectives are as follows:

- Na-dithionite solution type (i.e., bicarbonate and citrate) and iodine removal efficiency from sediments

- Na-dithionite concentration and iodine removal efficiency from sediments

- Identify the surface phase(s) that are dissolving and releasing iodine

- Long-term leaching of iodine from sediments after dithionite treatment

- Evaluate the applicable of dithionite treatment to sediments from different waste sites that may contain different co-contaminants and have iodine incorporated into different solid

To maximize the iodine removal from sediments, experiments used different reductant solutions, reductant concentration, and the time dependency of reduction. Experiments removing iodine from sediments were conducted at low sediment/water ratio in batch systems and at high sediment/water ratio in 1-D leach columns to evaluate the effect of continuous solution removal that would occur during field-scale injection. Changes in iodine incorporated into surface phases as a result of the reductive treatment were characterized by X-ray absorption near edge structure (XANES) and XRF. Changes in Fe oxides were also quantified by iron extractions as were changes in calcite (another phase that can incorporate iodine). Iodine-127 was primarily used because it exhibits similar geochemical behavior to I-129 and is present in detectable concentrations in all Hanford sediments, although some I-129 experiments were conducted.

Hanford area wells previously sampled for I-127 averaged 13.1 ± 2.3 µg L^{-1} and for I-129 averaged 0.0105 $\pm$ 0.0149 µg L^{-1} (1.85 ± 2.48 pCi L^{-1}) (Lee et al. 2017), whereas sediments averaged 0.016 ± 0.016 µg g^{-1} I-127 (Szecsody et al., 2017). Iodine-127 is present at all depths in groundwater as it is naturally occurring at low concentrations, although additional anthropogenic I-127 releases to the Hanford vadose zone have also migrated into groundwater. Although I-127 and I-129 varied with depth and location, the I-129 concentration was greatest just below the water table.

Although other technology evaluations in this report are focused on iodate immobilization, enhanced mobilization may be appropriate for enhancing capture with a groundwater P&T system. Currently, the Hanford Site is using the 200 West P&T system to develop a zone of hydraulic containment for I-129. In 2017, over 400 million gallons of water was injected across the three wells (average rate of 777 L/min) to reduce migration of the I-129 plume in the 200-UP-1 OU (DOE-EM 2009). Sequential liquid extractions

conducted on 15 vadose zone and aquifer sediments from the Hanford subsurface showed that of the total I-127 mass associated with the sediment $3.0 \pm 4.2\%$ was aqueous and $2.1 \pm 3.1\%$ was sorbed, with the remainder in operationally defined solid phases that included $27.5 \pm 16.4\%$ in a pH 5 acetate extraction, $46.5\% \pm 18.0$ in a pH 2.3 acetic acid extraction, and $20.9 \pm 13.1\%$ in an NH_4-oxalate extraction (Szecsody et al. 2017; Truex et al. 2017). Acetate extractions typically dissolve carbonates, although they can dissolve some Fe oxides, and the NH_4-oxalate extraction dissolves primarily amorphous Fe oxides (Chao and Zhou 1983). While these sequential extractions are operationally defined, these data highlight that some iodine is present in more mobile (aqueous/adsorbed) fractions while other fractions are less labile (Larner et al. 2006; Mossop and Davidson 2003). Whereas groundwater is predominantly iodate, identification of the iodine species in the vadose zone cores showed that five of eight cores were iodide dominated, two of eight cores were iodate dominated, and one core had equal iodide and iodate mass. While these results show that the vadose zone sediments and pore water are iodide-dominated, iodine species measurements in groundwater are nearly all iodate, although there are only a limited number of measurements. A vertical profile in groundwater at depths ranging from at the water table to 34 ft below the water table (Lee et al. 2017); iodide was 55% of the mass at the water table, but iodate dominated all deeper locations.

Because iodide and iodate exhibit low sorption, leaching of iodine-contaminated sediments should release iodide first (K_d 0.07 mL/g to 0.1, Rf in Hanford sediments 1.3 to 1.5; Truex et al. 2016), then iodate (K_d 0.3 mL/g to 1.2, Rf in Hanford sediments 2.4 to 6.2), so by 10 pore volumes (PVs), adsorbed iodide and iodate should be released from sediments. A comparison of iodine leaching behavior from 11 sediments from the B, T, and S complexes, however, indicated that while the highest iodine concentrations were released within the first few pore volumes, the amount of iodine mass leached by 10 PVs represented only $54.7\% \pm 14.2\%$ of the total iodine mass released from the sediment over 100 PVs. Therefore, while aqueous and adsorbed iodate/iodide is the most mobile mass (and needs to be remediated), this represents only 55% of the readily mobilized mass in the Hanford subsurface (Figure 6.1). Clearly, solid phases are being dissolved, releasing additional iodine species.

It has been hypothesized that iodine is incorporated in calcite, Fe-oxides, and possibly other precipitates. Slow dissolution of these phases can release iodine species to groundwater, even under natural conditions. For example, calcite in natural Hanford subsurface is in equilibrium with the aqueous calcium, magnesium, and carbonate aqueous species, but there is still continuous calcite dissolution and re-precipitation with no net dissolution or precipitation. During this exchange process, iodate can be released to aqueous solution. Calcite, amorphous Fe oxides such as ferrihydrite, and crystalline oxides such as goethite have moderate solubility, as opposed to very low solubility (stable) minerals such as quartz or apatite. In addition, waste operations can accelerate dissolution of some of these phases. In the Hanford 100K Area, P&T operations withdraw pH 7.5 water but reinject pH 5.5 to 6.2 water, which is causing some dissolution of calcite near injection wells and downgradient calcite precipitation once the pH has been neutralized. During this process, C-14 and Sr-90 incorporated in the calcite have been released to aqueous solution. If in iodate-laden sediments, the injection of acidic water dissolving calcite and some Fe-oxides would release significantly greater iodate into groundwater than the natural groundwater.
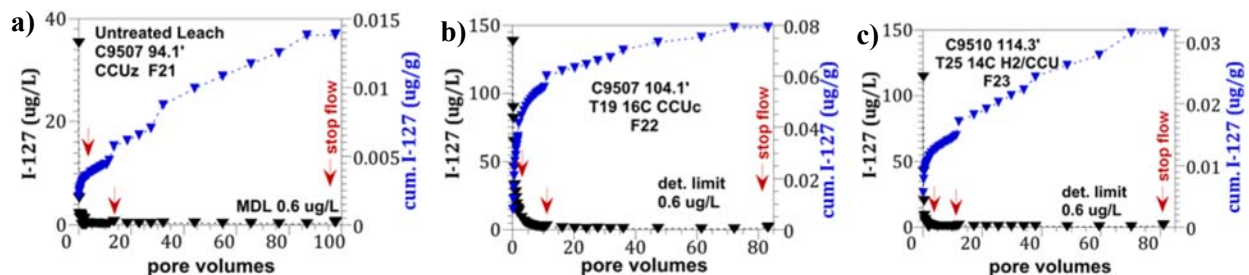
Figure 6.1.   Iodine-contaminated Hanford vadose zone sediments showing AGW leaching of: a) C9507 94.1' sediment, b) 9507 1104.1' sediment, and c) C9510 114.3' sediment.

Sodium dithionite ($Na_2S_2O_4$, sodium hydrosulfite) is a strong aqueous reductant that is used for industrial dyeing, pulp processing, water treatment, and cleaning in a wide variety of industries. In geosciences, it is used for enhanced oil recovery, as crystalline ferric iron extraction process (DCB extraction), and for creation of a subsurface reduced PRB (Szecsody et al. 1998). Sodium dithionite by itself will react with ferric oxides in sediment:

$$S_2O_4{}^{2-} + 4Fe^{3+} + 2H_2O <=> 4Fe^2 + 4H^+ + 2SO_3{}^{2-}$$
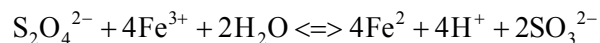
dissolving and reducing the ferric phases to multiple ferrous phases, including (1) adsorbed Fe^{2+}, (2) FeS, (3) $FeCO_3$ (Szecsody et al. 2004), and (4) structural Fe(II) in 2:1 clays (Stucki et al. 1984). The produced sulfite will oxidize to sulfate. Note that 1 mole of dithionite reduces 4 moles of iron and produces 4 moles of H^+, so the system (with no pH buffer) will become as acidic as pH 2.3, which results in mainly aqueous ferrous iron (along with dissolving other minerals; Szecsody et al. 2004). The addition of 4 moles of K_2CO_3 pH buffer at pH 12 with each mole of Na-dithionite results in an initial pH of 12, but after reaction with sediments, a pH of 8 to 9. This mixture of Na-dithionite and K_2CO_3 pH buffer has been successfully deployed at the Hanford 100D Area for chromate reduction and in a limited number of other field sites for chromate, trichloroethylene (TCE) (Vermeul et al. 2002), and energetic RDX remediation (Szecsody et al. 2001). Because the goal of the dithionite-K_2CO_3 treatment is to create solid ferrous phases (for a PRB), the pH needs to be neutral to alkaline (as ferrous iron desorbs under acidic conditions). A mixture of Na-dithionite, potassium carbonate, and sodium citrate (i.e., DCB extraction) has been used for decades for characterization of the total amount of amorphous and crystalline ferric oxide in sediments (Heron et al. 1994; Chao and Zhou et al. 1983). In contrast, the DCB extraction is designed to dissolve ferric oxides, reduce the iron, but maintain the ferrous iron in aqueous solution by complexation with citrate so that the total amount of ferrous iron can be measured.

For this study, Na-dithionite (with one or more additional chemicals) treatment of sediments is for (1) reduction of aqueous and adsorbed iodate as iodide species exhibit less sorption, and (2) dissolution of amorphous and crystalline ferric oxides that contain iodate/iodide, and maintain iodide (the product) aqueous. The efficiency of three different Na-dithionite solutions (i.e., Na-dithionite by itself, Na-dithionite and K_2CO_3, and DCB) are compared in terms of the efficiency for iodine removal from field-contaminated sediments.

6.2   Experimental Methods

Batch experiments were conducted to identify appropriate concentration ranges of dithionite to release and maintain iodine mobility by converting iodate to iodide and by dissolving iron oxides on sediment surfaces, releasing iodine species to aqueous solution. These experiments were designed to bound the appropriate concentration ranges and evaluate potential analytical interferences with iodine quantification.

6.2.1   Sediments

Iodine-contaminated subsurface sediments were collected from boreholes at the 200 West Area of the Hanford Site (Table 6.1). Because iodine speciation differed between vadose zone and aquifer sediments, both saturated and unsaturated sediments in different geologic formations beneath different waste sites were collected. Most sediments contained co-contaminants from former waste streams, which may influence iodine adsorption and incorporation processes. For example, sediments reacted with high ionic strengths (e.g., Na^+, NO_3^-, Table 6.1) would decrease sorption of iodide and iodate. In the sediments exposed to elevated uranium concentrations, there may also be competition between uranium and iodine for incorporation into calcite and Fe-oxides.

Table 6.1.   Major characteristics of iodine-contaminated sediments collected from the Hanford Site and used in experiments.

Sediment[a]	Well #	Depth (ft)	Geologic Formation	Co-contaminants
1	C9487	58.2 - 59.2	Hanford H2	Na, NO_3, ^{99}Tc, U
2, 2d[b]		230.0-231.0	Cold Creek	Na, NO_3, U
3	C9488	219.3–220.3	Cold Creek	Na, NO_3, Cr
4	C9507	94.1-95.1	Cold Creek	Na, NO_3, U, Cr
5		104.4-105.4	Cold Creek	Na, NO_3, U, Cr
6, 6d		137.1-138.1	Ringold	Na, NO_3, U
7, 7d	C9510	114.3-115.3	Hanford H2	Na, NO_3
8	C9411	258.0-259.0	Ringold	NO_3
9	C9567	284.0-285.0	Ringold	U
10	C9414	283.3-284.5	Ringold	U, ^{99}Tc
11, 11d	C9415	316.8-327.8	Ringold	NO_3, ^{99}Tc, U
12	C9412	296.4-297.4	Ringold	NO_3, ^{99}Tc, U
13, 13d	C9602	375.8-376.5	Ringold	Cr
14	C9497	237.0-238.0	Cold Creek	Na, NO_3

(a)   Sediments 8 to 13 are from the unconfined aquifer, others are vadose zone.
(b)   d: duplicate experiment or analysis.

6.2.2   Na-Dithionite Solution Chemistry and Concentration

Batch experiments were conducted to evaluate the efficiency of iodine removal from sediment using (1) 0.1 mol/L Na-dithionite, (2) 0.1 mol/L Na-dithionite and 0.4 mol/L K_2CO_3, and (3) 0.1 mol/L Na-dithionite and 0.4 mol/L K_2CO_3 and 0.6 mol/L Na-citrate. The batch experiments consisted of 3.0 g of sediment with 30 mL of the extraction solution in a 45-mL Teflon centrifuge tube for 200 h. In addition, a fourth experiment was conducted in which the 0.1 mol/L Na-dithionite and 0.4 mol/L K_2CO_3 solution was reacted with the sediment for 3 days, then a new 0.1 mol/L Na-dithionite and 0.4 mol/L K_2CO_3 was added each 3 days (repeated four times) to evaluate repeated treatment efficiency. The concentration of iodine (I-127) was measured in all four vials.

A series of batch experiments was conducted to evaluate the efficacy of variations of buffered Na-dithionite extractant solution (0.01 mol/L Na-dithionite, 0.04 mol/L K_2CO_3, and 0.004 $KHCO_3$) for removal of iodine from iodine-contaminated sediments. In these experiments, the Na-dithionite

concentrations in the final solutions were varied from 0.001 to 0.1 mol/L. The experiments were conducted in an anaerobic chamber to remove the influence of oxygen oxidizing the Na-dithionite solution. Selected experiments were repeated with the same solution, but with oxic water.

The batch experiments consisted of 3.0 to 10.0 g of sediment and 30 mL of the extraction solution in a 45-mL Teflon centrifuge tube. Samples of 3.0 mL were taken at multiple time periods, ranging from 0.1 to 100 h. Collected samples were passed through a 0.45-micron filter before iodine species analysis. Analyses were conducted by ion chromatography, liquid scintillation counting, or ICP-MS. Multiple iodine-contaminated sediments were used, and sequential liquid extractions were conducted before the leach studies. After the last liquid sample was taken, sequential liquid extractions were conducted to measure adsorbed and incorporated iodine.

6.2.3   Evaluate Solid Phases Mobilized by Na-dithionite

A series of batch experiments was conducted with varying reductant (Na-dithionite) concentration in different Hanford sediments, and the aqueous solutions were analyzed for ions that are from the dissolution of Fe/Mn oxides (Fe, Mn, Ti) and carbonates (Ca, Mg, U by ICP-OES, aqueous carbonate by carbon analyzer). These sediments were also analyzed for iron oxides before and after dithionite treatment using iron extractions and solid phase inorganic carbon (i.e., carbonates).

Sequential extractions were conducted to estimate specific association relationships of contaminants or other components with specific phases. The reagents used and their intended targets were as follows. AGW targeted aqueous contaminants. The extractant 0.5 mol/L HCl targeted the adsorbed fraction, pH 5 acetate targeted some carbonates and amorphous Fe oxides, pH 2.3 acetic acid targeted nearly all carbonates and Fe oxides, 0.1 M ammonium oxalate/oxalic acid targeted any remaining Fe-oxides, and 8 M nitric acid at 95°C targeted some aluminosilicates, phosphates, and oxides (defined as the hard to extract contaminant fraction).

The extractions were conducted in 45-mL Teflon centrifuge tubes at a sediment/liquid ratio of 1:2. For each set of 20 samples, a set of six preparation blanks and six blank spikes were performed. The set of six blanks consisted of the six solutions (i.e., extractions 1 through 6). The set of six blank spikes consisted of the six extraction solutions spiked with the contaminant(s) of interest. In addition, one duplicate sediment sample was conducted for each batch of 20 samples.

For the first extraction, 20 mL of AGW was mixed with 10 g of sediment in a 45-mL centrifuge tube (with O-ring seal) for 50 min on a slow (6-rpm) rotary mixer. The tube was then centrifuged at 3000 rpm for 10 min. Liquid was drawn off the top of the sediment and filtered (0.45-μm nylon/PVDF) for analysis. This process was then repeated for each of the other five extractants.

Additional extractions for total iodine in sediments were conducted based on previous research that demonstrated quantitative removal of iodine from certified standard sediments via extraction with 5% tetramethylammonium hydroxide (TMAH) (McNally 2011; Watts and Mitchell 2008). Briefly, 1 g of sediment was reacted with 20 mL of 5% TMAH (50-g/L solution) at 70°C for 3 h and shaken approximately every 15 min. Selected samples were digested in duplicate or triplicate to confirm reproducibility of this method. Upon sampling, all tubes were centrifuged and filtered as described for leaching experiments. Extractions for iron were also conducted before and after TMAH extractions to investigate whether these methods removed iodine that was associated with Fe phases. Amorphous Fe was extracted via 0.25 M NH_2OH-HCl at 70°C for 30 min. Crystalline and amorphous Fe were extracted with 0.3 M citrate – 0.06 M Na-dithionite – 1.0 M Na-bicarbonate (DCB) with reaction of 10 mL with 1 g of sediment at 80°C for 30 min. Total Fe was analyzed based on reaction of 10 mL of 5 M HCl with 1 g of sediment at room temperature for 5 days.

6.2.4   Evaluate Long-Term Stability of Iodine Remaining in Sediment

A series of batch experiments was conducted with selected sediments that received the dithionite treatment to evaluate the long-term stability of iodine remaining in the sediment after the dithionite extract (and iodine mobilization) was removed. These batch experiments used the sediments extracted as described in Section 5.1.1, but after the sediments had been washed three times with AGW.

The batch experiments consisted of 3.0 to 10.0 g of cleaned sediment and 35 mL of AGW in a 45-mL Teflon centrifuge tube, with 3.0-mL samples taken at multiple time periods ranging from 0.1 to 1500 h. The samples were passed through a 0.45-micron filter before iodine species analysis. Iodine species analysis was conducted by ICP-MS. Multiple iodine-contaminated sediments were used, and sequential liquid extractions were conducted before these leach studies. After the last liquid sample was collected, sequential liquid extractions were conducted to measure adsorbed and incorporated iodine.

Column experiments were also conducted to evaluate the rate at which iodine is released from sediments at near field sediment/water ratios using the dithionite solution, and the long-term immobilization of the remaining iodine in the sediment after dithionite-mobilized iodine is removed. These column studies were conducted at different flow rates on selected sediments used as described in Section 5.1.1. In contrast to the batch leaching experiments (Section 5.1.1), the column leach experiments had a high sediment/water ratio similar to that in the field, which will likely result in greater iodine species interactions with mineral or organic phases in the sediment and slower dissolution of Fe-oxides and iodine release.

In these column experiments, sediment was reacted with the AGW for different time periods as water flowed through the sediment (approximating groundwater flow through contaminated sediment). Each column experiment was unique in terms of the exact flow rate, mass of sediment, size of column, and the change in concentration of contaminant(s) leaching from the sediment.

Moist sediment was packed into a column, ranging in size from 0.77-cm diameter by 10-cm length to 2.6-cm diameter by 100-cm length. The weight of the moist sediment in the column was determined. The moisture content of the moist sediment was determined by weighing 3 to 5 g of moist sediment before and after drying for 48 h at 105°C. The packed column was then water-saturated by injecting AGW into one end of the column until water exited the effluent end of the column. The dry bulk density of the sediment was calculated from the dry sediment weight in the column divided by the column volume. The pore volume, or total water weight in the column, was calculated from the weight of the water in moist sediment plus weight of the water added to saturate the column. The porosity was calculated from the total water weight in the column divided by the column volume.

The injection solution (AGW) was modified to contain 80 mg/L bromide as a conservative tracer. The column experiment consisted of injecting AGW into one end of the column at a constant flow rate to achieve a 1- to 4-h residence time for a total duration of 10 to 200 PVs (depending on the contaminant). Liquid samples were collected in sufficient number and frequency to measure the change in concentration of the contaminant(s), which was typically 30 or more samples. These samples were collected using a timed fraction collector (Isco Foxy 200 or other), which contained either 4.5- or 15-mL falcon tubes to collect effluent samples. More effluent samples were collected in the first two pore volumes, with less frequent sample collection for subsequent pore volumes. Stop-flow events ranging from 10 to 1000 h with no flow were used to provide additional time for contaminants present in one or more surface phases on the sediment surface to partition into the pore water.

6.3 I-127 Results and Discussion

6.3.1 Iodine Surface Phase Characterization in Field-Contaminated Sediments

Iodine is present in vadose zone and aquifer sediments in multiple phases, from aqueous, adsorbed, and precipitated phases. To evaluate the efficiency of using Na-dithionite to remove iodine from sediments, characterization of the different iodine species in field-contaminated sediments prior to treatment was conducted. Sequential liquid extractions on 11 different sediments (Table 6.2) removed low concentrations of aqueous and adsorbed I-127 (Figure 6.2a, red squares) with much greater I-127 associated with the pH 5 and pH 2.3 acetate extractions (targeting carbonates; Figure 6.2a, orange and yellow diamonds,) and lower concentrations of I-127 in the ammonium oxalate extraction (targeting amorphous Fe-oxides, light green triangles). The nitric acid extraction was not conducted on all sediments, but showed additional I-127 in more difficult-to-dissolve phases. Both vadose zone and aquifer cores showed less than 10% of the total I-127 mass was aqueous and adsorbed, 50 to 80% was associated with both acetate extractions (targeting carbonates, although may also dissolve some Fe oxides), and 10 to 20% was associated with NH_4-oxalate extraction (targeting Fe oxides). Targeted removal of the mobile iodine (i.e., aqueous and adsorbed iodine) and easily dissolved iodine (i.e., in acetate or oxalate extractions) with dithionite treatment could effectively remove leachable iodine from sediments.

Analysis of the groundwater-extractable I-129 for select samples was conducted to compare the two isotopes. The vadose zone sediments 5, 6, and 7 showed an average I-127/I-129 ratio of 18.8 (i.e., low I-129), whereas aquifer sediment 8 had an I-127/I-129 ratio of 0.22 (Table 6.2). These results highlight that the two isotopes are likely from different sources and may be present in different solid phases.

A thin section of untreated sediment 5 was also analyzed by XANES to evaluate the valence state. Although the total I-127 in this sample was the highest of the field-contaminated sediments evaluated (1.26 µg g^{-1} removed via extractions, Table 6.2), the low concentrations made iodine oxidation state identification difficult (Figure 6.2b-c). The XANES analysis was inconclusive (approximately 50% iodate and 50% iodide) due to significant noise in the spectra at the low concentrations (Figure 6.2c). However, elemental analysis of three locations via µ-XRF suggested that iodine is present with predominantly iron phases (Figure 6.2b).

Table 6.2. Iodine-127 and -129 mass and rate of release in untreated (artificial groundwater) and dithionite/carbonate-treated sediments from both batch and column experiments.

Sed.	Treatment	Exp. Type	Rxn Time (h)	I-127 Rel. (μg/g)	I-129 Rel. (μg/g)	I-127 Rel. Rate (μmol IO$_3$ h^{-1} mol^{-1}Fe^{II})
1	AGW	1D leach	750	1.12E-02		7.65E-03
	AGW	batch	1000	8.11E-03		4.15E-03
	dith./CO$_3$	batch	170	1.94E-02		2.69E-02
4	AGW	batch	1000	7.00E-03		9.13E-03
	dith./CO$_3$	batch	170	2.32E-02		9.48E+01
	dith./CO$_3$	batch	300	3.45E-02		4.02E+00
	dith./CO$_3$	batch	1000	4.11E-02		4.36E-01
	AGW	1D leach	525	1.39E-02		9.61E-03
	dith./CO$_3$	1D leach	743	3.67E-01		8.28E+01
5	AGW	batch	1000	5.76E-02	1.49E-3[a]	1.92E-02
	dith./CO$_3$	batch	170	4.86E-01		5.93E+02
	dith./CO$_3$	batch	300	8.61E-01		6.44E+01
	dith./CO$_3$	batch	1000	1.05E+00		6.03E+00
	AGW	1D leach	525	7.93E-02		2.66E-02
	dith./CO$_3$	1D leach	743	1.26E+00		4.32E+01
6	AGW	batch	1000	1.01E-02	7.16E-3[a]	1.66E-03
	dith./CO$_3$	batch	170	4.06E-02	3.05E-2	1.92E-02
7	AGW	batch	1000	3.02E-02	1.85E-3[a]	2.14E-01
	dith./CO$_3$	batch	170	3.43E-01		1.11E+03
	dith./CO$_3$	batch	300	5.61E-01		1.05E+02
	dith./CO$_3$	batch	1000	6.87E-01		1.13E+01
	AGW	1D leach	525	3.17E-02		4.28E-01
	dith./CO$_3$	1D leach	743	8.63E-01		2.60E+01
7d	AGW	1D leach	750	1.33E-02		1.53E-01
	dith./CO$_3$	batch	170	3.39E-01		9.99E-01
8	AGW	batch	170	2.43E-3	1.08E-2	
	dith./CO$_3$	batch	170	4.80E-1	1.07E-1	

(a) 170 h
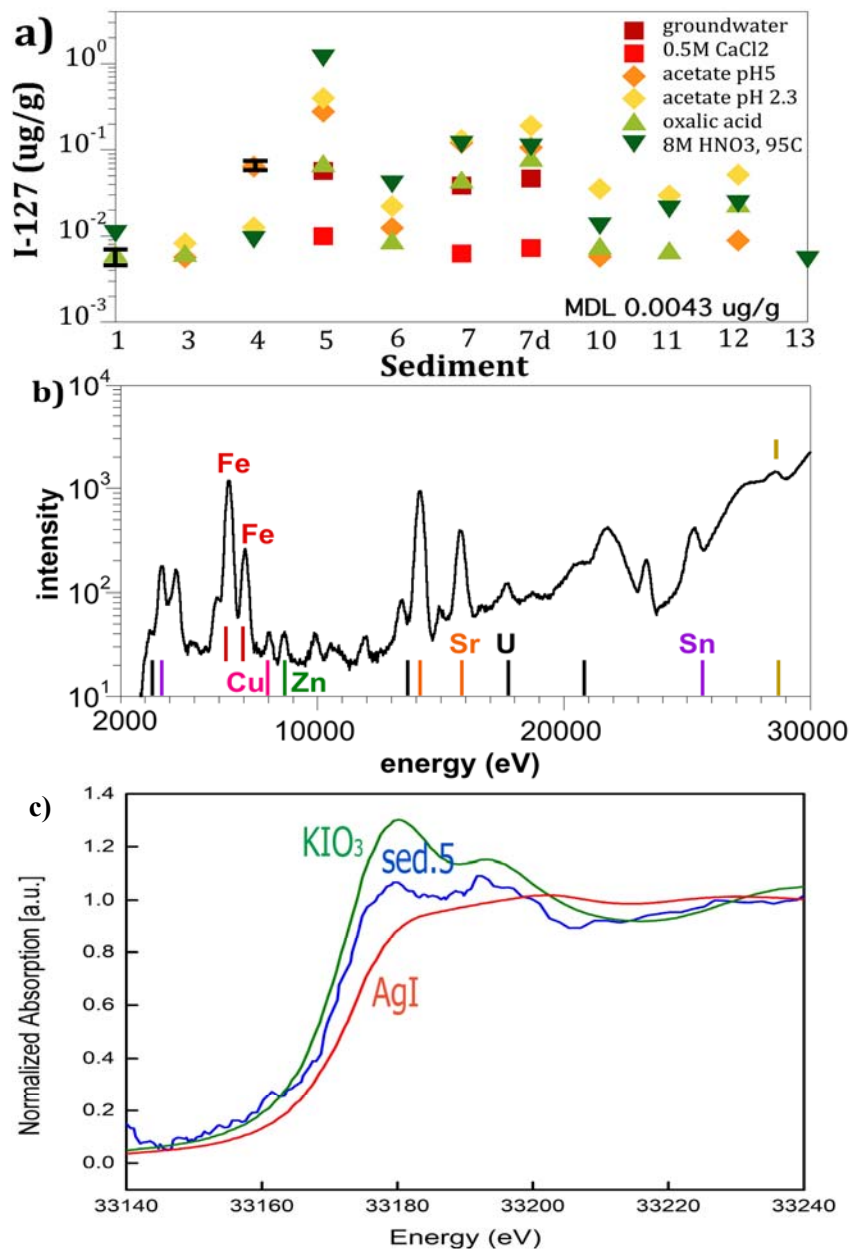
Figure 6.2. Iodine-127 present in field-contaminated sediments as shown by a) sequential liquid extractions, b) sediment 5 analysis by XRF elemental associations, c) sediment 5 XANES K-edge data confirming primary species as I^{+7}.

6.3.2   Different Na-Dithionite Solutions and I-127 Removal

Experiments with Na-dithionite with additional chemicals showed that the addition of the K_2CO_3 pH buffer enhanced the I-127 removal from the sediment by 20% (second vs. first set of bar graphs, Figure 6.3a), but the addition of Na-citrate decreased the I-127 removal by 7%. More time (i.e., reaction time of 1000 h versus 170 h) increased the I-127 removal from the sediment an average of 40%, even though the Na-dithionite itself is no longer reactive after a few days due to dissociation in water to sulfate, although FeS precipitates may have continued to react with Fe oxides. Additional time-dependency of I-127 removal is described in the next section. Repeated washing with a fresh Na-dithionite and K_2CO_3

every few days also increased I-127 removal from the sediment to 15% compared to the same solution and contact time with no solution replacement (last set of four bar graphs, Figure 6.3a). Note that this is a similar effect to injection of the solution into sediment (i.e., over time, fresh Na-dithionite solution contacts the sediment). Therefore, the recommended treatment is Na-dithionite with K_2CO_3, leaving the solution in situ. Since the ultimate products of Na-dithionite injection are Na^+, SO_4^{2-}, K_+, and CO_3^{2-}, previous field-scale injections have had regulatory approval to leave the spent solution in place. Experiments varying the Na-dithionite and K_2CO_3 solution concentration showed that while higher concentrations removed greater I-127 from the sediment, there was a decrease in efficiency at a Na-dithionite concentration > 0.03 mol/L (Figure 6.3b). With a 3 times increase in concentration from 0.01 to 0.03 mol/L Na-dithionite, I-127 extracted increased from 0.18 to 0.343 µg/g (90% increase), but the 3 times increase from 0.03 to 0.1 mol/L resulted in I-127 increase to 0.455 µg/g (33% increase).
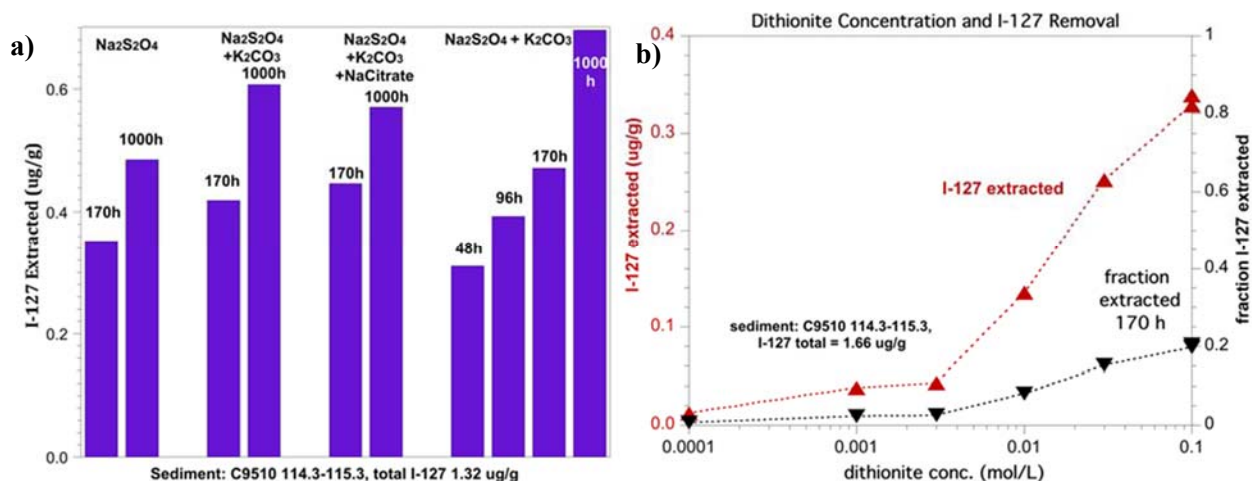
Figure 6.3.   Iodine removal from a field-contaminated sediment using a) Na-dithionite solutions of differing composition, and b) differing Na-dithionite concentrations.

A total of 21 different iodine-contaminated vadose zone and groundwater sediments from the Hanford 200 Area were used in Na-dithionite treatments, as described in the following sections. The I-127 removed by Na-dithionite/K_2CO_3 solution (purple diamonds, Figure 6.4) varied considerably, as the total I-127 in different sediments varied. For sediments that had complete sequential extraction I-127 analysis (9 of 21 sediments), the Na-dithionite treatment of different iodine-contaminated Hanford vadose zone and groundwater sediments removed $61.9 \pm 21.2\%$ of the iodine from the sediment, in contrast to the aqueous plus adsorbed fraction of $11.7 \pm 14.3\%$ of the iodine in the sediment. The total I-127 in sediments was measured by sequential liquid extractions, although in earlier studies, the most acidic extraction solutions were not measured by ICP-MS (so the total I-127 is inaccurately reported). Total I-127 values reported in Figure 6.4 are accurate, as they account for the total I-127 removed from the sediment by extractions, leaching, and dithionite treatment. Dithionite removed 30% to 80% of the I-127 from the sediment. As shown in Section 6.3.6, dithionite treatment and leaching removed 22 to 38 times more I-127 compared with untreated leaching, leaving an I-127-depleted sediment.
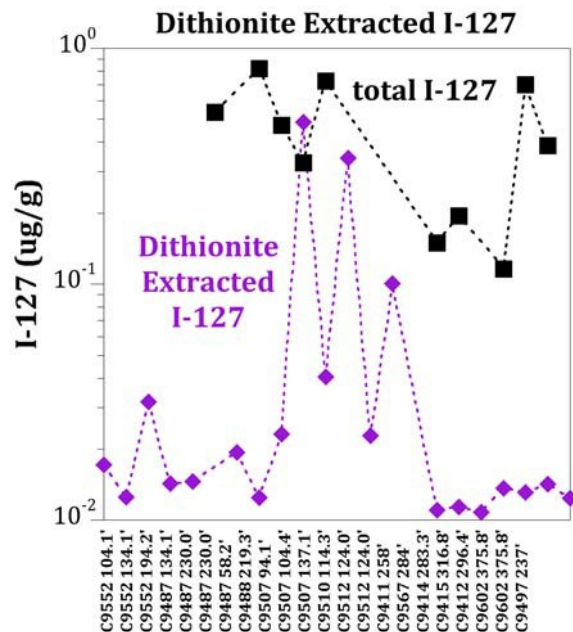
Figure 6.4.   Iodine removal from a field-contaminated sediments with Na-dithionite/K_2CO_3 in 170 h.

6.3.3   Contact Time and I-127 Removal with Na-Dithionite

Using a solution of 0.1mol/L Na-dithionite and 0.4 mol/L K_2CO_3 in three different sediments that were iodine-contaminated, the rate of iodine removal was evaluated. Over the first 140 h, the rate of iodine removal in these three different sediments showed a log-linear relationship (Figure 6.5a). After 144 h, the Na-dithionite/K_2CO_3 solution was removed to evaluate any additional release of iodine in the sediment. These experiments showed that over the next 1000 h, there was a slight increase in aqueous iodine (Figure 6.5b–d), although at a slower rate than in the Na-dithionite/K_2CO_3 solution. This indicates that although the Na-dithionite itself is no longer redox reactive, ferrous iron surface phases (i.e., adsorbed ferrous iron, FeS, and $FeCO_3$ precipitates) may be continuing to dissolve Fe oxides, releasing iodine into aqueous solution.
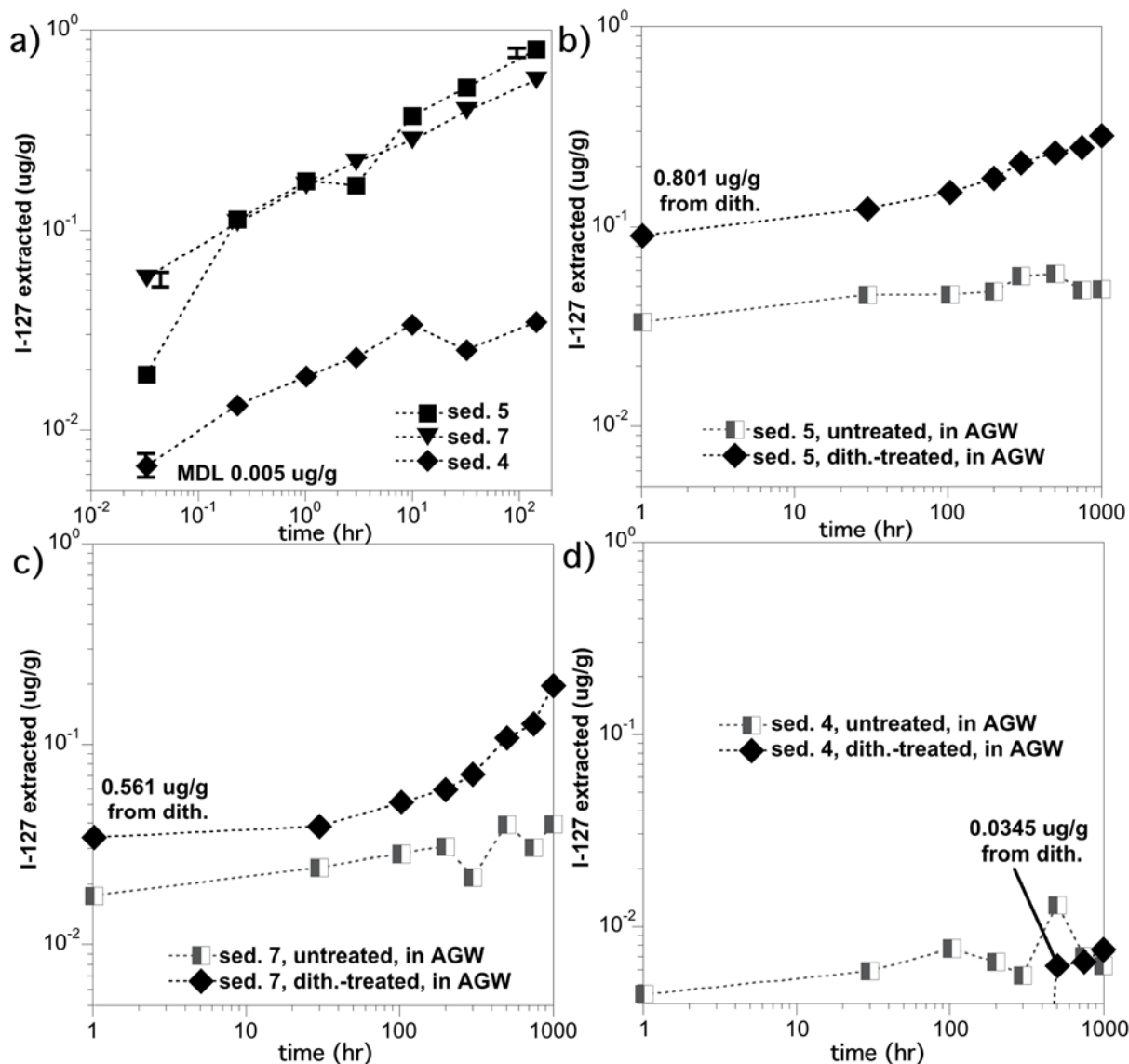
Figure 6.5.   Cumulative iodine removal in field-contaminated sediments in batch systems with 0.1 mol L^{-1} Na-dithionite + 0.4 mol L^{-1} K_2CO_3 solution for 170 h (a), followed by artificial groundwater after removal of the Na-dithionite/K_2CO_3 with a comparison of leaching for treated and untreated for sediment 5 (b), sediment 7 (c), and sediment 4 (d).

Comparison of the iodine release from untreated sediments to dithionite-treated sediments (after dithionite and released iodine has been replaced with AGW) shows that sediments treated with the Na-dithionite/ K_2CO_3 solution released iodine at a more rapid rate (Figure 6.5b–d). Again, this result indicates the dithionite treatment produced surface phases that are continuing to dissolve Fe oxides.

6.3.4   Effect of 1-D Flow in Sediment Columns on I-127 Removal

In order to evaluate the efficiency of Na-dithionite treatment as the solution flows through sediment at field scale (rather than batch experiments shown in the previous section), 1-D sediment columns were used in which a solution of 0.1mol/L Na-dithionite and 0.4 mol/L K_2CO_3 was injected for 170 h, then AGW

was injected into the sediment column for the next 570 h. Three sediments were used (C9507 104.4', C9510 114.3', C9517 94.1'), which were also dithionite-treated in batch systems (shown in the previous section). Untreated I-127 leach concentrations and cumulative mass are compared to I-127 leach concentrations and cumulative mass for the dithionite-treated sediments (Figure 6.6). Similar behavior observed in the three sediments included (1) I-127 aqueous concentrations were one to two orders of magnitude higher with dithionite treatment, (2) I-127 aqueous concentrations decreased two to three orders of magnitude for untreated and decreased one order of magnitude for dithionite-treated sediment, (3) the I-127 aqueous concentration for dithionite-treated sediments stayed higher than the untreated sediment for 120 to 150 PVs, and (4) leached mass for dithionite-treated sediment was one to two orders of magnitude higher than untreated sediment.

The higher I-127 leach concentrations for dithionite treatment was expected (Figure 6.6), as aqueous/adsorbed iodate was reduced and some Fe-oxides were dissolved (see Section 6.3.5.1 for details), releasing some solid phase iodate into solution, which was then reduced. Because the Na-dithionite/K_2CO_3 solution is only redox reactive for a few days (27-h dithionite dissociation half-life), dissolution of ferric oxides presumably occurs only during the same time period, releasing I-127 into aqueous solution. Because of that, it was expected that, during flow in these 1-D columns, once AGW was injected into the sediment columns (after 5 PVs), the aqueous I-127 concentrations for the dithionite-treated sediments would decrease to below concentrations in the untreated sediments. This was not the case, as aqueous I-127 concentrations in all three sediments stayed one to two orders of magnitude greater in the dithionite-treated sediments compared to untreated sediments even after 150 PVs of injected AGW. There are multiple ferrous phases created, including adsorbed Fe^{II}, FeS, and $Fe^{II}CO_3$ (described in Section 6.3.5.1), so the reduced sediment could continue to reduce any aqueous or adsorbed iodate, but would not be dissolving additional ferric oxides. The continued elevated I-127 aqueous concentrations in the dithionite-treated sediment, even after the pH has decreased to near groundwater concentration (Figure 6.7), appears to indicate that there is a continued slow reduction of iodate in the reduced sediment. It is likely that adsorbed iodate (which has a retardation factor < 6) would be quickly reduced to iodide and with less sorption remain mainly aqueous, so the mechanism slowly releasing I-127 (iodide) to aqueous solution from the sediment is not well understood.
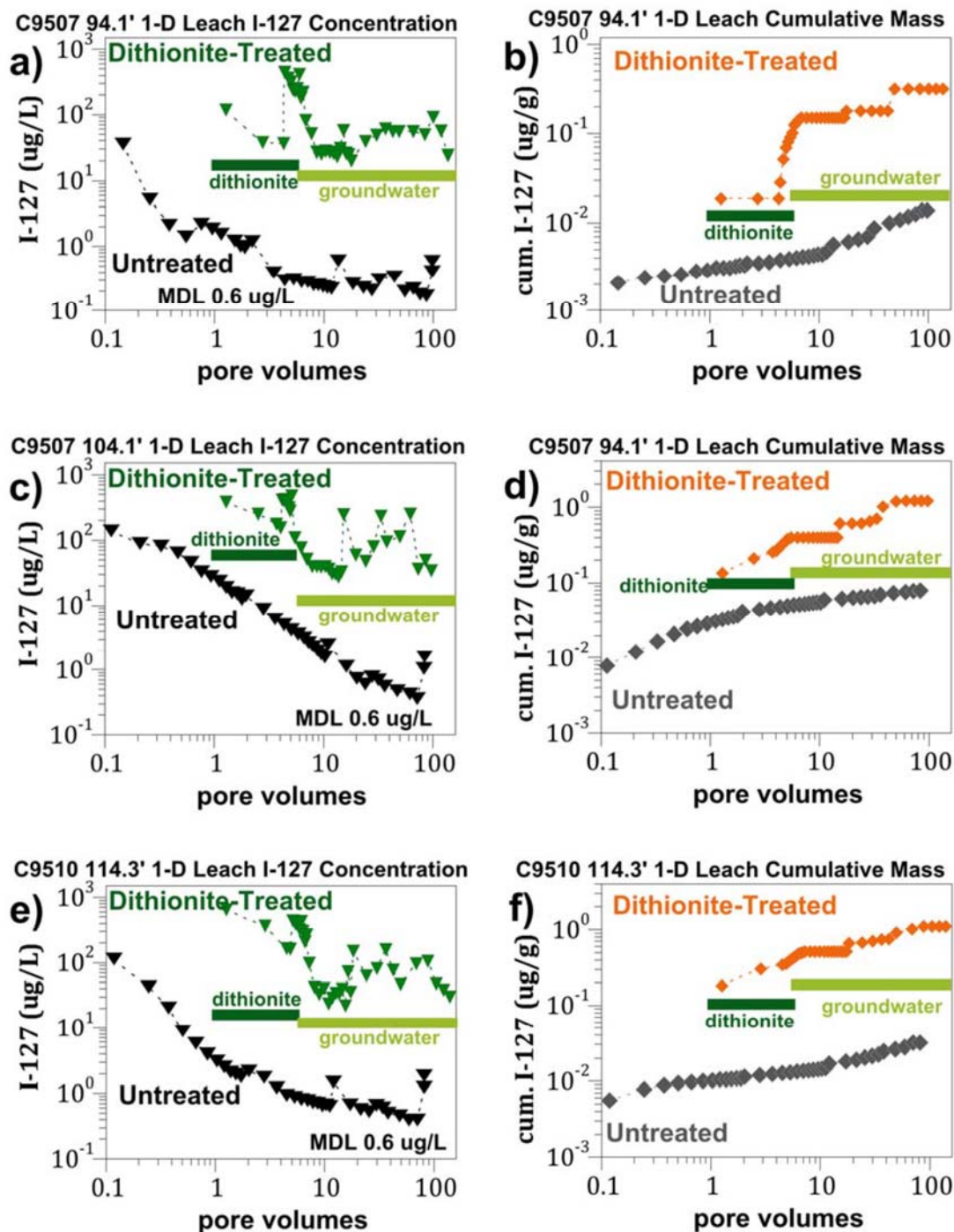
Figure 6.6.   Comparison of 1-D leaching behavior for untreated and dithionite-treatment of sediment from: a) C9507 94.1', b) C9507 104.1', and c) C9510 114.3'.
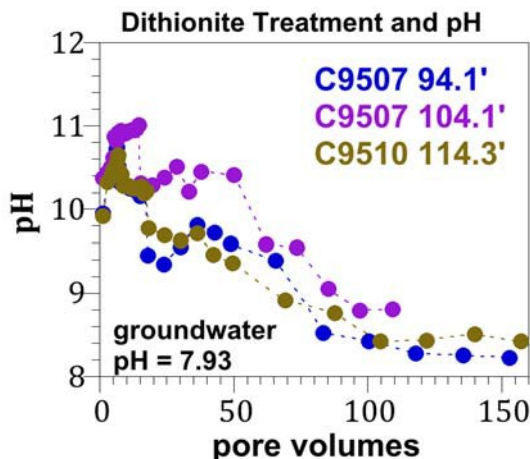
Figure 6.7.   Change in pH during leach of dithionite-treated sediments.

For remediation application to enhance iodine recovery during P&T, dithionite treatment of sediment has clearly shown that much more iodine can be removed from the sediment more quickly compared to leaching of just untreated sediment. However, it was expected that after Fe-oxides were dissolved and iodide advected from the sediments, I-127 concentrations in the dithionite-treated sediments would eventually be lower than in untreated sediments. Unfortunately, leaching experiments have shown continued elevated iodine concentrations 100 to 150 pore volumes after dithionite treatment (compared to untreated sediments). This observation needs to be investigated further as it may limit dithionite treatment use at field scale. It is possible that once the sediment is subsequently oxidized, the I-127 concentrations would decrease.

6.3.5   Effect of Dithionite Treatment on Sediment Surface Phases

Because the Na-dithionite/K_2CO_3 is well documented to dissolve amorphous and crystalline ferric oxides (Szecsody et al. 2004), sequential iron(II) and (III) extractions were conducted to quantify the extent of changes in the sediment, along with measurements of the aqueous iron (Heron et al. 1994). Inorganic carbon extractions were also conducted to evaluate any potential changes in calcite from the dithionite treatment. In addition, major and trace metals were also analyzed in dithionite-treated sediments to evaluate whether mobilized iodine was related to a different dissolving phase other than ferric oxides.

6.3.5.1   Iron Oxides

Comparing iron oxides before and after dithionite treatment, there was on average a 16% loss in Fe(III) phases, which corresponded to a gain in Fe(II) phases (last two columns in Table 6.3). The total Fe(II+III) remained constant (Figure 6.8a). The Na-dithionite/K_2CO_3 treatment was designed to dissolve Fe(III) oxides and create mainly immobile ferrous iron surface phases (i.e., adsorbed Fe(II), FeS, siderite), and the aqueous ferrous iron that remained in the spent high ionic strength treatment solution averaged 1.9 mg/L (0.065 µmol/g). There was no correlation between the aqueous ferrous iron and mobilized I-127 (Figure 6.8b) because while the mass of iodate in sediments varied two orders of magnitude, the mass of iron dissolved by the dithionite treatment was relatively constant between sediments. In contrast, for a synthetic Fe oxide precipitated from a solution also containing iodate, there should be a constant iodate/Fe ratio as the Fe oxide dissolves.

Table 6.3.   Iron characterization of sediments before and after Na-dithionite treatment.

Sediment		Fe^{II}CO$_3$, FeS (mg/g)	Other Fe^{II} (mg/g)	Am. + Crys. Fe^{III} (mg/g)	Other Fe^{III} (mg/g)	Total Fe^{III} (mg/g)	Fe^{III} Loss (%)	FeS Gain (mg/g)
C9487 58.2 - 59.2'	None	0.859	1.74	2.15	9.04	13.78		
	Dithionite/CO$_3$	1.873	1.64	1.57	7.00	12.09	23.3	1.014
C9507 94.1-95.1'	None	0.337	0.652	1.42	9.95	12.36		
	Dithionite/CO$_3$	1.208	0.993	0.83	9.45	12.48	9.6	0.871
C9507 104.4-105.4'	None	0.000	3.49	0.00	7.32	10.80		
	Dithionite/CO$_3$	0.000	2.88	0.00	5.42	8.30	25.9	0.000
C9507 137.1-138.1'	None	2.80	3.70	2.89	10.09	19.46		
	Dithionite/CO$_3$	3.05	2.49	1.630	9.61	16.78	13.4	0.249
C9510 114.3-115.3'	None	0.062	3.06	0.124	11.64	14.89		
	Dithionite/CO$_3$	0.891	2.23	0.000	8.34	11.46	29.1	0.829
C9510 114.3-115.3' (dup)	None	0.005	2.56	0.000	10.56	13.12		
	Dithionite/CO$_3$	0.878	1.89	0.000	9.06	11.83	14.2	0.873
C9414 283.3-284.5	None	0.237	1.72	0.746	9.81	12.51		
	Dithionite/CO$_3$	1.438	1.12	0.287	9.22	12.06	9.9	1.201
C9415 316.8-327.8	None	0.268	1.60	0.961	7.76	10.58		
	Dithionite/CO$_3$	1.398	1.18	0.262	6.99	9.83	16.8	1.130
C9412 296.4-297.4	None	0.179	2.17	1.12	9.67	13.14		
	Dithionite/CO$_3$	1.719	1.98	0.348	10.85	14.89	-3.8	1.540
C9602 375.8-376.5	None	0.204	0.429	0.569	6.60	7.80		
	Dithionite/CO$_3$	0.630	0.406	0.265	5.36	6.66	21.6	0.426
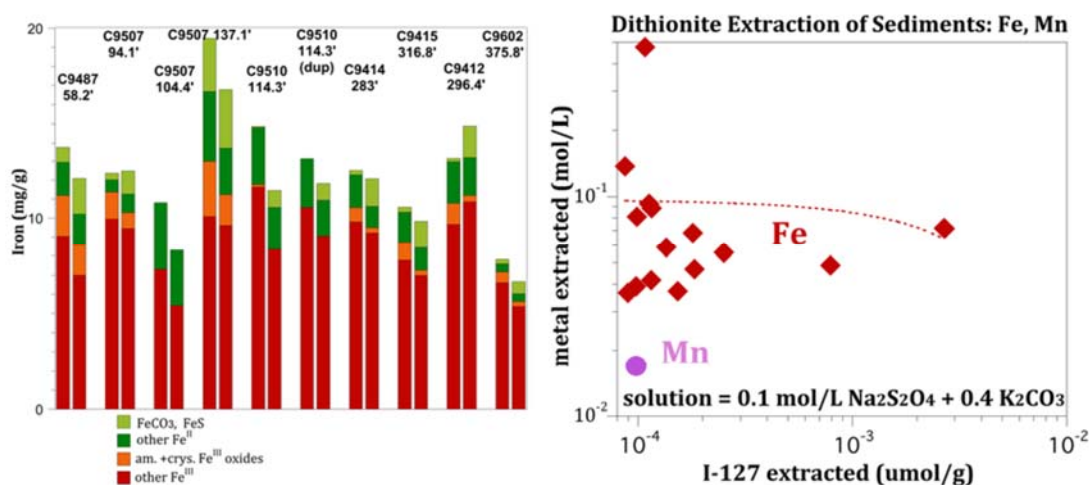
Figure 6.8.   Iron oxide characterization of sediments pre- and post- dithionite treatment.

6.3.5.2   Calcite Dissolution and Carbonate Precipitation

The inorganic carbon in sediments was also measured in selected untreated and dithionite-treated samples to evaluate whether calcite was being dissolved. Unfortunately, the Na-dithionite/K_2CO_3 treatment process results in the formation of multiple ferrous iron phases, including siderite ($FeCO_3$) along with adsorbed Fe(II) and FeS, using ferrous iron from ferric oxide dissolution and aqueous carbonate. The dithionite-treated sediments on average contained 98% greater solid phase carbonate compared with the same untreated sediment (Table 6.4). Because only two of seven sediments showed a small (3.3% and 3.8%) decrease in total inorganic carbonate and the remainder increased in carbonate precipitates, it is likely that the dithionite treatment does not dissolve calcite.

Table 6.4.   Inorganic carbon (IC) analysis on untreated and dithionite-treated sediments.

#	Sediment	Untreated (%IC)	Dith. Treat (%IC)	Increase (%)
E62.6	C9487 58.2 - 59.2'	0.105	0.180	71.9
E62.6 dup	C9487 58.2 - 59.2'	0.113	0.136	20.7
E62.8	C9507 94.1-95.1'	0.284	0.351	23.7
E62.9	C9507 104.4-105.4'	3.034	2.933	-3.3
E62.10	C9507 137.1-138.1'	0.010	0.054	464.6
E62.11	C9510 114.3-115.3'	1.384	1.331	-3.8
E62.21 dup 11	C9510 114.3-115.3'	1.29	1.383	7.4
E62.16	C9414 283.3-284.5'	0.018	0.059	226.2
E62.17	C9415 316.8-327.8'	0.016	0.040	141.8
E62.19	C9412 296.4-297.4'	0.178	0.278	56.2
E62.20	C9602 375.8-376.5'	0.016	0.028	79.0
E62.20 dup	C9602 375.8-376.5'	0.016	0.031	94.4
MCL		0.005	0.005	

Another approach to evaluate whether calcite in the untreated sediment is dissolving is to compare the untreated inorganic carbon (Table 6.4) against the aqueous Ca and Mg in dithionite-treated aqueous solution. With the inorganic carbon varying by over two orders of magnitude in different sediments, there was a relatively uniform aqueous concentration of Ca and Mg (Figure 6.9), indicating calcite is likely not being dissolved by the Na-dithionite treatment.
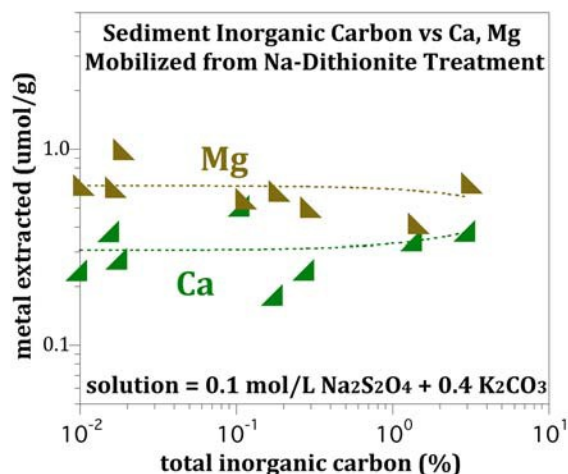
Figure 6.9.   Total inorganic carbon in untreated sediments and Ca, Mg mobilized from Na-dithionite treatment.

6.3.5.3   Dissolution of Other Minerals: Metals Mobilization

A number of major and trace metals were analyzed in dithionite-treated sediments to evaluate whether mobilized iodine was related to a different dissolving phase other than ferric oxides. Metals analyzed included Al, Ba, Ca, Fe, Mg, Mn, Mo, K, Si, Na, Sr, Ti, Zr, Bi, Cr, Co, Cu, Ag, P, and Zn. Aqueous concentrations of Mn, Bi, Cr, Co, Cu, and Zn were all below detection limits. The aqueous concentrations of I-127 and 10 metals mobilized in 21 different sediments by dithionite treatment showed no correlation of I-127 mobilized with any other mobilized metal (Figure 6.10). The 0.1 mol/L Na-dithionite and 0.4 mol/L K_2CO_3 solution contained high Al (19.0 mg/L) and P (8.5 mg/L), but low concentrations of I (< 1.26 µg/L), Ca (< 3.36 mg/L), Mg (< 0.27 mg/L), Fe (< 1.0 mg/L), Mn (< 0.24 mg/L), and Si (< 5.48 mg/L).
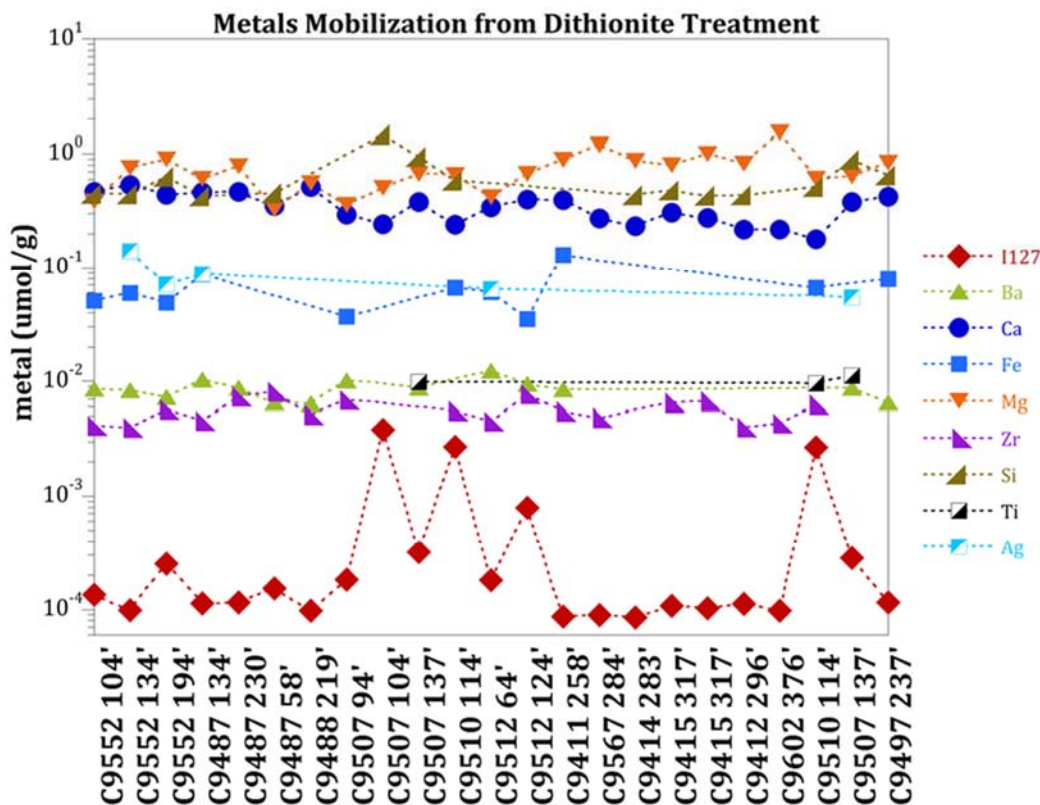
Figure 6.10. I-127 and other metals mobilized by Na-dithionite treatment.

The aqueous Si concentrations averaged 9.1 ± 4.1 mg/L (Figure 6.10), somewhat less than the 15 mg/L in the AGW used, indicating silica was not being dissolved (and may be precipitating). The Al aqueous concentrations averaged 5.0 ± 0.92 mg/L, which was less than the 19 mg/L in the dithionite solution, also suggesting some precipitation. The aqueous P concentrations of 4.1 to 6.3 mg/L were also less than the 8.5 mg/L in the dithionite solution, indicating phosphate precipitation. Both Na (at 0.2 mol/L) and K (at 0.8 mol/L) were present at high concentrations in the Na-dithionite/K_2CO_3 treatment solution. Aqueous concentrations of Mg averaged 9.4 mg/L and Ca averaged 7.4 mg/L, likely from a combination of desorption from ion exchange sites and dissolution of minerals. Sorbed cations on ion exchange sites (2 meq/100g or 20 µmol/g) could account for some of the ion concentrations observed but should be of similar proportion of the AGW (i.e., 70% Ca, 20% Mg, 8% Na, 2% K). Calcite was unlikely dissolving and producing the aqueous Ca and Mg as calcite contains 95% Ca and < 5% Mg. The sediment with the highest calcite (Table 6.4, C9507 104', 3.03% inorganic carbon) also did not have any greater aqueous Ca and Mg. A common mineral present in basalt (forsterite, $MgSiO_4$) may be dissolving in the dithionite solution. The lack of a correlation between the mass of I-127 in sediments and any mobilized metal (Figure 6.10) could indicate that there are no other phases (other than Fe oxides and possibly calcite) that are dissolving and contain iodine.

Silver was also present in some samples above the detection limits of 1.8 mg L^{-1} (Figure 6.10), although it was not present in the Na-dithionite/K-carbonate solution (< 0.2 mg L^{-1}). Therefore, there may be a trace metal associated with co-contaminants in the sediments. Simulations of trace metals and iodine in Geochemist Work Bench 10.0 (using the Minteq database) showed that Ag_2S and AgI should precipitate, so the iodine precipitation indicated in 1-D column studies (Figure 6.6) could be caused by the initial dissolution of a Ag-precipitate in the sediment by the alkaline Na-dithionite/K-carbonate solution and then slow AgI precipitation.

In order to prove that the iodate/iodide from reaction of the dithionite solution with sediments were from sediments and could be analyzed in the high ionic strength solution, a series of dithionite solutions were prepared and analyzed for iodine. The reduced and oxidized Na-dithionite/K_2CO_3 solution analyzed for I-127 showed that there were no iodine impurities in the dithionite or carbonate chemicals (Table 6.5). In addition, when I-127 was added to the high ionic strength Na-dithionite/K_2CO_3 solution, I-127 was accurately measured, so the dithionite (S_2O_4 mass of 128 g/mol) did not interfere with the I-127 mass analysis by ICP-MS. Therefore, I-127 reported in dithionite solution reaction with sediments was from the sediment.

Table 6.5.   Dithionite solutions analyzed for I-127.

Solution	Added Iodate (μg/L)	Added Iodide (μg/L)	Measured I-127 (μg/L)
0.06M $Na_2S_2O_4$ + 0.24M K_2CO_3	0.0	0.0	< 1.26
0.06M $Na_2S_2O_4$ + 0.24M K_2CO_3 (oxidized)	0.0	0.0	< 1.26
0.06M $Na_2S_2O_4$ + 0.24M K_2CO_3	150.0	0.0	135.0
0.06M $Na_2S_2O_4$ + 0.24M K_2CO_3	0.0	150.0	145.0

6.3.6   Mass of I-127 Removal by Na-Dithionite

The Na-dithionite/K_2CO_3 solution mobilized considerable I-127 from 200 Area Hanford subsurface sediments (Table 6.6, Figure 6.11). Batch (i.e., no flow) experiments showed that 170 h of solution treatment (light blue triangles, Figure 6.11) removed an average of 28.7% ± 20.4% of the total I-127 (black squares) associated with the sediment. Additional dithionite-sediment contact time (i.e., 300 h, 1000 h) removed a greater amount of iodine from the sediment (darker blue triangles, Figure 6.11). In 1-D columns where the dithionite solution was injected (170 h) then AGW (575 h), 61.9% ± 21.2% of the total I-127 was removed from the sediment. The total iodine in the sediment was difficult to measure, as sequential liquid extractions had to be pH neutralized and diluted before I-127 analysis (black squares, Figure 6.11). Early sequential liquid extractions had incomplete I-127 analysis because the most acidic extractions could not be analyzed by ICP-MS (red squares).
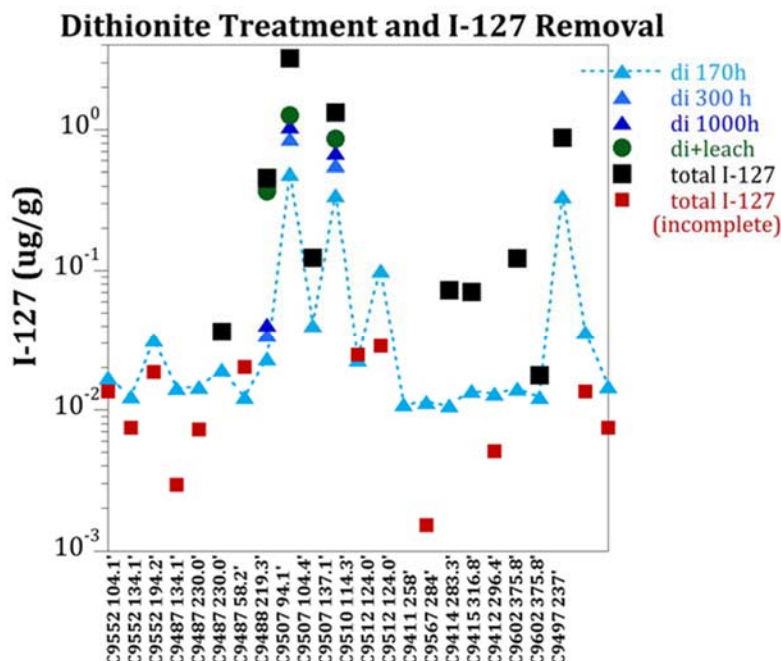
Figure 6.11. Na-dithionite/K_2CO_3 mobilization of I-127 from contaminated field sediments.

6.3.7   I-127 Mass Balance in Sediments Pre- and Post-Dithionite Treatment

Sequential liquid extractions that were conducted after 170 h dithionite treatment provided a measure of the total I-127 remaining in the sediment (Figure 6.12). These extractions showed that the fraction of I-127 removed by the dithionite treatment varied from 20% to 75% (Figure 6.12b). Sequential extractions conducted on sediments prior to dithionite treatment did not provide a complete measurement of the I-127 in sediments, as acetate and oxalic acid extractions were not analyzed in all cases, and the nitric acid extraction was not analyzed (Figure 6.13, Table 6.6). These extractions are, however, useful for identification of the first three mobile phases in the sediments. For the three sediments that were dithionite-treated in 1-D columns for 743 h (which removed significant I-127 from the sediment), a comparison of pre- and post-treatment sequential extractions does show that the oxalic acid extraction (which dissolves Fe oxides) decreased significantly. Because the 8 M nitric acid extraction was not analyzed for I-127 in pretreatment extractions, it is difficult to evaluate the full mass balance.

Table 6.6. Iodine-127 associated with sediments, characterized by sequential liquid extractions, dithionite treatment, and carbonate treatment.

Sediment Borehole Depth	Untreated Partial Seq. Extr. I-127[a] (µg/g)	Untreated 1000h CO$_3$ I-127[b] (µg/g)	Untreated 100 Pv leach I-127 (µg/g)	Dithionite Treat 170h extr. I-127 (µg/g)	Post Dith. Seq. Extr. I-127[c] (µg/g)	Dithionite Treat 300h extr. I-127 (µg/g)	Dithionite Treat 1000h extr. I-127 (µg/g)	Dithionite 1-D Treat I-127[d] (µg/g)	Post Dith. 1-D Leach extr. I-127[e] (µg/g)	Total I-127[e] (µg/g)
C9552 104.2-105.2'	1.36E-02	4.69E-03	0.00762	1.71E-02						
C9552 134.1-135.1'	7.44E-03	2.63E-03	0.00747	1.25E-02						
C9552 194.2-195.2'	1.87E-02	1.73E-02	0.00817	3.18E-02						
C9487 134.1-135.1'	2.94E-03	3.07E-03	0.00673	1.43E-02						
C9487 230.0-231.0'	7.25E-03	4.04E-03	0.00788	1.46E-02						
C9487 58.2 - 59.2'	5.25E-02	2.81E-03	0.0112	1.94E-02	1.69E-02					3.63E-02
C9488 219.3–220.3'	2.03E-02	4.83E-03	0.00699	1.24E-02						
C9507 94.1-95.1'	2.19E-01	2.30E-02	0.0138	2.32E-02		3.45E-02	4.11E-02	3.67E-01	8.63E-02	4.53E-01
C9507 104.4-105.4'	8.91E-01	1.07E-01	0.0793	4.86E-01		8.61E-01	1.05E+00	1.26E+00	1.97E+00	3.23E+00
C9507 137.1-138.1'	9.72E-02	2.12E-02		4.06E-02	8.36E-02					1.24E-01
C9510 114.3-115.3'	7.34E-01	6.84E-02	0.0317	3.43E-01		5.61E-01	6.87E-01	8.63E-01	4.56E-01	1.32E+00
C9512 64.2-65.2'	2.47E-02	6.07E-03		2.29E-02						
C9512 124-125'	2.86E-02	1.09E-02		1.00E-01						
C9411 258-259'	1.54E-03		0.00587	1.10E-02						
C9567 284-285'	2.45E-03		0.00847	1.14E-02						
C9414 283.3-284.5'	6.36E-03		0.01171	1.08E-02	6.17E-02					7.25E-02
C9415 316.8-327.8'	2.48E-03		0.0253	1.37E-02	5.69E-02					7.06E-02
C9415 316.8-327.8'	2.48E-03			1.31E-02						
C9412 296.4-297.4'	5.08E-03		0.01713	1.42E-02	1.08E-01					1.22E-01
C9602 375.8-376.5'	6.41E-03		0.01311	1.24E-02	5.30E-03					1.77E-02
C9510 114.3-115.3'	7.34E-01	6.84E-02	0.0317	3.39E-01	5.40E-01					8.79E-01
C9507 137.1-138.1'	9.72E-02	2.12E-02	0.0253	3.61E-02						
C9497 237-238'				1.47E-02						

(a) Sequential extractions 1-6, but not all extractions were analyzed (i.e., represents partial I-127)
(b) pH 9.3 0.1 M Na-CO3 extraction for 1000 h
(c) Sequential extractions 1-6, pH neutralized before analysis so all six analyzed (i.e., represents total I-127)
(d) Leached 100 PVs after 300 h of dithionite extraction of I-127
(e) Total I-127 is dithionite extracted + sequential extraction (after dithionite) + leached (in some cases)
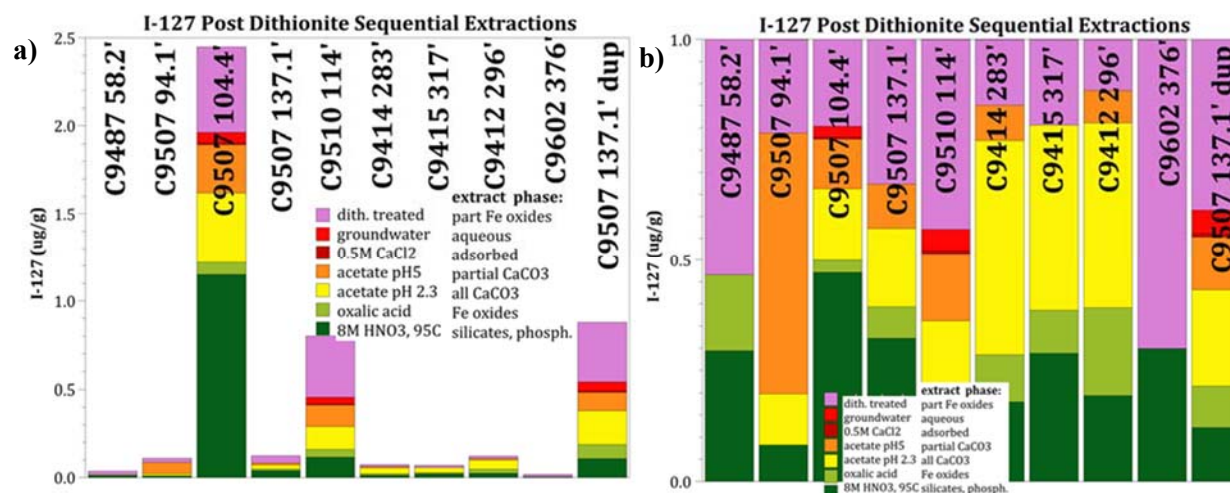
Figure 6.12. I-127 in field-contaminated sediments removed by dithionite/K$_2$CO$_3$ treatment then sequential liquid extractions, as shown by a) I-127 concentration (µg/g) and b) I-127 fraction of total.
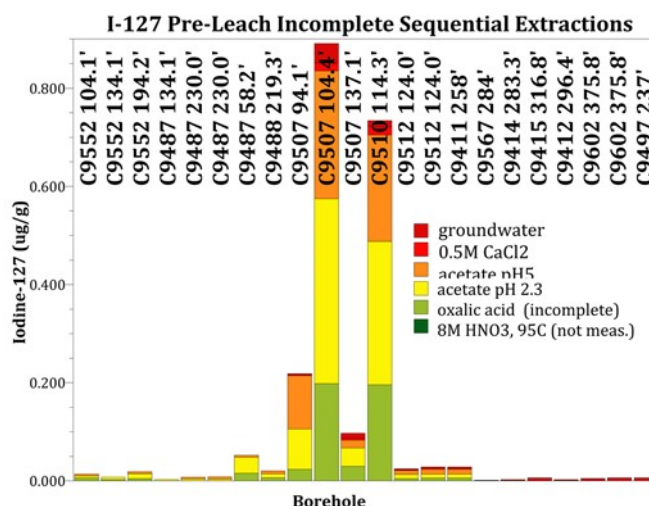
Figure 6.13. Untreated sediment sequential liquid extractions for I-127.

The high iodine removal from sediment using the Na-dithionite/K-carbonate solution indicates a pump and treat system at field scale should need much less volume of pumped groundwater to remove the iodine than it would with the addition of the reductant. While the Na-dithionite/K-carbonate treatment does greatly increase I-127 removal *mass* from sediment, it also needs to be demonstrated that the surface phases (i.e., amorphous Fe oxides, for example) that would slowly dissolve during groundwater flushing are dissolved more quickly with the Na-dithionite/K-carbonate solution. A comparison of iodine sequential extractions for (1) untreated, (2) untreated followed by leached, and (3) dithionite-treated followed by leached provides some information on changes in surface phases (Figure 6.6c). Sequential extractions for batch or 1-D leaching with dithionite generally showed a decrease in the fraction of iron oxide associated iodine (Figure 6.14, light green bars), but there was considerable variation in the total iodine released from the sediment. Therefore, sequential extractions have not consistently demonstrated that iodine in solid phases that are mobilized during groundwater leaching are the same solid phases that are dissolved by the dithionite-carbonate treatment. However, results do clearly demonstrate that the I-

129 is more easily extracted with dithionite treatment than I-127 as shown by the comparison of groundwater and dithionite extractions (Table 6.6).
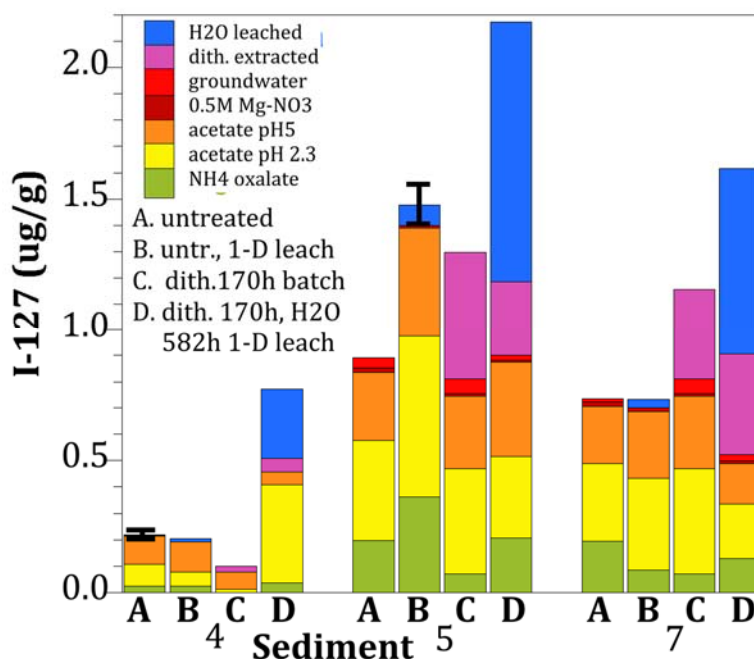
Figure 6.14. Comparison of pre- and post-dithionite treatment sequential liquid I-127 extractions for sediment 4 (C9507 104'), sediment 5 (C9507 94'), and sediment 7 (C9507 114').

Because most of the sequential liquid extractions are acidic, alkaline extractions were also conducted in an effort to evaluate the total iodine in the sediments. This pH 9.3 Na-carbonate extraction (1000 h), unfortunately, removed an average of 6.4% of the total I-127 in the sediment. This 1000-h carbonate extraction has been previously used to exchange aqueous carbonate in calcite to extract some of the uranium, which substitutes into the calcite structure. For I-127, this may indicate that the fraction in carbonates is small. In the sequential liquid extractions, the pH 5 Na-acetate extraction is also designed to dissolve a small fraction of carbonates. Note that multiple surface phases likely dissolve in the different extraction solutions, and amorphous ferrihydrite may partially dissolve in the pH 5 solution. Untreated sediment extractions indicate that this pH 5 Na-acetate extraction removed 27.5% of the I-127 in the sediment and post-dithionite treated extractions indicate that this pH 5 Na-acetate extraction removed 16.8% of the I-127 from the sediment. Because the dithionite treatment dissolves (by reductive dissolution) about a third of Fe oxides (a higher fraction of amorphous and less crystalline; Section 6.3.5.1), it is hypothesized that most Fe-oxides that contained I-127 were dissolved by the dithionite treatment and the pH 5 Na-acetate post dithionite treatment represents a portion of I-127 in calcite (i.e., 17%).

Another measure of "labile" iodine is the mass of iodine released after 100 PVs of groundwater leaching (although this is somewhat arbitrary). For uranium, this leached mass roughly equal to sequential extractions 1 (aqueous) + extraction 2 (adsorbed) + half of extraction 3 and 4 (presumed carbonates). For iodine, this sum of sequential extractions removed 18.4% of the iodine from sediments, whereas the 100 PV leach removed an average of 20.3% of the total iodine (Table 6.6).

6.3.8   Rate of I-127 Release from Sediments

Untreated release I-127 into aqueous solution and dithionite-treated sediments release a significantly greater mass, likely due to the partial dissolution of ferric oxides containing at least some of the I-127 associated with sediment solid phases. The rate of I-127 release from sediments (presumed from Fe-oxides and possibly other phases) was one to three orders of magnitude more rapid when the sediment was dithionite-treated in contrast to untreated sediments (Table 6.7).

Table 6.7.   Iodine release rates from sediments.

Sediment	Treatment	Exp. Type	Reaction Time (h)	I-127 Released (µg/g)	$Fe^{II}CO_3$, FeS (mg/g)	I-127 Release Rate (µmol IO_3 h^{-1} mol^{-1}Fe^{II})
C9487 58.2-59.2'	None	1D leach	750	1.12E-02	0.859	7.65E-03
	None	Batch	1000	8.11E-03	0.859	4.15E-03
	Dithionite	Batch	170	1.94E-02	1.873	2.69E-02
C9507 94.1-95.1'	None	Batch	1000	7.00E-03	0.337	9.13E-03
	Dithionite	Batch	170	2.32E-02	1.21	9.48E+01
	Dithionite	Batch	300	3.45E-02	1.21	4.02E+00
	Dithionite	Batch	1000	4.11E-02	1.21	4.36E-01
	None	1D leach	525	1.39E-02	1.21	9.61E-03
	Dithionite	1D leach	743	3.67E-01	1.21	8.28E+01
C9507 104.4-105.4'	None	Batch	1000	5.76E-02	1.32	1.92E-02
	Dithionite	Batch	170	4.86E-01	2.50	5.93E+02
	Dithionite	Batch	300	8.61E-01	2.50	6.44E+01
	Dithionite	Batch	1000	1.05E+00	2.50	6.03E+00
	None	1D leach	525	7.93E-02	2.50	2.66E-02
	Dithionite	1D leach	743	1.26E+00	2.50	4.32E+01
C9507 137.1-138.1'	None	Batch	1000	1.01E-02	2.68	1.66E-03
	Dithionite	Batch	170	4.06E-02	5.48	1.92E-02
C9510 114.3-115.3'	None	Batch	1000	3.02E-02	0.062	2.14E-01
	Dithionite	Batch	170	3.43E-01	0.891	1.11E+03
	Dithionite	Batch	300	5.61E-01	0.891	1.05E+02
	Dithionite	Batch	1000	6.87E-01	0.891	1.13E+01
	None	1D leach	525	3.17E-02	0.062	4.28E-01
	Dithionite	1D leach	743	8.63E-01	0.891	2.60E+01
C9414 283.3-284.5'	None	1D leach	750	1.17E-02	0.24	2.89E-02
	Dithionite	Batch	170	1.08E-02	1.44	1.94E-02
C9415 316.8-327.8'	None	1D leach	750	2.53E-02	0.268	5.54E-02
	Dithionite	Batch	170	1.37E-02	1.40	2.53E-02
C9412 296.4-297.4'	None	1D leach	750	1.71E-02	0.179	5.60E-02
	Dithionite	Batch	170	1.42E-02	1.72	2.14E-02
C9602 375.8-376.5'	None	1D leach	750	1.31E-02	0.204	3.77E-02
	Dithionite	Batch	170	1.24E-02	0.63	5.09E-02
C9510 114.3-115.3'	None	1D leach	750	1.33E-02	0.051	1.53E-01
	Dithionite	Batch	170	3.39E-01	0.878	9.99E-01

If the iodine release rate from the sediment was mainly controlled by Fe-oxides, then there should be a correlation between the concentration of ferrous iron phases (described in Section 6.3.5.1) and the I-127 release rate. However, while greater mass of FeS/FeCO$_3$ (one of several ferrous iron phases) resulted in greater I-127 release rates from the sediment, the correlation was poor, as the release rates in different dithionite-treated sediments varied up to three orders of magnitude with the same mass of ferrous iron (Figure 6.15a). This result implies ferrous phases are poorly characterized and/or are not controlling a significant portion of the iodine release from the sediment. While iron extractions have been used in other studies to characterize mass of ferrous and ferric phases, ferrous iron concentrations are low in these Hanford sediments.
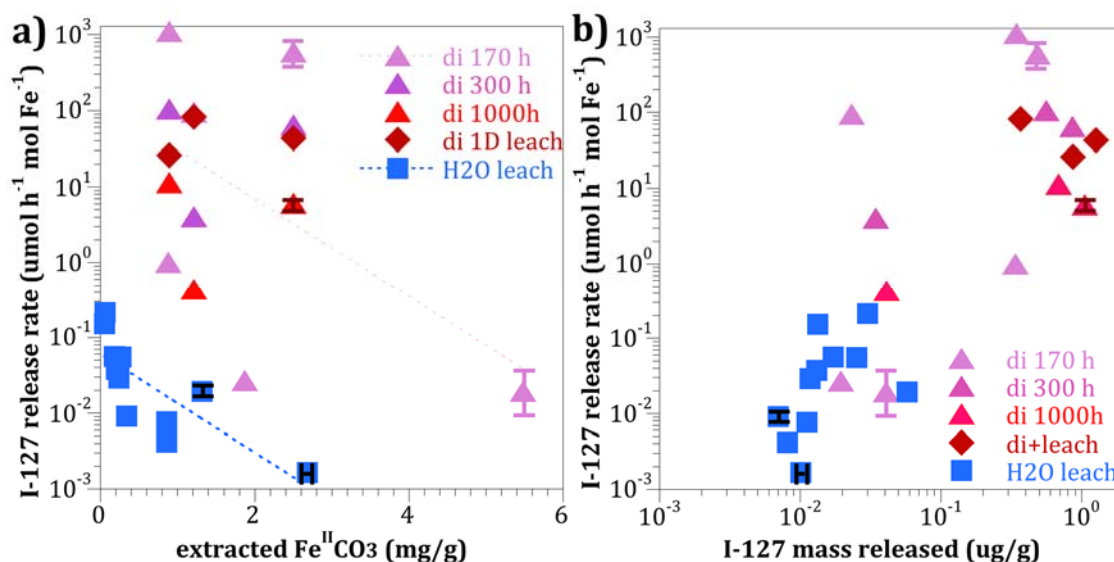
Figure 6.15. Iodine release rates in sediments as a function of a) FeS/FeCO$_3$ concentration, and b) iodine released mass.

There was a moderate correlation between the I-127 mass released from the sediment and the I-127 release rate (Figure 6.15b). Calculated release rates for three sediments that were extensively studied showed generally the highest release rate at 170 h experiments, with decreasing rates by 300 h, 1000 h, and in 750-h-long 1-D column leaching. This indicates that the efficiency of I-127 removal decreases, possibly as amorphous Fe oxides are initially (and rapidly dissolved), followed by slower dissolution of more crystalline Fe oxides, both of which contain some iodine.

6.4   I-129 Results and Discussion

6.4.1   Comparison of Iodine-129/127 in Hanford Sediments

To quantify the removal of iodine from sediments following equilibration with artificial groundwater or extraction with Na-dithionite, batch extractions were first conducted to estimate total I-129/127 initially present in sediments via a total iodine extraction (5% TMAH, tetramethyl ammonium hydroxide). The TMAH extractions were also compared with previous sequential extraction results conducted under acidic conditions (Figure 6.16, I-127 data from Table 6.6), which showed that some losses occurred with sequential extractions, especially in sediments with lower total I-127 concentrations.
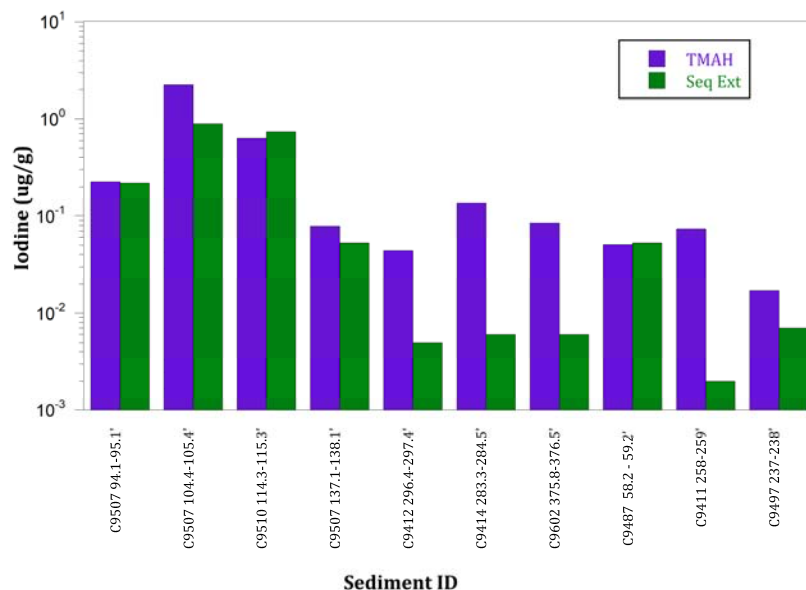
Figure 6.16. Comparison of total I-127 extracted via 5% TMAH (*purple*) in 50 g/L suspensions and sequential extractions *(green*, Figure 6.2a)* for sediments from the Hanford Site 200 West Area.

Figure 6.17 shows that I-129 concentrations ranged from 0.006 to 0.044 µg/g with the highest concentration measured in sample C9411 from the 200 West plume. Across the five samples analyzed for I-129, the sediment concentrations were positively correlated with depth ($R^2 = 0.98$, Figure 6.18). Further, there was more I-127 present in sediments as compared to I-129 with more variable concentrations spanning approximately three orders of magnitude (0.03 to 2.3 µg/g) for I-127. However, there was no apparent correlation in concentration with depth in the subsurface for I-127. These results suggest that I-127/129 each come from different sources. While it is known that I-129 is present from historical waste releases during plutonium production at the Hanford Site, large quantities of non-radioactive I-127 are due to its presence as a trace element in the nitric acid that was used in plutonium processing, and disposed in large quantities to constructed waste disposal facilities such as trenches, cribs, and ponds (Truex et al. 2017; Cantrell and Felmy 2012).
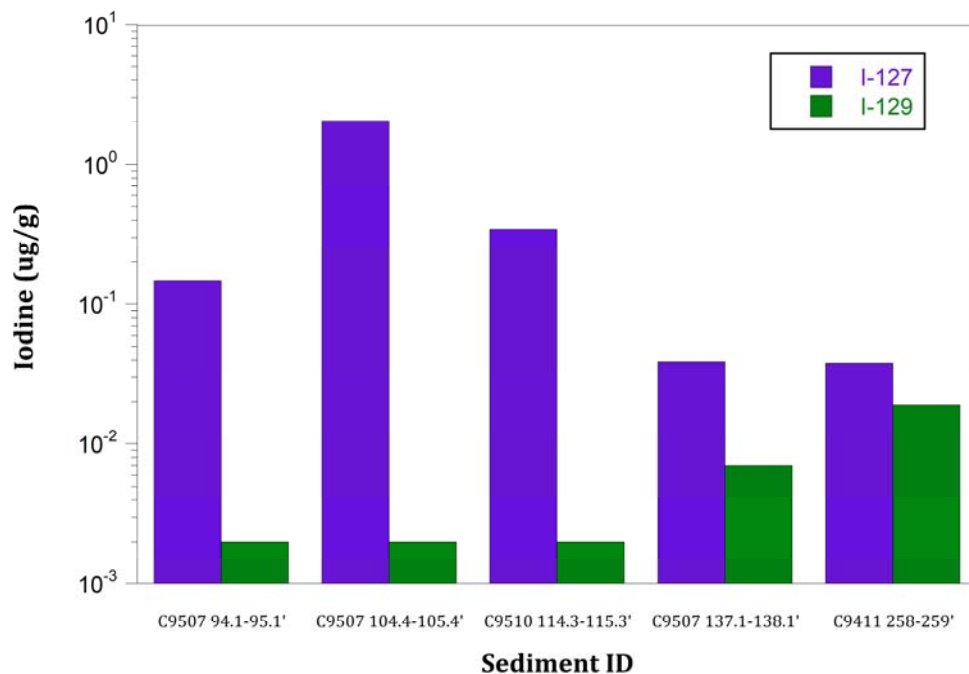
Figure 6.17. Comparison of total I-127 (*purple*) and I-129 (*green*) extracted via 5% TMAH in 50-g/L suspensions for sediments from the Hanford Site 200 West Areas.
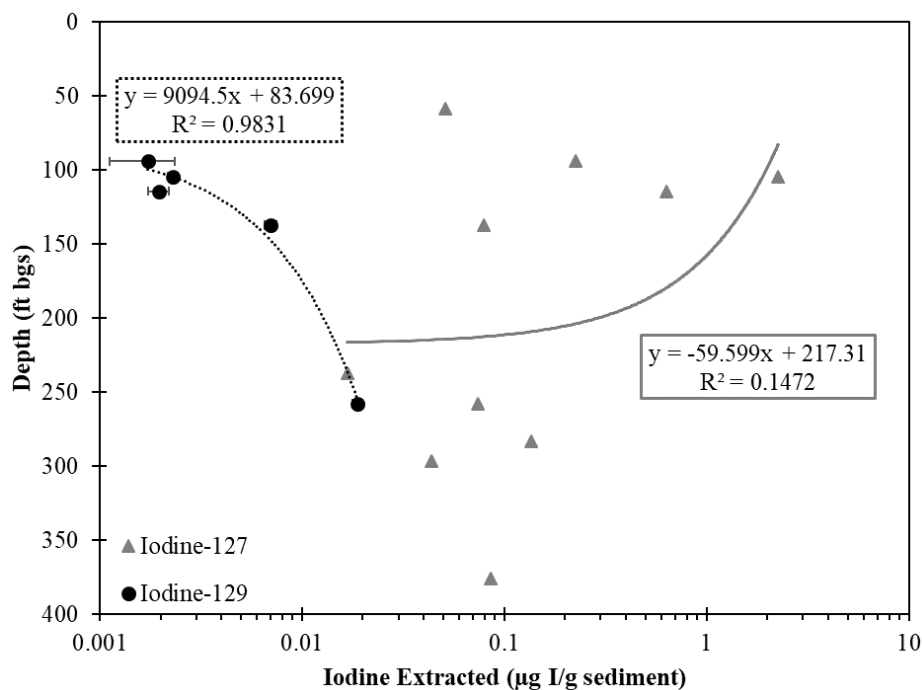
Figure 6.18. Comparison of total I-127 (*gray triangles*) and I-129 (*black circles*) extracted via 5% TMAH in 50-g/L suspensions with respect to depth for sediments from the Hanford Site 200 West Area, with dotted lines representing a linear fit of results.

6.4.2   Artificial Groundwater Extraction of Iodine-129 and Iodine-127

Batch experiments showed that I-129 was more readily leachable than I-127 from sediments with AGW (Figure 6.19) based on the fraction recovered as compared to the TMAH extractions. Further, in sediment C9411, more I-129 was extracted than I-127 (0.01 vs. 0.002 µg/g). Based on the recovery of iodine from artificial groundwater and TMAH extractions, apparent partitioning coefficients were estimated for both isotopes (Table 6.8). The coefficients are labeled as apparent partitioning coefficients because equilibrium may not have been reached and other processes in addition to desorption may be occurring. Nonetheless, these results confirm that I-129 is more readily mobilized in this system as compared to I-127. It must be noted that this result also highlights that the source of each isotope is ultimately different and makes a significant impact on their mobility. This result does not show that different isotopes of iodine generally exhibit different behavior in the environment but that the two isotopes present in this system exhibit different behavior due to different source conditions.
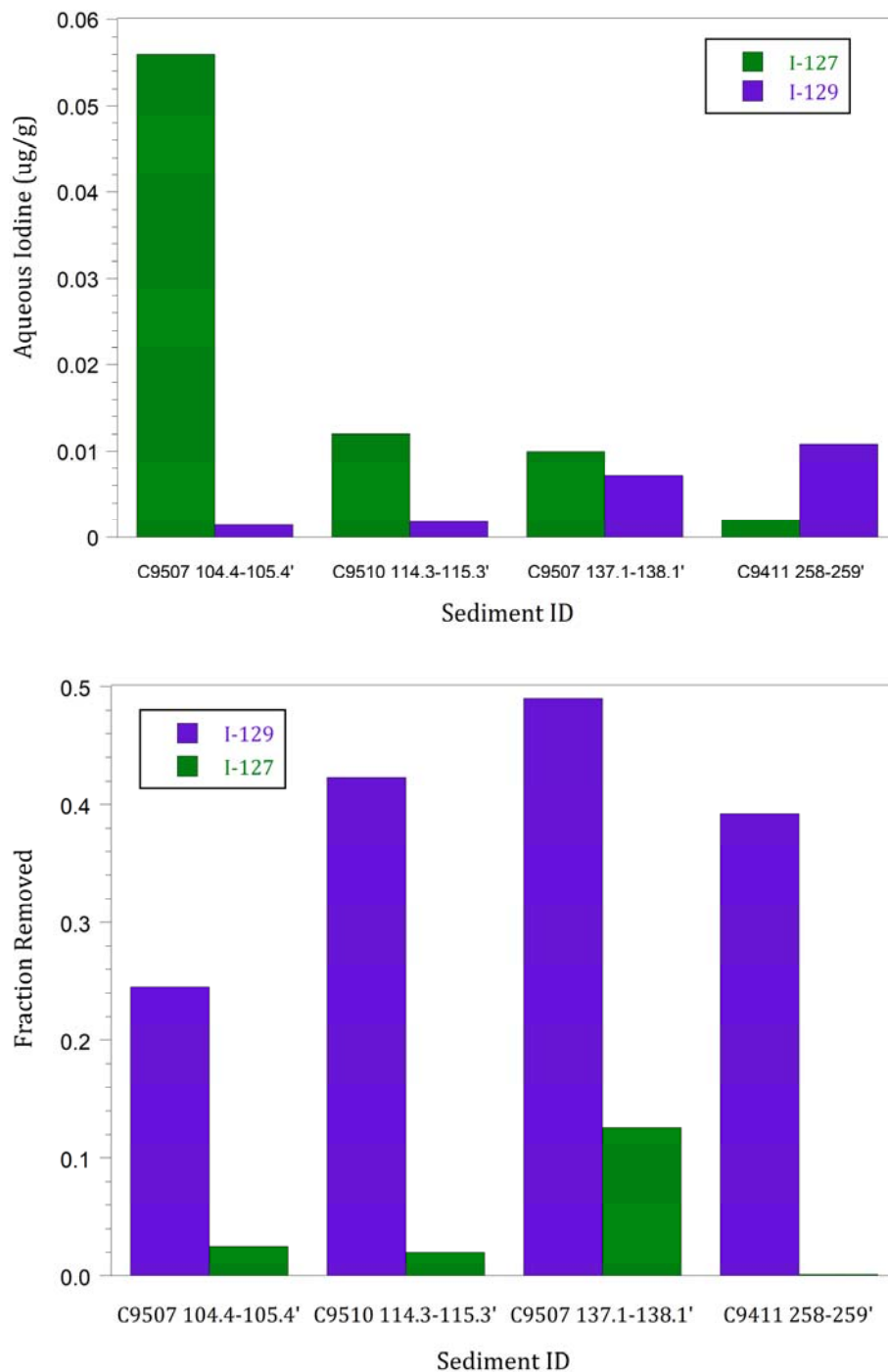
Figure 6.19. Iodine [I-127 in *green* and I-129 in *purple*] desorbed from Hanford Site sediments in µg/g (*top*) and fraction removed (*bottom*) following reaction of 250 g/L of sediments with artificial groundwater for 7 days. Note: I-129 data only shown for select samples.

Table 6.8. Summary of apparent partitioning coefficients measured via desorption of iodine from Hanford sediments (250 g/L) with artificial groundwater after 7 days.

Sediment ID	^{127}I K_d (mL/g)	^{129}I K_d (mL/g)
C9507 94.1-95.1'	144.6	NM
C9507 104.4-105.4'	165.5	*12.9*
C9510 114.3-115.3'	210.2	*5.8*
C9507 137.1-138.1'	28.3	*4.2*
C9412 296.4-297.4'	19.5	NM
C9414 283.3-284.5'	145.9	NM
C9602 375.8-376.5'	38.4	NM
C9487 58.2-59.2'	24.6	NM
C9411 258-259'	138.7	*7.0*
C9497 237-238'	3.7	NM
C9507 94.1-95.1'	25.4	NM

NM = not measured

6.4.3   Na-dithionite Treatment for Iodine-129/127 Mobilization

6.4.3.1   Comparison of Iodine-129/127 Removal by Na-Dithionite Solutions

Figure 6.20 summarizes results for extraction of both iodine isotopes with Na-dithionite. For all sediment samples reacted with Na-dithionite, I-129 recovery is greater than the amount extracted by TMAH. The greatest I-129 was removed from the sediment sample from within the I-129 plume in the 200 West area (C9411) with recovery of 3.9 times more I-129 than via the TMAH extraction which was previously reported to extract total iodine from sediments. It should be noted that less I-127 was leached with Na-dithionite as compared to TMAH for sediments with the exception of two of the ten samples (C9412 and C9507, 137.1-138.1'). Further, greater I-127/129 was removed in all extractions as compared to artificial groundwater reaction for the same period of time with 4 to 10.1 times more I-129 removed via Na-dithionite treatment. These results provide further evidence that I-129 is more readily leached from sediments than I-127 especially with Na-dithionite. Further, these data suggest that I-129 is more readily mobilized by the reductive extractant (Na-dithionite) that is generally used to target Fe phases as opposed to the TMAH extraction used in previous research.
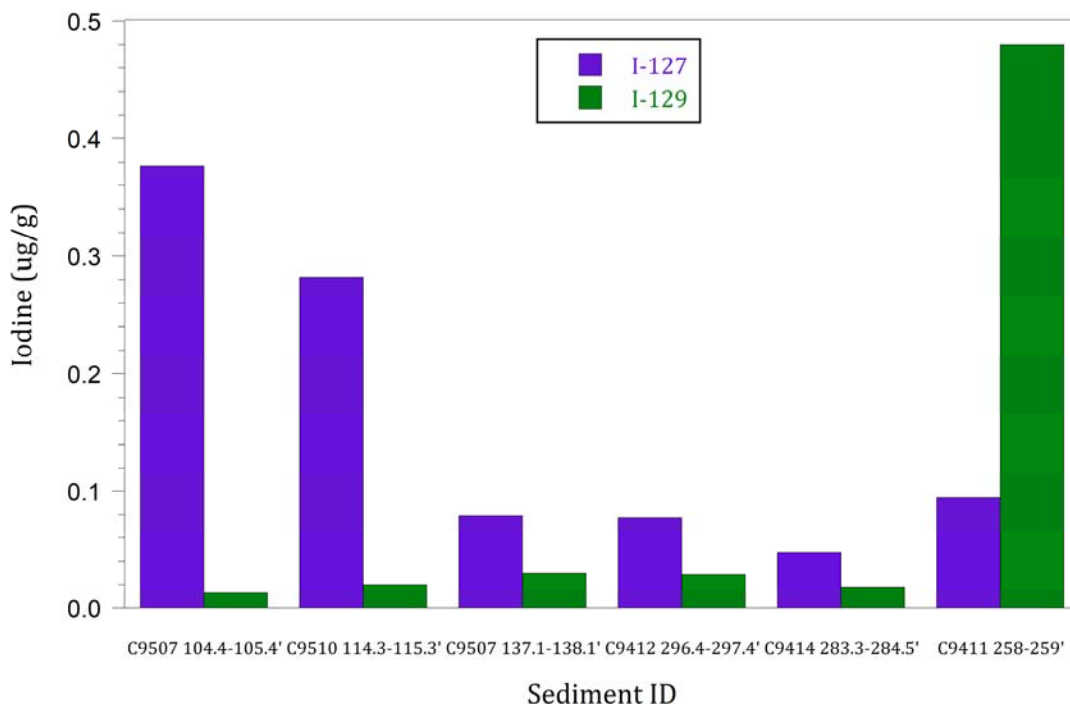
Figure 6.20. Comparison of iodine leaching with 0.1 M dithionite + 0.4 M potassium carbonate with 250-g/L sediment suspensions after 7 days with the concentration in µg/g for both I-127 (*purple*) and I-129 (*green*). Note: Results only shown for select samples for which I-129 analysis was completed and fraction removed cannot be computed as greater I-129 measured in dithionite extracts as compared to TMAH.

6.4.3.2   Comparison of Iodine-129/127 Removal with Iron Extractions

Additional experiments were conducted to investigate Fe phases and whether iodine was associated with iron phases. In these experiments, I-127 was measured in iron-specific extraction solutions (Figure 6.21). The extractions included (1) an amorphous ferric oxide extraction (NH_2OH-HCl), (2) amorphous and crystalline ferric oxide extraction (dithionite-citrate-bicarbonate, DCB), and (3) total ferrous/ferric extraction (5.0M HCl). Table 6.9 shows that the majority of Fe is present as Fe(III) with a significant fraction present as crystalline Fe. Further, Table 6.10 shows that Fe speciation does not change significantly following TMAH extractions, highlighting that these extractions are not extracting or altering Fe phases. Therefore, if iodine is co-precipitated with Fe phases, it is likely that it would not be extracted by TMAH as these data suggest that Fe phases are not dissolved by TMAH.

In general, there is a significantly greater amount of I-129 extracted via the Fe extraction (5.0 M HCl) as compared to the TMAH extraction, indicating (but not proving) that the iodine extracted by TMAH is not associated with Fe oxides. On average, $55\% \pm 17\%$ and $96.7\% \pm 1.4\%$ of total I-127 and -129, respectively, extracted in series with TMAH and then 5.0 M HCl was associated with the total Fe fraction (5.0 M HCl). These data suggest that (1) iodine is more readily removed by 5.0 M HCl as opposed to TMAH, (2) TMAH does not remove iodine from phases dissolved by 5.0 M HCl, and (3) TMAH may target different phases. These results provide secondary evidence that iodine may be strongly associated with Fe phases, especially for I-129.
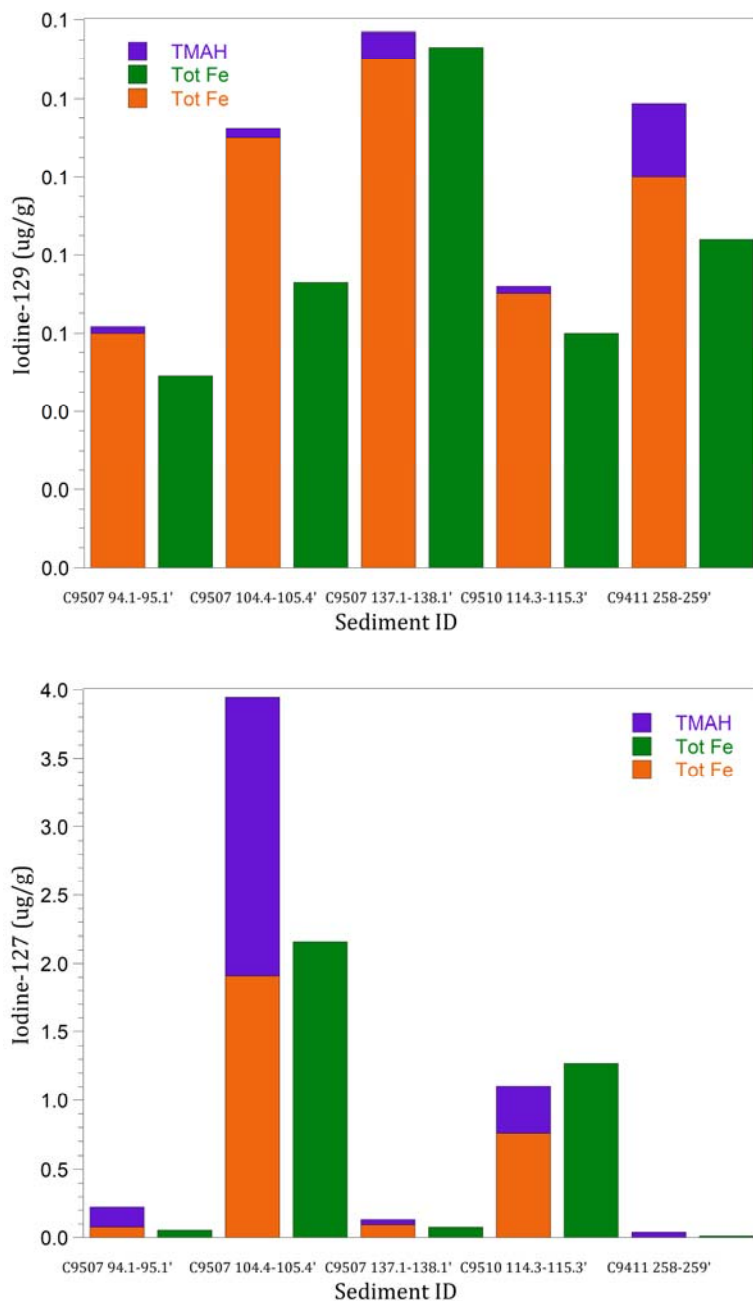
Figure 6.21. Summary of iodine in iron phases based on iron extractions (5.0 M HCl) for five sediments prior to TMAH extractions (*green*) and with the combined TMAH (*purple*) and iron extraction (*orange*), with I-129 (a) and I-127 (b).

Table 6.9. Summary of major components based on iron extractions for five sediments *prior* to 5% TMAH extractions, (1) amorphous iron via 0.25 M NH$_2$OH-HCl extraction, (2) crystalline and amorphous iron via DCB extraction, and (3) total iron via 5.0 M HCl extraction

Sample ID	% Amorphous	% Crystalline	% Fe(II)	% Fe(III)	Total Fe (mg/g)
C9507 94.1-95.1'	0.1%	21.8%	22.1%	77.9%	15.2
C9507 104.4-105.4'	0.0%	6.4%	25.6%	74.4%	8.5
C9507 137.1-138.1'	0.4%	4.0%	26.3%	73.7%	24.7
C9510 114.3-115.3'	0.0%	18.8%	24.7%	75.3%	13.4
C9411 258-259'	1.0%	14.3%	20.0%	80.0%	10.0

Table 6.10. Summary of major components based on iron extractions for five sediments *after* 5% TMAH extractions, (1) amorphous iron via 0.25 M NH$_2$OH-HCl extraction, (2) crystalline and amorphous iron via DCB extraction, and (3) total iron via 5.0 M HCl extraction

Sample ID	% Amorphous	% Crystalline	% Fe(II)	% Fe(III)	Total Fe (mg/g)
C9507 94.1-95.1'	0.5%	30.1%	23.9%	76.1%	13.3
C9507 104.4-105.4'	0.0%	5.0%	27.2%	72.8%	11.3
C9507 137.1-138.1'	0.8%	5.6%	32.7%	67.3%	16.9
C9510 114.3-115.3'	0.1%	18.1%	26.2%	73.8%	13.3
C9411 258-259'	1.4%	15.3%	21.3%	78.7%	10.2

6.4.4   Implications for Iodine-129 Mobilization for Pump-and-Treat

These results show that I-127 and I-129 exhibit different behavior in the Hanford subsurface likely due to their different sources, with the following major conclusions:

- Concentrations of I-127 are not correlated with depth but span approximately three orders of magnitude (0.03 to 2.3 µg/g via TMAH extraction). Further, I-129 and I-127 concentrations are not strongly correlated.

- Iodine-129 is more readily mobilized from sediments than I-127. For example, apparent partitioning coefficients for I-127 versus I-129 ranged from 210 to 3.7 mL/g and 4.2 to 12.9 mL/g, respectively, based on batch reactions of sediment with artificial groundwater.

- Na-dithionite extractions removed more iodine than artificial groundwater and extractants previously used for measuring total iodine in sediments (TMAH) (e.g., 4 to 10.1 times more I-129 was removed via Na-dithionite as compared to AGW). Further, iron-specific extractions removed significant amounts of iodine from sediments with 55% ± 17% and 96.7% ± 1.4% of total I-127 and -129, respectively, extracted in series with TMAH followed by 5.0 M HCl was associated with the total Fe fraction (5.0 M HCl).

Therefore, Na-dithionite may be a promising treatment for removal of I-129 in conjunction with pump and treat operations as it may remove significantly more I-129 than groundwater interaction with the sediments. However, future work is necessary to (1) identify whether anthropogenic iodine is associated with iron phases (potentially via laboratory experiments replicating Hanford conditions during waste

disposal), (2) identify whether citrate or another complexant is necessary to keep iron soluble and reduce secondary co-precipitation of iodine with iron phases, and (3) investigate the potential for natural variations in groundwater chemistry to mobilize iodine long term.

7.0 Materials for Iodine Immobilization

Above ground treatment of iodine, such as in the 200 West Area P&T system, is a potential groundwater remedial option for I-129 in the 200-UP-1 OU if materials with suitable properties can be identified. As a general target, based on the concentration range of I-129 in the 200-UP-1 OU, treatment to meet the required discharge standards would need to reduce I-129 from a maximum concentration of about 30 to 1 pCi/L (30-fold reduction). In addition, materials would need to achieve this reduction in the presence of I-127 concentrations that are typically about 1000 times higher than the I-129 concentration (Levitskaia et al. 2017). Thus, information about performance of treatment materials must consider this context for their deployment.

Potential engineered materials for specific uptake and sequestration of iodine for the range of expected iodine conditions have been evaluated. Materials were evaluated in terms of iodine uptake capacity, selectivity, affinity, and material stability. Material performance was compared with that for the materials currently in use at the 200 West P&T system: (1) Purolite A530E ion exchange resin and (2) Carbon Activated Corporation 011-55 granulated activated carbon. The following material categories were included in the evaluation: (1) iron oxide-influenced redox reactions and sorption, (2) sulfide phases, (3) reactions with bismuth-based materials, (4) organoclays, (5) aerogels, and (6) metal organic frameworks (MOFs). This initial laboratory scoping evaluation allowed candidate materials to be further tested if they showed sufficient promise for continued evaluation.

Ferrihydrite, bismuth oxy(hydroxide), and bismuth-cobalt-aluminum are the most promising materials, and the observed batch-test removal efficiency is sufficient to reduce concentrations of I-129 from 30 pCi/L to 1 pCi/L, even in the presence of a total iodine concentration loading (including I-127) in the groundwater is 1000 times higher than I-129. When available in sufficient quantities, the most promising materials were subsequently engineered into a viable form for deployment in the P&T system. In some cases, a viable form of the material was available commercially as hybrid ion exchange resins from ResinTech Inc. The promising materials were also embedded into polyacrylonitrile (PAN) beads. These engineered forms were then taken forward for kinetics testing and subsequent deployment in a column system, with relevant influent iodate concentrations and flow rates to verify removal efficiency.

7.1 Experimental Methods

Bench-scale tests were conducted to evaluate the efficacy of materials for treating targeted contaminants. Tests were conducted using methodologies reported in Mattigod et al. (2010a, 2010b) such that direct comparisons could be made to performance characteristics of materials previously evaluated and/or already in use. Candidate materials that met threshold screening criteria were further evaluated in a column configuration as an initial step in evaluating field-scale deployment.

7.1.1 Synthetic Groundwater

A synthetic groundwater was prepared for use in the experimental work using the recipe (Truex et al. 2017) shown earlier in Table 2.2.

7.1.2   Materials

7.1.2.1   Ion Exchange Resin

Purolite A530E (Purolite Company, Bala Cynwyd, PA) ion exchange resin was cleaned to remove residual metals left over from the manufacturing process by centrifuge washing two times for 15 min with distilled deionized water at a solution-to-solid ratio of 3:1, followed by centrifugation at 1700 rpm for 5 min. The resin is shipped in the chloride form and the excess chloride was removed by soaking the resin in distilled deionized water for 24 h. The resin was not centrifuged prior to decanting the water. The resin was rinsed once with distilled deionized water, the water was decanted, and then the resin was stored wet in a sealed poly bottle at room temperature while the moisture content was determined. The resin moisture content was determined using EPA Method 1314. The moisture content of the resin was calculated by weighing, nominally 1 to 3 g of wet resin in an individually tarred aluminum weighing boat and then the resin was dried in an oven for 24 h at $105\pm2°C$. The dried resin was weighed and returned to the oven for 2 h. This step was repeated until a constant weight was obtained. The dry weight of the resin was used as the basis to determine the solution-to-solid ratios, and to calculate the loading capacity. Thus, the dry weight of the resin used in the tests is reported along with the test results. Per the manufacturer's information, the total resin exchange capacity is 0.6 eq/L Cl⁻.

7.1.2.2   Granulated Activated Carbon (GAC)

Carbon Activated Corporation (CAC) 011-55 (coconut shell) GAC was selected since it is currently used in the 200 West P&T facility. The GAC was used "as-received," which is comparable to current P&T operations.

7.1.2.3   Iron Oxides

Iron oxides were selected to represent a range of redox conditions, from completely oxidized Fe(III) in ferrihydrite ($Fe(III)_5O_8H$), to mixed Fe(II)/Fe(III) in magnetite ($Fe(II)Fe(III)_2O_4$), to completely reduced Fe(II) in ferrous hydroxide ($Fe(II)OH_2$).

Synthetic 2-line ferrihydrite was prepared by titrating 0.092M $FeCl_3$ solution with 2M NaOH to a neutral pH (7.0). The precipitate that rapidly formed was agitated in a shaker overnight, followed by one last pH adjustment with 0.2 M NaOH to the neutral pH. After three rinses with deionized water and centrifugations at 5000 g, ferrihydrite was resuspended in deionized Milli-Q water and suspension density was calculated by dissolving a volume of ferrihydrite into 4 M HCl, reducing it with 10% hydroxylamine hydrochloride at pH 7, and analyzing Fe^{2+} using the ferrozine method (Stookey 1970).

The synthesis protocol for nano-magnetite has been reported in detail in Pearce et al. (2012). Briefly, Fe_3O_4 nanoparticles were synthesized under ambient conditions and in aqueous suspension by co-precipitating a stoichiometric mixture of $FeCl_2$ and $FeCl_3$ in 0.3 M HCl (pH < 1) with ammonium hydroxide (NH_4OH) solution in an anoxic glovebox. The precipitated nanoparticles were magnetically separated from the aqueous phase and washed twice with degassed and deionized milli-Q (>18 MΩ cm resistivity) water (DDW) to remove possible impurities, such as residual metal chlorides. After washing, the nanoparticles were resuspended in water prepared equivalently and stored inside the glovebox. The suspensions naturally equilibrated to a solution pH of ~8.5.

Micromagnetite particles were prepared following the method of Schwertmann and Cornell (2000). Oxidation of the $FeSO_4$ in an alkaline solution of KNO_3 at 90°C under a N_2 atmosphere yielded the magnetite particles, which were dried and stored under N_2 until analysis. Analysis following a new hybrid

oxidi-colorimetric method by Amonette and Matyáš (unpublished) revealed that micromagnetite was close to stoichiometric (~92%), with a composition of 70.96±0.41 wt% Fe_{Total} and 21.84±0.23 wt% Fe(II).

To synthesize ferrous hydroxide, $FeCl_2$ $4H_2O$ (14.00g, >95%, Fisher Scientific) was dissolved in DDW (400 g) in an anoxic glovebox. NaOH (10M, 8.2 mL) was added to the solution with shaking and it was left overnight to precipitate. The precipitated $Fe(OH)_2$ was filtered and dried for 24 to 48 h. Immediately prior to use, the dark oxidized surface layer was scraped off to reveal the white-green $Fe(OH)_2$, and the amount needed for testing was ground with a mortar and pestle.

7.1.2.4   Sulfide Phases

To synthesize iron sulfide (FeS) (1.0 g) in degassed, deionized water in an anoxic glovebox, a solution of $Fe(II)Cl_2 \bullet 2H_2O$ (1.65 g, 10 mL) was added to a solution of Na_2S (0.888g, 30 mL) to form a black precipitate. The precipitate was centrifuged (3000 rpm × 10 min) and washed with degassed, deionized water.

Potassium tin sulfide ($K_{2x}Mg_xSn_{3-x}S_6$, $x = 0.5$-1) was prepared by solid-state synthesis. A mixture of Sn (8.9 mmol, 1055 mg), Mg (4.7 mmol, 113 mg), K_2S (4.6 mmol, 204 mg), and S (15.7 mmol, 512 mg) was sealed under vacuum (10^{-4} Torr) in a fused silica tube and heated (10°C/h) to 550°C for 48 h, followed by cooling to room temperature at 100°C/h. The yellow polycrystalline product obtained was washed several times with water, acetone, and ether (in that order) (2 g, ~ 85% yield based on Sn). EDS analysis gave the average formula "$K_{1.3}Mg_{0.95}Sn_{2.1}S_6$" (Fard et al. 2015).

In a general procedure for tin sulfide (SnS), a mixture of solid $SnCl_2 \bullet 2H_2O$ (2.5 mmol) and $SnCl_4 \bullet 5H_2O$ (2.5 mmol) was suspended in 10 mL deionized water and the pH was adjusted to 12 by addition of NaOH while stirring. In a separate beaker, $Na_4S \bullet 9H_2O$ (15 mmol) was slowly added to 10 mL deionized water , and pH was adjusted first to 8 by drop-wise addition of 0.5 M NaOH, and then 12 by drop-wise addition of 2 M NaOH. The resulting Na_2S solution was slowly added to the Sn suspension, and the pH was adjusted to 12. The solution was stirred for 3 days at room temperature, transferred to a Teflon-lined autoclave, and kept at 110°C ± 5°C for 72 h to yield the aggregate. The obtained solid was gravity- filtered, washed with excess water until a neutral pH of the rinse water was obtained, and dried. The dried solid was ground into a fine powder using a mortar and pestle.

7.1.2.5   Bismuth-Based Materials

A typical synthesis for bismuth (oxy) hydroxide of the general structure $(BiO)_x(OH)(NO_3)_m(CO_3)_n$ involved suspending $Bi(NO_3)_3 \cdot 5H_2O$ and urea (2.7 mmol) in 50 mL ethylene glycol with stirring as described elsewhere (Qin et al. 2012). The mixture was subjected to solvothermal treatment at 150°C for 5 h in the Teflon liner of an autoclave vessel. The reaction mixture was allowed to cool to room temperature, and the ethylene glycol supernatant was decanted. The solid reaction product was collected via centrifugation (3500 rpm for 10 min). The solid was re-suspended in ultrapure water (10 mL/0.1 g sorbent), vortexed for 1 min, and collected by centrifugation. The washing procedure was repeated with ultrapure water for a total of five washes. The solid was then suspended in 100% methanol (10 mL/0.1 g sorbent), vortexed for 1 min, and collected by centrifugation. The methanol wash step was repeated twice more, and the product allowed to dry at room temperature. A comparable commercially-available bismuth-based material, bismuth subnitrate, was also obtained from Sigma Aldrich (Stock # B0426, Lot # MKCG7424).

The modified synthetic protocol for preparation of bismuth-cobalt-aluminum hydrotalcites was adapted from hydrothermal syntheses reported elsewhere (Byrappa and Yoshimura 2001). In a general procedure, the nitrate or chloride salts of Bi^{3+}, Co^{2+}, and Al^{3+} were dissolved in ~50 mL deionized water at a 2.5:2.5:1

molar ratio. The solution was stirred for about an hour, followed by the addition of 0.5 M NaOH solution while stirring until a pH of 8–9 was achieved. The mixture was stirred at room temperature for 3 days, transferred to a Teflon-lined autoclave, and kept at 110°C ± 5°C for 72 h to yield the aggregate. The obtained solid was gravity-filtered, washed with excess water until a neutral pH of the rinse water was achieved, and dried.

7.1.2.6 Organoclays

Two ORGANOCLAY® proprietary granular adsorption media samples were obtained from CETCO Mineral Technologies (Hoffman Estates, IL): CETCO MRM Organoclay and CETCO PM-200. Organoclays are composed of sodium bentonite that has been chemically altered to increase its sorption capacity for certain types of contaminants. MRM is a sulfur-impregnated organophilic clay granular filtration media that adsorbs non-aqueous phase liquids (NAPL) and dissolved low-solubility organics. It also sequesters mercury and arsenic from water. MRM has been formulated for use in groundwater P&T filtration, as PRB media, and as a solidification/stabilization additive to Portland cement. MRM contains a minimum of 25% quaternary amine loading. PM-199 is a granular adsorption media effective in removing oils, greases, other NAPL, and other dissolved high molecular weight/low solubility organics. PM-199 has been formulated for use in organophilic filtration media, bulk sediment capping, and as a solidification/stabilization additive. PM-199 contains 25% to 33% minimum quaternary amine loading.

7.1.2.7 Aerogels

Copper-functionalized silica aerogel was synthesized using a previously developed procedure (Matyáš et al. 2011). Briefly, granules of silica aerogel were hydrated in humidity-saturated air for 2 days. Following hydration, 3-(mercaptopropyl)trimethoxysilane [3-MPTMS; $HS(CH_2)_3Si(OCH_3)_3$, 95%] (Sigma Aldrich, St. Louis, MO) was distributed throughout the granules using a syringe at ~30 mL per 17 g of unhydrated sample. The wetted material was loaded into a 1-L high-pressure vessel and heated to 150°C, the vessel was filled with supercritical CO_2 at 24 MPa, and the sample was cooked for 24 h. Following this process, the thiol-modified aerogel (~12.5 g) was altered by installing the Cu(II) ions through treatment with 360 mL of 10 % $CuSO4·5H2O$ (99%, Sigma Aldrich) solution. About 60 mL of methanol was added to the solution to facilitate wetting of the moderately hydrophobic thiol-modified aerogel. The Cu^0 nanoparticles were produced on the silica aerogel pore surfaces by reducing the copper thiolate adduct ions at 165°C for 2 h under a 25 mL min^{-1} stream of 2.7% H_2 in Ar in a glass column.

7.1.2.8 Metal Organic Frameworks (MOFs) and Cationic Polymeric Networks (CPNs)

MOFs and CPNs with demonstrated efficient and selective anion capture were obtained from external collaborators for testing; SCU-101, SCU-102, and SCU-CPN-1-Cl were obtained from Professor Shuao Wang, Soochow University, China; Fe-BTC/PDA was obtained from Professor Wendy Queen, École Polytechnique Fédérale de Lausanne (EPFL), Switzerland.

1. SCU-101 and SCU-102 are a hydrolytically stable and radiation-resistant cationic MOF. SCU-101 has the chemical formula $[Ni_2(tipm)_2(C_2O_4)](NO_3)_2·2H_2O$ (tipm = tetrakis[4-(1-imidazolyl)phenyl]methane). These compounds exhibit fast removal kinetics, high sorption capacity, and unique molecular recognition derived sorption selectivity toward pertechnetate (TcO_4^-), and the anion exchange mechanism, shown in Figure 7.1a, is anticipated to be similar for IO_3^- (Zhu et al. 2017). The structure of SCU-102 is given in Figure 7.1b.

2. The synthesis of SCU-CPN-1-Cl is reported in Li et al. (2018). Briefly, SCU-CPN-1-Br, derived from the quaternization reaction between 1,1,2,2-tetrakis(4-(imidazolyl-4-yl) phenyl)ethene (TIPE) and 1,4-bis(bromomethyl)benzene, was soaked in saturated sodium chloride (NaCl) solution for 12 h to yield SCU-CPN-1-Cl. SCU-CPN-1-Cl demonstrates fast sorption kinetics and high sorption capacity

for anions and the exchange mechanism, shown in Figure 7.1c for ReO_4^-, is anticipated to be similar for IO_3^- (Li et al. 2018).

3. Fe-BTC (BTC = 1,3,5-benzenetricaboxylate) was prepared by heating a solution of iron(III) chloride hexahydrate (9.72 g) and trimesic acid (3.36 g) in DDW (120 mL) in a Teflon autoclave at 130°C for 72 h (Sun et al. 2018). The resulting solid was washed and purified prior to polymerization with polydopamine (PDA), and the structure is shown in Figure 7.1d. Fe-BTC exhibits rapid, selective removal of anions, such as $Cr(VI)O_4^-$, so it is anticipated to exhibit similar affinity for IO_3^- (Sun et al. 2018).
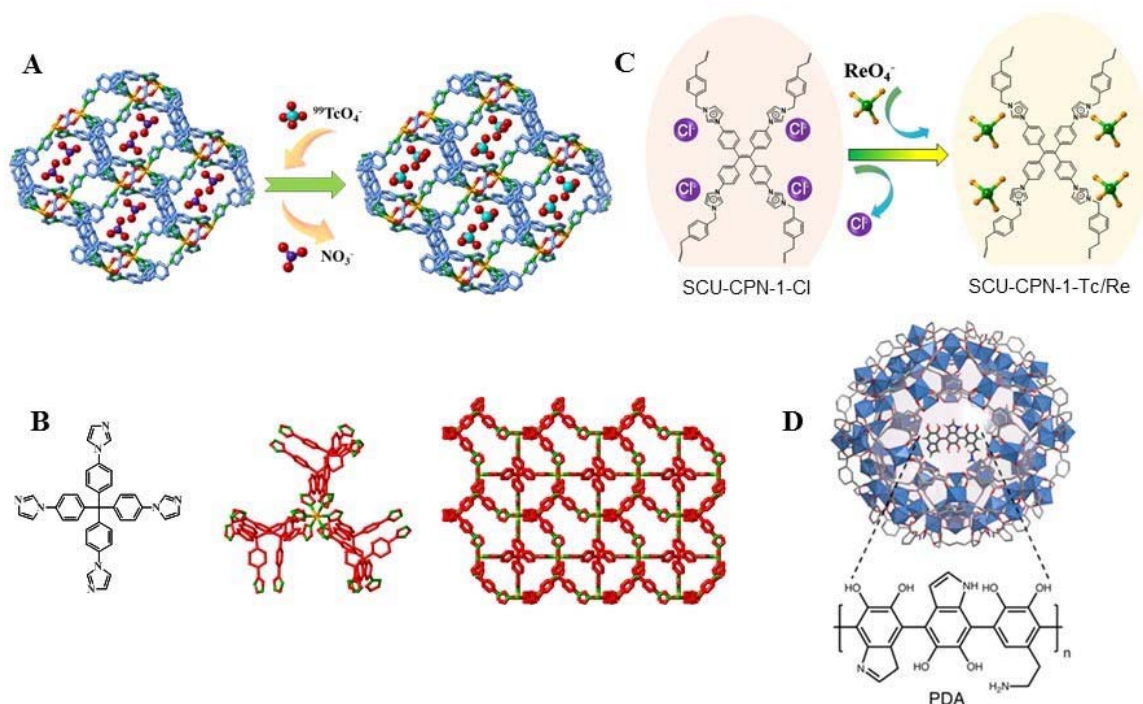
Figure 7.1. (A) Anion (TcO_4^-) exchange mechanism for SCU-101(atom color: Ni-orange; O-red; C-blue; N-green); (B) Structure of SCU-102 (atom color: Ni-orange; C-red; N-green); (C) Anion (ReO_4^-) exchange mechanism for SCU-CPN-1; (D) Polyhedral view of a large cage in the Fe-BTC with PDA embedded inside the channels.

7.1.3   Active Sorbent Deployment in Polyacrylonitrile (PAN) Beads

PAN fibers (X100, 3.3 dtex, 60 mm; Dralon GmbH, Dormagen, Germany) were dissolved in dimethyl sulfoxide (DMSO) at a ratio of 0.1 g PAN to 1.5 mL DMSO. Once fully dissolved, an active sorbent was added to the PAN/DMSO mixture and homogenized by stirring. After thorough mixing, the solution was dropped gently using a small pipette tip into a stirred water bath. Upon contact with water, the mixture formed PAN-active sorbent beads with a diameter of ~ 2 mm. After all beads were formed, they were transferred to a fresh deionized water bath to soak overnight. To eliminate residual DMSO, beads underwent 1 of 3 treatments: oven drying (50°C) until mass became stable, air drying, or rinse only in successive deionized water baths (5 × 50 mL). One batch of PAN-blanks (no active sorbent added) was made and PAN-blanks were used as controls. Consistent homogenization of the active sorbent in the PAN/DMSO matrix was difficult. The active sorbent would settle out if not constantly stirred. This was especially true for the ferrihydrite. Bismuth compounds were much finer powders that remained suspended longer but settled if given enough time. Thus, beads were made and tested in 0.1 g active sorbent batches and were not combined or divided. Individual beads were not compared because active

sorbent loading varied among beads. To assess the effect(s) of drying the beads prior to batch sorption testing, blank beads (0.1 g) were dried: (1) overnight in air or (2) overnight in an oven at 80°C.

7.1.4   Active Sorbent Deployment in Hybrid Ion Exchange Resins

Several ion exchange resins (Resin Tech Inc., West Berlin, NJ) were identified as potential candidates for iodine retention in the P&T facility. CHM-20 is a gel hybrid Type 2 strong base anion resin (dimethylethanolamine) with cerium oxide. ASM-125 is a chloride form gel hybrid Type 1 strong base anion resin (trimethylamine) containing hydrated iron oxide, used to treat pressurized water reactor water for antimony and silica. ASM-HP-10 is a chloride form gel hybrid Type 2 strong base anion resin (dimethylethanolamine) with hydrated iron oxide, used to remove arsenic, uranium, and other trace level contaminants from treated drinking water. Bi-form is a gel hybrid Type 1 strong base anion resin (trimethylamine). The active sorbent is homogeneously distributed throughout the resins. Corrections for the metal and moisture content per each resin were made according to assays provided by the manufacturer (see Table 7.1).

Table 7.1.   ResinTech resin characteristics.

Material	Type	Metal	Moisture Content (%)
CHM-20	Type 2 (dimethylethanolamine)	La = 2.69-3.13 g/kg Ce = 55.4 g/kg	-
ASM-10-HP	Type 2 (dimethylethanolamine)	Fe = 115 g/kg	45.1
ASM-125	Type 1 (trimethylamine)	Fe = 122 g/kg	45.9
Bi Form	Type 1 (trimethylamine)	Bi = 114g/kg	-

7.1.5   Batch Loading Tests

Solutions were prepared by adding the appropriate amount of sodium iodate (Fisher Scientific, Pittsburgh, PA) to simulated ground water to obtain 1.0 mg/L iodine. The pH of the starting solution containing iodate prior to addition of materials was 7.96.

Batch loading tests were conducted per PNNL Technical Procedure ESG-BSE-001, Rev. 3, where a mass of material and the appropriate amount of iodate solution to achieve the target ratio were placed into a 125-mL bottle or 50-mL falcon tube. The sizes of the bottles and tubes were chosen in an attempt to minimize headspace issues and volatilization concerns. Process blanks included solution blanks (initial iodate solution with no material) and material blanks (material in simulated groundwater with no iodate). Process blanks were prepared and handled in the same manner as all other loading tests. The bottles were sealed and placed on a shaker table set at 125 rpm to ensure the materials and iodate solution remained well mixed for the required 24-h period. All loading tests and process blanks were kept at room temperature. After the 24-h contact time, the bottles were removed from the shaker table and the solid materials were allowed to settle for 15 min. A 0.45-μm syringe filter was then used to separate the aqueous matrix from the sorbent. A 10-mL aliquot was removed, approximately 5-mL was pushed through the filter to prime the filter, and the remaining solution was placed into a 20-mL liquid scintillation vial.

Total iodine was analyzed on two different ICP-MS instruments based on equipment availability. The first instrument was an X-Series II ICP Mass Spectrometer from ThermoFisher Scientific and the second

instrument was an ELAN DRC II ICP Mass Spectrometer from PerkinElmer. The detection limit for total iodine is 0.0126 µg/L for both instruments. Two solution-to-solid ratios (200 and 1000) were used to span the range of predicted iodate uptake by the different materials. Actual material masses and solution volumes used in the batch tests were recorded and the tests were conducted in duplicate. After the 24-h sampling, the tubes from each test were returned to the shaker and re-sampled to obtain the > 30-day iodine loading sample. On additional tube for each test was prepared at a solution-to-solid ratio of 200.

After the 24-h batch loading test, the solid phase was extracted by centrifugation and analyzed by I K-edge X-ray absorption spectroscopy (XAS) on 20-BM-B at the Advanced Photon Source, Argonne National Laboratory, to determine the species of iodine present on the solid phase. Additional solid phase characterization included XRD to confirm the structure of the starting materials and SEM after reaction to examine the interaction between the iodine and the material.

7.1.6   Kinetics Screening

A limited kinetics test was performed on PAN-active sorbent materials, PAN-Bismuth (oxy)hydroxide (PAN-BIN), PAN-BSN, PAN-Ferrihydrite, and PAN-control) and two of the four resins (CHM-20 and ASM-HP-10). These were chosen based on best performance in earlier batch loading tests. To establish similar parameters for direct comparison to non-PAN batch loading results, a kinetics matrix of 0.1 g of sorbent in PAN-bead form at a 200 solution-to-solid ratio (in the same simulated groundwater composition as previous batch loading tests) at 7 time points (1, 3, 10,30, 120, 360, and 1440 min) was chosen. Total iodine was analyzed using the same instrumentation that was used for batch loading samples. The kinetics screening results were used to establish concentration and flow parameters for follow-up column testing.

7.1.7   Column Experiments

Flow-through column experiments were conducted with three PAN-sorbent materials, and the two ion exchange resins with the best performance determined by kinetics screening and batch loading tests. The goal of conducting column tests was to quantify iodine (in the form of iodate) uptake by each of the materials. Column experiment solutions were prepared using 200 West Area groundwater (filtered with 0.45-µm filter). All solutions used were 200 West Area groundwater amended with either 0.1 mg/L or 1 mg/L iodine (added as $NaIO_3$). The concentrations of the major components and contaminants of interest for this groundwater are shown in Table 7.2. The flow-through column experiments were conducted in PEEK columns that were 30 mm long with an inside diameter of 7.5 mm (volume 1.325 cm^3) with 5 µm frits and O-rings at each end. Each column was packed with test material, and pore volume of the column was determined for each. The solutions were pumped through the columns at a flow rate of either 4.5 or 25 mL/h. Due to the experimental nature of working with the PAN-sorbent materials, initial concentration of the solution and flow rate were adjusted depending on results. Effluent samples were collected with a fraction collector in pre-tared vials at intervals relevant to flow rate. After completion of the experiment, the vials were weighed to determine the cumulative volume of solution that passed through the column. All samples and blanks were analyzed for total iodine by ICP-MS.

Table 7.2. Major component and contaminant concentrations in the 200 West Area groundwater used in these studies.

Initial Composition	
Component	**Concentration (mg/L)**
Calcium	59.8
Chloride	19.1
Magnesium	20.6
Potassium	7.28
Silicon	28.2
Sodium	24.2
Strontium	0.22
Sulfate	73.7
Contaminant	**Concentration (µg/L)**
chromium	1.16
Total iodine (I-127 + I-129)	22.2
Nitrate	12,000
Tc-99	<0.03
U-238	2.04

7.2 Results

7.2.1 Iodine Loading Results

The initial and final iodine concentrations, the amount of dry material, and solution volumes are shown in Table 7.3 for the tests conducted at a solution-to-solid ratio of 200 and Table 7.4 for the tests conducted as a solution-to-solid ratio of 1000.

The initial and final total iodine concentrations for the most promising active sorbents, a new batch of bismuth (oxy)hydroxide (BIN-19), a commercially available bismuth-based material (BSN) and ferrihydrite (FeH), along with the different deployment mechanisms, are shown in Table 7.5 at a solution-to-solid ratio of 200, with a solution volume of ~20 mL and ~0.1 g of dry material. The pH of the solutions after iodine loading for the materials tested remained at 7.0-8.0, assuring predominance of iodate.

Potential uptake of calcium (Ca^{2+}), magnesium (Mg^{2+}), potassium (K^+), sodium (Na^+), and sulfur (S) from the synthetic groundwater by the materials (Table 7.6, with a solution-to-solid ratio of 200) was calculated as the difference between the initial concentration of the cations and the final concentration after 24-h incubation period. These results indicate the selectivity of the materials for iodine. A negative number indicates release of the element into solution from the material.

Table 7.3.   Iodate loading results for materials (solution-to-solid ratio = 200).

Material Tested	Iodine Initial Concentration (mg/L)	Iodine Final Concentration 0-1 day (mg/L)	Iodine Final Concentration >0-30 days (mg/L)	Mass of Material-Dry (g)	Soln. Vol. (mL)	Iodine Loading 0-1 day (mg/g)	Iodine Loading >0-30 days (mg/g)	K_d after 1 day (mL/g)	Iodine Species on Solid[a]	pH after Reaction
530E Resin	1.01	0.73	0.74	0.10	20.00	0.06	0.05	78.24	I^-	7.58
CAC GAC	1.01	0.73	0.68	0.11	21.11	0.06	0.07	76.68	I^-/IO_3^-	8.12
Ferrihydrite	1.02	0.05	0.04	0.10	17.11	0.17	0.17	3230.89	I^-/IO_3^-	7.26
Nano-magnetite	1.01	0.79	0.75	0.10	19.72	0.04	0.05	54.60	I^-	7.83
Ferrous Hydroxide	1.01	0.93	0.79	0.10	19.80	0.02	0.04	16.34	-	8.00
Potassium Tin Sulfide	1.01	1.01	0.99	0.10	20.81	0.00	0.00	0.00	-	8.54
Iron Sulfide	1.01	1.01	0.98	0.10	20.31	0.00	0.01	0.00	-	7.52
Tin Sulfide	0.99	0.79	0.82	0.10	20.08	0.04	0.03	51.97	-	7.33
Bismuth (oxy)hydroxide	1.01	0.00	0.00	0.11	21.01	0.20	0.20	201903.90	IO_3^-	8.04
Bi-Co-Al	0.99	0.02	0.00	0.10	20.18	0.19	0.20	12800.47	IO_3^-	7.75
Organoclay (PM-199)	1.02	0.82	0.79	0.10	20.78	0.04	0.05	51.95	I^-	7.95
Organoclay (MRM)	1.02	0.78	0.47	0.11	21.57	0.05	0.11	61.85	I^-	5.55
Cu-Silica Aerogel	1.01	0.85		0.11	21.47	0.03		37.35	IO_3^-	6.64
SCU-101 (MOF)	1.02	0.82	0.72	0.11	21.10	0.04	0.06	49.16	I^-	7.71
SCU-102 (MOF)	1.02	0.76	0.73	0.10	20.86	0.05	0.06	67.37	I^-	7.90
SCU-CPN (MOF)	1.02	0.24	0.23	0.11	21.17	0.16	0.16	635.77	I^-/IO_3^-	7.27
FeBTC-PDA (MOF)	1.02	0.41	0.25	0.11	21.42	0.12	0.15	287.36	I^-/IO_3^-	5.65

(a) Iodine species on the solid after 24-h batch sorption. Iodine speciation could not be determined for some materials as (1) the amount of iodine was below the detection limit of I K-edge XAS and (2) tin caused interference in the absorption spectrum at the I K-edge energy (33.17 KeV).

Table 7.4. Iodate loading results for materials (solution-to-solid ratio = 200).

Material Tested	Iodine Initial Concentration (mg/L)	Iodine Final Concentration 0-1 day (mg/L)	Iodine Final Concentration >0-30 days (mg/L)	Mass of Material-Dry (g)	Soln. Vol. (mL)	Iodine Loading 0-1 day (mg/g)	Iodine Loading >0-30 days (mg/g)	K_d after 1 Day (mL/g)
530E Resin	1.01	0.97	0.96	0.10	100.00	0.04	0.05	43.39
CAC GAC	1.01	0.81	0.78	0.12	105.80	0.21	0.23	254.66
Ferrihydrite	1.02	0.57	0.48	0.10	97.11	0.44	0.55	763.61
Nano-magnetite	1.01	0.82	0.80	0.10	99.72	0.19	0.21	232.56
Ferrous Hydroxide	1.01	1.00	0.98	0.10	99.50	0.01	0.03	11.96
Potassium Tin Sulfide	1.01	1.01	0.99	0.10	103.15	0.00	0.02	4.00
Iron Sulfide	1.01	1.00	1.00	0.10	100.18	0.01	0.01	12.05
Tin Sulfide	0.99	0.80	0.79	0.10	100.20	0.19	0.19	237.80
Bismuth (oxy)hydroxide	1.01	0.19	0.09	0.10	101.55	0.82	0.92	4204.12
Bi-Co-Al	0.99	0.45	0.37	0.10	101.05	0.54	0.62	1218.09
Organoclay (PM-199)	1.02	0.83	0.81	0.11	110.50	0.19	0.21	229.96
Organoclay (MRM)	1.02	0.83	0.28	0.11	111.10	0.19	0.74	225.96
Cu-Silica Aerogel	1.01	0.99	0.94	0.11	105.40	0.02	0.07	22.27
SCU-101 (MOF)	1.02	0.85	0.80	0.11	105.60	0.17	0.22	195.04
SCU-102 (MOF)	1.02	0.81	0.77	0.11	110.50	0.21	0.25	254.61
SCU-CPN (MOF)	1.02	0.66	0.65	0.11	105.30	0.36	0.37	554.88
FeBTC-PDA (MOF)	1.02	0.85	0.53	0.10	100.55	0.17	0.49	198.27

Table 7.5.   Iodine loading results (solution-to-solid ratio = 200).

Active Sorbent	Deployment Mechanism	Iodine Initial Concentration (mg/L)	Iodine Final Concentration (mg/L)	Iodine Loading (mg/g)	K_d (mL/g)
BIN-19	Synthesized powder	1.0700	0.00001	0.214	2,140,000
BSN	Commercially available powder	1.0700	0.00001	0.214	2,140,000
FeH	Synthesized powder	1.0750	0.0026	0.215	83,900
BIN-19	PAN beads	1.0800	0.0005	0.216	475,000
BSN	PAN beads	1.0050	0.0010	0.199	199,000
FeH	PAN beads	1.0800	0.0726	0.201	2780
BLA	PAN beads no active sorbent	1.0800	0.9667	0.023	23
CHM-20	Hybrid ion exchange resins	1.0050	0.0002	0.203	1,270,000
ASM-125	Hybrid ion exchange resins	1.0050	0.0018	0.200	114,000
ASM-HP-10	Hybrid ion exchange resins	1.0050	0.0002	0.201	857,000
Bi-Form	Hybrid ion exchange resins	1.0050	0.0129	0.198	15,400

(a) Mass of active sorbent corrected based on metal content of the resin.

Table 7.6. Iodine - Groundwater Constituent Loading Results for Materials (Solution-to-solid Ratio = 200)

Active Sorbent	Deployment Mechanism	Ca Uptake (µg/l)	Mg Uptake (µg/l)	K Uptake (µg/l)	Na Uptake (µg/l)	S Uptake (µg/l)
BIN-19	Synthesized powder	300	-25	15	130	14311
BSN	Commercially available powder	450	-60	15	130	14311
FeH	Synthesized powder	-150	200	30	-2375	15836
BIN-S	Silica substrate	200	20	50	5	13675
BIN-19	PAN beads	1500	355	515	135	13700
BSN	PAN beads	ND	ND	ND	ND	ND
FeH	PAN beads	5350	680	1110	885	9860
BLA	PAN beads no active sorbent	2550	500	770	-740	1100
CHM-20	Hybrid ion exchange resins	1750	200	-10	-10885	17011
ASM-125	Hybrid ion exchange resins	-5800	-10	-35	-590	17011
ASM-HP-10	Hybrid ion exchange resins	200	-15	-55	-1635	17011
Bi-Form	Hybrid ion exchange resins	-20550	15	15	-95	17011

ND   data not available

7.2.2   Kinetics

Kinetic experiments were performed to determine the rate of iodine uptake on the three best-performing sorbent materials in the batch sorption experiments. These materials included PAN-bismuth (oxy)hydroxide materials, PAN-ferrihydrite, PAN-bismuth subnitrate, two hybrid ion exchange resins, CHM-20 and ASM-HP-10. The experiments were performed at a solution-to-solid ratio of 200 in SGW spiked with 1 mg/L Iodine (as NaIO$_3$). The target amount of active sorbent for beads and resins was 0.1 g in order to provide a direct comparison to earlier batch loading tests results.

The selected time intervals chosen were 1, 3, 10, 30, 120, 360, and 1440 min. Similar to previous loading tests, the tests were prepared by adding the material and simulated groundwater to each tube and placing the tube on a shaker table set at 125 rpm for the indicated amount of time. At the end of the interval, 10-mL of solution was removed with a disposable syringe, and pushed through a 0.45-µm PES syringe filter with the first 5 mL used to prime the filter and the remainder collected as a sample.

The results for the PAN-sorbent materials are shown in Figure 7.2. PAN-beads without sorbent were used as a control. The three PAN-sorbent materials, bismuth (oxy)hydroxide (BIN), bismuth subnitrate (BSN) and ferrihydrite (FEH), had iodine loading values of 0.2018, 0.2014, and 0.1912 mg/g, respectively, after 24 h. For comparison, the three active sorbents in the absence of PAN had iodine loading values of 0.2141, 0.2142, and 0.2148 mg/g respectively after 24 h. All three PAN-sorbent materials demonstrated a sorption capacity sufficient to remove > 92% of the initial 1 mg/L iodine concentration under these specific conditions.
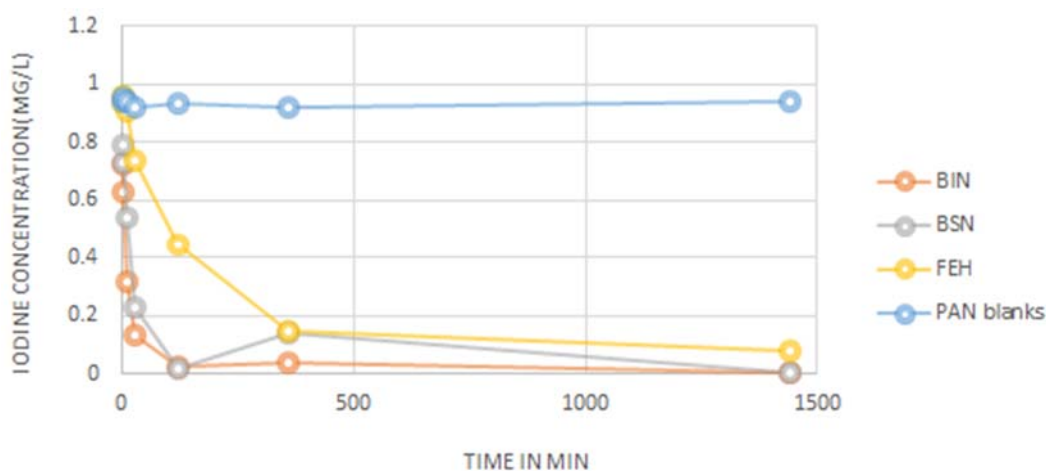
Figure 7.2.   PAN-active sorbent kinetics.

The two best-performing hybrid ion exchange resins (CHM-20 and ASM-HP-10) were selected for kinetic experiments and the results are shown in Figure 7.3. CHM-20 and ASM-HP-10 had iodine loading values of 0.2018, and 0.2014 mg/g, respectively, after 24 h. These two resins demonstrated a sorption capacity sufficient to remove > 99% of the initial 1 mg/L iodine concentration under these specific conditions.
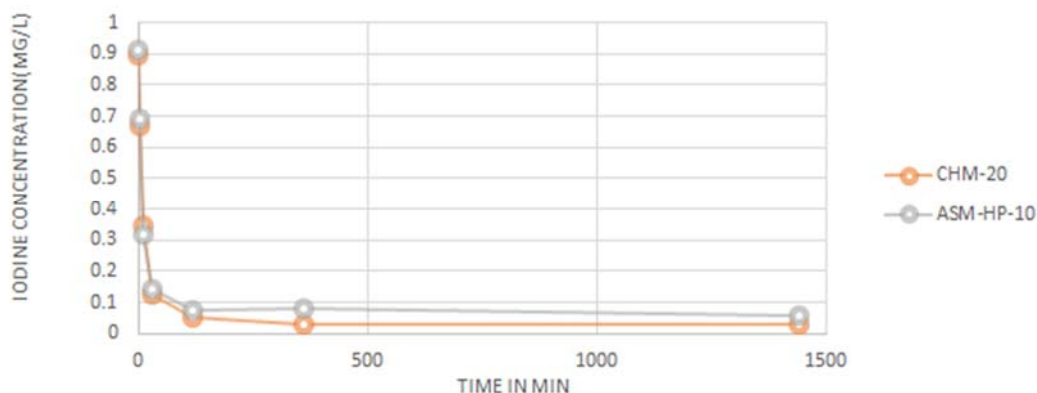
Figure 7.3.   Hybrid ion exchange resin kinetics.

7.2.3   Column Experiments

Initial flow-through column experiments were conducted with PAN-BSN beads to determine the optimum iodine concentration and flow rate to evaluate iodine uptake by the hybrid sorbents. Two starting solution concentrations of iodine (added as $NaIO_3$) were used (100 µg/L and 1000 µg/L) in 200 West Area groundwater (Table 7.2). The two columns for the 100-µg/L and 1000-µg/L concentrations were packed with PAN-bismuth subnitrate beads, 0.708 and 0.765 g, respectively, and the pore volumes were 0.848 and 1.140 mL, respectively. The flow rate for both tests was 25 mL/h, with effluent samples collected every 25 mL for 7 days. Iodine concentrations determined by ICP-MS are shown in Figure 7.4.
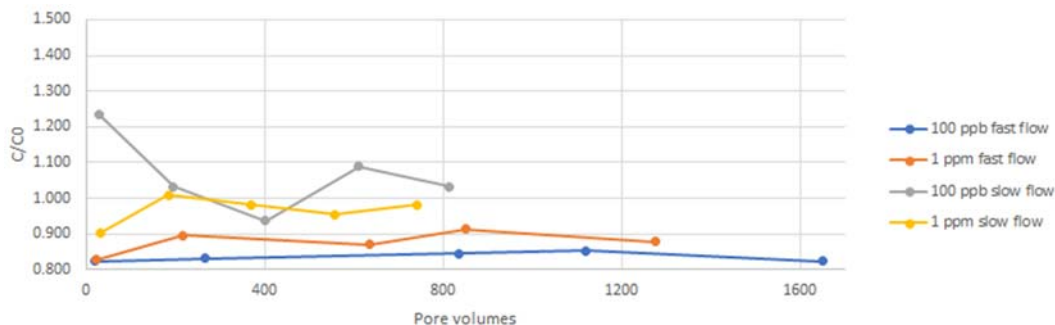
Figure 7.4.   Iodine breakthrough curves for PAN-bismuth subnitrate columns.

A second set of tests with PAN-BSN materials was run at the two concentrations with a slower flow rate and collection limited to once every 5 h. The columns for the 100-µg/L and 1000-µg/L concentrations were packed with PAN-bismuth subnitrate beads, 0.714 and 0.731 g, respectively, and the pore volumes were 1.033 and 1.009 mL, respectively. The flow rate for both tests was reduced to 4.5 mL/h. Iodine concentrations determined by ICP-MS are shown in Figure 7.4. The results indicate that little if any removal of iodate occurred on the PAN-bismuth subnitrate beads under the conditions used.

Column tests were conducted with the CHM-20 and ASM-10-HP hybrid ion exchange resins using an influent concentration of 100 µg/L iodine (added as $NaIO_3$) in 200 West Area groundwater (Table 7.2) at a flow rate of 25 mL/h for both columns. The CHM-20 and ASM-10-HP columns were packed with 0.922 and 0.935 g of resin, respectively, with pore volumes of 0.575 and 0.738 mL for each, respectively. Effluent samples were collected every 25 mL for 7 days. Iodine concentrations determined by ICP-MS are shown in Figure 7.5. Results indicate that CHM-20 sequestered iodate more effectively than

ASM-10-HP, with 50% breakthrough occurring at 324 PVs for CHM-20 and 268 PVs for ASM-10-HP. Three percent breakthrough occurred at 128 PVs for CHM-20 and 121 PVs for ASM-10-HP. Iodate peaks in the effluent above a C/C^0 of 1.0 were observed for both resins. These results suggest that a dynamic shift occurred in the exchangeable anions on the resins during the experiment. It is possible that the chloride initially occupying the exchange sites on the resins shifted to nitrate and that iodate has a greater selectively for exchange sites occupied by chloride relative to nitrate, resulting in the observed behavior. This behavior was more pronounced for ASM-10-HP than CHM-20.
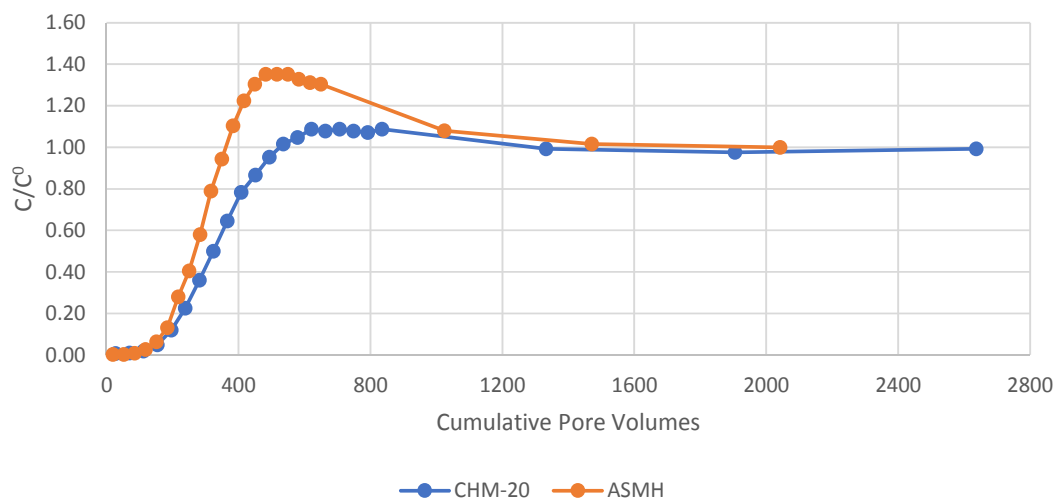
Figure 7.5.   Iodine breakthrough curves for CHM-20 (blue) and ASM-10-HP (orange) hybrid ion exchange resin columns.

A final pair of column tests were conducted with PAN-BIN and PAN-FEH sorbent beads at an influent concentration of 100 μg/L iodine (added as $NaIO_3$) in 200 West Area groundwater (Table 7.2) at a flow rate of 25 mL/h for both. The PAN-BIN and PAN-FEH columns were packed with 0.902 and 0.758 g of PAN-active sorbent respectively and pore volumes were 0.699 and 1.121 mL for each, respectively. Effluent samples were collected every 10 min for the first hour and every 25 mL after that up to a total of 50 h. Iodine concentrations determined by ICP-MS are shown in Figure 7.6. The results show significant breakthrough occurred at the first sampling point, indicating that in the current configuration, these materials would not be an effective sorbent for iodate.
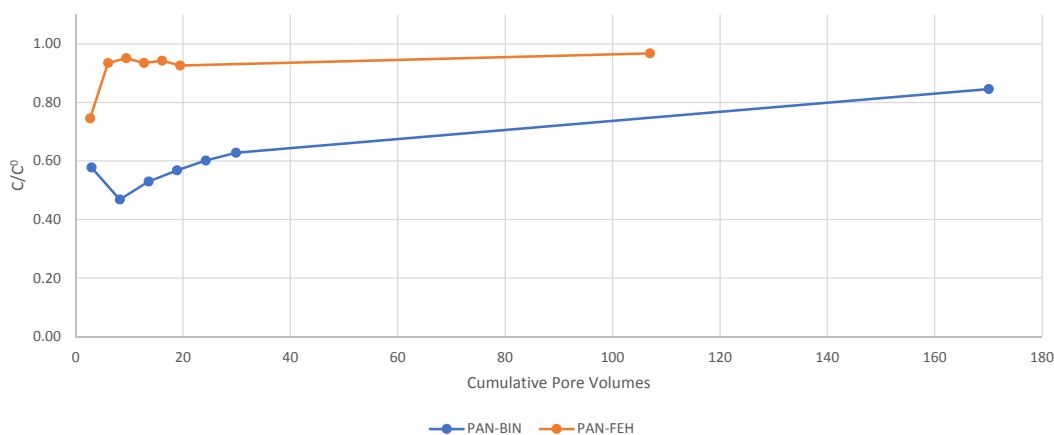
Figure 7.6.   Iodine breakthrough curves for PAN-bismuth (oxy)hydroxide (blue) and PAN-ferrihydrite (orange) columns.

7.3   Discussion

7.3.1   Material Evaluation

7.3.1.1   Baseline P&T Materials (Purolite A530E Ion Exchange Resin and Carbon Activated Corporation GAC)

The baseline materials currently deployed at the 200 West Area P&T, Purolite A530E ion exchange resin and Carbon Activated Corporation GAC, had similar distribution coefficients of 78 and 77 mL/g, respectively, for iodate at a solution-to-solid ratio of 200. The performance was lower for the A530E at the higher solution-to-solid ratio of 1000. The resin appears to have been at capacity for the solution-to-solid ratio of 200, consistent with results by Levitskaia et al. (2017), where spent resin from the P&T facility showed an I-127 loading of 44–58 µg/g. The CAC-GAC material showed additional capacity in the solution-to-solid ratio of 1000, with a loading increase by over a factor of 3. The higher surface area of the CAC-GAC compared to the resin may have contributed to this increased capacity. While the CAC-GAC and the A520E materials have capacity to remove iodine from solution, batch experiments indicate that the removal efficiency is significantly below that required to reduce concentrations of I-129 from ~30 pCi/L to 1 pCi/L considering the total iodine concentration loading that will be present due to I-127 in the groundwater at about 1000 times the I-129 concentration (Levitskaia et al. 2017). Column tests with relevant influent concentrations are needed to verify removal efficiency. Removal rate appears to be rapid, with the 1-day iodine loading on the CAC-GAC and the A520E similar to that for >30 days sample loading.

Analysis of the solid phase after reaction by I K-edge XAS revealed that the iodine speciation was no longer iodate, as was present in the starting solution, but was iodide for A530E and predominantly iodide, with a slight shift in the absorption edge due to the presence of some iodate, for CAC-GAC. This suggests that iodine loading onto the solid was not solely due to sorption, but changes in the solution chemistry caused reduction of a small fraction of the iodate to iodide, and this was preferentially sorbed onto the A530E and CAC-GAC. This is in agreement with previous studies by Parker et al. (2014), in which sorption of iodine was affected by iodine speciation in the 200 West Area groundwater. In this study, iodine loading on resins was increased by an order of magnitude when the iodine was converted to iodide.

7.3.1.2   Iron Oxides

The best-performing iron oxide material was ferrihydrite (Fe(III)5O8H), with loading values of 166 and 436 µg/g and K_d values of 3231 and 764 mL/g, at solution-to-solid ratios of 200 and 1000, respectively. The K_d value of 3231 mL/g at a solution-to-solid ratio of 200 is lower than that obtained for the batch sorption with ferrihydrite at a solution-to-solid ratio of 500 as described in Section 5 (K_d = 7826 mL/g), but those experiments were conducted in DDW and did not have the competing effects of the other ions present in the synthetic groundwater used here. Because loading on ferrihydrite increased for the solution-to-solid ratio of 1000 compared to the solution-to-solid ratio of 200, it was not at capacity at the solution-to-solid ratio of 200, also demonstrated by the near complete removal of iodine from solution in those tests. The observed batch-test removal efficiency in the solution-to-solid ratio of 200 (~20-fold) may be sufficient to reduce concentrations of I-129 from 30 pCi/L to 1 pCi/L even in the presence of the total iodine concentration loading due to I-127 in the groundwater at about 1000 times the I-129 concentration (Levitskaia et al. 2017). Column tests with relevant influent concentrations would be needed to verify removal efficiency. Removal rate appears to be rapid, with the 1-day iodine loading on the ferrihydrite similar to that for >30 days of loading.

Analysis of the ferrihydrite solid phase after reaction by I K-edge XAS revealed that the iodine speciation was predominantly iodate, with a reduction in the intensity of the white line due to the presence of some

iodide. The amount of iodate remaining in solution decreased slightly over the longer >30-day sorption test, and thus, iodate was not released back into solution, despite that fact that ferrihydrite is unstable and likely undergoing transformation to goethite.

Nano-magnetite (Fe_3O_4) performed less well, with loading values of 40 µg/g and K_d values of 55 mL/g, at a solution-to-solid ratio of 200, and an iodine loading of 190 µg/g and a K_d of 233 mL/g at the higher solution-to-solid ratio of 1000. These materials have a relatively high surface area that helps contribute to higher loading, although loading is not as high as for the ferrihydrite. The amount of iodate removed from solution did not change substantially over longer contact times. Analysis of the solid phase after reaction by I K-edge XAS revealed that the mechanism of iodine removal was by reduction of iodate to iodide.

Ferrous hydroxide ($Fe(OH)_2$) performed the worst of the iron oxides tested, with loading values of 20 and 10 µg/g, and K_d values of 16 and 12 mL/g, at solution-to-solid ratios of 200 and 1000, respectively. The iodine loading improved slightly with longer contact times. Iodine speciation on the solid could not be determined due to the low iodine loading.

These results suggest that sorption onto, or incorporation into, amorphous Fe(III)-bearing oxy(hydr)oxides, predominantly as iodate, is a promising option. Removal of iodate from solution by Fe(II)-bearing oxide-induced reduction to iodide is not an efficient process. There are challenges associated with deploying an amorphous Fe(III)-bearing oxides oxy(hydr)oxide, such as ferrihydrite, in the P&T system. The instability of ferrihydrite, and its gradual transformation to goethite over time, could affect iodine removal performance, although the lack of release of iodate into solution in the long-term tests performed here is promising. The nature of the ferrihydrite material requires that it be mixed with or coated on a support matrix, like silica sand. This process is of importance along with column configuration (e.g., the need for filters at each end) for deployment.

7.3.1.3   Sulfide Phases

Iron sulfide (FeS) and potassium tin sulfide ($K_{2x}Mg_xSn_{3-x}S_6$, x = 0.5-1, KMS) exhibited virtually no capacity for iodate update, with a very low iodine loading of <0.02 mg/g, irrespective of solution-to-solid ratio or contact time. Both materials have a significant reducing capacity and, in a sorption test conducted under the same conditions, demonstrated good loading capacity with respect to another potential oxyanion, pertechnetate (TcO_4^-). This highlights the importance of the uptake mechanism and reaction product for predicting material performance; e.g., technetium, as a transition metal, can be reduced to form a low solubility technetium sulfide, but if the iodate is reduced to iodide in this system, it is out-competed by the excess sulfide for available sorption sites.

7.3.1.4   Bismuth-Based Materials

The bismuth-based materials demonstrated the best performance of all the materials tested with respect to iodate immobilization. Bismuth (oxy)hydroxide had loading values of 200 and 820 µg/g and K_d values of 20,1904 and 4204 mL/g, at solution-to-solid ratios of 200 and 1000, respectively. Because loading on bismuth (oxy)hydroxide increased for the solution-to-solid ratio of 1000 compared to the solution-to-solid ratio of 200, it was not at capacity at the solution-to-solid ratio of 200, which was also demonstrated by the complete removal of iodine from solution in those tests. The observed batch-test removal efficiency in the solution-to-solid ratio of 200 (>1000-fold) is more than sufficient to reduce concentrations of I-129 from 30 pCi/L to 1 pCi/L, even in the presence of a total iodine concentration (i.e., including I-127) 1000 times the I-129 concentration (Levitskaia et al. 2017). Given the high performance of this material, an additional test was conducted under the same conditions, but at an iodate concentration more relevant to the concentrations of I-129 present in groundwater (0.6 µg/L). The bismuth oxy(hydroxide) completely removed the iodate from solution to below the detection limit of the instrument at a solution-to-solid ratio

of 200. This indicates that bismuth oxy(hydroxide) is a very promising material, but column tests would be needed to verify removal efficiency. At the lower solution-to-solid ratio (200), the rate of removal is good, with almost all of the iodate removed from solution within the first 24-h test period. The stability of the material is such that none of the iodine is released back into solution over the extended batch sorption tests (>30 days). At the higher solution-to-solid ratio (1000), 81% of the iodate was removed from solution in the first 24 h, and increased to 92% over the extended sorption test, suggesting that after the initial surface sorption sites become saturated, a kinetically slower process, possibly involving replacement of the interlayer anions (hydroxide, nitrate and carbonate) by the iodate, continues to remove iodate from solution. The speciation of iodine on the solid phase after the 24-h sorption test is iodate, confirming that redox-driven processes are not involved in the iodine immobilization mechanism.

Bismuth-cobalt-aluminum out-performed the rest of the materials tested, but was slightly less efficient than bismuth (oxy)hydroxide. Bismuth-cobalt-aluminum had loading values of 190 and 540 µg/g and K_d values of 12,800 and 1218 mL/g, at solution-to-solid ratios of 200 and 1000, respectively. The observed batch-test removal efficiency is more than sufficient to reduce concentrations of I-129 from 30 pCi/L to 1 pCi/L, even in the presence of a total iodine concentration loading due to I-127 in the groundwater at about 1000 times the I-129 concentration At the lower solution-to-solid ratio (200), 97% of the iodate is removed from solution within the first 24-h test period, and the remaining 3% removed over the extended batch sorption tests (>30 days). At the higher solution-to-solid ratio (1000), 54% of the iodate was removed from solution in the first 24 h, increasing slightly to 62% over the extended sorption test. The speciation of iodine on the solid phase after the 24-h sorption test was iodate. Removal rate appeared to be rapid, with the 1-day iodine loading on the ferrihydrite similar to that for >30 days of loading.

7.3.1.5   Organoclays

The two organoclays tested here, PM-100 and MRM, did not remove significant amounts of iodate from solution, despite a high capacity for iodide and pertechnetate removal reported in the literature (Li et al. 2014). Organoclay PM-100 had loading values of 40 and 190 µg/g and K_d values of 52 and 230 mL/g, at solution-to-solid ratios of 200 and 1000, respectively. This material removed virtually the same amount of iodate from solution, irrespective of the higher solution-to-solid ratio, suggesting that it was at capacity at the solution-to-solid ratio of 200. Much like the ion exchange resin, the performance of organoclay PM-100 did not significantly improve over the extended batch sorption tests. This is likely because organoclay PM-100 is functionalized with quaternary amine groups, as in the ion exchange resin, so any removal of iodate from solution is rapid. The observed batch-test removal efficiency in the solution-to-solid ratio of 200 was not sufficient to reduce concentrations of I-129 from 30 pCi/L to 1 pCi/L. As with the ion exchange resin, the iodine speciation on the solid was iodide, suggesting that changes in the solution chemistry, induced by the material, caused reduction of a small fraction of the iodate to iodide, and this was preferentially adsorbed onto the organoclay.

Organoclay MRM performed similarly in the 24-h sorption tests, with loading values of 50 and 190 µg/g and K_d values of 62 and 226 mL/g, at solution-to-solid ratios of 200 and 1000, respectively. Unlike organoclay PM-100, however, the performance of organoclay MRM did significantly improve over the longer sorption time of >30 days, with loading values increasing to 110 and 740 µg/g, at solution-to-solid ratios of 200 and 1000, respectively. Even with this improvement, however, the removal efficiency (3.6-fold) is still an order of magnitude too low. This improvement is likely related to a different mechanism for iodate immobilization, related to the sulfur in the sulfur-impregnated organoclay MRM. The speciation of iodine on the solid phase was iodide, implying reduction of iodate prior to immobilization on the organoclay, but the sulfur must remain associated with the clay as, in this case, it does not out-compete the iodide for sorption sites.

7.3.1.6   Aerogels

Despite literature precedent for aerogels to immobilize iodine (in the form of iodide and gaseous iodine), the copper-functionalized aerogel tested here was not able to remove significant quantities of iodate from solution. The aerogel had loading values of 30 and 20 µg/g and K_d values of 27 and 22 mL/g, at solution-to-solid ratios of 200 and 1000, respectively. This material removed similar amounts of iodate from solution, irrespective of the higher solution-to-solid ratio, suggesting that it was at capacity at the solution-to-solid ratio of 200. The speciation of iodine on the solid phase was iodate.

7.3.1.7   Metal Organic Frameworks and Cationic Polymeric Networks

The MOFs and CPNs demonstrated variable performance with respect to iodate immobilization. The CPN (SCU-CPN) performed the best, with loading values of 160 and 360 µg/g and K_d values of 636 and 557 mL/g, at solution-to-solid ratios of 200 and 1000, respectively. The observed batch-test removal efficiency in the solution-to-solid ratio of 200 (~4-fold) may not be sufficient for use in aboveground treatment. However, column tests with relevant influent concentrations are needed to verify removal efficiency. Removal rate appears to be rapid, with the 1-day iodine loading on the CPN only slightly less than that for >30 days of loading. The speciation of iodine on the solid phase was predominantly iodate, but a reduction in the intensity of the white line in the I K-edge XAS indicated that some iodide was also present. This result is of interest, as iodine is present as both iodate and iodide in Hanford groundwater. Many materials are selective for either iodate or iodide, but SCU-CPN demonstrated the capacity to immobilize both species on the solid phase.

FeBTC-PDA had loading values of 120 and 170 µg/g and K_d values of 287 and 198 mL/g, at solution-to-solid ratios of 200 and 1000, respectively. The observed batch-test removal efficiency is significantly below that required to reduce concentrations of I-129 from ~30 pCi/L to 1 pCi/L. However, column tests with relevant influent concentrations would be needed to verify removal efficiency. The performance of FeBTC-PDA did improve over longer loading times, especially at the high solution-to-solid ratio, with the extent of removal increasing from 17% at 1 day to 48% at > 30 days. Similar to SCU-CPN, the speciation of iodine on the solid phase was predominantly iodate, but with some iodide.

SCU-102 slightly outperformed SCU-101 at the low solution-to-solid ratio, with loading values of 50 µg/g and 40 µg/g and K_d values of 67 mL/g and 49 mL/g, respectively. However, they both reached the same loading value of 60 µg/g over the longer loading time. SCU-101 and SCU-102 behaved similarly at the higher solution-to-solid ratio with loading values of ~200 µg/g after 1 day and > 30 days. Because loading on SCU-101 and SCU-102 increased for the solution-to-solid ratio of 1000 compared to the solution-to-solid ratio of 200, it was not at capacity at the solution-to-solid ratio of 200. The speciation of iodine on the solid phase was iodide for both of these MOFs. This may explain the lower performance than that observed with SCU-CPN and FeBTC-PDA, as SCU-101 and SCU-102 could only immobilize the small amount of iodate that was reduced to iodide, whereas SCU-CPN and FeBTC-PDA could immobilize both iodate and iodide.

None of the MOFs/CPNs tested here were specifically designed for immobilization of iodate, so the fact that they removed some iodate from solution, and that the extent of removal depended on the structure and removal mechanism, suggests the MOF/CPN structure could be modified to improve performance with respect to immobilization of both iodate and iodide. However, given that these materials are relatively new, and that the synthesis can be complex, obtaining sufficient quantities for scaled-up testing will likely be difficult.

7.3.1.8 PAN-active Sorbent Composites

PAN-bismuth (oxy)hydroxide (PAN-BIN) and PAN-bismuth subnitrate (PAN-BSN) composites performed well in batch sorption experiments. PAN-BIN and PAN-BSN had IO_3^- loading values of 0.216 and 0.199 mg/g, respectively, which is almost identical to the active sorbent performance for BIN-19, and slight lower performance for BSN. The performance is influenced by the ability of the active sorbent to interact with IO_3^-, which depends on its distribution in the PAN bead and the available surface area. PAN-BIN and PAN-BSN also removed significant amounts of sulfur (13.7–16.15 mg/L) from solution, likely as the SO_4^{2-} anion, compared to the amount removed by the blank PAN beads, suggesting that these hybrid sorbents are not selective for IO_3^-, and performance may potentially suffer from competitive effects of other anions present in Hanford groundwater. The PAN-ferrihydrite (PAN-FEH) did not perform as well as the bismuth-based PAN composites with an iodine loading of 0.201 mg/g and a K_d value of 2775. This reduction in performance is due to the heterogeneous distribution of the active sorbent in the PAN beads.

7.3.1.9 ResinTech Hybrid Anion Exchange Resins

The amounts of ResinTech hybrid ion exchange resins used in the batch sorption experiments were such that the active sorbent was 0.1 g, based on the information provided in Table 7.1. ResinTech cerium- and iron-containing Type 2 hybrid ion exchange resins (CHM-20 and ASM-HP-10) performed the best of the hybrid sorbents for IO_3^- immobilization. CHM-20 and ASM-HP-10 had IO_3^- loading values of 0.203 and 0.201 mg/g and K_d values of 1,266,250 and 856,596 mL/g, respectively. The removal efficiency ($> 97\%$) of these hybrid materials was sufficient to reduce I-129 concentrations in the groundwater from 30 pCi/L to below the drinking water standard of 1 pCi/L. Even at the higher solution-to-solid ratio, both CHM-so and ASM-HP-10 removed the majority of the IO_3^- from solution, suggesting that they were not at capacity under these conditions. Both hybrid ion exchange resins removed significant amounts of sulfur from solution, likely as SO_4^{2-} (~17 mg/L), suggesting that these hybrid sorbents are not selective for IO_3^-, and performance may potentially suffer from competitive effects of other anions present in Hanford groundwater. The resins also released significant amounts of sodium into solution, which maybe a result of the resin synthesis protocol. The other iron- and bismuth-containing Type 1 hybrid ion exchange resins (ASM-125 and Bi-form) did not perform as well, with iodine removal efficiencies of 88% and 75% respectively, which is not sufficient to reduce the concentration of I-129 in groundwater from 30 pCi/L to below the drinking water standard of 1 pCi/L. This reduction in performance could be due either to the fact that the trimethylamine resin had a different amine content and did not perform as well as the dimethylethanolamine resin, or that the active sorbents in the resins were not as effective. Performance could be improved by optimizing the parent resin and by converting the active sorbent to a more efficient form, for example, by exchanging the chloride for nitrate or bicarbonate in the bismuth material.

7.3.2 Kinetics

All best-performing hybrid sorbents included in the kinetic experiments (PAN-BIN, PAN-BSN, PAN-FEH, CHM-20, and ASM-HP-10) exhibited rapid removal of IO_3^- from solution within 2 h. This rate of IO_3^- removal suggested that all hybrid sorbents should be suitable for column tests and the rates were used to establish the required flow rate.

7.3.3 Column Experiment

Column experiments were conducted to demonstrate capacity for each of the hybrid sorbents to remove at least 97% of IO_3^- from Hanford 200 Area groundwater, under flow conditions. The initial flow rate (25 mL/h) and starting IO_3^- concentration (100 μg/L) were chosen to represent a flow rate that would be practical for an ex situ P&T system, and the average groundwater concentration for iodine at the Hanford

Site. Columns were also run at a higher starting IO_3^- concentration (1000 µg/L) to ensure that breakthrough would be reached within the timeframe of the experiment. The results from column tests with the PAN-active sorbent composites indicate that little if any removal of IO_3^- occurred under the flow conditions tested. This could be due to the large size of the PAN-active sorbent composites (~2 to 3 mm), which meant that the volume of the column (1.325 cm^3) was insufficient to accommodate the batch experiment containing 0.1 g of the active sorbent, resulting in a lower amount than was used in the batch sorption and kinetics experiments. The size of the PAN-active sorbent composites and the packing procedure could also have impacted the flow path in the column, which, when combined with the short residence time in the column, could have severely reduced the efficiency of the active sorbent. To increase the residence time, the column experiment with PAN-BSN was repeated with a lower flow rate (4.5 mL/h) but no improvement in removal of IO_3^- was observed. Column experiments were also conducted with the best-performing ResinTech hybrid ion exchange resins (CHM-20 and ASM-HP-10), using an initial flow rate of 25 mL/h and a starting IO_3^- concentration of 100 µg/L. The performance of these resins was significantly better than the PAN-active sorbent composites under flow conditions. Results indicate that CHM-20 sequestered iodate more effectively than ASM-10-HP, with 50% breakthrough occurring at 324 PVs for CHM-20 and 268 PVs for ASM-10-HP. Three percent breakthrough occurred at 128 PVs for CHM-20 and 121 PVs for ASM-10-HP.

The best-performing hybrid resin (CHM-20) had an iodine loading of 8.35 µg/g in the column experiment at 3% breakthrough compared to 203 µg/g for the batch experiments at a solution-to-solid ratio of 200 and 1000 µg/g at a solution-to-solid ratio of 1000. (Virtually all of the iodine was removed from solution at both ratios, suggesting the hybrid resin was not a capacity.) The results from the column experiment were impacted to some extent by the flow rate of 25 mL/h, which is ~4 times faster than the optimum, but was chosen to be similar to the recommended flow rate for the Purolite A530E resin currently in use at the P&T. Column test conditions also included use of a small-diameter column. Under more optimal column conditions, the resin may perform better, potentially showing an improvement in capacity up to approximately an order of magnitude, which would be more consistent with the batch test results. At 100% breakthrough for the current column experiment parameters (400 PVs), the iodine loading would be 33 µg/g, which is similar to the I-127 loading of 35 µg/g on the spent DOWEX 21K resin for uranium (Campbell et al. 2018), and to the I-127 loading of 50 µg/g on the spent Purolite A530E resin for technetium (Levitskaia et al. 2017). However, column tests with Purolite A530E have shown that this resin can only sorb iodine in the form of iodide (I$^-$), and this may also be the case for DOWEX 21K. CHM-20 and ASM-10-HP are removing iodine in the form of iodate (IO_3^-), which is the dominant form of iodine in Hanford groundwater (Zhang et al. 2013). Additional testing would be required with CHM-20 and ASM-10-HP to determine their sorption capacity for iodide and organo-iodide, which are also present in Hanford groundwater. In terms of performance for their respective contaminants, CHM-20 had a capacity of 0.26 µM/g iodine at 100% breakthrough, which is comparable to the 0.20 µM/g of technetium that was present on the spent Purolite A530E, but much lower than the 77 µM/g of uranium on the spent DIONEX 21K resin. These contaminant loadings must, however, be considered within the context of the influent concentrations, which are on the order of 0.01 nM for technetium, 0.5 µM for uranium, and 0.3 µM for iodine.

Overall, the CHM-20 resin showed a potential for removal of iodine from Hanford, though with a low capacity. Some improvement in the measured capacity may be expected if column experiments were repeated with larger diameter columns and a lower flow rate to minimize the impact of the experiment conditions. In addition, performance of the hybrid resins could be further improved with additional development by (1) pre-conditioning the resin to convert from the chloride form into the bicarbonate or nitrate form to potentially mitigate apparent interactions with groundwater constituents; (2) changing the functional groups on the parent resin to higher amines, e.g., tributylamine; or (3) optimizing the amount of active sorbent, e.g., cerium hydroxide, within the hybrid resin.

8.0 Conclusions and Path Forward for Promising Technologies

Laboratory-based technology screening was conducted on five in situ treatment technologies and a suite of materials for ex situ removal of iodine from groundwater. Key findings from each of these efforts are summarized in the sections below. For the most promising technologies, additional detail is provided to outline an approach for further evaluation of the technology to determine the technology's efficacy and implementability under Hanford Site conditions.

8.1 Co-precipitation with Calcite

Co-precipitation of iodate with calcium carbonate was investigated using three methods. The first method, based on a study by Podder et al. (2017), showed that silica gel was effective at slowing the rate of calcite precipitation. It took approximately 2 weeks for the silica gel to form within the batch reactors. Subsequently, calcite crystals became visible in the batch reactors after another 2 weeks of equilibration in the silica gel. Separation of the calcite crystals from the silica gel proved to be challenging, confounding quantification of iodate loading within the newly formed calcite material. However, analysis of the silica gel/calcite precipitate demonstrated that the technology consistently removed approximately 60% of iodate from solution. It is interesting to note that this occurred across a wide range of iodate starting solution concentrations, from 100 to 396 mg/L. This finding indicates that the iodate removed from solution was largely associated with the silica gel vs. the calcite crystals.

The second method tested explored precipitating calcium carbonate in Hanford VZPW and AGW, which was based on previous testing that had shown an increase in iodate uptake when calcite-forming solutions were made in VZPW. Results from batch tests showed that 65% to 71% of iodine was removed with calcite in VZPW compared to 45% to 48% in AGW and 33% to 38% in DDI water (for concentrations 100 to 500 µg/L). Very little iodate was removed from any of the matrices when starting solution concentrations were high, i.e., 396 mg/L iodate. SEM analysis of calcium carbonate precipitates from the various solution matrices showed the presence of only calcite crystals in the DDI and AGW batch reactors. Conversely, SEM characterization of precipitates formed in the tests using VZPW as the contacting solution revealed calcite crystals, as well as needle-like crystals of the calcite polymorph aragonite. Due to their needle-like shape, aragonite crystals have a much higher surface-area-to-mass ratio vs. calcite crystals, which could explain the greater iodate removal in the VZPW vs. the other two matrices tested.

The final approach tested involved the formation of nano-calcite crystals. The nano-calcite was synthesized under elevated temperature and pressure following a method by Montes-Hernandez et al. (2007). Results showed that 76% to 83% of calcite was removed from solution (starting solutions concentrations ranged from 100 to 500 µg/L) over a period of 24 h. However, nearly all the uptake occurred prior to the first sample collected, which was collected 4 h after beginning the reaction. SEM images of precipitates from these tests revealed the presence of both large and nano-sized calcite crystals. Although this technique achieved the highest percentage of iodate removal from solution, the need for elevated pressure and temperature limits the practical implementation of this technology for in situ iodate removal.

Evaluation of the three calcite precipitation techniques clearly demonstrated the ability to remove iodate from Hanford-representative solutions at relevant total iodine solution concentrations. However, none of the approaches were effective at a high percentage (> 90%) of the iodate from solution. This presents a

serious shortcoming for in situ application, as technologies being considered for field deployment should be capable of order of magnitude (90% or greater) reduction in aqueous concentrations. Therefore, further testing of in situ formation of calcite for remediation of [129]I is not recommended.

8.2   Incorporation into Apatite/Carbonated Apatite

Precipitation of initially amorphous calcium-phosphate (which slowly crystallized into apatite) inconsistently removed a small amount of iodate from solution at pH 11 and above, and none at pH 9.0 and 7.5 (Figure 8.1a). The Campayo et al. (2011) paper hypothesize that iodate substitutes for OH- in the hydroxyapatite. In the 40 experiments performed as part of our study, many showed greater uptake during initial amorphous calcium phosphate precipitation, and less iodate uptake as the precipitate crystallizes to hydroxyapatite. The uptake from solution resulted in some adsorbed iodate (0% to 4%) and some iodate incorporated into apatite (0% to 6.5%), as measured by ion exchanging iodate off the apatite (for adsorbed), then dissolving the apatite in acid to measure the incorporated mass. The iodate loading in apatite ranged from 0.1 to as high as 10 mg iodate/g apatite starting with unrealistically high aqueous iodate solutions, but 11 to 30 µg iodate/g apatite starting with 200 µg/L iodate. Although this loading is reasonable for field-scale use, none of the 40 experiments showed iodate removal to 1.0 µg/L detection limits.

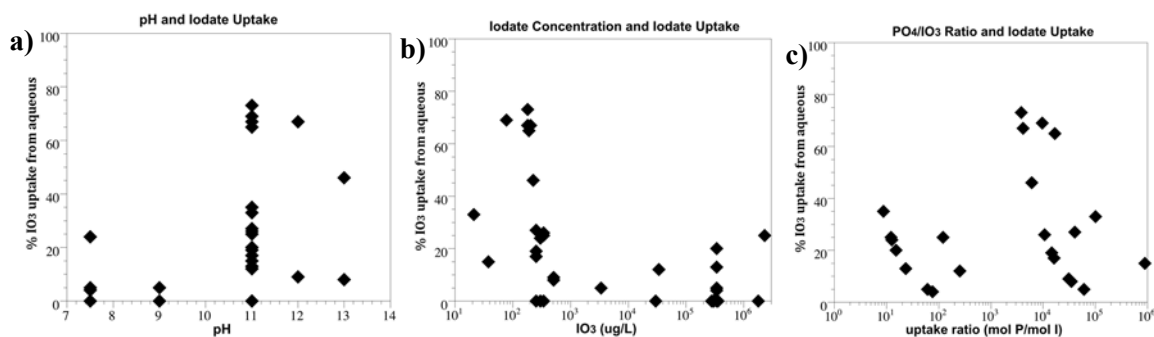Figure 8.1.   Iodate uptake from batch experiments as a function of a) pH, b) iodate concentration, and c) P/I ratio.

The rate of iodate removal from solution was calculated in time-course experiments and plotted as a function of the ratio of iodine to phosphate (Figure 8.2). A clear trend is observed where the most rapid iodate removal rates are observed in systems with the highest (> 1000 times) phosphate to iodate ratio.
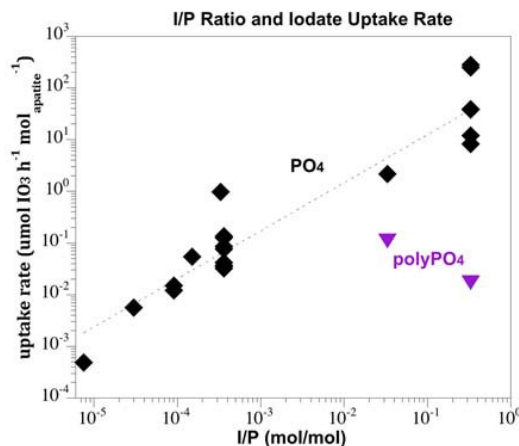
Figure 8.2.   Iodate uptake rate as a function of the I/P ratio.

To deploy in the field, iodate concentrations need to be reduced to < 1 µg/L. The phosphate (orthophosphate and polyphosphate) and carbonate-substituted apatite would not achieve this concentration reduction. While there is some uptake of iodate observed in laboratory batch experiments specifically at pH > 10 and low (< 200 µg/L) iodate concentration with high phosphate concentration, none of the experiments removed all of the iodate from aqueous solution. The most successful phosphate solution used only orthophosphate, which immediately precipitated, making it less practical for field-scale deployment. High phosphate concentrations have been successfully injected into Hanford sediments, including a polyphosphate solution (90% orthophosphate, 10% pyrophosphate at 70 mM) in the 300 Area, but only 1 of the 10 polyphosphate experiments performed as part of our study showed any iodate uptake. A Ca-citrate-phosphate solution has also been deployed at field scale (45 mM phosphate) in the 100N Area, but our laboratory studies with this solution mobilized more iodine due to the reducing conditions created.

As tested, little iodate was removed from solution via either sorption onto or incorporation into apatite; therefore, further testing of this technology for remediation of I-129 is not recommended.

8.3   Enhanced Sorption by Organic Carbon

A series of batch adsorption/desorption experiments was conducted to determine the effectiveness of several organic materials for sequestering iodate and iodide from Hanford groundwater. The organic materials that were evaluated in this study were chitin, lignin, and humic acid sorbed to a representative Hanford sediment. The results indicate that significant sorption of iodide occurred on chitin, with an average K_d value of 74.9 ± 4.3 mL/g. Sorption of iodate to chitin was minimal (K_d = 3.2 ± 4.0 mL/g). Sorption of both iodide and iodate to lignin was also minimal (K_d = 3.6 ± 3.5 and 4.8 ± 4.8 mL/g). Similarly, sorption of both iodide and iodate to HA-treated sediments was also minimal. Iodide K_d values for HA-treated sediment were 0.46 ± 0.05 mL/g, only slightly higher than that of untreated sediment 0.34 ± 0.05 mL/g. For iodate, HA-treated sediment had a K_d value of 0.58 ± 0.27 mL/g, which was lower than that of the untreated sediment, 1.13 ± 0.06 mL/g. It is possible that the humic acid acted as a competitor for iodate adsorption sites on the sediment; however, these differences are small.

Of the three organic carbon materials tested, only chitin showed potential as an in situ remediation technology for iodide (average K_d value of 74.9 ± 4.3 mL/g). However, iodine within the groundwater at 200-UP-1 is primarily in the form of iodate, which would limit the effectiveness of chitin as a removal technology. As such, further testing of this technology is not recommended.

8.4 Co-precipitation with and Sorption to Iron Oxides

The use of a pH 1.5 ferric iron solution to precipitate 2-line ferrihydrite (HFO) has a significant effect on reducing iodate mobility by (1) high iodate sorption to HFO and (2) incorporation of iodate into the precipitating HFO. The highest sorption capacity was found for HFO or goethite synthesized in a DDI water system followed by the iron oxides synthesized in AGW. Iodine sorption to HFO synthesized in AGW with sediments was also relatively high, with the iodine remaining adsorbed for prolonged periods.

The use of this in situ HFO precipitation technology was tested for immobilization of iodate in Hanford formation sediments as (1) source area treatment of iodine-contaminated sediment and (2) PRB to capture upgradient aqueous iodate. For source area treatment, the simultaneous injection of 100 µg/L iodate with the pH 1.5 ferric iron solution resulted in precipitation of 23% to 47% of the iodate likely within ferrihydrite (HFO). There may be additional decrease in iodine leaching release from precipitates in the sediments due to the HFO coating on surfaces; 80% to 95% of the iodine in contaminated sediments are in precipitates including Fe oxides and calcite. As a PRB, injection of 100 µg/L iodate into HFO-modified sediment showed complete removal for 170 PVs due to the low pH (i.e., high iodate sorption in the pH 1.5 to 5.0 sediment), after which 50% to 60% of the iodate was rapidly released into aqueous solution at a high concentration (up to 600 µg/L).

In addition, the fraction of iodate that remained immobile (40% to 50%) after 170 to 300 PVs is likely caused by iodate incorporation into HFO in these several week-long experiments. Although this approach is promising, more development is needed before field-scale implementation to further evaluate the long-term performance of iodate capture as well as potential negative impacts occurring from the injection (i.e., metals mobilization, permeability changes).

8.5 Dithionite-Enhanced Mobility

Whereas most in situ treatment technologies are designed to immobilize iodine, the Na-dithionite reduction technology is designed to enhance iodine mobility. The Na-dithionite mobilizes significant iodine due to Fe oxide dissolution in sediments and is designed to enhance P&T system efficiency. This technology is targeted at accelerating the removal of iodine from the surface by P&T in areas where sorption limits extraction efficiency. Leaching behavior of vadose zone and aquifer sediments under B, T, and S complexes have shown that only 55% of iodine mass is mobilized in the first 10 PVs (aqueous and adsorbed iodine), with the remainder removed over the next 100 PVs due to the slow dissolution of iodine from precipitates. Sediment characterization shows that only small fractions (i.e., 2% to 15%) of the iodate and iodide are adsorbed to the sediment, with the remainder present in one or more precipitates. The iodate and iodide associated with sediments may be bound to immobile natural organic matter, incorporated in calcite, incorporated in Fe oxides, or in other minerals.

Dithionite treatment of sediment enabled much greater (4 times or more) and rapid (one to three orders of magnitude) leaching of iodine from the sediment compared to leaching of untreated sediment. However, it was expected that after Fe-oxides were dissolved and iodide advected from the sediments, I-127 concentrations in the dithionite-treated sediments would eventually be lower than in untreated sediments. Although the geochemical behaviors of I-127 and I-129 are similar, extractions from field-contaminated sediments show that the precipitation pattern differs. Iodine-129 is more readily mobilized from sediments than I-127. For example, apparent partitioning coefficients for I-127 vs. I-129 ranged from 210 to 3.7 mL/g and 4.2 to 12.9 mL/g, respectively, based on batch reactions of sediment with AGW. Na-dithionite extractions removed more iodine than AGW and extractants previously used for measuring total iodine in sediments (TMAH) (e.g., 4 to 10.1 times more I-129 was removed via Na-dithionite as compared to AGW). Further, iron-specific extractions removed significant amounts of iodine from

sediments with 55 ± 17 and $96.7 \pm 1.4\%$ of total I-127 and -129, respectively, extracted in series with TMAH followed by 5.0 M HCl was associated with the total Fe fraction (5.0 M HCl). Because I-129 is more readily removed than I-127, lower Na-dithionite concentrations could be used for I-129 remediation within the P&T capture zone. Leaching studies with untreated and dithionite-treated sediments that contained high I-127 showed that significant I-127 was removed, but continued high I-127 concentrations in the treated sediment effluent may indicate the formation of a secondary precipitate, such as siderite, that incorporates some iodine. Although this technology is promising, additional work is necessary to (1) identify whether anthropogenic iodine is associated with iron phases (potentially via laboratory experiments replicating Hanford conditions during waste disposal), and (2) identify whether citrate or another complexant is necessary to keep iron soluble and reduce secondary co-precipitation of iodine with iron phases.

8.6 Materials for Iodine Immobilization

A wide range of materials was tested for capacity to remove iodate from synthetic groundwater containing competing anions. Ferrihydrite, bismuth oxy(hydroxide), and bismuth-cobalt-aluminum are the most promising materials, and the observed batch-test removal efficiency is sufficient to reduce concentrations of I-129 from 30 to 1 pCi/L, even in the presence of total iodine concentration loading due to I-127 in the groundwater at about 1000 times the I-129 concentration. Although the synthetic bismuth- based materials are only currently available in gram-quantities, efforts are underway to scale up their synthesis. When available in sufficient quantities, the promising materials were engineered into viable form for deployment in the P&T system. In some cases, a viable form of the material was available commercially as hybrid ion exchange resins from ResinTech Inc. The promising materials were also embedded into polyacrylonitrile (PAN) beads. The viable forms were then taken forward for kinetics testing and subsequent deployment in a column system, with relevant influent iodate concentrations and flow rates, to verify removal efficiency. ResinTech CHM-20, a cerium oxide/hydroxide hybrid with a Type 2 (dimethylethanolamine) parent anion exchange resin, performed the best with respect to iodate removal in a column system using 200 West Area groundwater with an influent iodine concentration of 100 µg/L (added as sodium iodate) and a flow rate of 25 mL/h. The performance of the CHM-20 hybrid resin can be characterized as marginal, with an iodine capacity under the conditions tested of 33 µg/g at 100% breakthrough. There is a potential for improving resin performance by optimizing the parameters for the column experiments and tuning the resin composition. However, the CHM-20 resin capacity is substantially lower in relation to the influent contaminant loading based on expected I-127 concentration in groundwater than the capacity/loading ratio of the current resins in use at the 200 West P&T facility for uranium and Tc-99. Therefore, significant improvements through resin development would be needed to enable its use as an effective iodate treatment application.

9.0 Quality Assurance

This work was performed in accordance with the Pacific Northwest National Laboratory (PNNL) Nuclear Quality Assurance Program (NQAP). The NQAP complies with the United States Department of Energy Order 414.1D, *Quality Assurance,* and 10 CFR 830 Subpart A, *Quality Assurance Requirements*. The NQAP uses NQA-1-2012, *Quality Assurance Requirements for Nuclear Facility Application* as its consensus standard and NQA-1-2012 Subpart 4.2.1 as the basis for its graded approach to quality.

The information associated with this report should not be used as design input or operating parameters without additional qualification.

10.0 References

10 CFR 830, Subpart A. 2011. "Quality Assurance Requirements." *Code of Federal Regulations*, Washington, DC: U.S. Department of Energy.

ASME NQA-1-2012. *Quality Assurance Requirements for Nuclear Facility Applications*. New York, NY: The American Society of Mechanical Engineers.

DOE Order 414.1D. 2011. *Quality Assurance*. Washington, DC: U.S. Department of Energy. Approved 4/25/2011.

Bird GA and W Schwartz. 1997. "Distribution coefficients, K_ds, for iodide in Canadian Shield lake sediments under oxic and anoxic conditions." *Journal of Environmental Radioactivity* 35(3):261–279. DOI: 10.1016/S0265-931X(96)00062-8.

Byrappa K and M Yoshimura. 2001. *Handbook of Hydrothermal Technology: A Technology for Crystal Growth and Materials Processing*, Norwich, NY: Noyes Publications/William Andrew Publishing LLC. ISBN 0-8155-1445-X.

Campbell EL, TG Levitskaia, MS Fujimoto, VE Holfeltz, S Chatterjee, and GB Hall. 2018. *Analysis of Uranium Ion Exchange Resin from the 200 West Pump-and-Treat Facility*. PNNL-28062. Richland, WA: Pacific Northwest National Laboratory.

Campayo L, A Grandjean, A Coulon, R Delorme, D Vantelon and D Laurencin. 2011. "Incorporation of iodates into hydroxyapatites: a new approach for the confinement of radioactive iodine." *Journal of Materials Chemistry* 21(44):17609–17611. DOI: 10.1039/C1JM14157K.

Cantrell KJ and AR Felmy. 2012. *Plutonium and Americium Geochemistry at Hanford: A Site-Wide Review*. PNNL-21651, Richland, WA: Pacific Northwest National Laboratory.

Cantrell KJ, RJ Serne, and GV Last. 2003. *Hanford Contaminant Distribution Coefficient Database and Users Guide*. PNNL-13895, Rev. 1. Richland, WA: Pacific Northwest National Laboratory.

Chao TT and L Zhou. 1983. "Extraction techniques for selective dissolution of amorphous iron oxides from soils and sediments." *Soil Science Society of America Journal* 47(2):225–232. DOI: 10.2136/sssaj1983.03615995004700020010x.

Couture RA and MG Seitz. 1983. "Sorption of anions of iodine by iron oxides and kaolinite." *Nuclear and Chemical Waste Management* 4(4):301–306. DOI: 10.1016/0191-815X(83)90055-4.

Demirkanli DI, MJ Truex, JE Szecsody, MM Snyder, JJ Moran, MK Nims, AR Lawter, CT Resch, DL Saunders, NP Qafoku, SR Baum, BD Williams. 2018. Contaminant Attenuation and Transport Characterization of 200-DV-1 Operable Unit Sediment Samples from Boreholes C949+7, C9498, C9603, C9488, and C9513. PNNL-27524. RPT-DVZ-CHPRC-0004 Rev 0.0. Pacific Northwest National Laboratory, Richland, WA.

Denham M and C Eddy-Dilek. 2016. "Sustainable Remediation of Radionuclides By a Common Sense Approach to Enhanced Attenuation – 16441." In *WM2016 Conference*. March 6–10, 2016, Phoenix, AZ. Available at http://www.wmsym.org/archives/2016/pdfs/16441.pdf.

DOE. *In situ remediation integrated program: Technology summary*. 1994. DOE/EM-0134P.

DOE. 1996. *Iodine-129 Contamination: Nature, Extent, and Treatment Technologies*. DOE/RL-95-89. Richland, WA: U.S. Department of Energy.

DOE. 2012. *Record of Decision for Interim Remedial Action Hanford 200 Area Superfund Site 200-UP-1 Operable Unit*. 12-AMRP-0171. Richland, WA: U.S. Department of Energy, Richland Operations Office. Available at https://pdw.hanford.gov/arpir/index.cfm/viewDoc?accession=0091413.

DOE. 2016. *Hanford Site Groundwater Monitoring Report for 2016*. DOE/RL-2016-67. Richland, WA: U.S. Department of Energy.

DOE. 2017. *UP-1 Evaluation Plan for Iodine.* DOE/RL-2015-69, Rev. 0. Richland, WA: U.S. Department of Energy, Richland Operations Office.

DOE-EM. 2009. *Remedial Investigation/Feasibility Study for the 200-UP-1 Groundwater Operable Unit*. DOE/RL-2009-122 Rev 0. Richland, WA: CH2M Hill Plateau Remediation Company.

Du T, D Tamboli, Y Luo and V Desai. 2004. "Electrochemical characterization of copper chemical mechanical planarization in KIO_3 slurry." *Applied Surface Science* 229(1):167–174. DOI: 10.1016/j.apsusc.2004.01.062.

Fard ZH, CD Malliakas, JL Mertz and MG Kanatzidis. 2015. "Direct Extraction of Ag^+ and Hg^{2+} from Cyanide Complexes and Mode of Binding by the Layered $K_2MgSn_2S_6$ (KMS-2)." *Chemistry of Materials* 27(6):1925–1928. DOI: 10.1021/acs.chemmater.5b00374.

Fuhrmann M, Sa Bajt and MAA Schoonen. 1998. "Sorption of iodine on minerals investigated by X-ray absorption near edge structure (XANES) and ^{125}I tracer sorption experiments." *Applied Geochemistry* 13(2):127–141. DOI: 10.1016/S0883-2927(97)00068-1.

Geiszler, KN. 2016. Solubilization of Metals from Solids using a KOH-KNO_3 Fusion. PNNL Technical Procedure, PNNL-ESL-Fusion, Rev. No.:2

Hartman MJ, LJ Morasch and WD Webber. 2004. *Hanford Site Groundwater Monitoring for Fiscal Year 2003*. PNNL-14548. Richland, WA: Pacific Northwest National Laboratory.

Heron G, C Crouzet, ACM Bourg and TH Christensen. 1994. "Speciation of Fe(II) and Fe(III) in Contaminated Aquifer Sediments Using Chemical Extraction Techniques." *Environmental Science & Technology* 28(9):1698–1705. DOI: 10.1021/es00058a023.

Hou XL, CL Fogh, J Kucera, KG Andersson, H Dahlgaard and SP Nielsen. 2003. "Iodine-129 and Caesium-137 in Chernobyl contaminated soil and their chemical fractionation." *Science of the Total Environment* 308(1):97–109. DOI: 10.1016/S0048-9697(02)00546-6.

Kekli, A, A Aldahan, M Meili, G Possnert, N Buraglio, and R Stepanauskas. 2003. "I-129 in Swedish rivers: distribution and sources." *Science of the Total Environment* 309(1):161–172. DOI: 10.1016/S0048-9697(03)00010-X.

Larner BL, AJ Seen and AT Townsend. 2006. "Comparative study of optimised BCR sequential extraction scheme and acid leaching of elements in the certified reference material NIST 2711." *Analytica Chimica Acta* 556(2):444–449. DOI: 10.1016/j.aca.2005.09.058.

Lee BD, JE Szecsody, N Qafoku, EM McElroy, SR Baum, MM Snyder, AR Lawter, CT Resch, BN Gartman, L Zhong, DL Saunders, BD Williams, JA Horner, II Leavy, BB Christiansen, RE Clayton and KC Johnson. 2017. *Contaminant Attenuation and Transport Characterization of 200-UP-1 Operable Unit Sediment Samples*. PNNL-26894. Richland, WA: Pacific Northwest National Laboratory.

Levitskaia TG, EL Campbell, SD Chatterjee, and GB Hall. 2017 *Analysis of Technetium Ion Exchange Resin from the 200 West Pump-and-Treat Facility*. PNNL-26933; RPT-DVZ-AFRI-049, Rev. 0. Richland, WA: Pacific Northwest National Laboratory.

Li D, DI Kaplan, AS Knox, KP Crapse and DP Diprete. 2014. "Aqueous ^{99}Tc, ^{129}I and ^{137}Cs removal from contaminated groundwater and sediments using highly effective low-cost sorbents." *Journal of Environmental Radioactivity* 136:56–63. DOI: 10.1016/j.jenvrad.2014.05.010.

Li K, Y Zhao, P Zhang, C He, J Deng, S Ding and W Shi. 2016. "Combined DFT and XPS investigation of iodine anions adsorption on the sulfur terminated (001) chalcopyrite surface." *Applied Surface Science* 390:412–421. DOI: 10.1016/j.apsusc.2016.08.095.

Li J, X Dai, L Zhu, C Xu, D Zhang, MA Silver, P Li, L Chen, Y Li, D Zuo, H Zhang, C Xiao, J Chen, J Diwu, OK Farha, TE Albrecht-Schmitt, Z Chai and S Wang. 2018. "^{99}TcO$_4^-$ remediation by a cationic polymeric network." *Nature Communications* 9(1):3007. DOI: 10.1038/s41467-018-05380-5.

Mattigod SV, EC Golovich, DM Wellman, EA Cordova and RM Smith. 2010a. *Uranium Adsorption on Ion-Exchange Resins - Batch Testing*. PNNL-20135. Richland, WA: Pacific Northwest National Laboratory.

Mattigod SV, EC Golovich, DM Wellman, EA Cordova and RM Smith. 2010b. *Tc-99 Adsorption on Selected Activated Carbons Batch Testing Results*. PNNL-20136. Richland, WA: Pacific Northwest National Laboratory.

Matyáš J, G Fryxell, B Busche, K Wallace and LS Fifield. 2011. "Functionalized Silica Aerogels: Advanced Materials to Capture and Immobilize Radioactive Iodine." In *Ceramic Materials for Energy Applications*, pp. 21-32. eds: Y Katoh, KM Fox, H Lin, I Belharouak, S Widjaja and D Singh. DOI: 10.1002/9781118095386.ch3.

McNally SR. 2011. *The Status of Iodine and Selenium in Waikato Soils*. Master of Science Thesis, University of Waikato, Hamilton, New Zealand. Available at https://hdl.handle.net/10289/5375.

Mehta S. 2017. "Geochemical evaluation of uranium sequestration from field-scale infiltration and injection of polyphosphate solutions in contaminated Hanford sediments." *Applied Geochemistry* 84:133-153. DOI: 10.1016/j.apgeochem.2017.06.009.

Montes-Hernandez G, F Renard, N Geoffroy, L Charlet and J Pironon. 2007. "Calcite precipitation from CO_2–H_2O–$Ca(OH)_2$ slurry under high pressure of CO_2." *Journal of Crystal Growth* 308(1):228–236. DOI: 10.1016/j.jcrysgro.2007.08.005.

Mossop KF and CM Davidson. 2003. "Comparison of original and modified BCR sequential extraction procedures for the fractionation of copper, iron, lead, manganese and zinc in soils and sediments." *Analytica Chimica Acta* 478(1):111–118. DOI: 10.1016/S0003-2670(02)01485-X.

Parker KE, EC Golovich and DM Wellman. 2014. *Iodine Adsorption on Ion-Exchange Resins and Activated Carbons– Batch Testing*. PNNL-23730; RPT-DVZ-AFRI-021, Rev. 0. Richland, WA: Pacific Northwest National Laboratory.

Pearce CI, O Qafoku, J Liu, E Arenholz, SM Heald, RK Kukkadapu, CA Gorski, CMB Henderson and KM Rosso. 2012. "Synthesis and properties of titanomagnetite ($Fe_{3−x}Ti_xO_4$) nanoparticles: A tunable solid-state Fe(II/III) redox system." *Journal of Colloid and Interface Science* 387(1):24–38. DOI: 10.1016/j.jcis.2012.06.092.

Podder J, J Lin, W Sun, SM Botis, J Tse, N Chen, Y Hu, D Li, J Seaman and Y Pan. 2017. "Iodate in calcite and vaterite: Insights from synchrotron X-ray absorption spectroscopy and first-principles calculations." *Geochimica et Cosmochimica Acta* 198:218–228. DOI: 10.1016/j.gca.2016.11.032.

Qin F, G Li, R Wang, J Wu, H Sun and R Chen. 2012. "Template-Free Fabrication of Bi_2O_3 and $(BiO)_2CO_3$ Nanotubes and Their Application in Water Treatment." *Chemistry – A European Journal* 18(51):16491–16497. DOI: 10.1002/chem.201201989.

Qafoku NP, AR Lawter, DH Bacon, L Zheng, J Kyle and CF Brown. 2017. "Review of the impacts of leaking CO_2 gas and brine on groundwater quality." *Earth-Science Reviews* 169:69–84. DOI: 10.1016/j.earscirev.2017.04.010.

Schwertmann U and RM Cornell. 2000. *Iron Oxides in the Laboratory: Preparation and Characterization*, Weinheim, Federal Republic of Germany: Wiley-VCH. ISBN 3-527-29669-7.

Serne RJ., Bjornstad BN., Schaef HT., Williams BA., Lanigan DC., Horton DG., Clayton RE., Mitroshkov AV., LeGore VL., O'Hara MJ., Brown CF., Parker KE., Kutnyyakov IV., Serne JN., Last GV., Smith SC., Lindenmeier CW., Zachara JM., Burke DS. 2008. *Characterization of Vadose Zone Sediment: Uncontaminated RCRA Borehole Core Samples and Composite Samples*. PNNL-13757-1, Rev.1. Pacific Northwest National Laboratory; Richland, WA.

Serne RJ, JH Westsik, BD Williams, HB Jung and G Wang. 2015. *Extended Leach Testing of Simulated LAW Cast Stone Monoliths*. PNNL-24297. Richland, WA: Pacific Northwest National Laboratory.

Sheppard MI, DH Thibault, J McMurry and PA Smith. 1995. "Factors affecting the soil sorption of iodine." *Water, Air, and Soil Pollution* 83(1):51–67. DOI: 10.1007/bf00482593.

Shigeno Y, K Kondo and K Takemoto. 1980. "Functional monomers and polymers. LXX. On the adsorption of iodine onto chitosan." *Journal of Applied Polymer Science* 25(5):731–738. DOI: 10.1002/app.1980.070250502.

Stookey LL. 1970. "Ferrozine---a new spectrophotometric reagent for iron." *Analytical Chemistry* 42(7):779–781. DOI: 10.1021/ac60289a016.

Strickland CE, AR Lawter, NP Qafoku, JE Szecsody, MJ Truex and G Wang. 2017a. *Evaluation of Iodine Remediation Technologies in Subsurface Sediments: Interim Status Report*. PNNL-26957. Richland, WA: Pacific Northwest National Laboratory.

Strickland CE, CD Johnson, BD Lee, N Qafoku, JE Szecsody, MJ Truex and VR Vermeul. 2017b. *Identification of Promising Remediation Technologies for Iodine in the UP-1 Operable Unit*. PNNL-26934. Richland, WA: Pacific Northwest National Laboratory.

Stucki JW, PF Low, CB Roth and DC Golden. 1984. "Effects of oxidation state of octahedral iron on clay swelling." *Clays and Clay Minerals* 32(5):357–362. DOI: 10.1346/ccmn.1984.0320503.

Sumner ME. 2000. "Section D, Soil Fertility and Plant Nutrition." In *Handbook of Soil Science*. Boca Raton, FL: CRC Press.

Sun DT, L Peng, WS Reeder, SM Moosavi, D Tiana, DK Britt, E Oveisi and WL Queen. 2018. "Rapid, Selective Heavy Metal Removal from Water by a Metal–Organic Framework/Polydopamine Composite." *ACS Central Science* 4(3):349–356. DOI: 10.1021/acscentsci.7b00605.

Szecsody JE, KM Krupka, MD Williams, KJ Cantrell, CT Resch and JS Fruchter. 1998. *Uranium Mobility During In Situ Redox Manipulation of the 100 Areas of the Hanford Site*. PNNL-12048. Richland, WA: Pacific Northwest National Laboratory.

Szecsody, J., Rockhold, M., Oostrom, M., Moore, R., Burns, C., Williams, M., Zhong, L., Fruchter, J., McKinley, J., Vermeul, V., Covert, M., Wietsma, T., Breshears, A., and Garcia, B., 2009, Sequestration of Sr-90 Subsurface Contamination in the Hanford 100-N Area by Surface Infiltration of a Ca-Citrate-Phosphate Solution, Pacific Northwest National Laboratories, PNNL-18303.

Szecsody JE, JS Fruchter, MA McKinley, CT Resch and TJ Gilmore. 2001. *Feasibility of In Situ Redox Manipulation of Subsurface Sediments for RDX Remediation at Pantex*. PNNL-13746. Richland, WA: Pacific Northwest National Laboratory.

Szecsody JE, JS Fruchter, MD Williams, VR Vermeul and D Sklarew. 2004. "In situ chemical reduction of aquifer sediments: Enhancement of reactive iron phases and TCE dechlorination." *Environmental Science & Technology* 38(17):4656–4663. DOI: 10.1021/es034756k.

Szecsody JE, BD Lee, AR Lawter, N Qafoku, CT Resch, SR Baum, II Leavy and VL Freedman. 2017. *Effect of Co-Contaminants Uranium and Nitrate on Iodine Remediation*. PNNL-26955. Richland, WA: Pacific Northwest National Laboratory.

Szecsody JE., Truex MJ., Qafoku NP., Wellman DM., Resch T., Zhong L. 2013. Influence of acidic and alkaline waste solution properties on uranium migration in subsurface sediments. *J. Contam. Hydrol.* 151, 155-175

Truex MJ, BD Lee, CD Johnson, N Qafoku, GV Last, MH Lee and DI.Kaplan. 2015. "Conceptual Model of Iodine Behavior in the Subsurface at the Hanford Site." PNNL-24709. Richland, WA: Pacific Northwest National Laboratory.

Truex MJ, BD Lee, CD Johnson, NP Qafoku, JE Szecsody, JE Kyle, M Tfaily, MMV Snyder, AR Lawter, M Oostrom, G Tartakovsky, II Leavy, EM McElroy, D Appriou, R Sahajpal, MM Carroll, GV Last, MH Lee, and DI Kaplan. 2016. *Conceptual Model of Iodine Behavior in the Subsurface at the Hanford Site*. PNNL-24709, Rev. 1. Richland, WA: Pacific Northwest National Laboratory.

Truex MJ, JE Szecsody, N Qafoku, CE Strickland, JJ Moran, BD Lee, M Snyder, AR Lawter, CT Resch, BN Gartman, L Zhong, MK Nims, DL Saunders, BD Williams, JA Horner, II Leavy, SR Baum, BB Christiansen, RE Clayton, EM McElroy, D Appriou, KJ Tyrrell and ML Striluk. 2017. *Contaminant Attenuation and Transport Characterization of 200-DV-1 Operable Unit Sediment Samples*. PNNL-26208; RPT-DVZ-AFRI-037. Richland, WA: Pacific Northwest National Laboratory.

Um W and RJ Serne. 2005. "Sorption and transport behavior of radionuclides in the proposed low-level radioactive waste disposal facility at the Hanford site, Washington." *Radiochimica Acta* 93(1):57–63. DOI: 10.1524/ract.93.1.57.58295.

Vermeul VR, MD Williams, JE Szecsody, JS Fruchter, CR Cole and JE Amonette. 2002. "Creation of a Subsurface Permeable Reactive Barrier Using In Situ Redox Manipulation." In *Handbook of Groundwater Remediation using Permeable Reactive Barriers: Applications to Radionuclides, Trace Metals, and Nutrients*, pp. 163–192. ed: DL Naftz. San Diego, CA: Academic Press.

Wan, J.; Larsen, JT.; Tokunaga, TK. and Zheng, Z. 2004. pH neutralization and zonation in alkaline-saline tank waste plumes. *Environ. Sci. Technol.* 38, 1321–1329

Watts MJ and CJ Mitchell. 2008. "A pilot study on iodine in soils of Greater Kabul and Nangarhar provinces of Afghanistan." *Environmental Geochemistry and Health* 31(4):503. DOI: 10.1007/s10653-008-9202-9.

Wang, G.; Um, W.; Wang, Z.; Reinoso-Maset, E.; Washton, NM.; Mueller, KT.; Perdrial N.; O'Day, PA. and Chorover, J. 2017. Uranium Release from Acidic Weathered Hanford Sediments: Single-Pass Flow-Through and Column Experiments. *Environ. Sci. Technol.* 51, 11011–11019.

Wang, G.; Qafoku, NP.; Szecsody, JE.; Strickland, CE.; Brown, CF.; Freedman, VL. 2019. Time-dependent iodate and iodide adsorption to Fe oxides. *ACS Earth Space Chem.* (accepted)

Wellman DM, JP Icenhower, AP Gamerdinger and SW Forrester. 2006. "Effects of pH, temperature, and aqueous organic material on the dissolution kinetics of meta-autunite minerals, $(Na, Ca)_{2-1}[(UO_2)(PO_4)]_2 \cdot 3H_2O$." *American Mineralogist* 91(1):143–158. DOI: 10.2138/am.2006.1807.

Xu C, DI Kaplan, S Zhang, M Athon, Y-F Ho, H-P Li, CM Yeager, KA Schwehr, R Grandbois, D Wellman and PH Santschi. 2015. "Radioiodine sorption/desorption and speciation transformation by subsurface sediments from the Hanford Site." *Journal of Environmental Radioactivity* 139:43–55. DOI: 10.1016/j.jenvrad.2014.09.012.

Yamashita T and P Hayes. 2008. "Analysis of XPS spectra of Fe^{2+} and Fe^{3+} ions in oxide materials." *Applied Surface Science* 254(8):2441–2449. DOI: 10.1016/j.apsusc.2007.09.063.

Zhang S, C Xu, D Creeley, Y-F Ho, H-P Li, R Grandbois, KA Schwehr, DI Kaplan, CM Yeager, D Wellman and PH Santschi. 2013. "Iodine-129 and Iodine-127 Speciation in Groundwater at the Hanford Site, U.S.: Iodate Incorporation into Calcite." *Environmental Science & Technology* 47(17):9635–9642. DOI: 10.1021/es401816e.

Zhu L, D Sheng, C Xu, X Dai, MA Silver, J Li, P Li, Y Wang, Y Wang, L Chen, C Xiao, J Chen, R Zhou, C Zhang, OK Farha, Z Chai, TE Albrecht-Schmitt and S Wang. 2017. "Identifying the Recognition Site for Selective Trapping of $^{99}TcO_4^-$ in a Hydrolytically Stable and Radiation Resistant Cationic Metal–Organic Framework." *Journal of the American Chemical Society* 139(42):14873–14876. DOI: 10.1021/jacs.7b08632.

Pacific Northwest
National Laboratory

902 Battelle Boulevard
P.O. Box 999
Richland, WA 99354
1-888-375-PNNL (7665)

www.pnnl.gov